

**University of Alberta**

**First-Row Transition Metal-Mediated Reactions: Catalytic Ester  
Hydrogenolysis, Aerobic Alkane Oxidation, and [5+2] Ring-Expansion  
Reactions**

by

**Shaohui Yu**

A thesis submitted to the Faculty of Graduate Studies and Research  
in partial fulfillment of the requirements for the degree of

Doctor of Philosophy

Department of Chemistry

©Shaohui Yu  
Spring 2014  
Edmonton, Alberta

Permission is hereby granted to the University of Alberta Libraries to reproduce single copies of this thesis and to lend or sell such copies for private, scholarly or scientific research purposes only. Where the thesis is converted to, or otherwise made available in digital form, the University of Alberta will advise potential users of the thesis of these terms.

The author reserves all other publication and other rights in association with the copyright in the thesis and, except as herein before provided, neither the thesis nor any substantial portion thereof may be printed or otherwise reproduced in any material form whatsoever without the author's prior written permission.

## Abstract

The research described in this dissertation focuses on first-row transition metal catalyzed and mediated organic reactions. The first part of the thesis involves the exploration of the catalytic reactivity of phosphoranimide-supported tetrametallic nickel and cobalt clusters, while the second part focuses on the development of stoichiometric cobalt/iron-mediated ring-expansion reactions.

The ester hydrogenolysis reactions catalyzed by the new nickel cluster proceeded under remarkably mild conditions. Both nickel and cobalt catalysts show unique selectivity for ester  $sp^3$  C–O bond activation, affording the corresponding carboxylic acids and alkanes by simple hydrogenolysis. Other relevant reactions catalyzed by this cluster include ketone hydrogenation and an unprecedented new reduction of benzyl aldehyde, in which sequential Tishchenko and ester reduction reactions are involved.

The catalytic aerobic alkane oxidation reactions were developed, remarkably, using the same nickel and cobalt clusters. Despite the air-sensitive nature of the clusters, the air-oxidized catalysts mediate aerobic oxidation, activating  $sp^3$  C–H bonds in hydrocarbons and functionalized organics to afford mainly ketones at elevated temperatures. The investigated substrates include alkyl arenes, ethers and non-functionalized hydrocarbons. Oxidation occurs selectively at the methylene positions  $\alpha$  to the activating groups, which

include either phenyl groups or oxygen atoms. For alkanes, tertiary C–H bonds appear to be more reactive than secondary C–H bonds, suggesting a free radical process, at least at some point(s) in the overall transformation.

For cobalt-mediated [5+2] cyclopentenyl/alkyne ring-expansion reactions, the narrow substrate scope defined in previous studies limits the potential for developing applications. Two synthetic routes for preparing unsymmetrical cobalt(I) cyclopentadiene precursors were examined, including reduction of unsymmetrical cobaltocenium compounds and replacement of ethylene ligands with cyclopentadiene in cobalt(I) bisethylene complexes. The attempted [5+2] ring-expansion reactions afford unsymmetrical cobaltocenium compounds as the major products, instead of the desired seven-membered ring formation.

Based on DFT calculations conducted by Salai and Nakamura, a new strategy for [5+2] ring-expansion reaction was proposed. Instead of  $\eta^4$ -cyclopentadiene cobalt (I) complexes, an  $\alpha$ -diimine iron(0) alkyne complex is protonated in the presence of cyclic alkene. However, the reaction generates an ammonium derivative from ligand reduction and no ring-expansion products are obtained. New ligand design is required for the further investigations.

## **Acknowledgements**

I would like first to express my gratitude to my supervisor Prof. Jeff Stryker for providing invaluable education, guidance and strong support for my entire Ph.D. career.

I would also like to acknowledge the current and past Stryker group members that I have been working with: Dr. Bryan Chan, Dr. Rick Bauer, Dr. Owen Lightbody, Dr. Kai Ylijoki, Dr. Robin Hamilton, Dr. Jeremy Gauthier, Jeffrey Quesnel, Dominique Herbert, Verner Lofstrand, Jeffrey Bunquin, Ting Zhao, Dr. Tao Bai, Kirsten Tomlin, Devin Reaugh, Colin Diner, Md Jewel, Adam McKinty, Fraser Pick, Chao Han. In particular, I wish to thank Bryan and Rick for their help when I first joined the group.

I would also express my thanks to the staff in analytical labs at the University of Alberta for offering high-quality services in NMR, MS, EA, X-ray, etc. Special thanks would go to Wayne Moffat, Marc-Andre Hoyle and Miranda Skjel for GC-MS and EA services as well as Jing Zheng for HR-MS analysis.

Finally, I would like to thank my family, especially my parents, for the encouragement and my wife, Xi Wang, for her support.

## Table of Contents

Preface	1
Part I: Ester Hydrogenation and Aerobic Alkane Oxidation Catalyzed by the Phosphoramidate-Supported Nickel Cluster	5
Part I Introduction	5
Chapter 1: Nickel/ Cobalt-Catalyzed Ester Hydrogenation Reactions	7
1.1 Introduction	7
1.2 Results and Discussion	22
1.3 Conclusion	71
1.4 Future work	72
Chapter 2: Nickel -Catalyzed Aerobic Alkane Oxidation Reactions	75
2.1 Introduction	75
2.2 Results and Discussion	101
2.3 Conclusion	137
2.4 Future work	138
Part II: Study towards Cobalt/ Iron-Mediated Mediated [5+2] Ring-Expansion Reactions	139
Part II Introduction	139

Chapter 3: Study towards Cobalt-Mediated Mediated [5+2] Ring-Expansion Reactions	143
3.1 Introduction	143
3.2 Results and Discussion	150
Chapter 4: New strategy towards Iron-Mediated Mediated [5+2] Ring-Expansion Reactions	179
4.1 Introduction	179
4.2 Results and Discussion	182
Part II Conclusion	184
Part II Future work	185
Chapter 5: Experimental Information	186
Appendix I	271
References	288

## List of Tables

<i>Title</i>	<i>Page</i>
Table 1-1: A summary of reducing reagents used for ester reduction	11
Table 1-2: Comparison for ester hydrogenation reactions between nickel/cobalt clusters with literature catalysts	24
Table 1-3: Ester hydrogenation reactions catalyzed by nickel and cobalt clusters	25
Table 1-4: Benzyl benzoate reduction optimization	32
Table 1-5: Results of parallel reactions using CaH <sub>2</sub> for the cationic effect study	37
Table 1-6: Effect of the hydrogen pressure on ester hydrogenation reactions	38
Table 1-7: Modes of oxidative addition of Ni(COD) <sub>2</sub> to ester substrates	57
Table 1-8: Comparison of <sup>13</sup> C NMR signals between $\epsilon$ -caprolactone and the polymers	65
Table 2-1: Comparison of four generations of Gif systems	98
Table 2-2: A summary of the aerobic alkane oxidation reactions	103
Table 2-3: Two categories of substrates that have high or low boiling points	105
Table 2-4: Oxidation of ethylbenzene	110
Table 2-5: Solvent optimization for ethylbenzene oxidation	115
Table 3-1: A summary of cobaltocene derivatives oxidation using halogens	158
Table 3-2: Reduction of substituted cobaltocenium compounds with alkyllithium	166
Table 5-1: A summary of GC and mol percent for toluene in prepared diethyl ether solutions	189

## List of Figures

<i>Title</i>	<i>Page</i>
Figure I1-1: Structure of phosphoranimide-supported nickel/cobalt cluster	5
Figure 1-1: Triglycerides' structure and their synthesis	7
Figure 1-2: Examples of fruit flavors	8
Figure 1-3: PETE's structure and its synthesis	9
Figure 1-4: Resonance structure of esters	10
Figure 1-5: Structures of potassium hydridoruthenate complexes	11
Figure 1-6: Structures of Noyori-type complexes	14
Figure 1-7: Structures of ruthenium complexes with amino-phosphino-bridged ligands	14
Figure 1-8: Relative trend in ester reduction	27
Figure 1-9: Type A and B for oxidative addition of Ni(COD) <sub>2</sub> to esters	56
Figure 2-1: Orbital diagram of molecular oxygen	77
Figure 2-2: Diastereomers of 1,1'-oxodiisochromane	120
Figure 3-1: X-ray crystal structure of [(1-Me-3- <sup>t</sup> BuCp)Co(Cp)][BF <sub>4</sub> ]	165
Figure 3-2: Isomeric structures of cyclopentadiene cobalt(I) complexes	167
Figure 4-1: Structures of cobalt(I) complexes	181
Figure 5-1: Calculation of toluene yield (y-value)	188

## List of Abbreviation

Å	Angstrom
Acac	Acetylacetonate
Bu	Butyl group
COD	Cyclooctadiene
Cp	$\eta^5$ -Cyclopentadienyl
Cp*	$\eta^5$ -Pentamethylcyclopentadienyl
DFT	Density Function Theory
Et	Ethyl group
Equiv.	Equivalents
g	Grams
h	Hours
HOMO	Highest Occupied Molecular Orbital
Hz	Hertz
IR	Infrared
<i>J</i>	Coupling constant
L	Ligand
LUMO	Lowest Unoccupied Molecular Orbital
Me	Methyl
ml	millilitre
mmol	millimoles
MO	Molecular Orbital
M. S.	Molecular Sieves
NMR	Nuclear Magnetic Resonance
Nu	Nucleophile
OAc	Acetate

OTf	Triflate
Ph	Phenyl group
ppm	Parts per million
Pr	Propyl group
R	Alkyl group
rpm	Revolutions per minute
RT	Room temperature
<i>t</i> Bu	<i>tert</i> -butyl group
THF	Tetrahydrofuran
TMS	Trimethylsilyl
TOF	Turnover frequency
Tol	Toluene
TON	Turnover number
UV	Ultraviolet
VSEPR	Valence shell electron pair repulsion
X	Halogen atom
$\delta$	Chemical Shift
$\eta$	Hapticity
$\Delta$	Heating
$\mu$ L	Microlitre

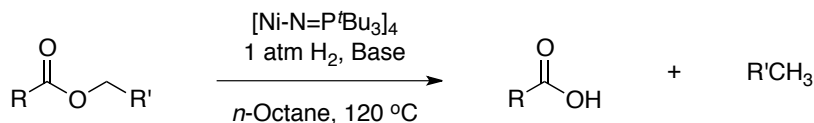
## Preface

The surge in organometallic chemistry has greatly promoted applications in organic synthesis over the past several decades. Modern transition-metal complexes have demonstrated diverse appeal and display important reactivities. They not only mediate organic transformations stoichiometrically, but also serve as catalysts for numerous reactions. Industrially important transition metal-catalyzed reactions include the widely recognized olefin metathesis and cross-coupling reactions.<sup>1,2</sup> In general, the precious second- and third-row metals have been the most thoroughly investigated, whereas the late first-row transition metals remain relatively unexplored. Due to their abundance, availability and low toxicity, first-row transition metals are now drawing more and more research interest.

My research has been focused on first-row transition-metal catalyzed and mediated organic reactions. This dissertation consists of two parts: the first part describes the study of nickel- and cobalt-catalyzed ester hydrogenation and aerobic alkane oxidation reactions in chapter 1 and chapter 2, respectively; the second half covers the research directed towards cobalt and iron-mediated [5+2] ring-expansion reactions in chapter 3 and chapter 4, respectively. The last chapter 5 provides the supporting information for all related experiments discussed in this dissertation. These chapters are summarized below.

Chapter 1 introduces esters and their corresponding industrial applications, research about ester reduction reactions in laboratory and reductive ester upgrading strategies in industry. The remaining part of this chapter is devoted to my discovery of ester hydrogenation using structurally novel nickel and cobalt catalysts and subsequent discussion about its unique reaction patterns, substrate scope and preliminary mechanistic studies (Eq. p-1).

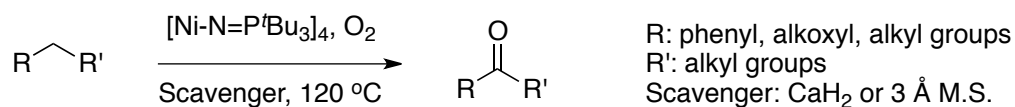
### Equation p-1



R, R': alkyl, aryl groups; Base: NaH or CaH<sub>2</sub>

Chapter 2 begins with an introduction to the alkanes, their industrial utility and the corresponding challenges for catalytic selective alkane activation. Subsequently, alkane C-H bonds activation and alkane oxidation chemistry are briefly discussed, including Shilov chemistry, biological oxidations with metalloenzymes, the Gif iron system and other synthetic catalysts. The last part of chapter 2 describes and discusses my discovery of aerobic alkane oxidation reactions catalyzed by novel nickel and cobalt clusters, including condition optimization, exploration of substrate scope and a preliminary mechanistic study (Eq. p-2).

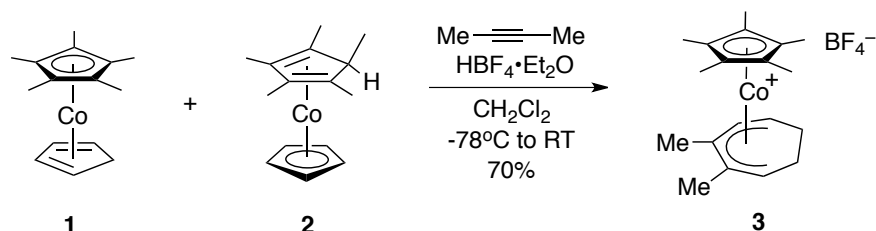
### Equation p-2



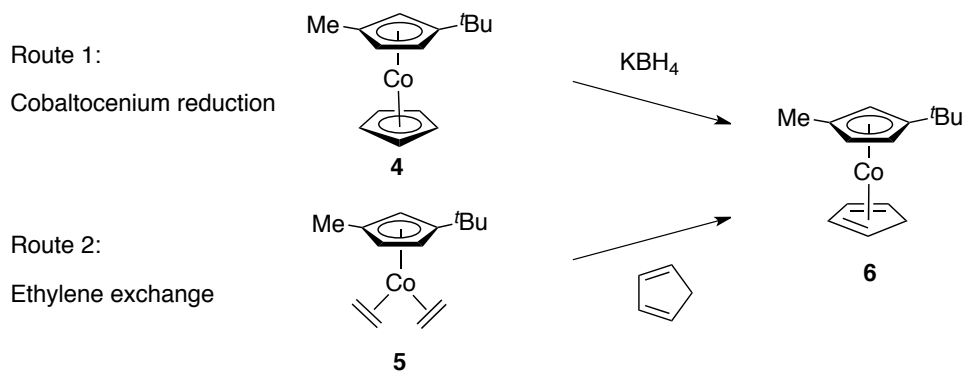
Chapter 3 introduces previously studied cobalt-mediated [5+2] ring-expansion reactions (Eq. p-3) and some promising preliminary results obtained using the cobalt systems bearing disubstituted cyclopentadienyl ligands. The next part of this chapter focuses on the synthesis of novel cobalt(I)-cyclopentadiene complexes **6** with disubstituted cyclopentadienyl ligands. Two synthetic routes were investigated: (1) the reduction of unsymmetrical cobaltocenium compounds **4** and (2) ligand exchange starting from the

cobalt(I) bis(ethylene) complex **5** and cyclopentadiene (Scheme p-1). The last section provides the results and discussion pertinent to the attempted cyclopentenyl ring-expansion reactions.

### Equation p-3

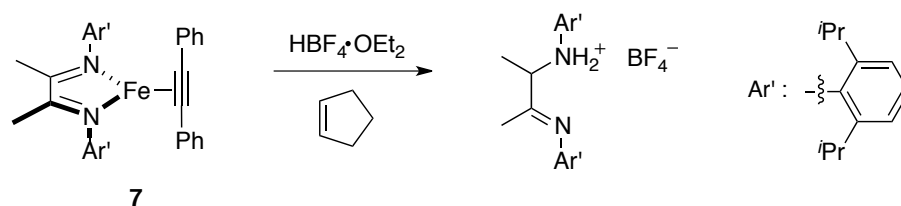


### Scheme p-1



Chapter 4 covers a new approach to ring-expansion reactions using low valent iron alkyne complexes **7** as precursors. DFT calculations of similar ring-expansion reactions, performed by collaborators, are provided as theoretical support for this novel ring-expansion strategy. Our investigation of ring-expansion reactions will be presented and followed by a discussion of the undesired results (Eq. p-4).

### Equation p-4

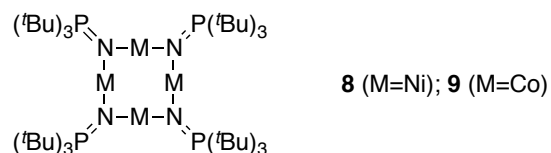


Chapter 5 includes all the experimental information pertinent to Chapters 1 to 4. Detailed reaction procedures are provided for every reaction reported in the thesis. Spectroscopic data and analytical results of each reaction are also incorporated.

## Part I: Low-Coordinate Nickel and Cobalt Clusters-Catalyzed Reactions: Ester Hydrogenation and Aerobic Alkane Oxidation

A novel class of structurally-unique, low-coordinate nickel and cobalt clusters was recently developed in our group.<sup>3</sup> The low-valent nickel(I) and cobalt(I) centers are supported by phosphoranimide ligands to form tetrameric clusters,  $[\text{Ni-N}=\text{P}^t\text{Bu}_3]_4$  **8** and  $[\text{Co-N}=\text{P}^t\text{Bu}_3]_4$  **9** (Figure I1-1). The four metal centers of the complex are coplanar, bridged by the electron-rich nitrogen atoms of the phosphoranimide. Each metal center is coordinated to two phosphoranimide ligands in a linear arrangement. The absence of any additional ancillary ligands in the clusters results in some unique properties and unprecedented reactivity.<sup>3</sup> In our group, significant research effort has been devoted to exploring potential applications of the clusters for catalyzing industrially important processes and novel organic reactions.

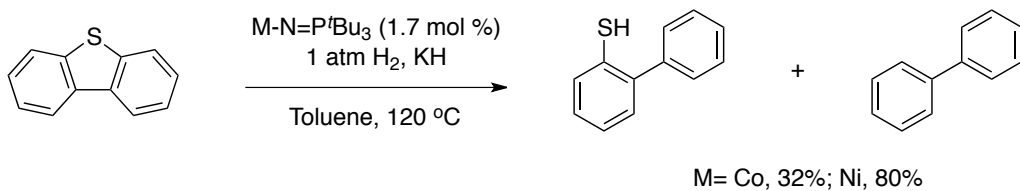
**Figure I1-1** Structure of phosphoranimide-supported nickel/cobalt cluster



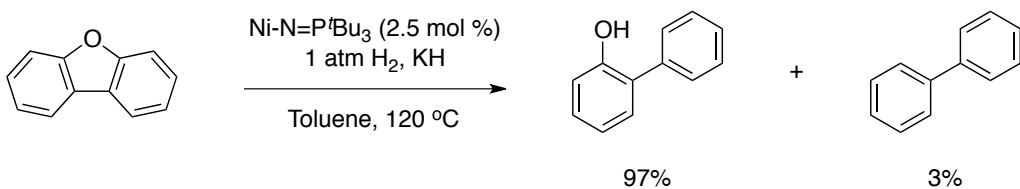
The clusters demonstrate robust reactivity for alkene/alkyne hydrogenation at low temperature and low hydrogen pressure. The clusters have been specifically designed to catalyze hydrodesulphurization and hydrodeoxygenation reactions under mild conditions (Eq. I1-1, 2).<sup>4</sup> In addition to these previous discoveries, I have now found that the clusters also show remarkable hydrogenation and, surprisingly, oxidation abilities under appropriate conditions. Therefore the first part of the dissertation will present two new reaction processes catalyzed by the unique nickel and cobalt clusters **8** and **9**. More

specifically, in Chapter 1, ester hydrogenation reactions are discussed, while Chapter 2 covers aerobic alkane oxidation reactions, each starting with the same precatalyst complex.

**Equation I1-1.**



**Equation I1-2.**



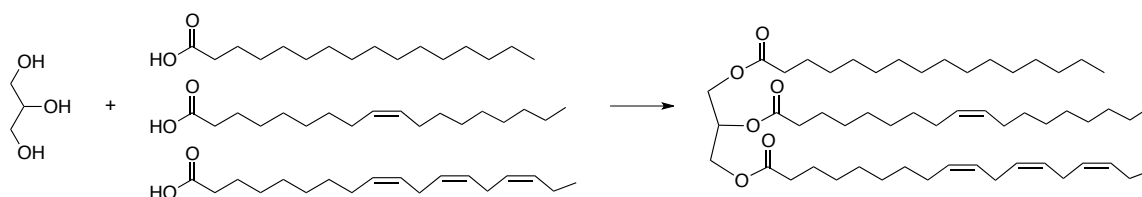
# Chapter 1: Ester Hydrogenation Reactions Catalyzed by Phosphoranimide-Supported Nickel/Cobalt Clusters

## 1.1 Introduction

### 1.1.1 Introduction to Esters

Esters are extensively present in nature and the economy with diverse utilities and applications. Naturally occurring ester derivatives are abundant, consisting mainly of triglycerides and a range of terpenoids that provide different fruit flavors. In the world of industry, chemicals possessing ester functional group are produced on large scale for commercial purposes, such as ethyl acetate, which is widely used as an organic solvent. In addition, the polyester industry provides an enormous range of plastic materials annually, such as PET, PTT, etc. Nowadays, ester derivatives have been widely applied in energy, food, materials and other industries, significantly improving the overall human wellbeing.

**Figure 1-1.** Triglycerides' structure and their synthesis

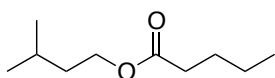


Triglycerides are the major component of lipids that are extensively present in organisms. In nature, lipids are typically present as vegetable oils in plants, fats in animals, oils in algae. In general, triglycerides are derived from glycerol and fatty acids (Figure 1-1). The three fatty acid moieties are usually different in a triglyceride molecule. Moreover, between

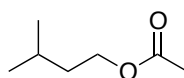
different organisms, triglycerides vary in the length of carbon chains and the degree of unsaturation. Generally speaking, vegetable oils mainly consist of unsaturated triglycerides, while animal fats contain more saturated triglycerides. Lipids possess the highest energy density among the three biomass categories, classified as lignin, lipids and carbohydrates.<sup>5</sup> Therefore, lipids are considered to be the most promising biomass feedstock for renewable fuels. The current utilization of triglycerides includes blending in petrodiesel and conversion to biodiesel, a fatty acid methyl ester (FAME).<sup>6</sup>

Fruit flavors are terpenoids, simple and fragrant alkyl esters present in a variety of fruits. Apples, bananas, pears, strawberries are distinguished by their unique aromas caused by corresponding esters. For instance, apple flavor includes isopentyl valerate and banana flavor is caused by isoamyl acetate (Figure 1-2). Manufactured or naturally extracted fruit flavors are broadly utilized as food or beverage additives in food industry.<sup>7</sup>

**Figure 1-2.** Examples of fruit flavors



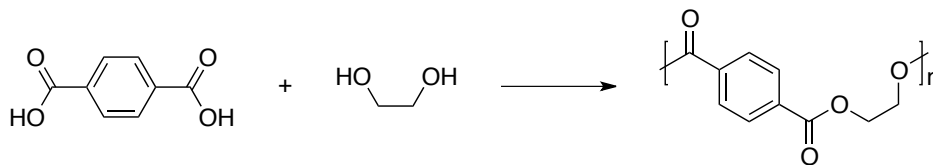
Apple flavor:  
isopentyl valerate



Banana flavor:  
isoamyl acetate

Polyesters are a group of polymers with ester linkages in their main chain. Naturally occurring polyesters include cutin and plant cuticles, covering all aerial surfaces of plants. Manufactured polyesters are represented by polyethylene terephthalate (PETE), an esterification product of ethylene glycol and terephthalic acid (Figure 1-3). PETE is widely used in the production of commodity items in daily life, such as clothes, bottles, ropes, etc.<sup>8</sup>

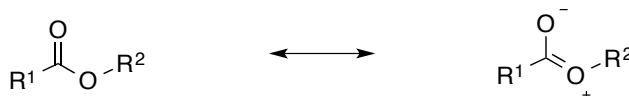
**Figure 1-3.** PETE's structure and its synthesis



Despite the diversity of ester derivatives in nature and industry, they all possess the same ester functional group and share similar chemical properties. The ester group is represented as  $R^1(C=O)OR^2$ , which is composed of acyl ( $R^1C=O$ ) and alkoxy ( $OR^2$ ) moieties. The presence of the carbonyl group in the ester renders the  $\alpha$ -protons acidic, as observed in other carbonyl compounds, such as aldehydes and ketones. However, esters are generally less acidic than ketones and aldehydes, as confirmed in experiments and as can be seen through pKa value comparison. Meanwhile, the carbonyl carbons in esters are more resistant towards nucleophilic attack than those in ketones and aldehydes. Therefore, esters remain less active than ketones and aldehydes in many reactions.

This decreased reactivity is attributed to the presence of an alkoxy group connected to the carbonyl group in esters. The improved stability of the ester group can be rationalized by the contribution of its resonance structures (Figure 1-4). From the point of view of the Frontier Molecular Orbital theory, the interaction between  $n$ -electrons and  $\pi^*$  orbital lowers the energy of the non-bonding allyl-like  $\pi^2$ -orbital, which is the HOMO in the ester group. Therefore, the ester compounds are more thermodynamically stabilized than the corresponding ketone/aldehyde derivatives.

**Figure 1-4.** Resonance structure of esters



### 1.1.2 Ester Reduction Reactions

The reduction of esters is more challenging than the reduction of corresponding ketones and aldehydes due to the increased inertness of esters. Mild reducing reagents (e.g., NaBH<sub>4</sub>) reduce aldehydes and ketones efficiently, but remain ineffective towards ester substrates.<sup>9</sup> One exception is that LiBH<sub>4</sub> in THF can reduce esters to the corresponding alcohols slowly.<sup>10</sup> The reactivity of LiBH<sub>4</sub> is attributed to the lithium counterion coordination to the substrate as a Lewis acid. Catalytic hydrogenation of esters is very challenging and remains largely unexplored, whereas catalytic aldehyde and ketone hydrogenations are well established. In particular, asymmetric hydrogenation of ketones is of great value in the production of enantiopure compounds and has widespread applications in organic synthesis.<sup>11</sup>

The primary strategies for ester reduction involve the use of either very reactive reagents or mild reductants with addition of metal catalysts (Table 1-1). Aluminum hydride reagents are commonly used for ester reduction, including LiAlH<sub>4</sub> and DIBAL-H. LiAlH<sub>4</sub> reduces esters to alcohols, while DIBAL-H converts esters to aldehydes at low temperatures. Milder reagents used for ester reduction include NaBH<sub>4</sub>,<sup>12</sup> silanes<sup>13</sup> and dihydrogen,<sup>14</sup> but the addition of catalysts is required to effect the reduction efficiently. Among all reducing reagents, molecular hydrogen appears to be most attractive, due to its atom economy, abundance, and reduced waste generation.

**Table 1-1.** A summary of reducing reagents used for ester reduction

Reducing reagent	Direct reduction		Catalyst required		
	LiAlH <sub>4</sub>	DIBAL-H	NaBH <sub>4</sub>	R <sub>3</sub> Si-H	H <sub>2</sub>

### ***Ester hydrogenation***

Molecular hydrogen has long been considered as an ideal reducing reagent, especially for large-scale process. The advantages include industrial availability, mild chemical properties as a reducing reagent, and the generation of non-hazardous byproduct, H<sub>2</sub>O. However, hydrogenation of esters is regarded as a difficult task. Thus, only a few effective catalysts have been reported in the literature, predominantly comprised of relatively expensive ruthenium complexes.

**Figure 1-5.** Structures of potassium hydridoruthenate complexes



**10**

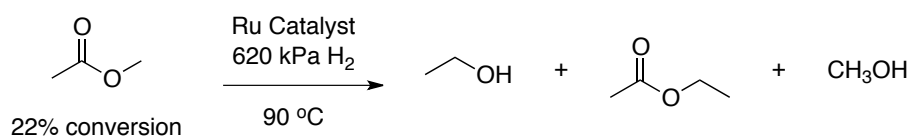


**11**

The central challenge for ester hydrogenation reactions is the development of efficient catalytic systems. Transition-metal complexes are so far the only and most effective catalysts available. The first homogeneous catalysts for ester reduction were reported in 1981, albeit with limited success. In this work, potassium hydridoruthenate complexes **10** and **11** were prepared and characterized (Figure 1-5).<sup>15</sup> They were later tested for the reduction of various carbonyl derivatives. The substrate scopes of each complex are restricted, limited to activated esters bearing electron-withdrawing groups (e.g.,

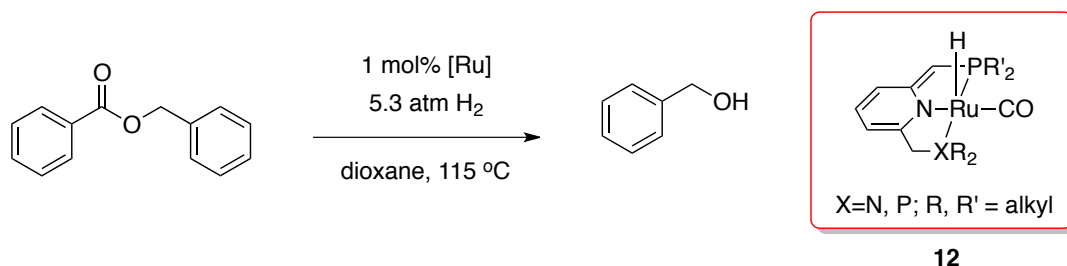
CF<sub>3</sub>CO<sub>2</sub>Me). The most noteworthy achievement in this work was the hydrogenation of methyl acetate to the alcohols catalyzed by complex **11**, which is claimed as the first example of aliphatic ester hydrogenation by any homogeneous catalyst (Eq.1-1).<sup>16</sup> Subsequently, many more ruthenium complexes were developed for ester hydrogenation. Selected examples include H<sub>4</sub>Ru<sub>4</sub>(CO)<sub>8</sub>(PBU<sub>3</sub>)<sub>4</sub>, Ru(CO)<sub>2</sub>(CH<sub>3</sub>CO<sub>2</sub>)<sub>2</sub>(PBU<sub>3</sub>)<sub>2</sub>, etc.<sup>17,18</sup> However all of these catalysts are associated with the same disadvantages: narrow substrate scope and requirement of additives in large amount, including zinc<sup>19</sup> and inorganic acids<sup>20</sup>.

### Equation 1-1

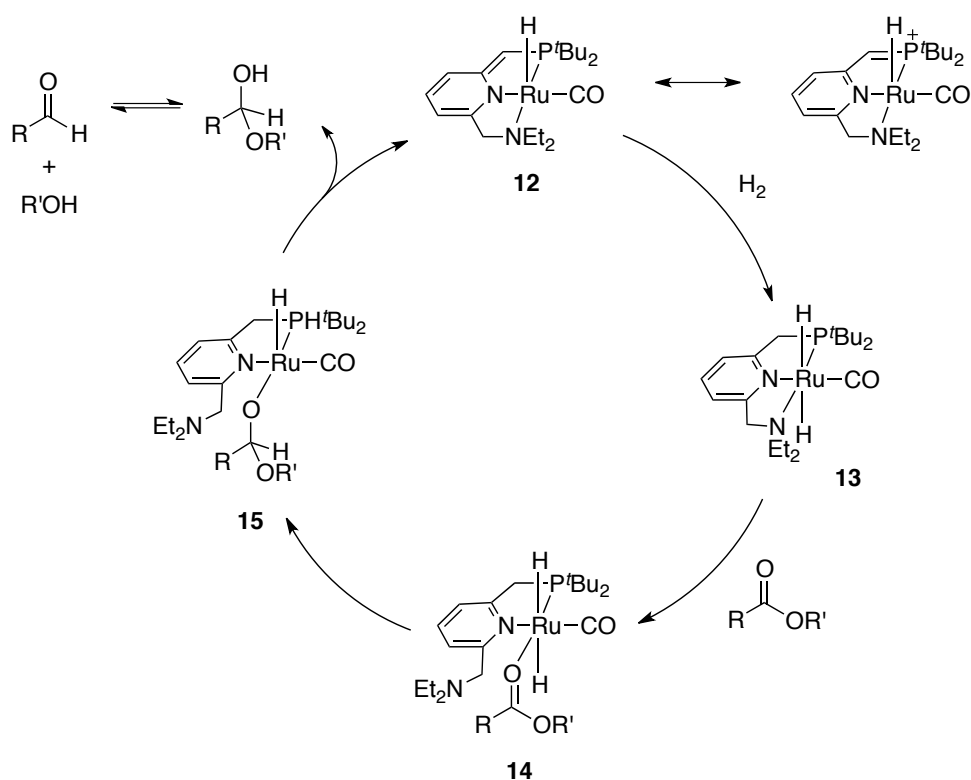


The breakthrough in ester hydrogenation came with the development of modern pincer ligands and the PNN ruthenium complex **12** by Milstein, *et al.*, in 2006 (Eq. 1-2).<sup>21</sup> This complex is an efficient catalyst for the reduction of aliphatic esters under mild conditions, affording corresponding alcohols. The proposed mechanism of the reduction involves dissociation of the amine “arm” of the ligand to leave a vacant coordination site, followed by ester binding to the ruthenium center forming complex **14** and subsequent transfer of hydride to the carbonyl carbon (Scheme 1-1). The resulting hemiacetal compound is dissociated from the ruthenium complex **15** to generate the aldehyde, which is reduced to alcohol in a similar fashion but at a faster rate.

### Equation 1-2



### Scheme 1-1



The Saudan research group has explored the possibility of applying the ketone hydrogenation catalysts to ester substrates. This study was focused on the ruthenium complexes chelated by N, P ligands **16**, **17**, known as the most efficient catalysts for ketone hydrogenation.<sup>22</sup> Noyori-type complexes **16**, **17** are incompetent to reduce esters, but

several ruthenium complexes with amino-phosphino-bridged ligands **18**, **19** and **20** demonstrate extraordinary reactivity towards ester groups (Figure 1-6, 7). Another attractive feature of this reaction is that the catalyst remains inert toward olefin hydrogenation. As a result, these are particularly suitable as catalysts for the synthesis of oleyl alcohols.

**Figure 1-6.** Structures of Noyori-type complexes

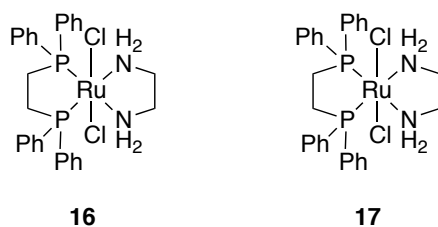
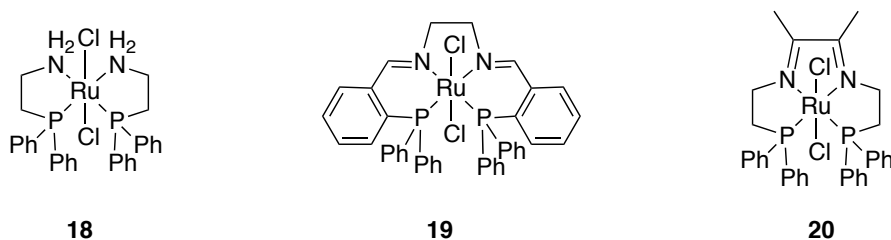


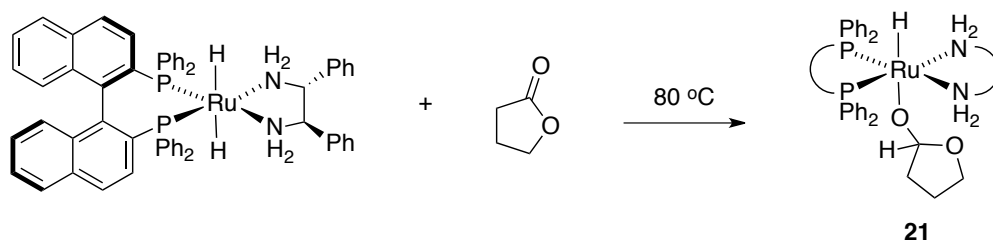
**Figure 1-7.** Structures of ruthenium complexes with amino-phosphino-bridged ligands



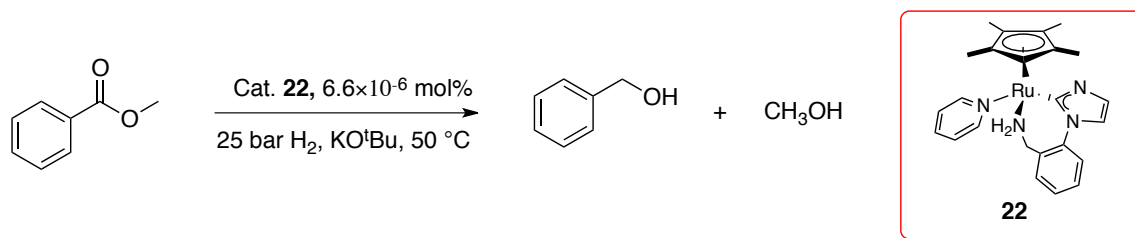
Ruthenium complexes have also been developed in the Bergens, Morris and Gusev groups, among others. Bergens' work features the observation of a catalytic intermediate, the ruthenium-hemiacetaloxide **21** (Eq. 1-3).<sup>23</sup> Morris and coworkers developed a new and powerful ruthenium catalyst **22** bearing an N-heterocyclic carbene ligand (Eq. 1-4).<sup>24</sup> This is quite different from the previous catalysts, which mostly contain N, P-ligands. In addition to the invention of new ruthenium complexes, Gusev and coworkers also reported an

analogous osmium catalyst for ester hydrogenation.<sup>25</sup> Osmium is notoriously expensive and cannot be used for mass-scale processes.

### Equation 1-3



### Equation 1-4

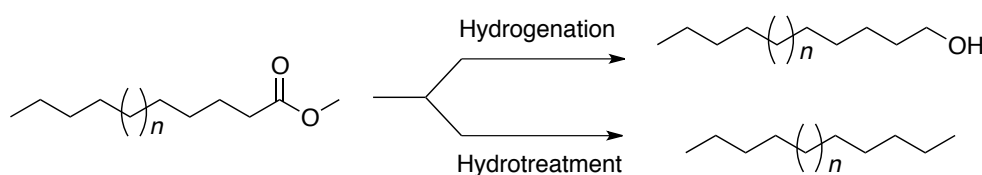


Although research into ester hydrogenation has been fruitful in recent years, the periodic table still remains largely unexplored. The developed catalysts are limited to expensive ruthenium and osmium metals. Meanwhile, the reactions also require high hydrogen pressure, typically more than 5 atm. The reaction patterns lack diversity, as alcohols are produced exclusively from these reactions.

### 1.1.3 Industrial ester hydrogenation

In contrast to the early-stage ester hydrogenation research in the academic laboratory, industrial upgrading of esters using molecular hydrogen has been applied to various processes. Hydrotreatment and hydrogenation constitute the two main industrial practices currently. In both cases, heterogeneous transition metal compounds are deployed as catalysts under forcing conditions, but the product distribution varies. Alcohols are generally obtained from hydrogenation, while alkanes are selectively produced from hydrotreatment (Scheme 1-2). More precisely, ester hydrogenation produces fatty alcohols as an important commodity, while ester hydrotreatment is in development as a bio-fuel refinery technique to upgrade esters to higher-quality liquid fuels.

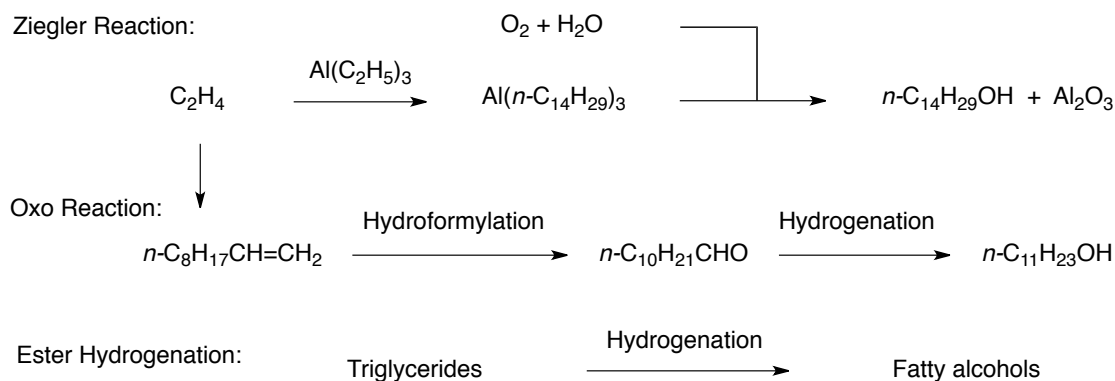
**Scheme 1-2**



Fatty alcohols are valuable chemicals with broad applications as detergents and surfactants in the cosmetics, food and pharmaceutical industries.<sup>26-28</sup> More specifically, long-chain alcohols are applied as emulsifiers in cosmetic products, plasticizers for softening fabrics, carriers in medicine, etc.<sup>27</sup> Fatty alcohols are naturally occurring in waxes, but their supply heavily relies on industrial production. The first industrial process began in the early twentieth century by reducing natural esters with sodium metal, a process known as the Bouveault-Blanc reduction.<sup>29</sup> Nowadays, the best developed industrial processes for fatty alcohol production include Ziegler and Oxo processes, along with the hydrogenation of fatty esters and acids.<sup>30</sup> Ziegler and Oxo processes produce synthetic alcohols from petroleum feedstock, whereas ester hydrogenation converts bio-derived esters to natural

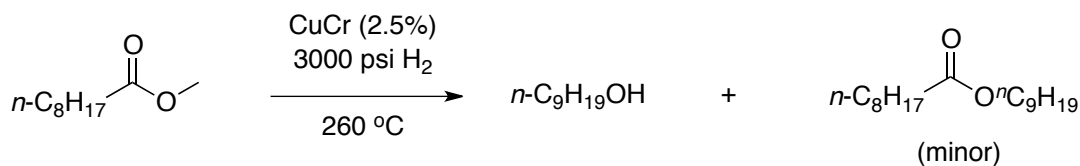
alcohols (Scheme 1-3). The ester hydrogenation process contributes about 40 percent of the worldwide supply of fatty alcohols.<sup>30</sup>

### Scheme 1-3



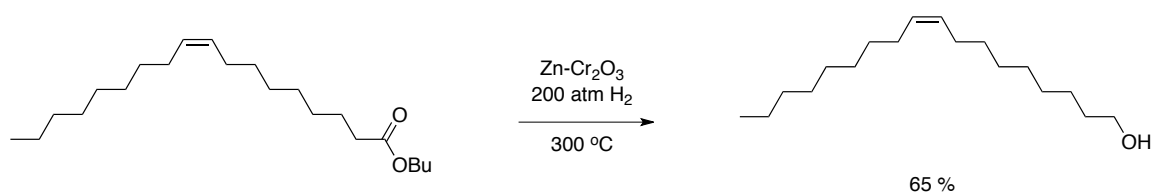
Copper chromites are the most common catalysts used in the ester hydrogenation industry. Typical operating conditions require high hydrogen pressures (200-300 atm) and high temperatures (250-300 °C) (Eq. 1-5).<sup>31</sup> Other catalytic systems have been developed, including palladium-rhenium and rhodium-tin bimetallic mixtures.<sup>32</sup> The catalysts are not selective towards ester functional groups, also reducing olefin moieties. As a result, both functional groups are hydrogenated to afford saturated fatty alcohols.

### Equation 1-5



Unsaturated fatty alcohols are a class of value-added alcohol derivatives, which have broad applications in cosmetic commodities. The most common unsaturated alcohols in the market are oleyl alcohols. Generally, the hydrogenation of olefin functionality is easier than ester hydrogenation. This tendency raises a challenge for the development of catalysts possessing the opposite reactivity. Zinc–chromite oxide was discovered in 1937 to be an active catalyst for the production of unsaturated alcohols from unsaturated esters at 300 °C and under 200 atm hydrogen pressure (Eq. 1-6).<sup>33</sup> Many other bimetallic catalytic systems were reported afterwards, including cobalt-tin,<sup>26</sup> ruthenium-tin,<sup>34</sup> and iron oxide-zinc catalysts,<sup>32</sup> among others.

#### Equation 1-6

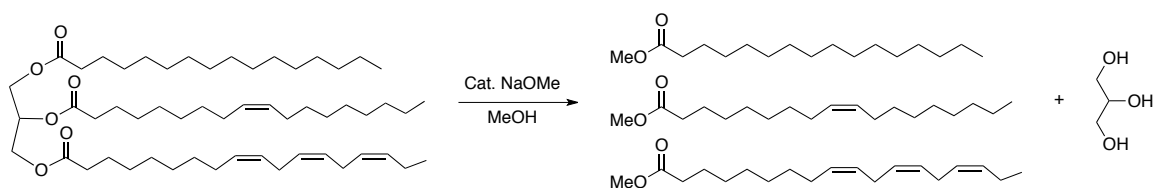


#### 1.1.4 Industrial ester hydrotreatment

Ester hydrotreatment is a different industrial process compared to ester hydrogenation. Ester hydrotreatment produces saturated alkanes by complete removal of the oxygen content in the ester starting materials. It is a refinery technology to produce high-quality liquid fuels and has been applied to the upgrading of triglyceride feedstock and biodiesels to renewable diesel fuels, which are saturated long-chain hydrocarbons identical to petroleum diesels.

Triglycerides are valuable biomass, but cannot be utilized directly as fuels. In the bio-fuel industry, triglycerides are converted to biodiesels by transesterification (Eq. 1-7).<sup>35</sup> However, biodiesels are still problematic when used in diesel engines. Significant disadvantages include high cloud point, high viscosity, low volatility and poor oxidation stability, which together cause a series of problems in fuel flow, engine compatibility, storage, etc.<sup>36</sup> The problems are mostly associated with the high oxygen content as well as the presence of unsaturation. However with the development of new capabilities to solve these problems, ester hydrotreatment provides an opportunity for the upgrading of triglycerides and biodiesels.

### Equation 1-7

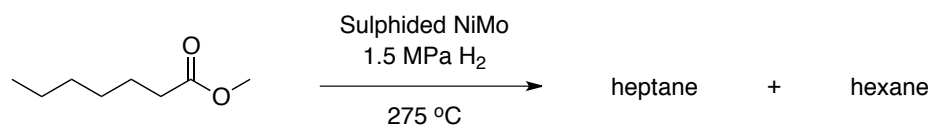


In industry, petroleum refinery infrastructures are ideal facilities for ester hydrotreatment. Therefore, ester hydrotreatment can take advantage of existing facilities and will reduce the capital investment requirements drastically. As a consequence, catalyst development becomes an essential challenge for ester hydrotreatment. Current research not only focuses on modifying the commercialized petroleum catalysts, but also at the development of novel catalytic systems.

Commercially available petroleum hydrodesulphurization (HDS) catalysts have been evaluated in ester hydrotreatment. In 2005, Senol successfully utilized HDS catalysts to

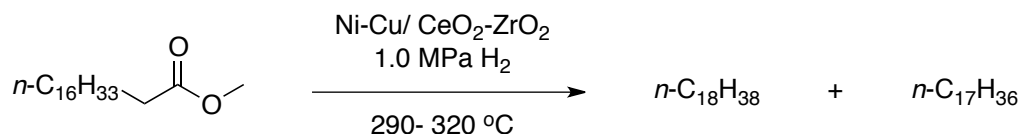
realize the reduction of esters to alkanes under industrial process conditions (250-300 °C, 1.5 MPa H<sub>2</sub>) (Eq. 1-8).<sup>37</sup> In this study, the applied HDS catalysts are alumina-supported and sulphided NiMo and CoMo. However, the stability of the catalysts is not satisfactory due to over-desulphurization of the catalysts, which appears to be a general problem in bio-oil hydroprocessing.<sup>38</sup> Further studies from Senol suggest that water formation inhibits the reactivity of the catalysts and that simultaneous addition of H<sub>2</sub>S is necessary to maintain catalytic performance.<sup>39</sup> However, as biomass has very low sulfur content, the industrial process for ester hydrotreatment with HDS catalyst would require continuous addition of sulfur-containing compounds, which is not practical.

#### Equation 1-8



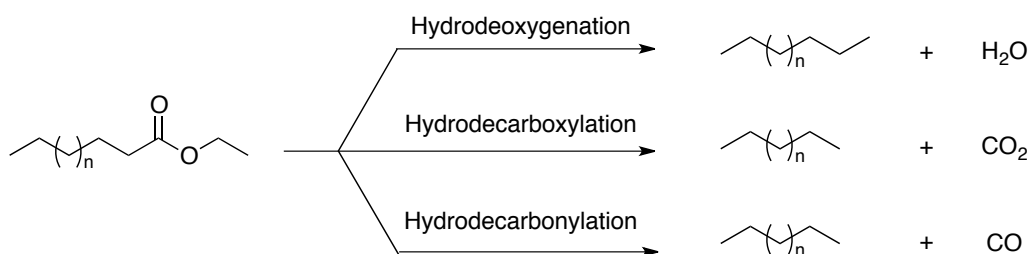
As an alternative, non-sulphided catalysts have been developed. The CeO<sub>2</sub>-ZrO<sub>2</sub> supported Ni-Cu bimetallic system reported by Yakovlev *et al.*, is capable of catalyzing the reduction of biodiesel to renewable diesel at 280-330 °C and 1.0 MPa of H<sub>2</sub> (Eq. 1-9).<sup>40</sup> In this system, copper is proposed to facilitate nickel oxide reduction and prevent the methanization of CO or CO<sub>2</sub> at the operating temperature. Moreover, catalysts based on precious metals have also been reported, including Pd/C, Pt/H-2SMS, etc.<sup>41,42</sup>

#### Equation 1-9

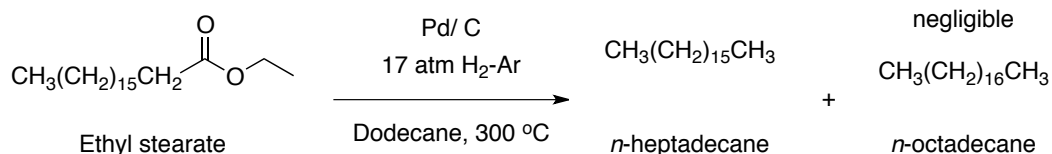


The full mechanism for the ester hydrotreatment reactions has not been established. However based on product analysis, three reaction pathways have been proposed (Scheme 1-4). The pathways include hydrodeoxygenation, hydrodecarboxylation and hydrodecarbonylation, which would correspond to the formation of H<sub>2</sub>O, CO<sub>2</sub> and CO as byproducts, respectively.<sup>43</sup> The alkanes formed from hydrodeoxygenation pathway are one-carbon longer than that from other two pathways. In general, hydrodeoxygenation is the main pathway in hydrotreatment reaction, which is generally accompanied by lesser amounts of the other two pathways.<sup>44</sup> However hydrodecarboxylation as the predominant pathway has also been reported. One example is the reduction of ethyl stearate catalyzed by Pd/C at high temperatures, which affords *n*-heptadecane as a major product with only negligible amount of *n*-octadecane (Eq. 1-10).<sup>45</sup>

**Scheme 1-4**



**Equation 1-10**



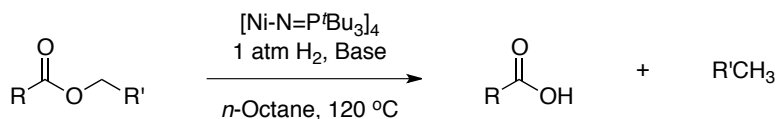
In conclusion, research into ester hydrogenation has been actively pursued over the past several decades. Many research groups have been focusing on the development of *homogeneous* catalysts. However, the catalysts developed so far are mostly ruthenium complexes, incompatible with economical large-scale applications. On the other hand, industrial research has been centered on the development and improvement of *heterogeneous* catalysts. *To the best of our knowledge, homogenous first-row transition-metal catalysts have never been reported to perform ester hydrogenation reactions.* In the results and discussion section, my study of nickel and cobalt cluster-catalyzed ester hydrogenation reactions under relatively mild conditions will be presented.

## **1.2 Results and discussion**

### *1.2.1 Overview of ester hydrogenation*

Since the discovery and characterization of phosphoranimide-supported low-coordinate nickel and cobalt clusters in our group, a series of reactions have been developed employing the clusters as catalysts for energetically difficult reactions, such as hydrodesulphurization and hydrodeoxygenation. During my exploration of other catalytic reactivity of these nickel and cobalt clusters, ester hydrogenation reactions under mild conditions were discovered. The reactions involve the hydrogenolysis of alkyl C–O bond in the esters to afford carboxylic acids and alkanes as products (Eq. 1-11). This reaction pattern is unique and potentially exploitable, as the  $sp^3$  C–O bond is selectively activated in the presence of the  $sp^2$  C–O bond in carboxylic ester substrates.

### Equation 1-11



R, R': alkyl, aryl groups; Base: NaH or CaH<sub>2</sub>

The ester hydrogenation reactions presented herein are distinct from all homogenous and heterogeneous catalysts currently available in literature (Table 1-2). As discussed, the reported homogenous catalysts are exclusively based on two types of precious metals, ruthenium and, occasionally, osmium. In comparison, the nickel and cobalt clusters are low-cost base metal catalysts and therefore much more economically viable for future industrial applications. Meanwhile, all reported ruthenium and osmium-catalyzed reactions generate alcohols as the sole products, whereas in the nickel/cobalt-catalyzed ester hydrogenation reactions, only alkanes and carboxylic acids are obtained. In comparison to the heterogeneous catalysts reported in literature, the phosphoramidate-supported nickel and cobalt clusters are advantageous because they are hydrocarbon-soluble and require much milder reaction conditions. The heterogeneous base metals applied in industrial ester reduction processes require considerably higher hydrogen pressure and more elevated reaction temperatures.

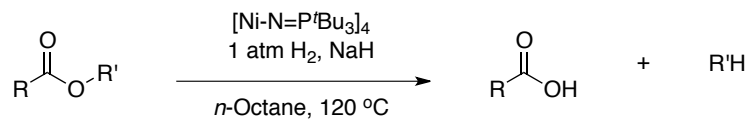
**Table 1-2.** Comparison for ester hydrogenation reactions between nickel/cobalt clusters with literature catalysts

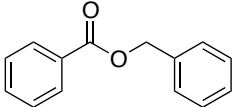
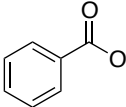
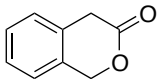
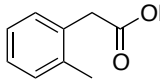
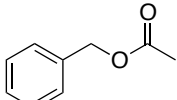
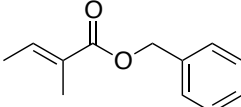
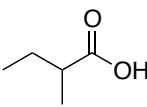
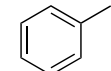
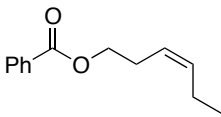
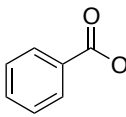
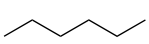
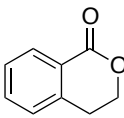
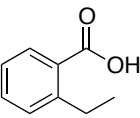
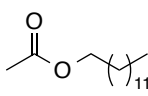
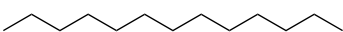
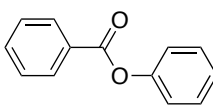
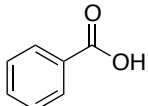
	This research	Literature	
Catalysts	Ni/Co Clusters	Homogeneous	Heterogeneous
Metals	Ni, Co	Ru, Os	Ni, Co, Cu, Fe, Pd, Pt...
Products	Alkanes and Carboxylic Acids	Alcohols	Alkanes or Alcohols
Conditions	100 °C, 1 atm H <sub>2</sub>	> 50 °C, > 4 atm	> 280 °C, > 10 atm

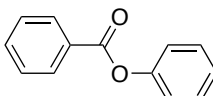
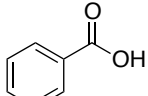
### 1.2.2 Detailed results: catalytic hydrogenation of esters

Generally speaking, the ester hydrogenation reactions we developed are conducted using the nickel cluster **8** as catalyst, under basic conditions and with mild heating. The reaction is generally performed in *n*-octane solution with the addition of insoluble NaH or CaH<sub>2</sub> as a proton scavenger, at 100-120 °C and under 1 atm of H<sub>2</sub>. The scavenger is required either as a base to deprotonate the carboxylic acid as it is formed or to promote turnover of the catalyst, or both. A summary of these ester reduction reactions is presented in Table 1-3. The substrate scope includes benzyl esters and alkyl esters. The influence of  $\alpha$ -hydrogen atoms on ester functional group has also been assessed.

**Table 1-3.** Ester hydrogenation reactions catalyzed by nickel and cobalt clusters

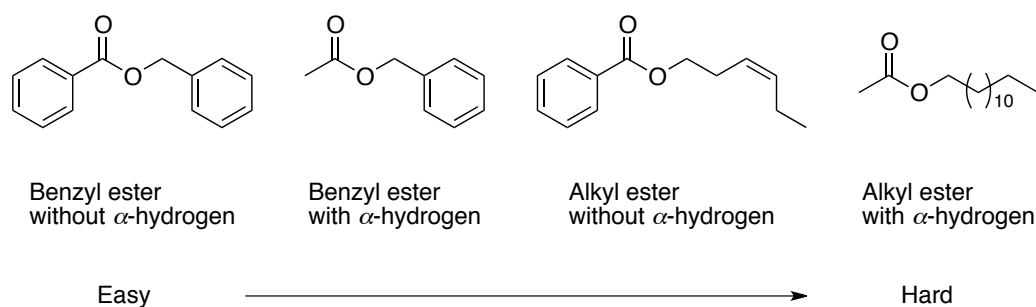


Entry	Ester substrate	Products	Catalyst Loading	Scavenger	Yield (%)
1		 + 	2.0	CaH <sub>2</sub>	100
2		 + 	2.0	CaH <sub>2</sub>	55.2
3		 + Ca(OAc) <sub>2</sub>	2.0	CaH <sub>2</sub>	100
4		 + 	2.0	CaH <sub>2</sub>	100
5		 + 	2.0	NaH	75
6			2.0	NaH	97
7			2.0	CaH <sub>2</sub>	0.8
8		 + 	25	None	52.8 <sup>a</sup>

9			+		5.0	CaH <sub>2</sub>	30.3 <sup>b</sup>
<p>a. GC yield of benzene, when the catalyst load is 25 mol% per nickel cluster.</p> <p>b. Isolated yield of benzoic acid, when the catalyst load is 5 mol% per nickel cluster.</p>							

Among the substrates, benzyl esters without acidic  $\alpha$ -hydrogen atoms are the most reactive in these hydrogenation reactions. This is probably due to the fact that the benzylic C–O bond is weaker than the alkyl C–O bond. Meanwhile, the absence of  $\alpha$ -hydrogens allows the use of strong bases like NaH as both scavenger and promoter. The strong base accelerates the reaction – details will be discussed shortly. Furthermore, benzyl esters bearing acidic  $\alpha$ -hydrogen atoms can also be completely reduced, in the presence of a weaker base scavenger (CaH<sub>2</sub>). However, the rate of this reaction is much slower. For hydrogenation of alkyl esters, the use of stoichiometric NaH is generally required in order to obtain a good yield. However, NaH can only be used as an additive when no acidic  $\alpha$ -hydrogen is present in the alkyl ester substrate. Otherwise, NaH competitively converts the ester to the corresponding enolate and causes undesired Claisen condensation reactions.<sup>46</sup> Being the most challenging substrates evaluated so far, enolizable alkyl esters undergo reductions at the slowest rate and give low yields. Thus, the relative ease of hydrogenation is closely associated with the presence of benzylic C–O bond and absence of  $\alpha$ -hydrogens (Figure 1-8).

**Figure 1-8.** Relative trend in ester reduction

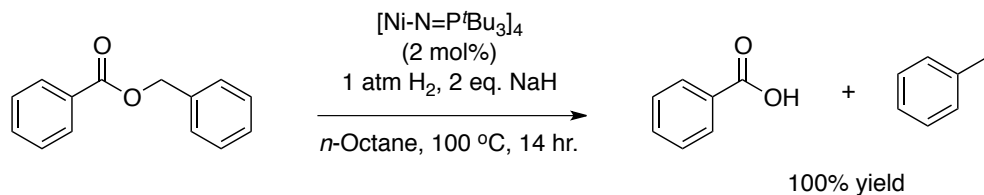


### 1.2.3 Hydrogenolysis of benzyl benzoate

During my exploration of the nickel and cobalt cluster-catalyzed reactions, the reduction of benzyl esters appeared to proceed more readily than the corresponding alkyl esters. Such a reactivity difference is mostly associated with the weakness of the benzyl C–O bond. In this study, the scope of benzyl esters investigated includes benzyl benzoate, benzyl acetate, 3-isochromanone and benzyl tiglate, listed as entries 1 to 4 in Table 1-3, respectively.

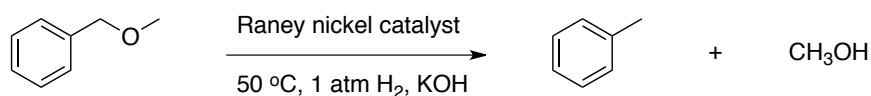
The first substrate to undergo successful reduction was benzyl benzoate (Eq. 1-12). The reason for choosing this substrate was the subsequent simple work-up procedure. Classical ester hydrogenation of benzyl benzoate would result in two equivalents of the benzyl alcohol instead of a mixture of two alcohol species. However, and quite unexpectedly, only toluene and benzoic acid were isolated as products, as identified and confirmed by various analytical methods. Benzoic acid was isolated and its identity determined by  $^1\text{H}$  NMR spectroscopy, while toluene was detected and quantified using GC-MS analysis and observed on the  $^1\text{H}$  NMR spectrum of the crude product mixture.

### Equation 1-12



Before proceeding to a detailed discussion about this reduction, a comparison between the nickel(I) cluster **8** and Raney nickel is warranted. In general, Raney nickel has been regarded as the most activated heterogeneous nickel(0) reagent. Its enhanced reactivity is mostly due to its very high surface area, with excess dihydrogen embedded in the porous structures. Raney nickel is capable of benzylic C–O bond activation of benzyl ethers and has been employed as a reagent for the hydrogenolysis of benzyl ethers to free alcohols (Eq. 1-13).<sup>47</sup> However, despite of its strong reducing ability, Raney nickel has never been reported to activate the  $\text{sp}^3$  C–O bond in benzyl esters. In comparison, phosphoramidate-supported nickel cluster has not only demonstrated benzylic C–O bond activation in ether substrates investigated earlier by Jeff Bunquin, but also in benzylic esters as covered in this chapter.

### Equation 1-13



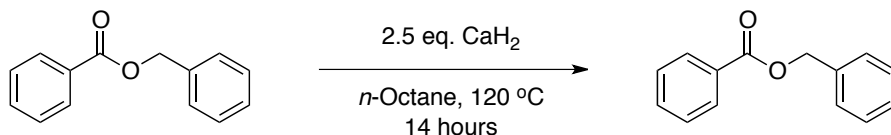
#### 1.2.4 Optimization of benzyl benzoate hydrogenolysis

Benzyl benzoate was used as a model compound in the optimization of conditions for ester hydrogenation reactions. A series of experiments have been conducted to establish the

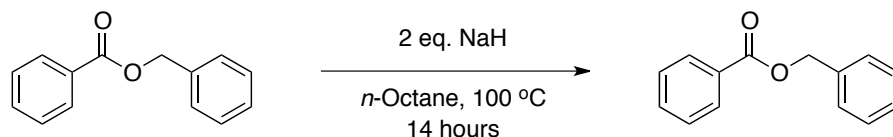
efficiency of the catalysts and determine the effects of the scavenger, solvent, temperature, as well as pressure on the reaction. These experimental results are summarized in Table 1-4. The optimal conditions (entry 13) call for the use of insoluble NaH as a scavenger, *n*-octane as solvent, maintained at 100 °C under 1 atm of hydrogen pressure.

To prove that the catalytic reactivity is due to the nickel or cobalt cluster, background experiments in the absence of any catalyst have been conducted (Table 1-4, entries 1 to 3). The control reactions were performed at high temperature with a suspension of NaH or CaH<sub>2</sub> in *n*-octane containing benzyl benzoate (Eq. 1-14, 15). For the reaction using CaH<sub>2</sub>, benzyl benzoate is the only organic compound detected in GC analysis besides solvent (Eq. 1-16). For reactions using NaH as a scavenger, when the reaction temperature is 100 °C or lower, no reaction occurs. However, when the temperature is raised to 120 °C, a side reaction was detected that goes very slowly. The side product is benzyl alcohol, produced in 3.2% GC yield after 14 h at 120 °C. Insofar as the side reaction produces a totally different product, it would not significantly interfere with the ester reduction. These experiments thus validate the catalytic role played by the nickel or cobalt cluster in ester hydrogenation.

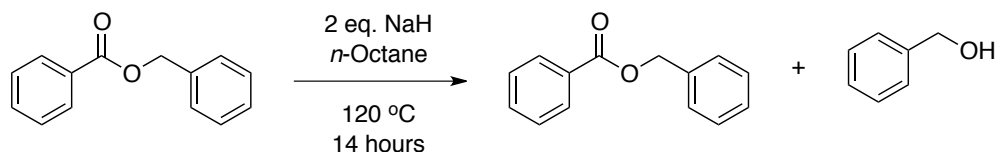
#### Equation 1-14



### Equation 1-15

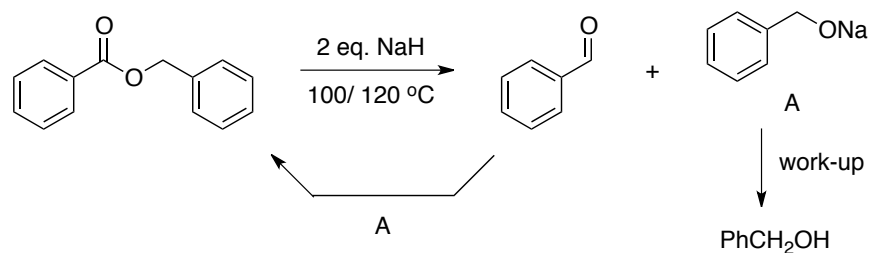


### Equation 1-16

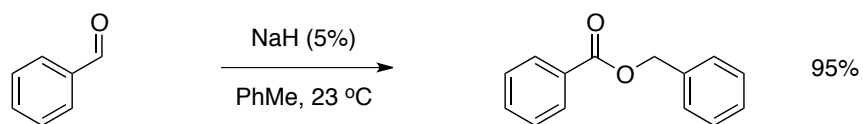


In the control experiment using NaH at 120 °C, the formation of benzyl alcohol presumably involves the nucleophilic addition of NaH to the carbonyl carbon of benzyl benzoate (Scheme 1-5). The resultant benzaldehyde intermediate is then converted to benzyl benzoate by the Tishchenko reaction, which is catalyzed by sodium benzyloxide. After a work-up procedure, benzyl alcohol is detected as the sole product. In the literature, the NaH-catalyzed Tishchenko reaction has been reported (Eq. 1-17).<sup>48</sup> NaH is thus capable of reducing benzaldehyde to sodium benzyloxide, which is proposed to be the actual catalyst for the Tishchenko reaction.

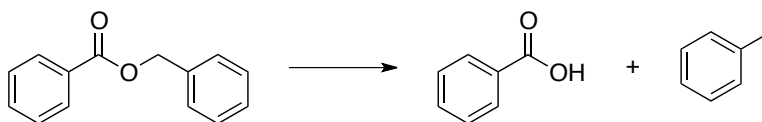
### Scheme 1-5



### Equation 1-17



After the confirmation of the catalytic reactivity of the clusters, a set of comparative experiments was conducted to evaluate the reactivity of nickel and cobalt clusters toward ester hydrogenation and determine the scope of the reaction. Among the four clusters listed in Table 1-4, entries 4 to 7, the phosphoramidate-supported nickel(I) cluster **8** appears to be most promising catalyst to afford quantitative conversions. In comparison, the phosphoramidate-supported cobalt(I) cluster is much less reactive under the same conditions, while the tetramethylated cobalt(II) cluster and its oxidized mixed valent cobalt cluster<sup>49</sup> appear to be completely inactive. For reactions with both nickel(I) and cobalt(I) cluster, the same products are obtained, toluene and benzoic acid. As discussed below, [Ni-N=P<sup>t</sup>Bu<sub>3</sub>]<sub>4</sub> can be generally applied for to the hydrogenolysis of other substrates.

**Table 1-4.** Benzyl benzoate reduction optimization

Entry	Catalyst	Catalyst (mol%)	Solvent	Scavenger	Temp (°C)	Time (hr)	Yield (%)
1	-	-	<i>n</i> -octane	NaH	100	14	0
2	-	-	<i>n</i> -octane	NaH	120	14	0 <sup>a</sup>
3	-	-	<i>n</i> -octane	CaH <sub>2</sub>	120	14	0
4	[Ni-N=P <sup>t</sup> Bu <sub>3</sub> ] <sub>4</sub>	2	<i>n</i> -octane	CaH <sub>2</sub>	120	14	100
5	[Co-N=P <sup>t</sup> Bu <sub>3</sub> ] <sub>4</sub>	2	<i>n</i> -octane	CaH <sub>2</sub>	120	14	2.4
6	[Me-Co-N=PEt <sub>3</sub> ] <sub>4</sub>	2	<i>n</i> -octane	CaH <sub>2</sub>	120	14	0
7	[Me-Co-N=PEt <sub>3</sub> ] <sub>4</sub> [BF <sub>4</sub> ]	2	<i>n</i> -octane	CaH <sub>2</sub>	120	14	0
8	[Ni-N=P <sup>t</sup> Bu <sub>3</sub> ] <sub>4</sub>	2	THF	CaH <sub>2</sub>	120	14	85.8
9	[Ni-N=P <sup>t</sup> Bu <sub>3</sub> ] <sub>4</sub>	2	benzene	CaH <sub>2</sub>	120	14	55.7
10	[Ni-N=P <sup>t</sup> Bu <sub>3</sub> ] <sub>4</sub>	2	<i>n</i> -octane	-	120	14	7.0
11	[Ni-N=P <sup>t</sup> Bu <sub>3</sub> ] <sub>4</sub>	1	<i>n</i> -octane	CaH <sub>2</sub>	120	14	59.3
12	[Ni-N=P <sup>t</sup> Bu <sub>3</sub> ] <sub>4</sub>	1	<i>n</i> -octane	CaH <sub>2</sub>	120	28	100
13	[Ni-N=P <sup>t</sup> Bu <sub>3</sub> ] <sub>4</sub>	1	<i>n</i> -octane	NaH	100	14	100 <sup>b</sup>
14	[Ni-N=P <sup>t</sup> Bu <sub>3</sub> ] <sub>4</sub>	1	<i>n</i> -octane	MgH <sub>2</sub>	100	14	20.2
15	[Ni-N=P <sup>t</sup> Bu <sub>3</sub> ] <sub>4</sub>	2	<i>n</i> -octane	K <sub>2</sub> CO <sub>3</sub>	120	14	9.0
16	[Ni-N=P <sup>t</sup> Bu <sub>3</sub> ] <sub>4</sub>	2	<i>n</i> -octane	proton sponge	120	14	8.2
17	[Ni-N=P <sup>t</sup> Bu <sub>3</sub> ] <sub>4</sub>	2	<i>n</i> -octane	zinc	120	14	9.4
18	[Ni-N=P <sup>t</sup> Bu <sub>3</sub> ] <sub>4</sub>	2	<i>n</i> -octane	CaH <sub>2</sub>	100	14	74.9
19	[Ni-N=P <sup>t</sup> Bu <sub>3</sub> ] <sub>4</sub>	2	<i>n</i> -octane	CaH <sub>2</sub>	80	14	21.0
20	[Ni-N=P <sup>t</sup> Bu <sub>3</sub> ] <sub>4</sub>	2	<i>n</i> -octane	CaH <sub>2</sub>	60	14	8.0

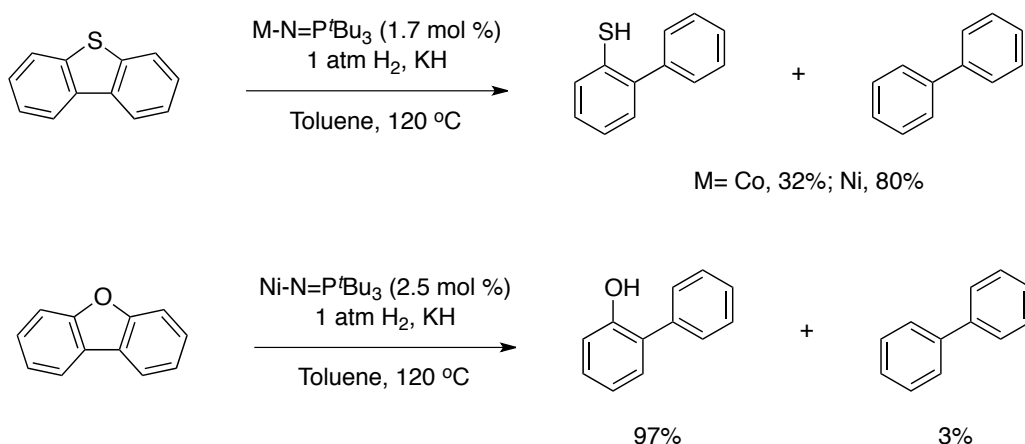
a. PhCH<sub>2</sub>OH is formed with 3.2% GC yield

b. PhH is formed as the product

The solvent system for ester reduction is carefully chosen. Appropriate solvents have to be inert to both catalysts and scavengers. Because the electron-rich nickel(I) and cobalt(I) clusters are likely to activate carbon-halogen bonds, halogenated organic solvents are excluded. In addition, the basicity of both the phosphoranimide ligand and the scavenger also limits the use of protic solvents, such as alcohols and ketones. Several possible solvents have been screened, as represented in entries 4, 8, and 9 of Table 1-4. Tetrahydrofuran, benzene and *n*-octane are all reasonable solvents that afford good to excellent yields. The best solvent is *n*-octane as the corresponding reaction affords quantitative reduction of ester compound and simplified product isolation. Meanwhile, *n*-octane has low toxicity and a high boiling point that would allow heating reactions to high temperatures without generating excessive pressure.

Compared to solvent effects, the choice of basic scavenger is more crucial for the ester reduction reaction. In previous hydrodesulfurization and hydrodeoxygenation reactions, potassium hydride or another strong base is required to neutralize the thiols and alcohols generated in the reactions (Eq. 1-18). Accordingly, in the ester hydrogenation reaction, the formation of acidic product(s) is also expected. Therefore, we concluded that a base would be indispensable before we conducted any additional ester hydrogenation reactions.

### Equation 1-18



A control experiment, as shown in entry 10 of Table 1-4, was conducted to determine experimentally if a base was indeed necessary. The reaction in the absence of base gives small amount of toluene and benzoic acid as final products, before the reaction stops. The results suggest that nickel(I) cluster **8** is capable of reducing the benzyl benzoate by itself at the beginning of the reaction. However the reaction quickly shuts down after the catalysts are deactivated. Therefore addition of base as a scavenger is essential for the ester hydrogenation reaction.

Scavengers that have been tested are listed in entries 4 and 12-16, and consist of sodium hydride, calcium hydride, magnesium hydride, potassium carbonate, 1,8-bis(dimethylamino)naphthalene (also known as proton sponge), and zinc. Generally the reactions were conducted with 2 mol% of nickel(I) tetramer **8** as a catalyst. The results suggest that both NaH and  $CaH_2$  are efficient scavengers, as all corresponding reactions go to completion within 14 h.

To compare the reactivity between calcium hydride and sodium hydride, reactions with lower loading of the nickel cluster have been conducted (entries 11 and 13, Table 1-4). When the nickel cluster loading is lowered to 1 mol%, the reaction with 2 equivalents of NaH goes to completion at 100 °C. On the other hand, the reaction with 2.5 equivalents of CaH<sub>2</sub> at 120 °C affords a 59.3% GC yield of toluene. These results imply that NaH is more efficient than CaH<sub>2</sub> as a scavenger and directly accelerates the reaction rate.

The remaining scavengers are not effective and the corresponding reactions only afford a low, presumably stoichiometric, yield. Magnesium hydride was tested as a hydride reagent because the magnesium cation could in principle function as a Lewis acid, potentially activating the ester functional group. Potassium carbonate and proton sponge were tested as examples of weak bases with minimal direct interaction with esters. The latter is also soluble in the reaction medium. Zinc of course, is not a base, so it is distinct from other scavengers. Zinc is not expected to react with esters bearing  $\alpha$ -hydrogens; however as a scavenger for carboxylic acid, zinc is not efficient enough to replace NaH/CaH<sub>2</sub>. Generally speaking, for these scavengers, it is possible that the capture of carboxylic acid occurs less readily, if it occurs at all, and results in rapid deactivation of catalyst. Therefore, the corresponding ester hydrogenation reactions afford low, if any, conversions.

In summary, scavengers are essential for these catalytic ester hydrogenation reactions and have a critical impact on the reaction rate. Based on the experimental results, NaH and CaH<sub>2</sub> are efficient scavengers for ester hydrogenation reactions without inducing significant diversion of the esters. A strong base is necessary, but the base can be insoluble in the reaction medium.

### 1.2.5 Cation effects in scavenger bases

Although NaH and CaH<sub>2</sub> are both metal hydride reagents, the difference between them is significant (entries 11 and 13, Table 1-4). Similar phenomenon is also observed in hydrodesulphurization reactions employing the same catalysts, in which KH is much more effective than NaH as a scavenger. Both NaH and CaH<sub>2</sub> are regarded as strong bases, though with different basicities, kinetic and thermodynamic. The varied effectiveness from one to the other may come from the difference in basicities or a more specific cationic effect of the metal.<sup>50</sup>

The effect of potassium and sodium cations was subsequently studied. To evaluate the effect of Na<sup>+</sup>/K<sup>+</sup> cation, parallel reactions were conducted for comparison, listed as entries 1 and 2, and then 3 and 4 in Table 1-5. In each set of the parallel reactions, NaBF<sub>4</sub> or KPF<sub>6</sub> was added to only one of the reactions and the rest of the experimental parameters including concentration, stirring rate, temperature, etc, were carefully controlled to be as similar as possible. Since the reduction of *cis*-3-hexenyl benzoate with CaH<sub>2</sub> as a scavenger affords slow conversion, this reaction was selected as a model (Eq. 1-19). If the cationic effect is significant, the conversion is expected to increase appreciably upon addition of the potassium salt. Based on GC analysis of the organic fraction and the amount of benzoic acid isolated, the presence or absence of potassium and sodium cations has little or no effect on the reaction (Table 1-5). Therefore, basicity is more likely to be the reason behind the variation in the scavenger effectiveness.

#### Equation 1-19

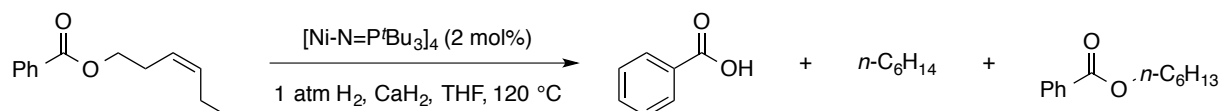


**Table 1-5.** Results of parallel reactions using CaH<sub>2</sub> for the cationic effect study

Entry	Additive	PhCO <sub>2</sub> <i>n</i> -C <sub>6</sub> H <sub>11</sub> GC Yield (%)	GC Yield of <i>n</i> -hexane (%)	PhCO <sub>2</sub> H GC/Isolated Yield (%)
1	NaBF <sub>4</sub>	95.1	0.8	4.1 <sup>1</sup>
2	-	93.4	1.1	5.5 <sup>1</sup>
3	KPF <sub>6</sub>	98.7	1.3	17.4 <sup>2</sup>
4	-	98.6	1.4	13.6 <sup>2</sup>

1. GC yield of benzoic acid
2. Isolated yield of benzoic acid

The effect of temperature on the ester reduction has also been evaluated. A series of experiments at various temperatures were conducted, as listed in entries 4, 18-20 in Table 1-4. Benzyl benzoate hydrogenation reactions were performed at 20 °C intervals from 60 °C to 120 °C. The results indicate that as the temperature decreases, the conversion drops significantly. The reaction at 60 °C affords only 8.0% GC yield of toluene. For the reaction at 80 °C, the toluene GC yield increased to 21%. The reactions at 100 and 120 °C both produce toluene and benzoic acid in much higher yields. Therefore, the ester hydrogenation reaction is typically conducted at or above 100 °C.

An investigation into the influence of hydrogen pressure has also been carried out. Two parallel reactions were conducted at different H<sub>2</sub> pressures, while all other reaction conditions were kept the same (Eq. 1-20). The reaction at 300 psi H<sub>2</sub> pressure affords *a much lower yield of toluene* than the analogous reaction performed at 14.7 psi (1 atm) of H<sub>2</sub>

(Table 1-6). This result establishes that the increased hydrogen pressure strongly inhibits the ester hydrogenation reaction, presumably by forcing the equilibrium toward the formation of saturated nickel hydride species. Correspondingly, unsaturated nickel hydride species might be capable of activating esters, whereas saturated ones remain inert.

### Equation 1-20

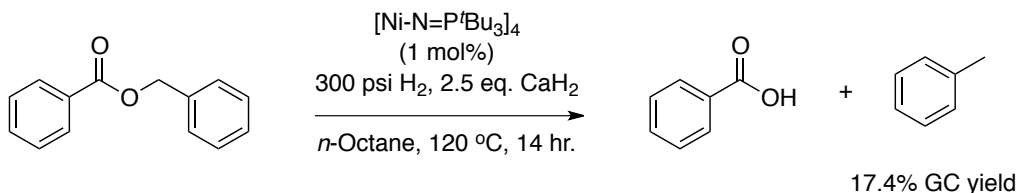
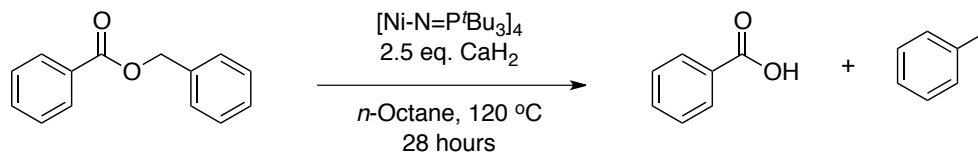


**Table 1-6.** Effect of the hydrogen pressure on ester hydrogenation reactions

Entry	Catalyst	Catalyst load (mol%)	H <sub>2</sub> pressure	Toluene GC yield (%)
1	[Ni-N=P <sup>t</sup> Bu <sub>3</sub> ] <sub>4</sub>	1.0	1 atm= 14.7 psi	59.3
2	[Ni-N=P <sup>t</sup> Bu <sub>3</sub> ] <sub>4</sub>	1.0	300 psi	17.4

To identify if the nickel cluster is deactivated upon heating for 14 h, a hydrogenolysis experiment with a much longer reaction time was conducted. When the catalyst loading is 1 mol%, the GC-MS yield of toluene is 59.3% after 14 h (Entry 1, Table 1-6). This reaction is repeated under the exact same conditions and left for 28 h (Eq. 1-21). From GC-MS analysis, toluene is the only compound left in the organic fraction together with *n*-octane solvent. This result proves that the catalyst remain active after 14 h of reaction time and is capable of driving the reaction to completion given longer reaction time.

### Equation 1-21



The reaction in Entry 1, Table 1-6 was used for the calculation of turn over number (TON) and turn over frequency (TOF) for the nickel cluster. In the experimental section of ester hydrogenolysis, detailed experiments are provided to establish a relationship between GC and actual yield of toluene. The GC yield of toluene (59.3%) converted to the actual yield is 85.9%, giving a TON of 85.9. Meanwhile, the reaction time is 14 h, giving a TOF of  $6.13\text{ h}^{-1}$ . These data are calculated based on a reaction using  $\text{CaH}_2$ . For reaction using  $\text{NaH}$  as a scavenger, the reaction is quantitative with 1 mol% catalyst after 14 h. The corresponding TON is at least 100 and TOF is  $7.14\text{ h}^{-1}$  at a minimum.

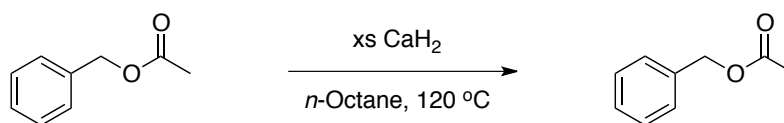
Thus, a range of reaction parameters has been examined, including catalyst, solvent, scavenger, temperature, and hydrogen pressure. The phosphoramidate-supported nickel cluster,  $[\text{Ni-N=P}^t\text{Bu}_3]_4$ , is, at this point, the most powerful catalyst identified for benzyl ester hydrogenolysis. In order to reduce esters efficiently, however,  $\text{NaH}$  or  $\text{CaH}_2$  is required as a scavenger. The reaction proceeds efficiently above  $100\text{ }^\circ\text{C}$  and hydrogen pressure should remain at 1 atm.

#### 1.2.6 Substrate Scope. Hydrogenation of other benzyl esters

The detailed study of the effect of various parameters in benzyl benzoate reduction provides a solid foundation for further substrate scope exploration. Benzyl acetate is a more challenging substrate than benzyl benzoate due to the presence of acidic  $\alpha$ -protons.

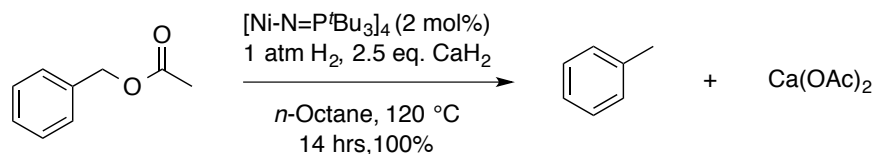
The most efficient scavenger, NaH, deprotonates benzyl acetate readily, therefore a weaker base is required to allow the reduction to occur without inducing side reactions. To test if CaH<sub>2</sub> causes side reactions, a background experiment was performed in the absence of the nickel cluster (Eq. 1-22). The *n*-octane solution containing benzyl acetate and calcium hydride was heated to 120 °C. Based the GC-MS analysis, this control reaction failed to produce any new compound(s) making CaH<sub>2</sub> an appropriate scavenger for the hydrogenation reaction of benzyl acetate.

### Equation 1-22



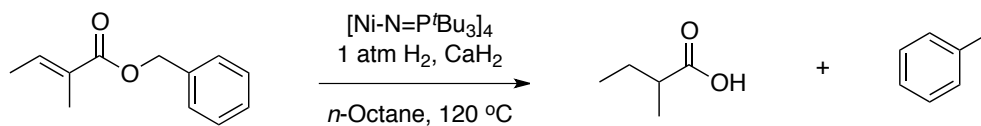
The reduction of benzyl acetate was carried out by using 2 mol% of nickel(I) cluster **8** with the addition of excess CaH<sub>2</sub> (Eq. 1-23). The reaction proceeds smoothly, with the formation of white precipitate. GC-MS analysis of the organic fraction confirms the formation of toluene as the only product in the organic phase and a complete consumption of benzyl acetate. The white solid was dissolved in D<sub>2</sub>O to obtain a <sup>1</sup>H NMR spectrum. The broad singlet peak at 1.89 ppm can be readily assigned to the methyl group of calcium acetate. The reduction of benzyl acetate is thus successful and again demonstrates the selectivity for benzyl C–O activation.

### Equation 1-23



Benzyl tiglate is a benzyl ester that contains an olefin moiety. This substrate was subjected to ester hydrogenation reaction to determine if the benzyl C–O activation is preferred over olefin hydrogenation. Since  $\text{CaH}_2$  is a decent scavenger for benzyl acetate, it was used again in the benzyl tiglate reduction (Eq. 1-24). Even if hydrogenation of double bond happens fastest, it is unlikely that  $\text{CaH}_2$  will induce undesired reactions of the intermediate ester. The hydrogenation of benzyl tiglate under standard conditions affords toluene and 2-methylbutanoic acid quantitatively, as concluded by GC-MS analysis and  $^1\text{H}$  NMR spectroscopy. The result indicates that the hydrogenation of both the olefin moiety and benzyl C–O bond are complete within 14 h of reaction time.

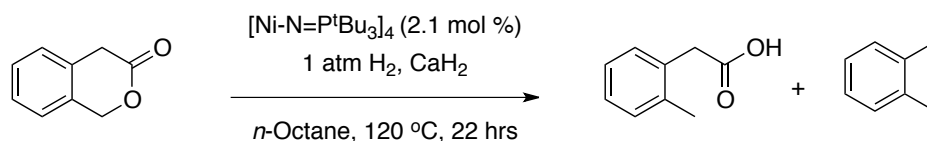
### Equation 1-24



3-isochromanone is a substrate similar to benzyl acetate, as both are enolizable benzyl esters. Since 3-isochromanone is a lactone, if successful the reaction would generate a single product and both product isolation and characterization would be more convenient. Due to the fact that 3-isochromanone is not very soluble in *n*-octane solution, THF was used as the solvent (Eq. 1-25). This reaction proceeds more slowly than benzyl benzoate

reduction, as the conversion to *o*-tolylacetic acid is 55.2% after 14 h. The known product, *o*-tolylacetic acid was obtained as a white solid and confirmed by <sup>1</sup>H NMR spectroscopy.<sup>51</sup> GC-MS analysis of the organic fraction also identifies *o*-xylene as a minor product.

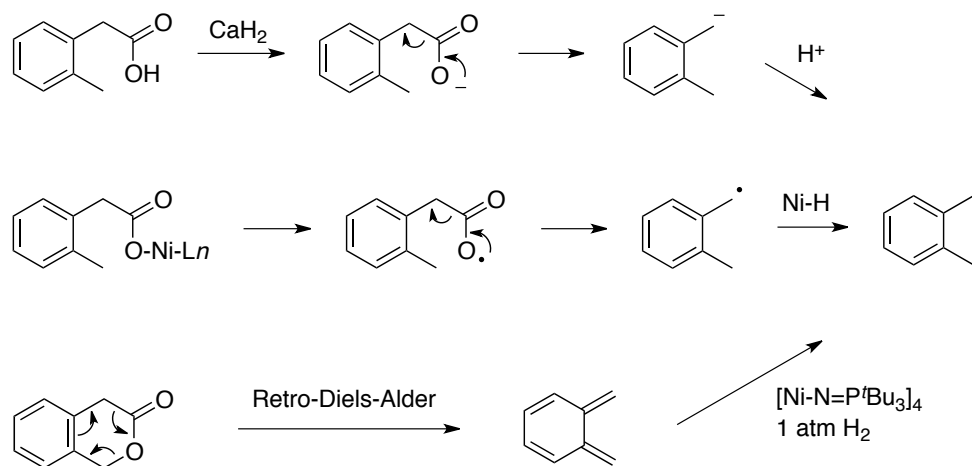
### Equation 1-25



The slower reaction rate of 3-isochromanone hydrogenolysis is attributed to the relatively higher energy of this conformationally constrained lactone. More specifically, benzyl benzoate can rotate freely to adopt the thermodynamically more stable *s*-trans conformation. This conformation is stabilized by two hyperconjugative effects: one of the oxygen lone pairs overlaps with the  $\pi^*$ -carbonyl orbital, while the other aligns nicely with  $\sigma^*$ -carbonyl orbital.<sup>52</sup> In contrast, 3-isochromanone is locked in an *s*-cis conformation and moreover, it is also destabilized by dipole-dipole interactions.<sup>53</sup> As a consequence, for 3-isochromanone, equilibrium may shift toward the formation of 3-isochromanone enolate, resulting in a decrease in the reduction rate.

In the above reaction, the *o*-xylene can be derived from a decarboxylation pathway arising from either the corresponding carboxylic acid or the nickel carboxylate intermediate, and could involve an anionic or radical pathway. Alternatively, the production of *o*-xylene might be expected from 3-isochromanone via retro-Diels-Alder reaction, followed by hydrogenation (Scheme 1-6). However, the reported retro-Diels-Alder reaction of 3-isochromanone is conducted by pyrolysis at 565 °C,<sup>54</sup> a considerably higher temperature than required for ester hydrogenation.

### Scheme 1-6



In summary, a range of benzyl esters, with and without acidic  $\alpha$ -protons can be reduced using nickel(I) cluster as the catalyst under mild conditions, including benzyl benzoate, benzyl acetate, benzyl tiglate and 3-isochromanone. The nickel-catalyzed hydrogenolysis of benzyl esters is now well established and reasonably general in scope.

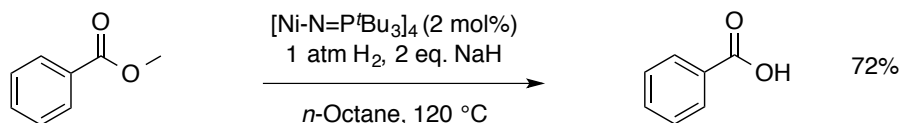
#### 1.2.7 Alkyl ester hydrogenation

In comparison to benzyl esters, the reduction of alkyl esters is more difficult, due to the stronger alkyl C–O bond. Alkyl esters can be further divided into two categories depending on the presence or absence of acidic  $\alpha$ -hydrogens. Alkyl esters without  $\alpha$ -hydrogens are relatively easier to reduce, while enolizable alkyl esters remain challenging based on our current understanding. The scavenger is crucial in alkyl ester reduction reactions. Reactions using NaH as a scavenger gave significantly improved yields, compared to

analogous reactions employing  $\text{CaH}_2$  as a scavenger. The alkyl esters that can be reduced in good yield include methyl benzoate, *cis*-3-hexenyl benzoate and 3,4-dihydroisocoumarin, as detailed below.

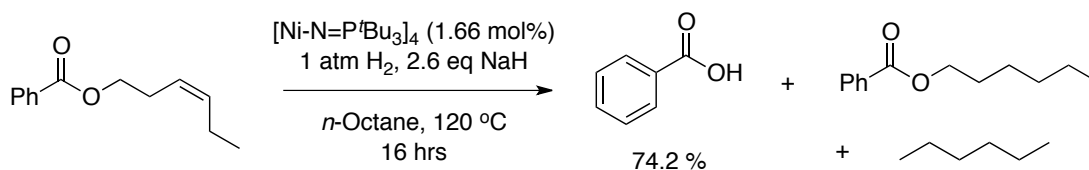
Methyl benzoate undergoes reduction reasonably well (Eq. 1-26). In order to maintain a high conversion, NaH is again required as a scavenger. The reaction produces a considerable amount of white precipitate, which can be isolated and assayed as benzoic acid (72%) by  $^1\text{H}$  NMR spectroscopy. For methyl benzoate, the hydrolysis of the  $\text{sp}^3$  C–O bond generates methane as the alkane component. Due to its gaseous nature and the apparatus used for the reaction, the gas was not detected. Therefore, in order to confirm the formation of alkanes, other alkyl esters were also used as substrates.

#### Equation 1-26



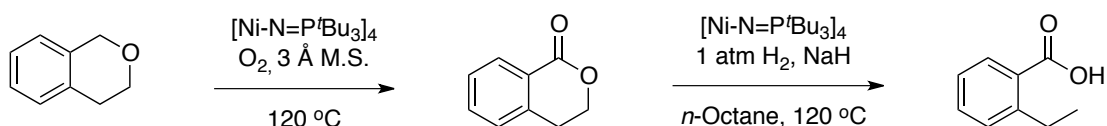
*Cis*-3-hexenyl benzoate can also be reduced in a good yield using NaH as a scavenger (Eq. 1-27). The reaction involves initial olefin hydrogenation followed by selective activation of the alkyl C–O bond to produce benzoic acid and hexane. Benzoic acid was isolated and characterized by  $^1\text{H}$  NMR spectroscopy. Hexane was observed by GC-MS analysis. Some hexyl benzoate was also recovered from alkene hydrogenation without ester cleavage.

### Equation 1-27



3,4-Dihydroisocoumarin is another lactone, therefore only a single product is expected from hydrogenation. The reaction affords *o*-ethylbenzoic acid in 97% isolated yield (Eq. 1-28). The isolation and characterization of this product provides substantial evidence for the formation of both carboxylic acid and alkane components in acyclic hydrogenolysis. Furthermore, the yield of the product can be readily determined, whereas the volatile alkane products are more difficult to quantify. As 3,4-dihydroisocoumarin is not commercially available, it was synthesized by a novel catalytic aerobic oxidation of isochroman (Eq. 1-28). Surprisingly, this oxidation reaction is catalyzed by the same nickel precatalyst cluster that mediates reduction. Details of our investigation of aerobic oxidation reactions are presented in Chapter 2.

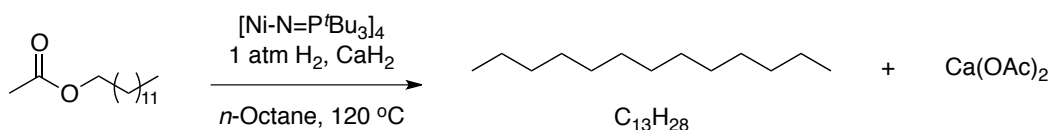
### Equation 1-28



Several simple alkyl esters have also been examined in hydrogenation reactions, but the conversions to cleavage products are still not satisfactory. In particular, alkyl esters bearing acidic  $\alpha$ -hydrogens remain as challenging substrates. The difficulty is primarily associated with the lack of suitable scavengers, as NaH competitively deprotonates the esters and

CaH<sub>2</sub> is too inefficient to be practical. In one example, the hydrogenation of tridecyl acetate was performed with CaH<sub>2</sub> as a scavenger. Tridecane was observed in GC-MS analysis, but merely in 0.8% yield (Eq. 1-29).

### Equation 1-29



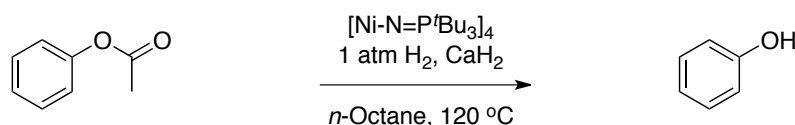
#### 1.2.8 The hydrogenation of aryl esters

Aryl esters do not contain an sp<sup>3</sup> C–O bond in the ester functional group, representing the final type of ester substrate studied in this investigation. Since the aryl and acyl C–O bonds are both sp<sup>2</sup> hybridized and are correspondingly strong bonds, the activation of aryl esters is expected to be more difficult. Moreover, selective activation only of one of the two sp<sup>2</sup> C–O bonds represents another challenge for aryl esters. For this study, we selected phenyl acetate and phenyl benzoate as simple model substrates.

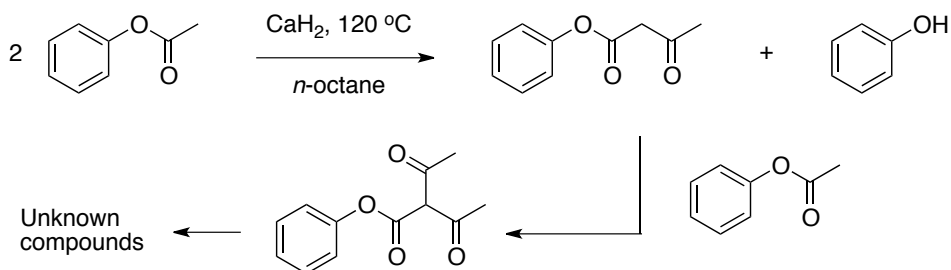
The hydrogenation of phenyl acetate in the presence of CaH<sub>2</sub> at 120 °C affords phenol as the only observable product (Eq. 1-30). Phenol appears to be the hydrogenation product from acyl C–O bond activation, but it is not: a control experiment conducted in the absence of catalyst establishes that phenol comes from side reactions mediated by CaH<sub>2</sub>, the major of which appears to be Claisen condensation (Scheme 1-7). Phenyl acetoacetate is not observed in the GC-MS analysis. However, it is possible that phenyl acetoacetate undergoes further condensations with phenyl acetates to form more complicated byproducts. In

comparison, the same side reactions are not observed in a control experiment using benzyl acetate, probably because benzyl alcohol is not as a good leaving group as phenol. Alternatively, phenyl acetate decomposition to phenol and ketene cannot be excluded as a plausible, possibly catalyzed, pathway. Such decomposition is common in industrial process using solid Brønsted acids as catalyst.<sup>55</sup>

### Equation 1-30



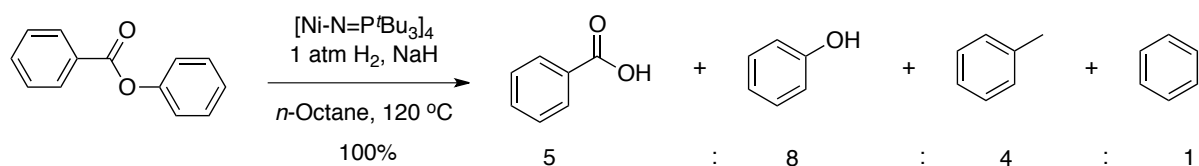
### Scheme 1-7



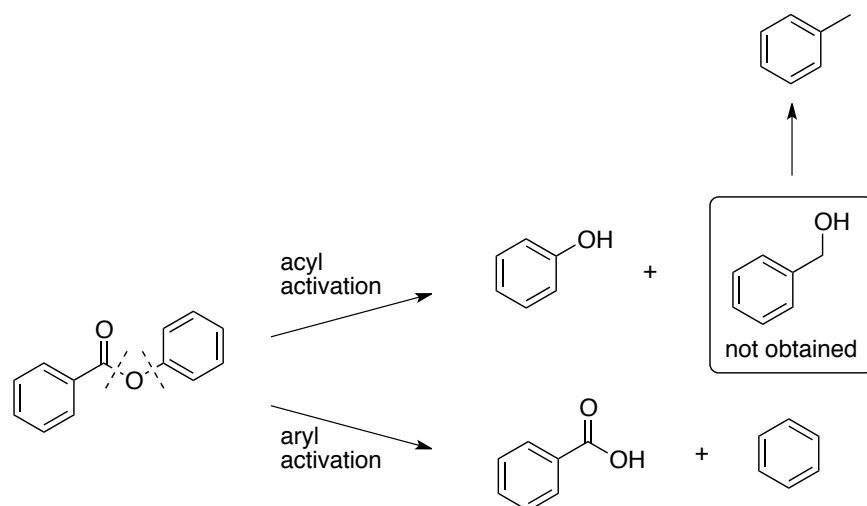
Phenyl benzoate was selected as a second aryl ester substrate, as it does not bear acidic  $\alpha$ -hydrogens. Although aldol-type side reactions are no longer possible, the hydrogenation reaction using NaH as a scavenger at 120 °C gives a complicated product mixture, which includes benzene, toluene, benzoic acid and phenol (Eq. 1-31). In the GC-MS analysis, benzene and toluene are observed in a ratio of 1.0 : 5.3, respectively. The  $^1\text{H}$  NMR spectrum of the precipitated solids reveals that both benzoic acid and phenol are present, with an integration ratio of 1.0 : 1.6. In theory, these compounds can be generated from two

distinct pathways, involving acyl and aryl C–O bond activation, respectively. Phenol and toluene, the deoxygenation product of benzyl alcohol, are anticipated to form through acyl C–O bond activation, while benzene and benzoic acid are formed via the aryl C–O bond activation pathway (Scheme 1-8).

### Equation 1-31



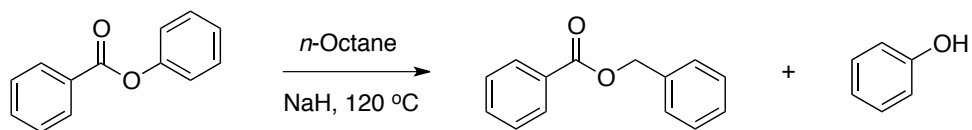
### Scheme 1-8



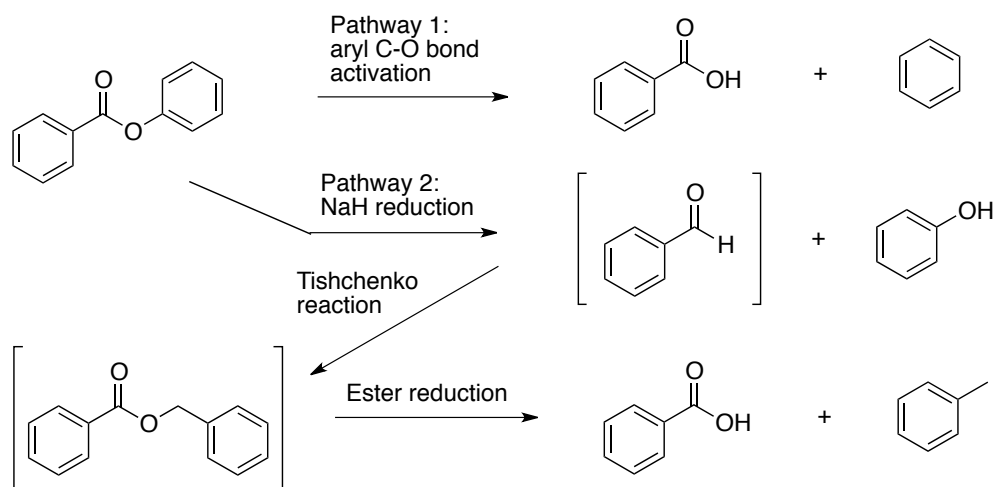
A control experiment with NaH alone was conducted to reveal background reactions (Eq. 1-32). Indeed, phenyl benzoate is converted to benzyl benzoate and phenol at 120 °C, similar to the reaction observed between NaH and benzyl benzoate. The reaction probably

involves a nucleophilic attack of NaH to the acyl carbon to form sodium phenoxide and benzaldehyde (Scheme 1-9). Tishchenko dimerization of benzaldehyde to form benzyl benzoate is then catalyzed by sodium phenoxide. This control experiment reveals that in the phenyl benzoate hydrogenation, the toluene is produced from the catalyzed reduction of benzyl benzoate, while the phenol is produced from the undesired reaction between NaH and phenol benzoate. Thus, phenyl benzoate reduction involves an aryl C–O bond activation to produce benzoic acid and benzene. Meanwhile, undesired side reactions, including NaH-induced reduction, benzyl benzoate formation, and subsequent catalytic ester reduction afford phenol, benzoic acid and toluene byproducts.

### Equation 1-32

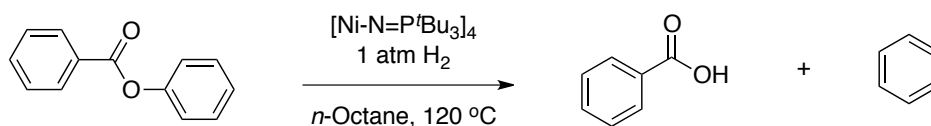


### Scheme 1-9



The NaH-induced side reactions complicate the phenyl benzoate reduction. To observe the inherent selectivity of the nickel cluster in aryl ester reduction, a reaction without the addition of base was carried out (Eq. 1-33). The reaction was conducted with 25 mol% of the nickel cluster while heating to 120 °C under 1 atm of H<sub>2</sub>. There is indeed a stoichiometric reaction between the ester substrate and the nickel center(s). The GC-MS analysis revealed that benzene was obtained in 52.8% conversion as the only product, along with recovered starting material. The benzoic acid produced has also been isolated and identified. The products are formed from a highly selective activation of aryl C<sub>sp2</sub>-O bond in the presence of the acyl C-O bond. According to Gary, in the phenyl benzoate molecule, the bond dissociation energies for aryl and acyl C-O bonds are about 94±5 and 64±5 kcal mol<sup>-1</sup>, respectively.<sup>56</sup> Therefore, the nickel cluster selectively activates the very much stronger aryl C-O bond.

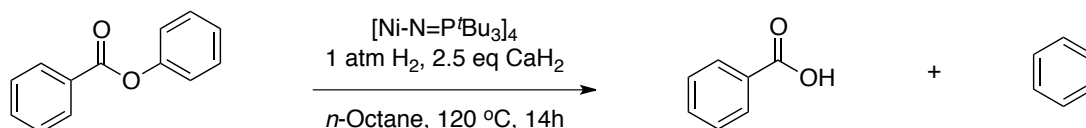
### Equation 1-33



To conduct the phenyl benzoate hydrogenation reaction catalytically while minimizing the scavenger induced side reactions, CaH<sub>2</sub> was then added as a scavenger. The catalyst loading was decreased to 5 mol% with respect to the nickel cluster, while other reaction conditions remained the same (Eq. 1-34). After the reaction, the organic fraction, analyzed by GC-MS, identified benzene as the single volatile product in a GC yield of 32.8%, which corresponds to 70.0% actual yield. Benzoic acid was also isolated as the salt and determined by <sup>1</sup>H NMR

spectroscopy. This result indicates that this reaction can be performed cleanly and catalytically by using  $\text{CaH}_2$  as a proton scavenger, but the TON is only 14 per nickel cluster over a period of 14 hrs.

### Equation 1-34



In summary, the hydrogenolysis of aryl esters can be conducted catalytically. The strong aryl C–O bond is activated selectively in the presence of the weaker acyl C–O bond. However, the reaction is largely limited to esters without acidic  $\alpha$ -hydrogens, given that enolizable aryl esters may give aldol background reactions.

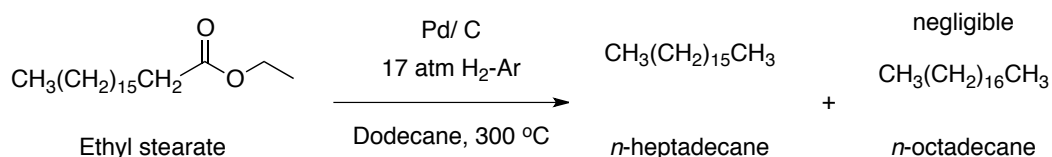
#### 1.2.9 Discussion on the selectivity and mechanism of reduction reaction

To this point, ester hydrogenation reactions have been applied to the reduction of benzyl, alkyl and aryl esters. The reactions demonstrate high selectivity towards alkyl or aryl C–O bond activation while acyl C–O bond activation is not observed. Such selectivity is not commonly encountered in ester reduction reactions, but a few examples have been reported in the literature, including ester hydrogenation with a Pd/C catalyst and stoichiometric ester reduction using organotin hydride as the reductant.

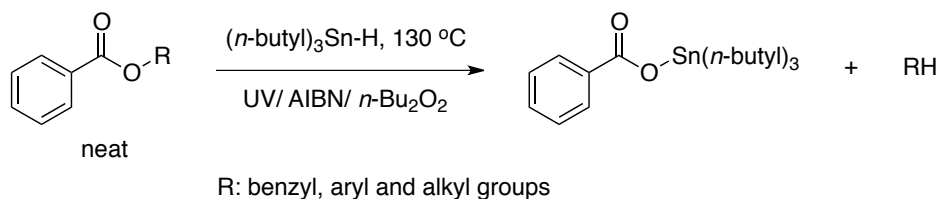
As discussed in the introduction, Pd/C is capable of selective alkyl C–O bond activation. The overall reaction also involves a decarboxylation step, releasing carbon dioxide (Eq. 1-35).<sup>45</sup> The ester reduction with tri-*n*-butyltin hydride is completely different, a hydrostannolysis

reaction forming the tin carboxylate compound and the corresponding hydrocarbon (Eq. 1-36).<sup>57</sup> This is a radical chain reaction, which requires irradiation or the addition of a radical initiator, such as AIBN or *n*-Bu<sub>2</sub>O<sub>2</sub>. The substrate scope for this reaction is rather broad and various alkyl and benzyl benzoates can be reduced, including steric bulky *t*-butyl benzoate.

### Equation 1-35



### Equation 1-36



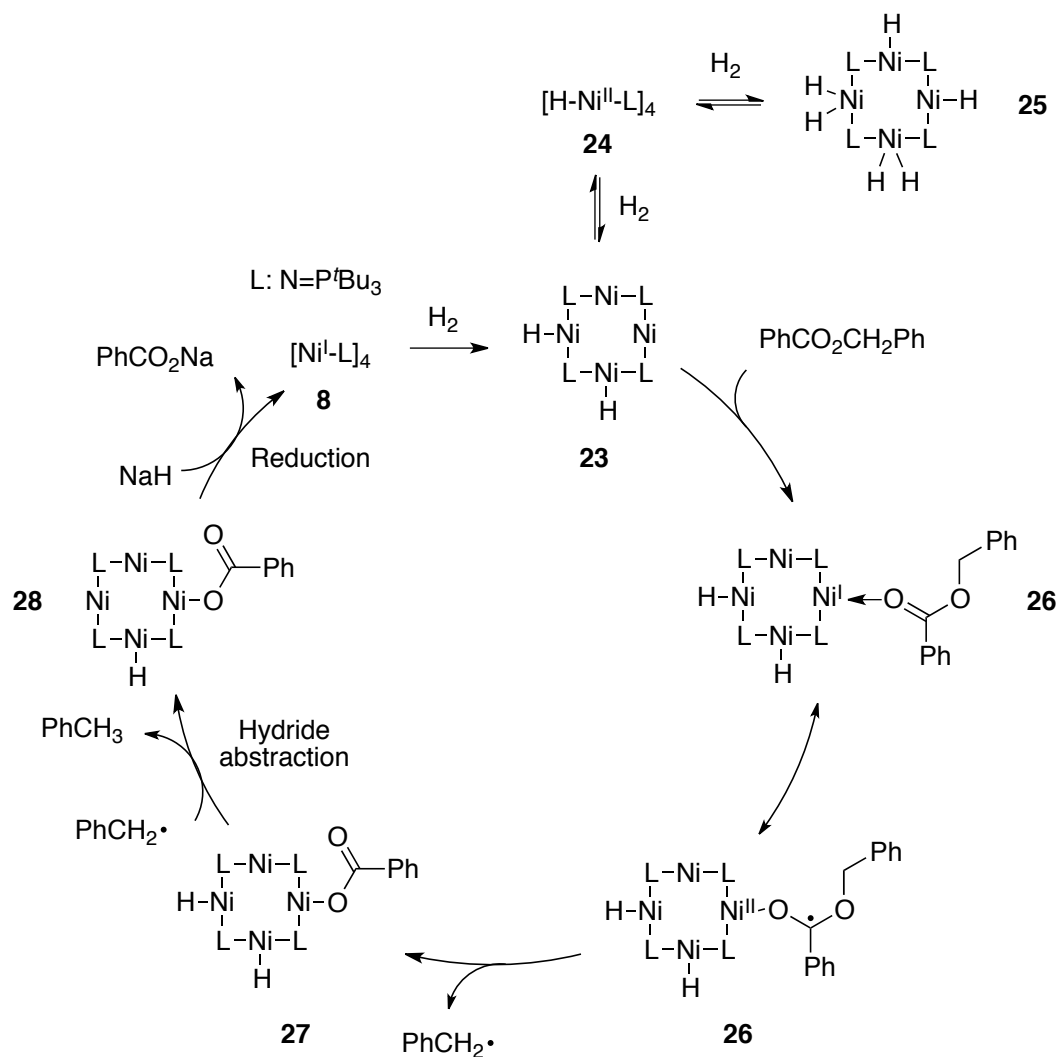
Compared to the activation of an alkyl C–O bond, acyl C–O bond activation is nearly more universal in the ester reduction literature. Important examples for this type of reactions include reductions using reactive metal hydrides (DIBAL-H, LiAlH<sub>4</sub>) and ruthenium/osmium-catalyzed ester hydrogenation reactions.<sup>21,25</sup> In the industrial process for fatty alcohol production, the acyl C–O bond in raw ester feed can also undergo cleavage. All of these reactions share the common feature of acyl C–O bond activation. For the ester hydrotreatment reactions under harsh industrial conditions, acyl and alkyl C–O bonds are both activated, and detailed mechanistic information remains unclear. In general, the majority of ester reduction reactions involve acyl C–O bond activation and many of them utilize a stoichiometric nucleophilic reagent or Lewis acidic reductant.

The nickel and cobalt cluster-catalyzed ester hydrogenation reactions reported herein are thus unprecedented. The reaction appears to be mechanistically distinct from all other reported ester hydrogenation reactions. The reasons for this unique selectivity remain unresolved. Two general mechanistic proposals have been developed, involving either a radical or a nonradical oxidative addition pathway.

The nickel(I) cluster **8**, we propose reacts initially with the first equivalent of hydrogen fast at room temperature to form a dihydride nickel(I)/(II) cluster **23**. Then a second addition of hydrogen to complex **23**, maybe reversible, affords a tetrahydride nickel(II) complex **24** (Scheme 1-10). It is possible that a further addition of hydrogen to complex **24** could happen and form a hexahydride Ni(II)/ Ni(III) complex **25**. Moreover, in complexes **23-25**, hydride may bridge to nickel centers rather than behave as a terminal ligand. These reactions between nickel cluster **8** and hydrogen are included in both mechanisms.

For the radical pathway, an ester substrate coordinates to one nickel(I) **8** center, followed by a internal single electron transfer step to afford a stabilized radical intermediate **26**. The subsequent step is the homolysis of the benzylic C–O bond to afford a nickel(II) carboxylate complex **27** and a benzylic radical. The radical then abstracts a hydrogen atom from the nickel hydride complex **28** to release toluene product. In the last step, the remaining nickel hydride complex is deprotonated by sodium hydride, releasing, sodium benzoate and regenerating the active catalyst **8**.

**Scheme 1-10**



An alternative nonradical mechanistic pathway could involve a selective oxidative addition of low-valent nickel to the ester substrate (Scheme 1-11). In this hypothesis, the mixed valent nickel(I)/(II) cluster **23** is also formed from nickel(I) cluster **8** by hydrogenation(s). Complex **23** activates an ester substrate by binuclear oxidative addition to either the acyl



### 1.2.10 Discussion: Selectivity in Oxidative Addition

The oxidative addition of low valent nickel reagents to ester compounds has been previously observed in both stoichiometric transformations and catalytic reactions. In general, the selectivity for C–O bond activation in ester group reduction is reagent- and condition-dependent, as the selectivity varies if any of the metal complexes, ester substrates, or ligands is changed. Examples of selective activation of aliphatic, phenyl and acyl C–O bonds have all been observed in various reactions. However, the selectivity in C–O bond activation of ester compounds is not always exclusive. In some reactions, mixtures of products are obtained as a result of competitive activation of different C–O bonds.

**Figure 1-9.** Type A and B for oxidative addition of Ni(COD)<sub>2</sub> to esters



In 1976, Yamamoto reported different types of C–O bond activation in ester substrates by Ni(COD)<sub>2</sub> in the presence of various ligands (Figure 1-9).<sup>58</sup> In these reactions, a new nickel(0) complex is formed *in situ*, which cleaves the C–O bond by oxidative addition. The selectivity for C–O bond activation is largely dependent on the substrate (Table 1-7). For phenyl acetate, activation of acyl C–O bond is preferred when Ni(COD)<sub>2</sub> is used in combination with various ligands. However, when PEt<sub>3</sub> is added as a ligand, both acyl and phenyl C–O bonds are cleaved. On the contrary, for alkenyl esters, the alkenyl C–O bond is predominantly activated in most reactions.

**Table 1-7.** Modes of oxidative addition of Ni(COD)<sub>2</sub> to ester substrates<sup>a</sup>

	None	PPh <sub>3</sub>	PCy <sub>3</sub>	PEt <sub>3</sub>	bpy <sup>b</sup>	Ni(PPh <sub>3</sub> ) <sub>4</sub> <sup>c</sup>
Phenyl carboxylate	-	A	A	A+B	A	A+B
Alkenyl acetate	B	B	A+B	-	B	-

a. Symbols A and B is abbreviated for Type A and B reactions in Figure 1-9, respectively.

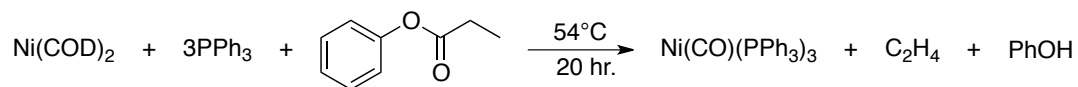
b. bpy = 2,2'-bipyridine

c. Ni(PPh<sub>3</sub>)<sub>4</sub> is used to replace Ni(COD)<sub>2</sub>.

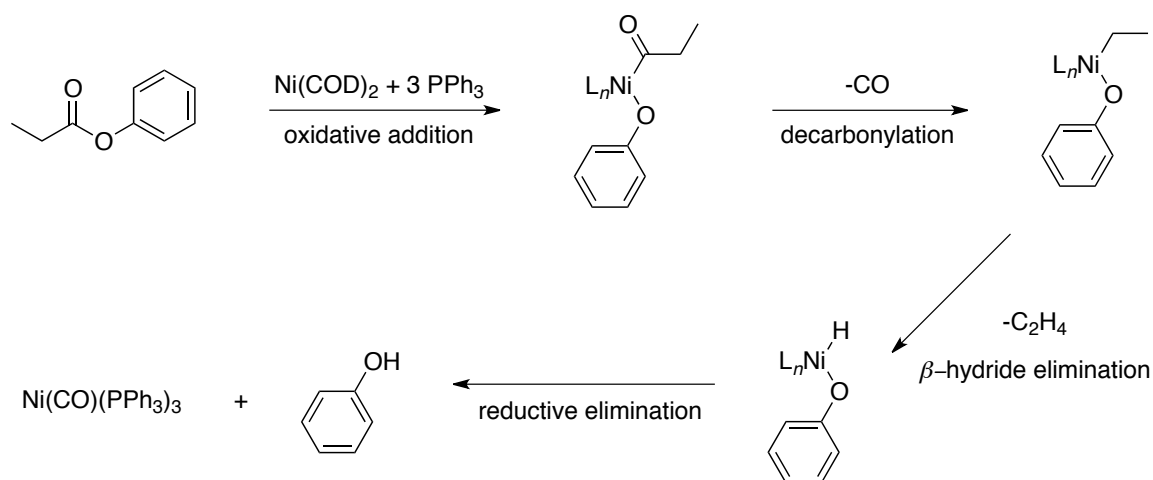
In 1980, Yamamoto reported a more detailed study on phenyl ester activation by Ni(COD)<sub>2</sub> or dialkyl Ni(II) species.<sup>59</sup> His study established a detailed reaction mechanism involving the oxidative addition to ester compounds. Consistent with the previous study, the acyl C–O bond is selectively cleaved in aryl esters. One representative reaction has been selected for a detailed discussion.

When Ni(COD)<sub>2</sub> and three equivalents of PPh<sub>3</sub> are added to phenyl propionate, ethylene, phenol and Ni(CO)(PPh<sub>3</sub>)<sub>3</sub> are obtained in 1:1:1 ratio (Eq.1-37). The products isolated indicate that the reaction involves the oxidative addition of Ni(0) species to the acyl C–O bond, followed by decarbonylation, β-hydride elimination and reductive elimination processes (Scheme 1-12).

### Equation 1-37

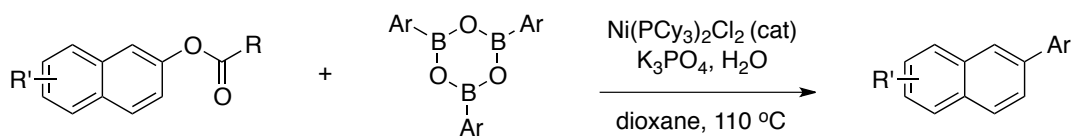


### Scheme 1-12

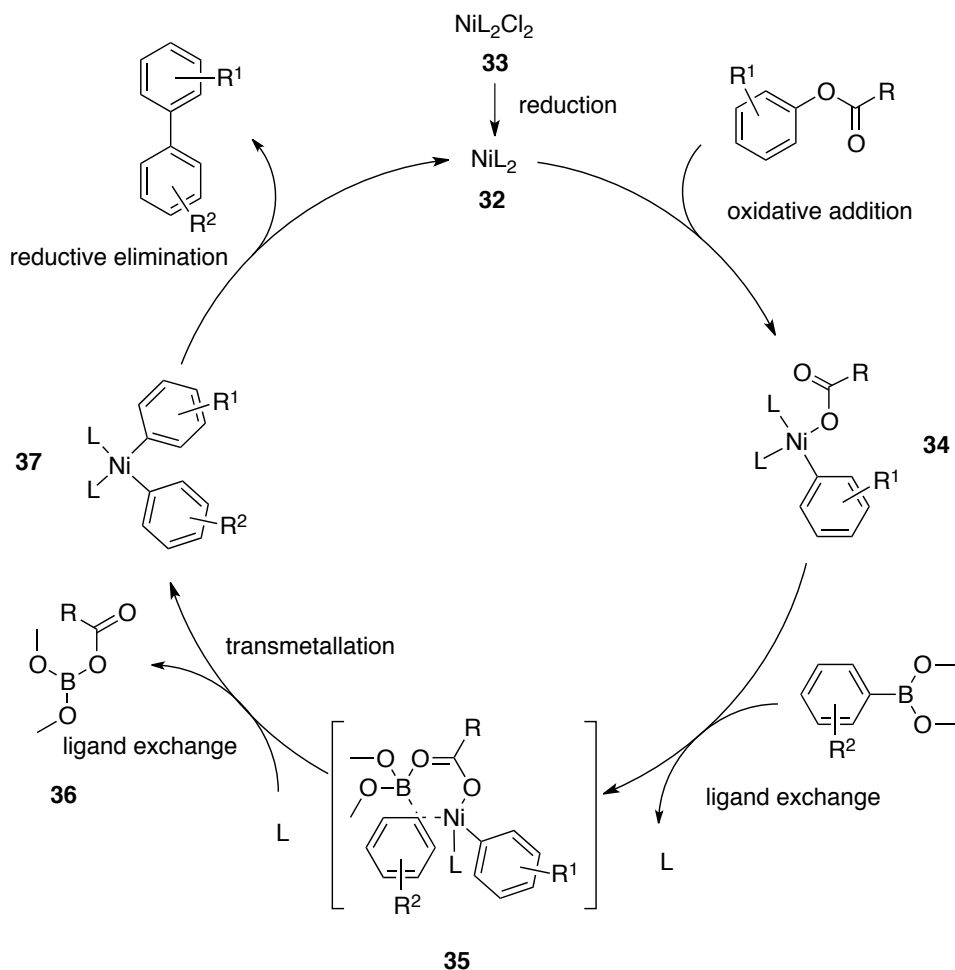


The activation of aryl C-O bond has also been observed in cross-coupling reactions, in which phenyl acetate is used as the substrate in place of aryl halides. In 2008, Shi reported the nickel-catalyzed cross-coupling reaction between phenyl esters and arylboroxines to afford the coupled biphenyl product (Eq. 1-38).<sup>60</sup> The proposed mechanism involves ester oxidative addition, transmetalation and reductive elimination (Scheme 1-13). The oxidative addition step is selective, involving cleavage of the stronger aryl C-O bond (106 kcal/mol) in the presence of a weaker acyl C-O bond (80 kcal/mol).<sup>61</sup> This selectivity is opposite to what is observed in aryl ester activation reactions using  $Ni(COD)_2$  and phosphine ligands in Scheme 1-12.

### Equation 1-38



**Scheme 1-13**

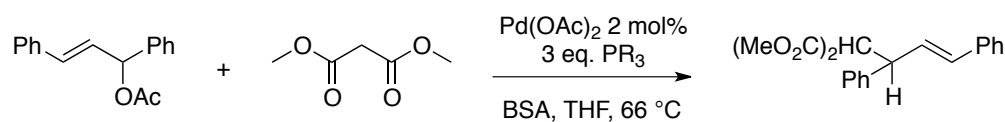


DFT calculations from Liu's group provide a plausible mechanism for the selectivity observed in Shi's reactions.<sup>61</sup> The activation of aryl C–O bond has a higher activation barrier of +22.9 kcal/mol compared to acyl C–O bond activation with a barrier of +14.2 kcal/mol. However the corresponding transmetallation step requires +33.1 kcal/mol following the acyl C–O bond activation, but only +31.2 kcal/mol after aryl C–O bond activation. Therefore, the pathway involving acyl C–O activation has an overall higher

energy barrier and the reactions largely undergo aryl C–O bond pathway to afford biphenyl products.

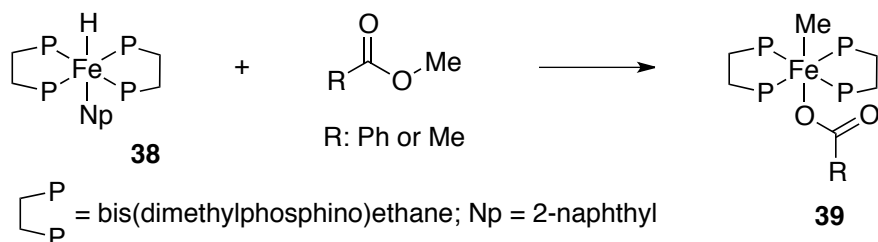
The previous discussion focuses mainly on the selectivity in aryl esters; however, activations of other types of esters have also been reported. For reactions involving allyl esters, the activation of  $sp^3$  C–O bond occurs predominantly. An established example occurs during the Tsuji-Trost reaction, which activates allylic esters in the presence of carbon nucleophiles to form a new C–C bond (Eq. 1-39).<sup>62</sup> In that reaction, an oxidative addition of a Pd (0) species occurs exclusively at the weaker allyl C–O bond to form allyl Pd(II) intermediates. Prior coordination of the alkene to the metal before oxidative addition significantly lowers activation barrier. Overall, the mechanism is an intramolecular activation of the adjacent allylic C–O bond.

### Equation 1-39



For non-activated alkyl esters, the selective alkyl C–O activation has also been demonstrated. In 1978, the Jesson group reported the activation of methyl benzoate or acetate by the iron(II) species **38** (Eq. 1-40).<sup>63</sup> The methyl C–O bond has been selectively activated and the corresponding iron(II) carboxylate complexes **39** are well characterized.

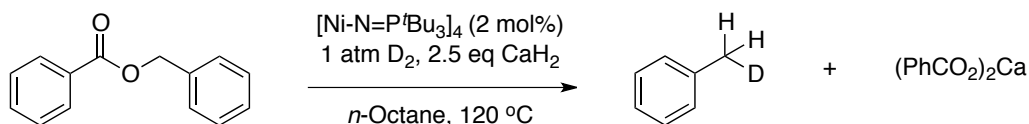
### Equation 1-40



In our examples of ester hydrogenation, the selective oxidative addition of the nickel/cobalt cluster, presumably already hydrogenated, to one of the C–O bonds in ester is certainly a logical mechanistic pathway. However, the two major differences between nickel cluster **8** and other nickel reagents and catalysts remain the number of involved metal centers and equally importantly, their respective oxidation states.

A deuterium labeling experiment has been conducted to determine the origin of the hydrogen atom in toluene product (Eq. 1-41). High resolution GC-MS analysis confirms that the quantitative product is the mono-deuterated toluene. Non-deuterated toluene is not obtained from this experiment. This verifies that the new hydrogen atom in toluene comes from the hydrogen gas and not calcium hydride or solvent.

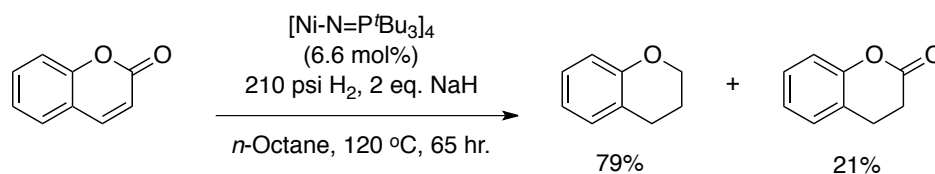
### Equation 1-41



### 1.2.11 New reaction pattern in ester hydrogenation

The majority of ester substrates tested in hydrogenation reactions involve alkyl/aryl C–O bond activation. However, one exception to this generalization was observed, involving selective deoxygenation of the carbonyl oxygen. Hydrogenation of dihydrocoumarin produces an ether compound, isochroman, as the major product (Eq. 1-42). This is a novel reaction pattern in the study of ester hydrogenation, for the carbonyl oxygen is removed while forming two new C–H bonds. Isochroman was identified and characterized by  $^1\text{H}$  NMR spectroscopy and GC-MS analysis.

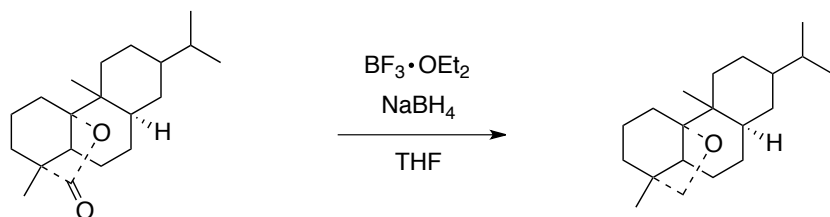
#### Equation 1-42



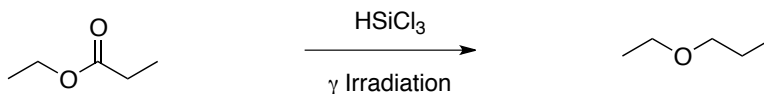
To the best of our knowledge, such a reaction pattern has not been previously observed in ester hydrogenation reactions. In literature, reactions proceeding from esters to ethers are very few and mostly limited to the use of hydrosilanes as reducing reagents. One exception involves the use of the boron trifluoride/sodium borohydride reagent, discovered in 1962 (Eq. 1-43).<sup>64</sup> In 1969, trichlorosilane became the first reported silane to reduce carboxylic esters to their corresponding ethers (Eq. 1-44).<sup>65</sup> Triethylsilane is more regularly used as the reducing agent and various additives/catalysts are required to promote the reactions. In 2001, a mixture of titanium tetrachloride and trimethylsilyl trifluoromethanesulfonate was used in combination with triethyl silane for the reduction of esters to ethers (Eq. 1-45).<sup>66</sup> More recently, a variety of metal complexes have also been utilized as catalysts for

this hydrosilylation, including iridium(III) bromide,<sup>67,68</sup> triruthenium carbonyl cluster,<sup>69</sup> and acetylmanganese carbonyl complexes,<sup>70</sup> etc.

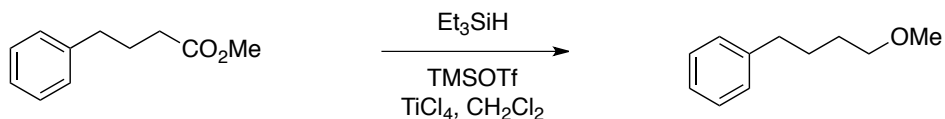
#### Equation 1-43



#### Equation 1-44



#### Equation 1-45



#### 1.2.12 Miscellaneous catalytic reactions

During the study of ester hydrogenation, some other relevant reactions have been discovered. Two major types are ring-opening lactone polymerization and reduction of benzaldehydes. Lactone hydrogenation reactions produce unanticipated polymers instead

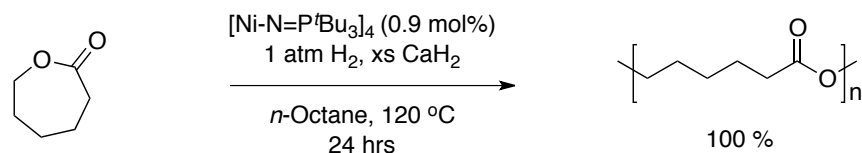
of the carboxylic acids. The hydrogenation of benzaldehydes affords unexpected products, including carboxylic acids and hydrocarbons.

### 1.2.13 Lactone polymerization

When aliphatic lactones are used as substrates in catalytic hydrogenation reactions, the products obtained are polyesters. The expected alkyl carboxylic acids from the hydrogenolysis of  $sp^3$  C–O bond are not obtained. Hence these are indeed lactone ring-opening polymerization reactions. Two lactone substrates have been briefly studied,  $\epsilon$ -caprolactone and 16-hexadecanonalide.

The reaction of  $\epsilon$ -caprolactone with the Ni(I) catalyst **8** at 1 atm of hydrogen pressure produces a plastic solid (Eq. 1-46). The material is insoluble in water, hexane or diethyl ether, but can be dissolved in dichloromethane. The solid is identified as ring-opening polymerization product based on  $^1\text{H}$  NMR,  $^{13}\text{C}$  NMR spectroscopy and HR-MS analysis.<sup>71</sup> A comparison between the  $^{13}\text{C}$  NMR spectrum of the starting material and product is listed (Table 1-8). The spectrum appears to be similar, bearing same number of signals with similar chemical shifts. However, the  $^1\text{H}$  NMR spectra for both compounds are very different, as polyester spectrum exhibits four resonances whereas  $\epsilon$ -caprolactone exhibits only two. Further HR-MS analysis confirms the product as the polyester with a broad range of molecular weight ( $M+Na/Z$ ) from 1247 to 7644.

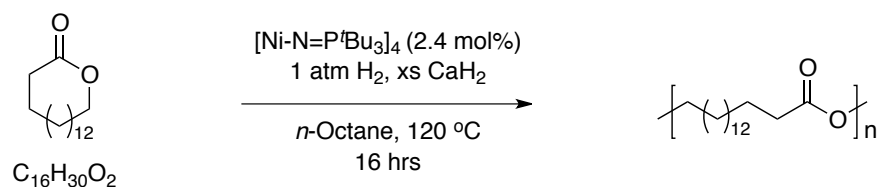
#### Equation 1-46



**Table 1-8.** Comparison of  $^{13}\text{C}$  NMR signals between  $\epsilon$ -caprolactone and the polymers

	Chemical shift (ppm)					
$\epsilon$ -caprolactone	176.22	69.30	34.57	29.34	28.93	22.99
polymer	173.12	63.75	33.73	27.96	25.14	24.18
dimer	173.42	63.01	34.55	28.14	24.61	24.58

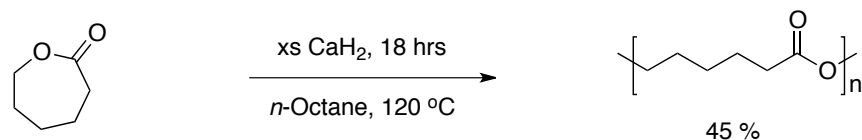
Polymerization of macrolactones is considered to be more difficult than lactones with smaller ring sizes.<sup>72</sup> On the other hand, for macrolactones, the chance of reducing the ester linkage is greater than in small-sized lactones. Therefore, 16-hexadecanone was selected for catalytic ester hydrogenation. In the event, however, the presence of the 16-membered ring in the lactone fails to direct the reaction to reduce carboxylic acid derivatives. The reaction still affords the ring-opening polymerization polyester (Eq. 1-47). The MS analysis using matrix-assisted laser desorption/ionization technique indicates a broad distribution of molecular weight from 500 to 3700.

**Equation 1-47**

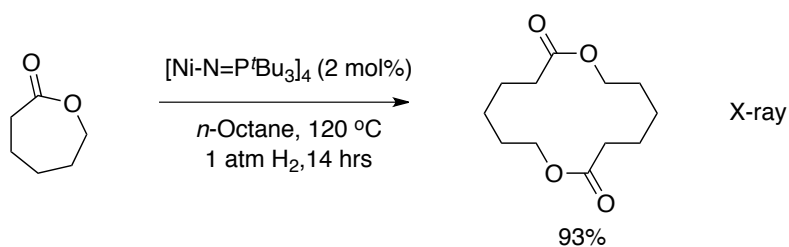
To understand the polymerization reaction, two separate control experiments were conducted using either  $\text{CaH}_2$  or the nickel cluster **8**. The first control experiment with  $\text{CaH}_2$  alone shows that lactone polymerization also occurs, but the consumption of monomer is not completed over the same time period (Eq. 1-48). To understand whether or not the

nickel cluster is catalyzing the polymerization, the second control experiment is performed in the absence of  $\text{CaH}_2$  (Eq. 1-49). This reaction catalytically produces a white solid that is distinct from the liquid  $\epsilon$ -caprolactone monomer. In addition, the product has a different solubility compared to  $\epsilon$ -caprolactone polymers. This solid is soluble in diethyl ether, whereas the polymers remain insoluble. The structure of the product was determined by X-ray crystallography as  $\epsilon$ -caprolactone dimer, 1,8-dioxacyclotetradecano-2, 9-dione. The  $^{13}\text{C}$  NMR spectra for the monomer, dimer and polymer are very similar and have been listed for comparison in Table 1-8.

#### Equation 1-48



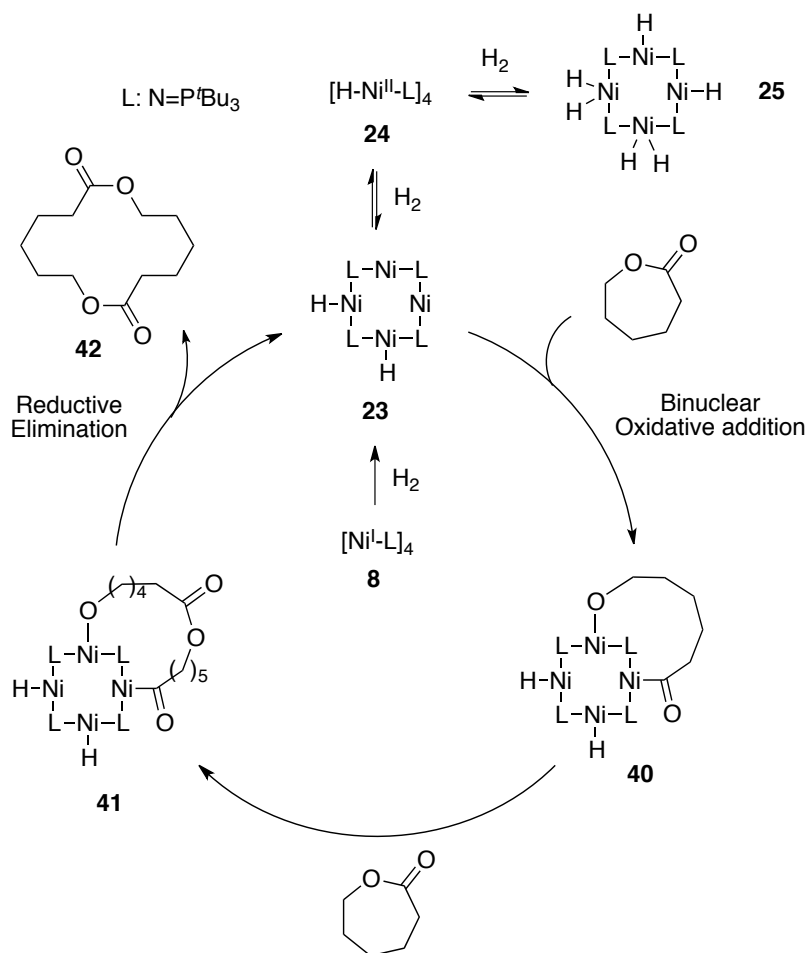
#### Equation 1-49



Preparation of the  $\epsilon$ -caprolactone dimer generally requires multistep transformations with the assistance of protecting groups.<sup>73-75</sup> Oligomerization of  $\epsilon$ -caprolactone has also been reported, but the products include a mixture of dimer, trimer, tetramer and etc.<sup>76</sup> In contrast, nickel catalyzed lactone dimerization reaction appears to be efficient and selective.

The reaction pathway may involve acyl C–O bond activation to form a bridged intermediate **40** (Scheme 1-14). The alkyl oxide then attacks another  $\epsilon$ -caprolactone to form a new intermediate **41**, from which a reductive elimination step affords a dimer **42**. After the reaction, significant amount of product was found accumulated at the top part of the glass bomb, indicating that the dimer sublimes from the reaction solution. The sublimation may drive the dimerization process to completion and also protect the dimer from further reaction.

**Scheme 1-14**

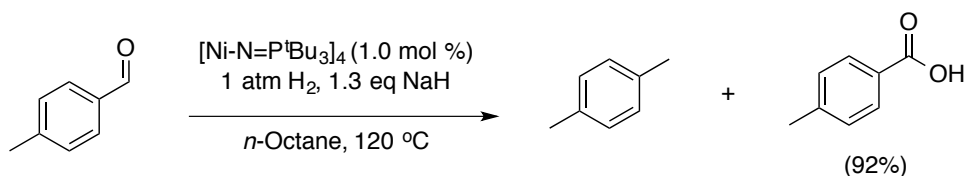


For the polymerization reaction, the overall process could involve two pathways: one is the calcium hydride catalyzed  $\epsilon$ -caprolactone polymerization, the other nickel cluster catalyzed dimerization pathway. The dimers may be consumed as a building block in polymerization reaction before it escapes the reaction solution. Therefore, the dimerization process accelerates the reaction rate in the conversion of  $\epsilon$ -caprolactone to polymers.

#### 1.2.14 Benzaldehyde hydrogenation/hydrogenolysis

The hydrogenation of *p*-methylbenzaldehyde catalyzed by nickel cluster **8** has also been investigated. However, the reactions using NaH as a scavenger produced unexpected products, *p*-xylene and *p*-methylbenzoic acid, in equimolar amounts (Eq. 1-50). The direct aldehyde hydrogenation product, *p*-methylbenzyl alcohol, was not observed. Based on the products generated, it is deduced that the reaction involves the initial formation of *p*-methylbenzyl *p*-methylbenzoate *in situ* (Scheme 1-14). The proposed pathway to this intermediate is a Tishchenko reaction named after Russian chemist Tishchenko, with subsequent hydrogenolysis of the benzyl ester in one pot.

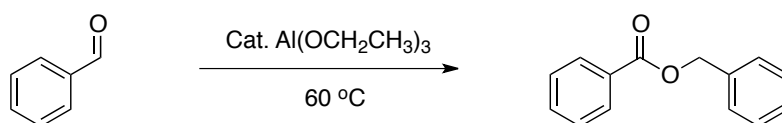
#### Equation 1-50



The Tishchenko reaction is an aldehyde condensation process to form the corresponding ester compound. The reaction was discovered by Claisen and improved by Tishchenko using an aluminum alkoxide as a catalyst (Eq. 1-51).<sup>77</sup> Surprisingly, this reaction is not

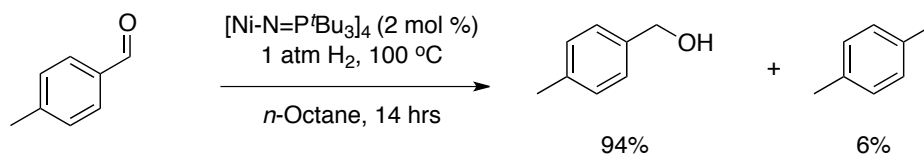
named after the discoverer, Claisen, but the developer, Tischtschenko. Furthermore, the reaction name was simplified to Tishchenko reaction. Nowadays, a large number of homogeneous and heterogeneous catalysts have been developed for Tishchenko reactions.<sup>78</sup>

### Equation 1-51



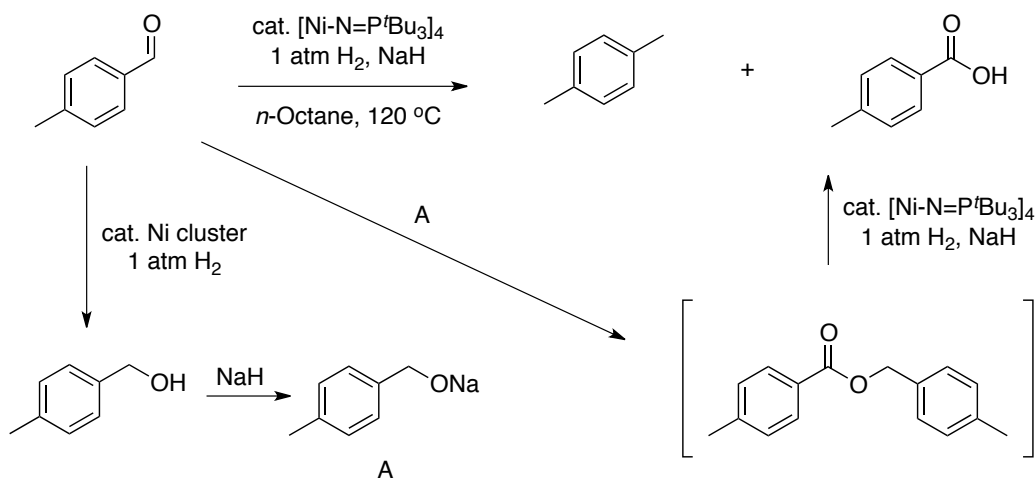
In the unanticipated *p*-methylbenzaldehyde reduction, the actual catalyst carrying out the Tishchenko reaction is unknown. Therefore, a control experiment was necessary for the identification of the catalyst. The reaction without added scavenger was expected to confirm that the nickel hydride catalyzes the aldehyde condensation (Eq. 1-52). However, this reaction produces, cleanly, 94% *p*-methylbenzyl alcohol and 6% *p*-xylene based on GC-MS analysis. The nickel hydride is not the catalyst for Tishchenko reaction, but instead catalyzes aldehyde hydrogenation, which proceeds to completion. Indeed, this catalytic hydrogenation reaction is attractive for many applications, since the catalyst requires very mild conditions and no additives. This reaction establishes a new project in the group, developing catalytic, scavenger-free hydrogenation of aldehyde and ketone substrates.

### Equation 1-52



Based on the control experiment and previous ester reductions, a mechanistic pathway for the conversion of *p*-methylbenzaldehyde to carboxylic acid and xylene can be proposed (Scheme 1-15). The hypothesis involves initial hydrogenation of aldehyde to alcohol. After that, NaH reacts with the *p*-methylbenzyl alcohol to form the alkoxide, which has been reported to be a catalyst for Tishcheko reaction.<sup>78</sup> It is also possible that the alkoxide catalyst is a nickel alkoxide. The *p*-methylbenzyl *p*-methylbenzoate generated *in situ* then undergoes hydrogenolysis, catalyzed by the nickel cluster, to afford the observed products.

**Scheme 1-15**



In conclusion, we have reported a series of ester reduction reactions catalyzed by nickel and cobalt clusters, which show high selectivity in the activation of the ester and acyl C–O bonds in the ester functional group. The reactions uniquely generate carboxylic acids and alkanes, a process closely related to green diesel production in the industrial ester refinery. The catalysts provide a valuable model system for understanding industrial nickel catalysts.

### 1.3 Conclusion

In summary, we have developed ester hydrogenolysis reactions using  $[\text{Ni-N}=\text{P}^t\text{Bu}_3]_4$  **8** as a precatalyst, which proceed under mild reaction conditions (1 atm  $\text{H}_2$ , 120 °C). In these reactions, benzyl/alkyl/aryl C–O single bonds can be selectively activated in the presence of acyl C–O bonds, forming the corresponding carboxylic acid salts and hydrocarbons as products. Such selectivity is unprecedented in catalytic ester reduction processes. In the literature, the reported homogeneous catalysts are mostly ruthenium complexes, which hydrogenate esters exclusively to alcohol products. In addition, our ester hydrogenolysis reactions are quite distinct from the industrial hydrogenation/hydrotreatment processes using heterogeneous catalysts.

Generally speaking, the ester hydrogenolysis reactions we developed require the addition of  $\text{CaH}_2$  or  $\text{NaH}$  as a proton scavenger. The substrate scope is relatively broad, including benzyl, alkyl and aryl esters. In these reactions, benzyl C–O bond activation appears to be kinetically easier than C–O bond activation of alkyl/aryl esters. The presence of an aromatic ring at the acyl position in alkyl esters is essential to obtaining useful reaction rates. It seems that coordination of the aromatic ring to the nickel center(s) in the active catalyst is necessary to promote activation of alkyl C–O bond. The most challenging substrates under current conditions are alkyl esters with no aromatic functionality, which fail to undergo significant hydrogenolysis.

The chemical structure of the active catalyst remains undetermined. However, when mercury was added in a benzyl benzoate hydrogenolysis reaction, the reaction became stalled. The GC yield of toluene decreased to a merely 2% in this mercury test reaction. This result suggested that the real catalyst is more likely to be heterogeneous.<sup>79</sup> More effort is needed to reveal the true nature of the real catalyst.

## 1.4 Future work

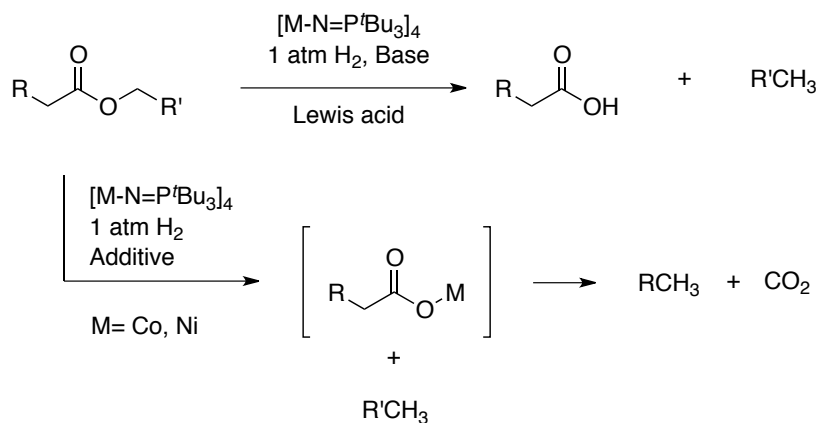
Problems associated with ester reduction mainly rise from the use of a strongly basic scavenger, which consequently narrows the substrate scope of this reaction. In addition, the employment of base is a general disadvantage for the entire series of nickel/cobalt cluster-catalyzed reactions, which include hydrodesulphurization and hydrodeoxygenation. Therefore the development of new catalysts stable under acidic conditions or selective nonbasic scavengers could serve as a general solution for this problem. However, the design and development of such catalysts are incredibly challenging.

### Equation 1-53



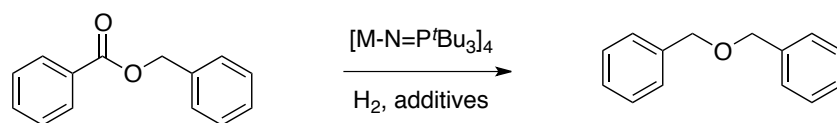
For the ester hydrogenation reactions, the current conditions using CaH<sub>2</sub> as a base is rather ineffective in reducing aliphatic esters bearing acidic  $\alpha$ -hydrogens, such as triglycerides and tridecyl acetate (Eq. 1-53). Future work is required to improve the efficiency in the reduction of these challenging substrates. Possible strategies include addition of Lewis acid to activate ester compounds, exploration of non-basic scavengers and the use of new additives to promote the decarboxylation step (Scheme 1-16). Furthermore, if decarboxylation can be designed as the dominant pathway, no protic compounds would be produced in principle and therefore the addition of base would no longer be necessary. Hence, for this proposed methodology, the acidic  $\alpha$ -hydrogens in aliphatic esters would not pose a serious challenge.

### Scheme 1-16

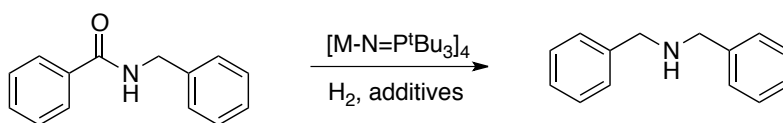


Future work is also required for the exploration of ester reduction to give ethers. The ester substrate scope for this deoxygenation reaction has to be further extended. However the embedded challenge under current conditions is that the hydrogenolysis of alkyl or aryl C–O bonds is the dominant reaction pathway for many ester compounds. To expand the substrate scope for deoxygenation, new reaction conditions have to be developed so that C–O single bond hydrogenolysis can be minimized (Eq. 1-54). Furthermore, other carbonyl compounds may also be deoxygenated. Amides can potentially be an important class of substrates. A parallel investigation by Ting Zhao in our group suggests the C–N bond activation in amide substrates does not occur under hydrogenation conditions. There thus exists the possibility to hydrogenate amides to amines under appropriate conditions (Eq. 1-55). The deoxygenation of aldehydes and ketones to alkanes is expected to be equally difficult; as such carbonyl compounds have demonstrated other reaction patterns. More specifically, aldehydes undergo Tishchenko reactions prior to being reduced, while acetophenone hydrogenation affords an alcohol product (Scheme 1-17) that does not undergo further reduction. Overall, further investigation may be required to study the reduction of ester or related carbonyl derivatives.

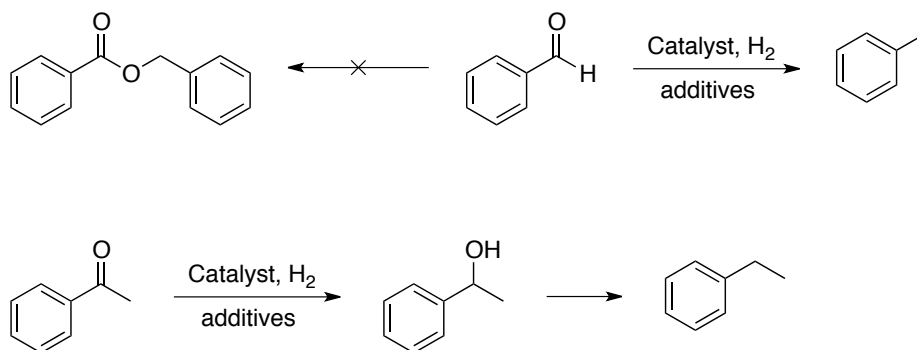
### Equation 1-54



### Equation 1-55



### Scheme 1-17



## Chapter 2: Aerobic Alkane Oxidation Catalyzed by Phosphoranimide-Supported Nickel and Cobalt Clusters

### 2.1 Introduction

#### 2.1.1 Oxidation Reactions and Oxidants

Oxidation exists ubiquitously on this planet. The oxidation reaction is one of the most fundamental reactions in chemical research and has wide industrial applications. Generally speaking, oxidation is a broad research topic covering many intensively explored areas, such as alkene epoxidation,<sup>80</sup> alcohol oxidation,<sup>81-83</sup> etc. There are also numerous reactions named after their discoverers or developers in the field of oxidation, including Swern oxidation, Wacker-Tsuji oxidation, Baeyer-Villiger oxidation, Oppenauer oxidation, Corey-Kim oxidation, etc.<sup>84</sup>

To conduct oxidation reactions in the desired and controllable fashion, a large number of oxidizing reagents and systems have been developed over the decades. The oxidants can be classified into different categories including peroxides, strong acids, halogens, hypohalites, periodinanes, metal oxides, etc. These reagents contain either weak hetero-heteroatom bonds or electron-deficient highly oxidized atoms, such as transition metals, halogens, nitrogen and sulphur. The most commonly used oxidants at high oxidation state include Dess-Martin reagent, Cr(VI) and Mn(VII) compounds, etc.<sup>85</sup>

In spite of the large number of oxidants available, performing clean oxidation reactions without releasing noxious pollutants is still incredibly challenging, especially on industrial scale. In general, the current challenges facing oxidation reactions mainly include poor atom efficiency, high toxicity, high cost and large volumes of waste generation.<sup>86</sup> Many

oxidation reactions generate large amounts of byproducts, which usually contain halogens, transition metals and other hazardous components.

Nowadays, ecological sustainability is becoming an increasingly important issue in every aspect of the modern society. Accordingly, the industrial processes involving oxidation reactions have to grow beyond the old fashion, and need to be conducted in a more economical and clean way in order to cultivate sustainable development. The development of inexpensive, efficient and environmentally friendly oxidizing reagents is the key to realizing this goal and enhancing long-term maintenance of the planet's well being.

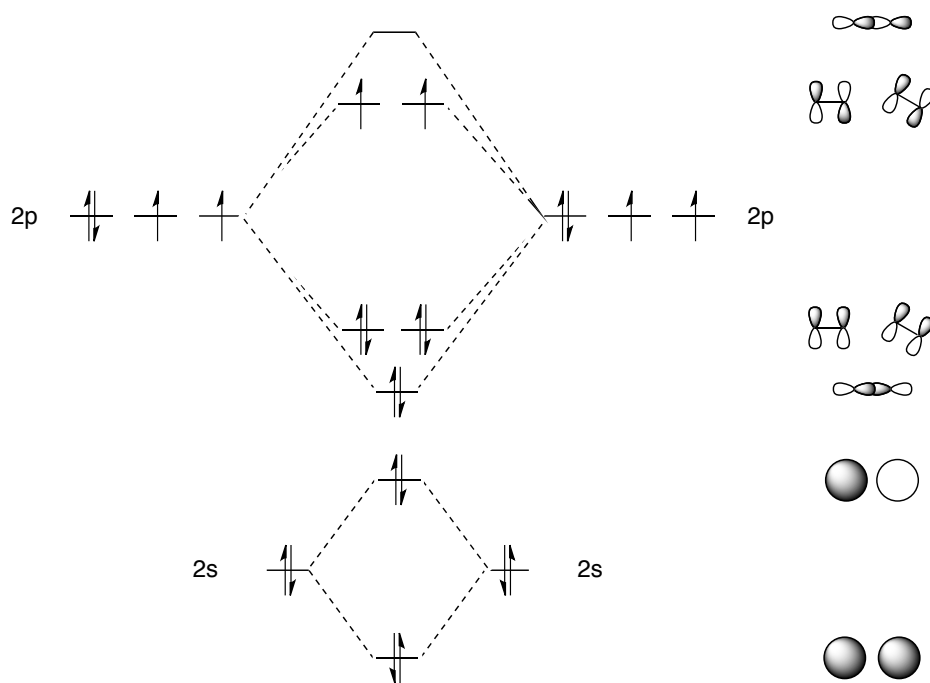
### *2.1.2 Introduction to molecular oxygen ( $O_2$ )*

Molecular oxygen is regarded as an ideal oxidant in various aspects. First, dioxygen is abundant on the planet, constituting about 20.9% of atmosphere by volume. Therefore, oxidation reactions using air can avoid any additional expense for other oxidizing reagents. Second, purified dioxygen is also readily available on industrial scale at low cost. Current industrial dioxygen manufacturing methods include air liquification and water electrolysis.<sup>87</sup> Third, compared to other corrosive and toxic oxidants, molecular oxygen is mild and easy to handle. Finally, the ultimate byproduct of the oxidation reaction is water, which can be directly released to the ecosystem. Therefore, developing oxidation reactions with molecular oxygen is not only scientifically appealing, but also beneficial in the economic and environmental points of views.

The presence of the heteroatom-heteroatom bond indicates the oxidizing ability of molecular oxygen. This is not simply a well-accepted opinion, but also supported by experimental measurements. The redox potential of molecular oxygen is 1.23 V with respect to water. In comparison, the redox potential is 1.09 V for bromine and 1.36 V for

chlorine with reference to their corresponding halides.<sup>88</sup> The data imply that as an oxidant, molecular oxygen is stronger than bromine, but weaker than chlorine. Furthermore, Frontier Molecular Orbital theory provides a more accurate description on the oxidizing ability of dioxygen molecule than VSEPR theory. As depicted in orbital diagram (Figure 2-1), the HOMO of the  $O_2$ , consists of two energetically equivalent  $\pi^*$  orbitals, each of which is occupied by a single unpaired electron. The molecular orbital diagram below also demonstrates that the triplet spin state with diradical character is the ground state molecular oxygen.

**Figure 2-1.** Orbital diagram of molecular oxygen



### 2.1.3 Reactions using O<sub>2</sub> as an oxidant

As a promising oxidizing reagent, molecular oxygen has been utilized in many oxidation reactions. The majority of these reactions are catalyzed reactions that play important roles in organic synthesis; these currently attract intensive research interest. On the contrary, uncatalyzed reactions using dioxygen are much less popular and most of them have no significant synthetic utility.

The most common uncatalyzed aerobic oxidation reaction is the flammable combustion of organic molecules. Combustion is a highly exothermic radical-chain reaction, leading to the formation of synthetically unattractive carbon dioxide.<sup>89</sup> This is a traditional way to generate energy with a history over thousands of years in human society.

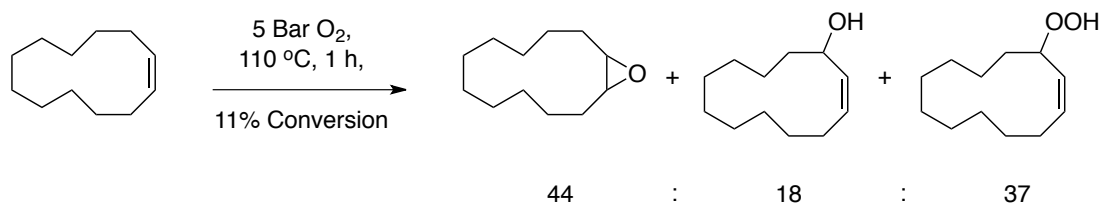
Another general type of uncatalyzed aerobic oxidation reactions, generally termed autoxidation, occurs in long-term chemical and fuel storage. For example, autoxidation of diethyl ether leads to the formation of diethyl ether hydroperoxide, which can be further polymerized to form highly explosive diethyl ether peroxides (Eq. 2-1).<sup>90</sup> Molecules with an olefin moiety can be oxidized slowly at the allylic position in air to give oxygenated products; this is the decomposition process in biodiesel storage, as well as for many other chemicals.<sup>35</sup> Therefore, antioxidants are added as a common adduct to many chemicals to prevent the undesired auto-oxidation process.

#### Equation 2-1



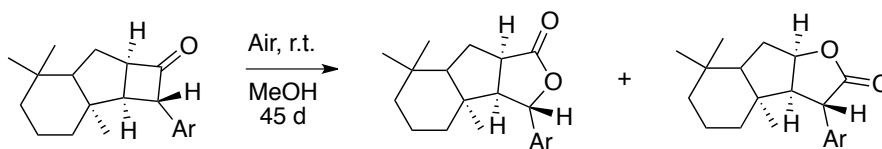
Uncatalyzed aerobic oxidations in organic synthesis remain scarce, as very few organic compounds react directly with molecular oxygen at a satisfactory rate. The reported examples are generally restricted to cyclic alkenes, which include cyclododecane, cyclooctene and 1,5,9-cyclododecatriene. These reactions are usually conducted at a temperature range between 70 °C to 110 °C. Cyclooctene and 1,5,9-cyclododecatriene oxidations afford the corresponding epoxides with high chemoselectivity.<sup>91</sup> However, for cyclododecane oxidation reaction, hydroperoxide, alcohol and epoxide are all present as final products (Eq. 2-2).<sup>92</sup>

### Equation 2-2



There is also an interesting report of an unusual uncatalyzed Baeyer-Villiger oxidation of cyclobutanone in air (Eq. 2-3).<sup>93</sup> The reaction occurs at room temperature in methanol over 45 days to expand the strained cyclobutanone derivatives to a mixture of  $\gamma$ -butyrolactone compounds. The regioselectivity of oxygen atom insertion varies depending on the substitution pattern of the aryl groups.

### Equation 2-3



In summary, uncatalyzed aerobic reactions are mostly used in uncontrolled energy production and may cause hazardous problems in chemical storage. In organic synthesis, direct reactions between molecular oxygen and organic molecules are usually slow and have limited utility. The addition of catalysts is essential to enhance the reaction rate and improve the yield.

#### *2.1.4 Catalytic aerobic oxidation reaction*

Compared to the uncatalyzed reactions, the catalyzed reactions using molecular oxygen as an oxidizing reagent bear more synthetic applications. These reactions are rather diverse and therefore a broad range of organic transformations has been realized. According to Jiao, et al.,<sup>94</sup> the reactions can be generally classified into three categories: dehydrogenative oxidation, oxidative coupling, and aerobic oxidation with oxygen-atom incorporation.

Dehydrogenative oxidation involves the removal of hydrogen atoms from organic molecules. These well-documented conventional reactions include alcohol oxidation to aldehyde or ketone derivatives.<sup>86</sup> More recently, a series of novel reactions have been developed, including the direct esterification of alcohols,<sup>95</sup> amide synthesis from alcohol and amine,<sup>96</sup> conversion of substituted cyclohexanones to phenol derivatives and dehydration of aldehydes to the corresponding  $\alpha,\beta$ -unsaturated aldehydes, among other things.<sup>97</sup>

The scope of oxidative coupling is rather broad, covering reactions involving carbon-carbon, carbon-heteroatom and even heteroatom-heteroatom bond formation. Common examples include homo-coupling,<sup>98</sup> oxidative amidation, oxidative Heck coupling, Wacker-

type oxidation, and cycloaddition.<sup>94</sup> Research in this field is also closely correlated to other frontier research areas, such as C–H activation and cross-coupling reactions.<sup>99,100</sup>

Oxygen atom transfer aerobic oxidation reactions have been demonstrated using simple substrates: alkanes, alkenes and alkynes to afford ketones, epoxides, diketones, and many other oxygenated products.<sup>101–103</sup> Furthermore, oxygen incorporation has also been performed on substrates bearing functional groups, to build the structurally more complicated molecules efficiently.<sup>104–107</sup>

Among the diverse oxidation reactions using O<sub>2</sub> as the terminal oxidant, alkane partial oxidation reactions are attracting more research attention due to their commercial potential and challenging nature. The rest of this chapter focuses on the alkane oxidation reactions, covering an introduction to the alkanes, fundamental C–H activation processes, and selective catalytic alkane oxidation reactions.

### *2.1.5 Introduction about alkanes*

Alkanes are saturated hydrocarbons that are abundant in fossil fuel reservoirs such as petroleum and natural gas. Various saturated hydrocarbon compounds are present as important components in crude oils. Meanwhile, methane is the major constituent of natural gas.<sup>108</sup> Currently, alkanes are mainly produced from petroleum-based industries and serve primarily as a source of transportation fuels.

Alternatively, alkanes are also utilized as a valuable feedstock for the production of value-added commodity and specialty chemicals, including alcohols, ketones, and aldehydes. Under current technology for petrochemical synthesis, the transformation involves indirect multi-step manipulations, such as energy-intensive thermal cracking,<sup>109</sup> olefin

polymerization,<sup>110</sup> conversion to syngas<sup>111</sup> or other inefficient processes. Ideally, alkanes could be potentially converted to fine chemicals in a single catalytic oxidation step. However, this direct conversion is not yet practical in industry.

Today many researchers find the idea of oxidizing alkanes to fine chemicals using O<sub>2</sub> directly exciting. If successfully developed to industrial standard, it would provide value-added petrochemicals in a much more efficient, economical, and environmentally cleaner way. Meanwhile, such selective technology would be particularly valuable for natural gas upgrading. Under ambient temperature and atmospheric pressure, methane exists in gas form, which renders the full utilization challenging and expensive.<sup>112</sup> Therefore, an easy conversion of methane to liquid compounds such as methanol, formaldehyde, or methyl formate would largely eliminate the difficulties in natural gas transportation and storage, while providing an alternative energy /chemicals source.

Partial oxidation of alkanes has been targeted in research for decades; however, many difficulties lie in the research and appear to be insurmountable. The relative inertness of alkanes remains as the major challenge for the further development of alkane oxidation. The alkane molecules are composed of only sp<sup>3</sup> C–H and sp<sup>3</sup> C–C bonds without any  $\pi$  or *n*-electrons. Both C–H and C–C bonds are strong  $\sigma$  bonds, in which the bond energy is approximately 100 kcal/mol.<sup>113</sup> As a result, the thermal reaction between alkanes and molecular oxygen requires very high temperatures to occur. For instance, the auto ignition temperature for butane is 405 °C.<sup>114</sup> In addition, alkanes are also resistant to many other strong oxidizing reagents. Experiments have been conducted by adding *n*-hexane to concentrated sulfuric acid, boiling nitric acid, potassium permanganate or chromic acid and *n*-hexane, yet no activation of the *n*-hexane was observed.<sup>115</sup>

Compounding the problem, the enhanced reactivity of partially oxidized products leads to another challenge for alkane oxidation reactions. These oxygenated compounds are generally more reactive than the alkane starting material. The incorporation of the oxygen atom into the alkane activates the adjacent C–H bonds due to the electronegativity and hyperconjugative effects of the oxygen atom. As a consequence, reactions usually proceed to fully oxidized products, whereas partially oxidized intermediates are rarely produced in any appreciable amount. The most problematic case occurs in methane oxidation, from which carbon dioxide is obtained as the major oxidation product. Methanol and formaldehyde are not accessible due to their higher reactivity compared to methane.

The chemo- and regioselectivity of C–H activation represents another challenge in alkane oxidation reactions. Though primary, secondary and tertiary C–H bonds can be differentiated by radical species, many existing reactions still suffer from low chemoselectivity. Moreover, regioselectivity among the same type of C–H bonds (e.g., two chemically inequivalent methyl groups) is exceptionally difficult, as the alkane substrates do not possess any directing group to guide C–H activation to a particular position. Taking the linear alkanes for example, these hydrocarbons only consist of internal methylene groups and terminal methyl groups. Since all methylene groups share very similar electronic and steric properties, they can be hardly distinguished in chemical reactions.

#### *2.1.6 Alkane $sp^3$ C–H activation and related oxidation reactions*

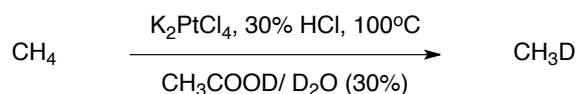
Though alkanes are relatively inert compounds, a variety of reagents have been discovered/developed to activate the saturated hydrocarbons. The reagents can be roughly categorized as super acids (e.g., HF-SbF<sub>5</sub>), free radicals, peracids, carbenes and more abundantly, transition metal complexes.<sup>116</sup> Over the past thirty years, a significant number of organometallic complexes have been developed to activate alkyl C–H bonds.

Transition-metal complexes capable of C–H activation are diverse in their electronic and structural properties. According to Bercaw,<sup>117</sup> the activation of aliphatic C–H bond by transition metal complexes can be classified into five mechanism-based categories: (1) electrophilic activation by high-valent electron-deficient complexes, (2) oxidative addition with low-valent electron-rich ‘late’ transition metals, (3) sigma-bond metathesis by alkyl or hydride ‘early’ transition-metal complexes, (4) 1,2-addition to metallocarbene or nitrene complexes, and (5) metalloradical activation by rhodium(II) porphyrin complexes. Among the five categories, the C–H activation via (1) electrophilic activation and (2) oxidative addition reactions have been intensively investigated, resulting in a deeper mechanistic understanding. In this thesis, our main focus will be on the first two categories of reactions; C–H bond activation involving sigma-bond metathesis, 1,2-addition and metalloradical activation will not be covered in any detail.

The electrophilic activation of  $sp^3$  C–H bond by high-valent metal complexes is a promising and effective strategy to oxidatively functionalize aliphatic compounds. A considerable number of transition metal complexes have been demonstrated to activate alkyl C–H bond stoichiometrically. Some of them have been further developed into catalysts for alkane oxidation reactions.

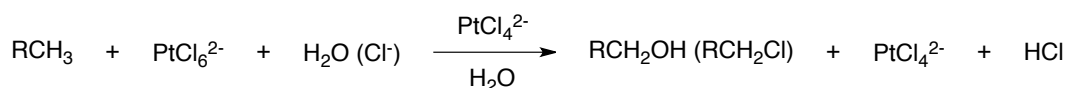
In 1969, Shilov reported his pioneering work for electrophilic C–H bond activation in alkanes.<sup>118</sup> The hydrogen-deuterium (H/D) exchange in methane or ethane is observed, catalyzed by  $K_2PtCl_4$  under acidic condition at 100 °C. The experiments were performed in a mixture of deuterated acetic acid and deuterium oxide (30%), to which hydrochloric acid was added (Eq. 2-4).

#### Equation 2-4



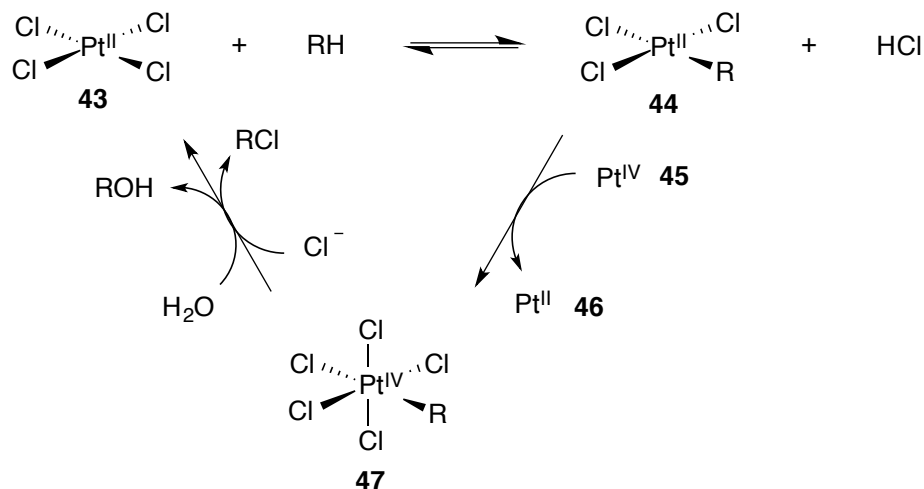
Based on the observations from the above experiments, Shilov and co-workers then made significant progress toward realizing catalytic alkane oxidation reactions in 1972 (Eq. 2-5).<sup>119</sup> The reactions were conducted with PtCl<sub>2</sub> catalyst under strongly acidic conditions at 120 °C, although stoichiometric amounts of H<sub>2</sub>[PtCl<sub>6</sub>] were used as the oxidant. The reaction affords terminal alcohols and the corresponding alkyl halide as major products.

#### Equation 2-5



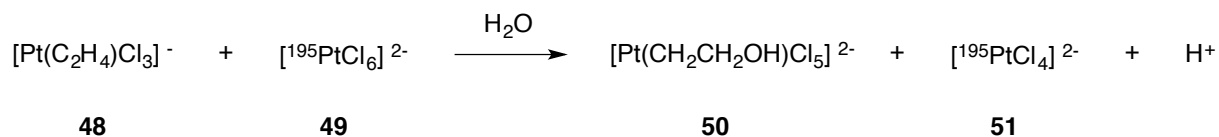
This activation pattern differs from typical radical reactions, in which the methyl groups are not competitively activated. The mechanistic hypothesis proposed by Shilov involves three steps: (1) the activation of an alkane C–H bond by Pt(II)Cl<sub>4</sub><sup>2-</sup> to form an alkylplatinum(II) intermediate **44**; (2) oxidation by the Pt(IV) complexes **45** to generate an alkylplatinum(IV) species **47**; and (3) the reaction of the alkylplatinum intermediate with H<sub>2</sub>O and Cl<sup>-</sup> to regenerate the Pt(II) catalyst **43** and release the alcohol and/or alkyl halide products (Scheme 2-1).<sup>120</sup>

### Scheme 2-1



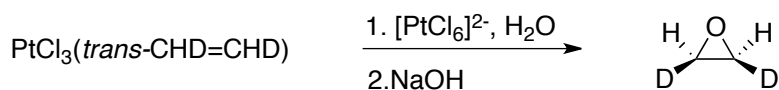
In 1990's, Bercaw and co-workers provided a more detailed mechanistic investigation of the Shilov system, conducting in-depth kinetic, isotopic labelling, and stereochemistry studies.<sup>121</sup> For the second step, <sup>195</sup>Pt isotopic labeling experiments suggest an alkylplatinum(IV) intermediate **50** is formed from oxidation mediated by Pt(IV)Cl<sub>6</sub><sup>2-</sup> **49** rather than the suggested alkyl group migration to the platinum(IV) center **49** (Eq. 2-6). This discovery indicates the possibility of developing Pt(II)-catalyzed reactions using cheaper terminal oxidizing reagents. Indeed, several corresponding reactions have been developed by employing electrochemical oxidation or O<sub>2</sub> in combination with copper salts or heteropoly acids.<sup>122-124</sup>

### Equation 2-6

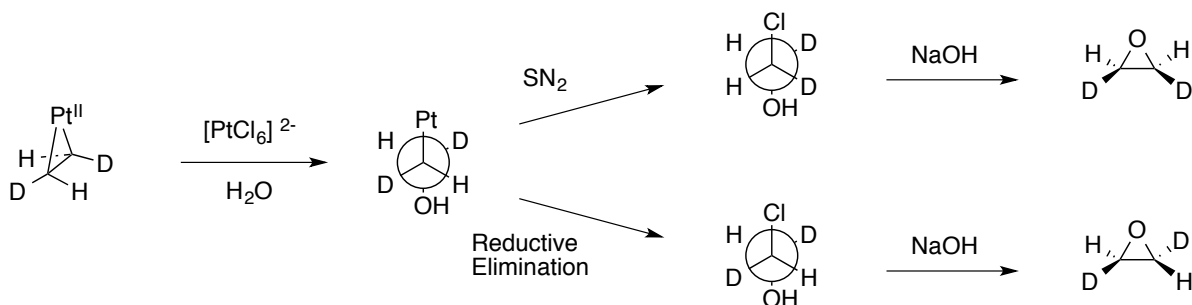


In addition, Bercaw also studied the stereochemistry of the Shilov reaction. A reaction was performed using *trans*-1,2-dideuterioethylene to produce d<sub>2</sub>-1-chloroethanol. After treating with sodium hydroxide solution, the product was identified as *cis*-ethylene-d<sub>2</sub> oxide (Eq. 2-7). The result suggests that after the formation of alkylplatinum (IV) intermediate **50**, the reduction step is an S<sub>N</sub>2 displacement with H<sub>2</sub>O or Cl<sup>-</sup>. Alternatively, if the pathway involves a reductive elimination, the product would be a different isomer, *trans*-ethylene-d<sub>2</sub> oxide, which was not observed in this experiment (Scheme 2-2).

### Equation 2-7



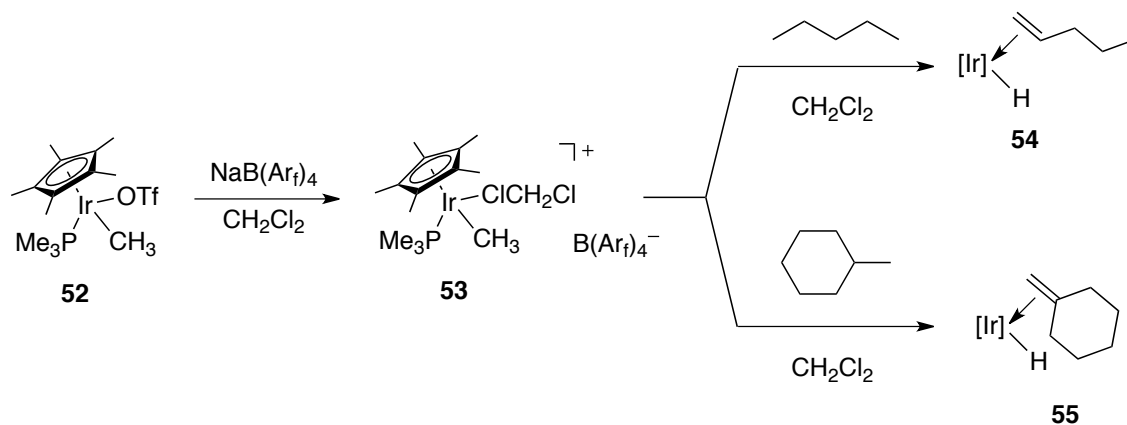
### Scheme 2-2



In 1995, Bergman *et al.*, reported an iridium-mediated electrophilic C–H activation reaction at a remarkably mild temperature (10 °C).<sup>125</sup> The iridium(III) complex, Cp\*(PMe<sub>3</sub>)IrMe(ClCH<sub>2</sub>Cl)<sup>+</sup>BAR<sub>4</sub><sup>-</sup> **53**, is prepared from Cp\*(PMe<sub>3</sub>)IrMe(OTf) **52** by the addition of sodium tetraarylborate in dichloromethane. Cp\*(PMe<sub>3</sub>)IrMe(ClCH<sub>2</sub>Cl)<sup>+</sup>BAR<sub>4</sub><sup>-</sup> **53**

activates the aliphatic C–H bond in hydrocarbons, such as pentane and methylcyclohexane, to afford the corresponding cationic olefin hydride complexes **54**, **55** (Eq. 2-8).

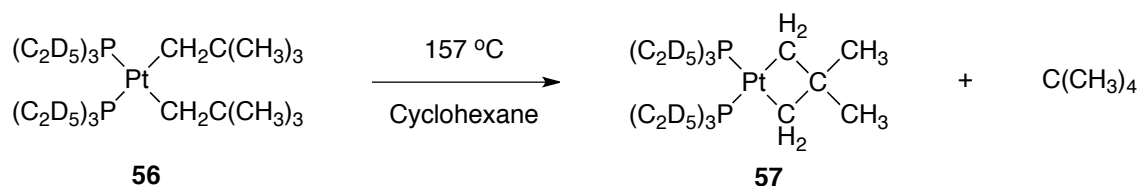
### Equation 2-8



In summary, high-valent transition metal complexes are an important class of organometallic compounds that are capable of C–H activation. Many complexes that are capable of electrophilic C–H activation have been reported, illustrated by Shilov’s and Bergman’s examples.

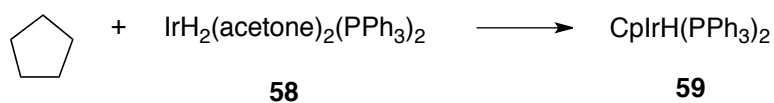
Alternatively, however, *electron-rich* low valent ‘late’ transition-metal complexes can also activate aliphatic C–H bonds by a non-radical mechanism. Such complexes activate C–H bonds by concerted oxidative addition. Early discoveries involve intramolecular C–H bond activation (“orthometallation”) of the coordinating ligands. As the example illustrated, the activation of the neopentyl group is observed in dineopentylbis(triethylphosphine) platinum(II) complex **56**, producing a more rigid 3,3-dimethylcycloplatinabutane complex **57**, as reported by Whitesides in 1979 (Eq. 2-9).<sup>126</sup>

### Equation 2-9

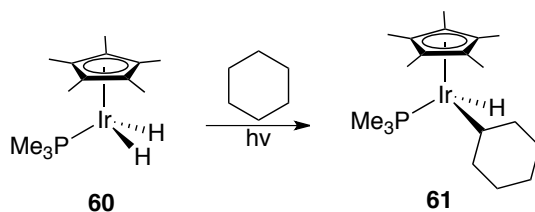


Intermolecular alkane activation reactions were developed shortly afterwards. In 1979, Crabtree discovered the iridium-mediated dehydrogenation reaction of cyclic alkanes to form new  $\pi$ -bonded ancillary ligands. For instance, the dehydrogenation of cyclopentane by IrH<sub>2</sub>(acetone)<sub>2</sub>(PPh<sub>3</sub>)<sub>2</sub> **58** led to the formation of CpIrH(PPh<sub>3</sub>)<sub>2</sub> **59** (Eq. 2-10).<sup>127</sup> In 1982, Bergman and Graham independently reported photochemical C–H activation reactions of cyclohexanes and neopentanes with Cp\*Ir(PMe<sub>3</sub>)(H)<sub>2</sub> **60** and Cp\*Ir(CO)<sub>2</sub> **62**, respectively (Eq. 2-11, 12).<sup>128,129</sup> Subsequently, an ever-increasing number of low valent complexes have since then been developed to activate alkanes stoichiometrically by oxidative addition.

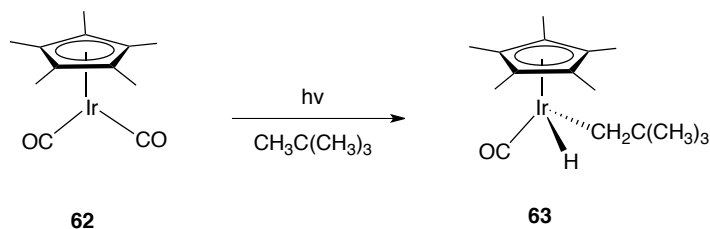
### Equation 2-10



### Equation 2-11

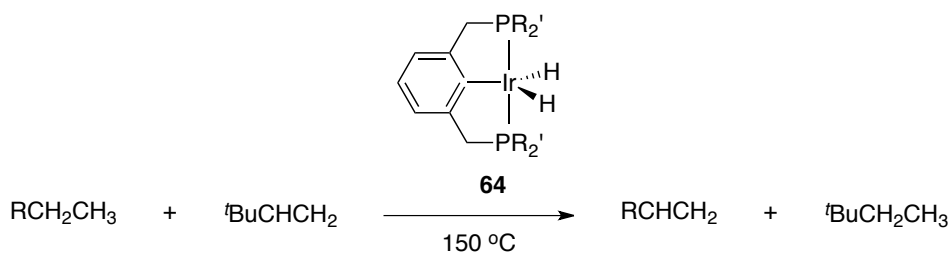


### Equation 2-12

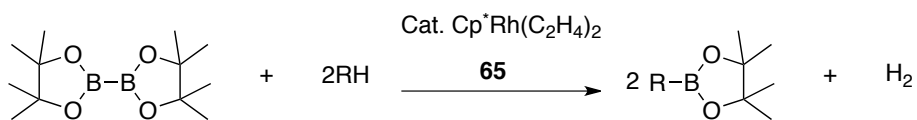


More recently, *catalytic* alkane functionalization reactions have also been developed using low valent transition-metal catalysts. The alkane dehydrogenation catalyzed by iridium complex **64** has been developed, in which terminal alkenes can be obtained from alkanes (Eq. 2-13). In another example, the borylation of alkanes is mediated by rhodium catalyst **65**, producing alkylboron compounds (Eq. 2-14). These catalysts, however, are sensitive to oxidants, so low valent transition-metal complexes are inherently not applicable as catalysts for alkane oxidation reactions.

### Equation 2-13



### Equation 2-14

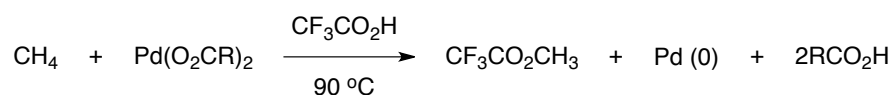


### 2.1.7 Alkane oxidation with oxidants other than O<sub>2</sub>

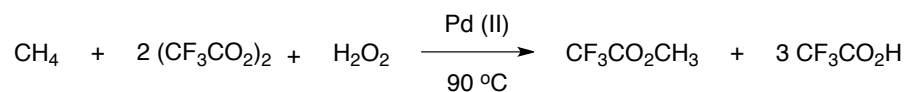
Though different types of organometallic compounds are capable of activating the aliphatic C–H bonds, very few of them can be further developed into alkane oxidation catalysts. Established catalysts are predominantly high valent transition-metal complexes. Besides the discussed PtCl<sub>2</sub> catalyst in Shilov system, many other high valent transition-metal catalysts are reported.

Palladium(II) complexes have also been demonstrated to activate the saturated hydrocarbons. In 1987, Sen group developed palladium(II)-mediated alkane oxidation reactions in trifluoroacetic acid at 90 °C (Eq. 2-15).<sup>130</sup> Adamantane and methane are oxidized to the corresponding 1-adamantyl and methyl trifluoroacetates. Palladium(0) metal is precipitated during the reactions. In 1991, Sen developed the corresponding palladium-catalyzed methane oxidation reactions with the addition of hydrogen peroxide and trifluoroacetate (Eq. 2-16).<sup>131</sup> Methyl trifluoroacetate was formed as a stable product resisting further oxidation. The added trifluoroacetic anhydride absorbs water generated from the reaction and therefore protects methyl trifluoroacetate from undergoing ester hydrolysis to form the more reactive methanol.

#### Equation 2-15



#### Equation 2-16



Sulfuric acid has also been used as an oxidant in several alkane oxidation reactions with various transition or post-transition metal catalysts, mainly involving Pt(II), Pd(II), or Hg(II) species. In 1993, Periana reported mercury(II)-catalyzed methane oxidation in sulfuric acid to generate methyl bisulphate (Eq. 2-17).<sup>132</sup> This catalytic reaction was developed from the known methane oxidation with stoichiometric amount of mercuric triflate, in which methyl triflate is produced and mercuric triflate is reduced to mercurous triflate (Eq. 2-18). In the catalytic reaction, the sulfuric acid is used to oxidize the mercury species with the release of sulphur dioxide. In 1998, Periana first demonstrated methane oxidation with a bidiazine platinum(II) complex **66**. The reactions are also conducted in hot sulfuric acids to generate methyl bisulphate (Eq. 2-19).<sup>133</sup>

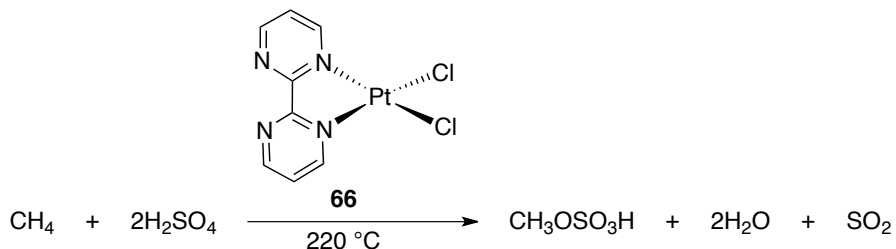
#### Equation 2-17



#### Equation 2-18

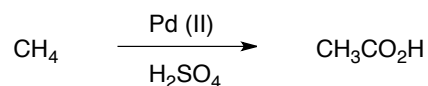


#### Equation 2-19

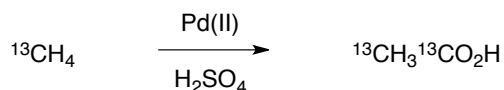


The oxidative condensation of methane, discovered by Periana in 2003, is distinct from the previous methane oxidation reactions.<sup>134</sup> The methane oxidation reaction is catalyzed by palladium(II) sulphate in sulfuric acid at 180 °C to produce mainly acetic acid, along with methanol in a much smaller amount (Eq. 2-20). The <sup>13</sup>C-labeling experiment confirms methane as the carbon source for both carbons in the C<sub>2</sub> product (Eq. 2-21). The proposed pathway involves an oxidation of methane to methanol and subsequently to carbon monoxide. The carbonylation process of methylpalladium(II) species **67** ultimately leads to the formation of acetic acid (Scheme 2-3).

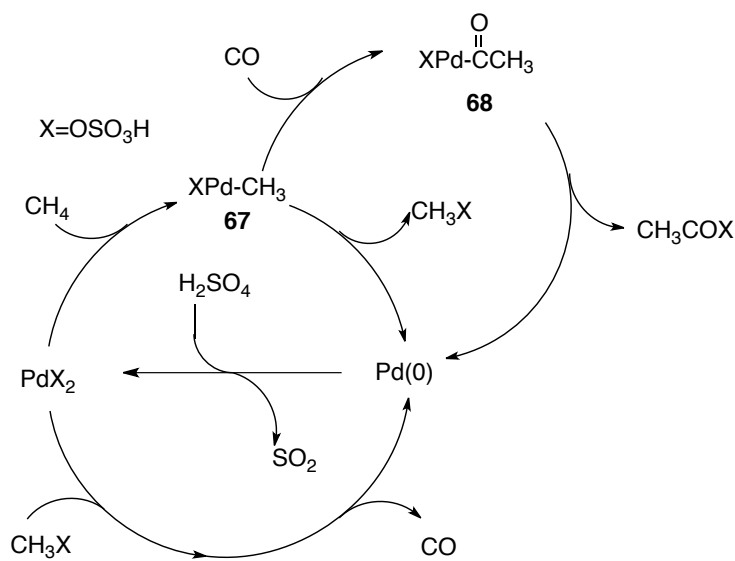
### Equation 2-20



### Equation 2-21

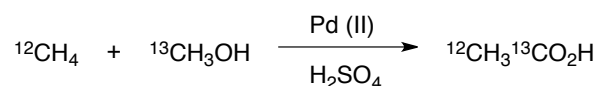


### Scheme 2-3



This hypothesis is supported by a series of mechanistic studies. A control experiment, carried out with a mixture of methane and methanol, resulted in the consumption of both starting materials and the formation of acetic acid; methanol is thus an intermediate of the reaction. Moreover, a reaction with  $^{13}\text{C}$ -enriched methanol and non-labelled methane provides a  $^{13}\text{C}$ -labelled acetic acid where  $^{13}\text{C}$  is exclusively present on the carbonyl carbon of the product (Eq. 2-22). This result proves that the carbonyl carbon in the acetic acid comes from methanol and methyl group of the product from methane.

### Equation 2-22



These pioneering discoveries contribute substantially to the development of partial alkane oxidation. However, significant drawbacks are still closely tied with the discussed reactions, such as the requirement for expensive catalysts, corrosive oxidants, and the generation of toxic gas(es), which together suppress applications of the reactions in industry. To develop mild and green alkane oxyfunctionalization reactions, it is crucial to use clean oxidants. The ideal choice would be developing methods that use molecular oxygen as an oxidant.

#### 2.1.8 Aerobic alkane oxidation in metalloenzymes

Nature demonstrates aerobic alkane oxidation reactions in a wide range of prokaryotic and eukaryotic microorganisms. Various classes of enzymes have been naturally evolved to catalyze the partial oxidation of alkanes. These enzymes are all metalloenzymes, since they

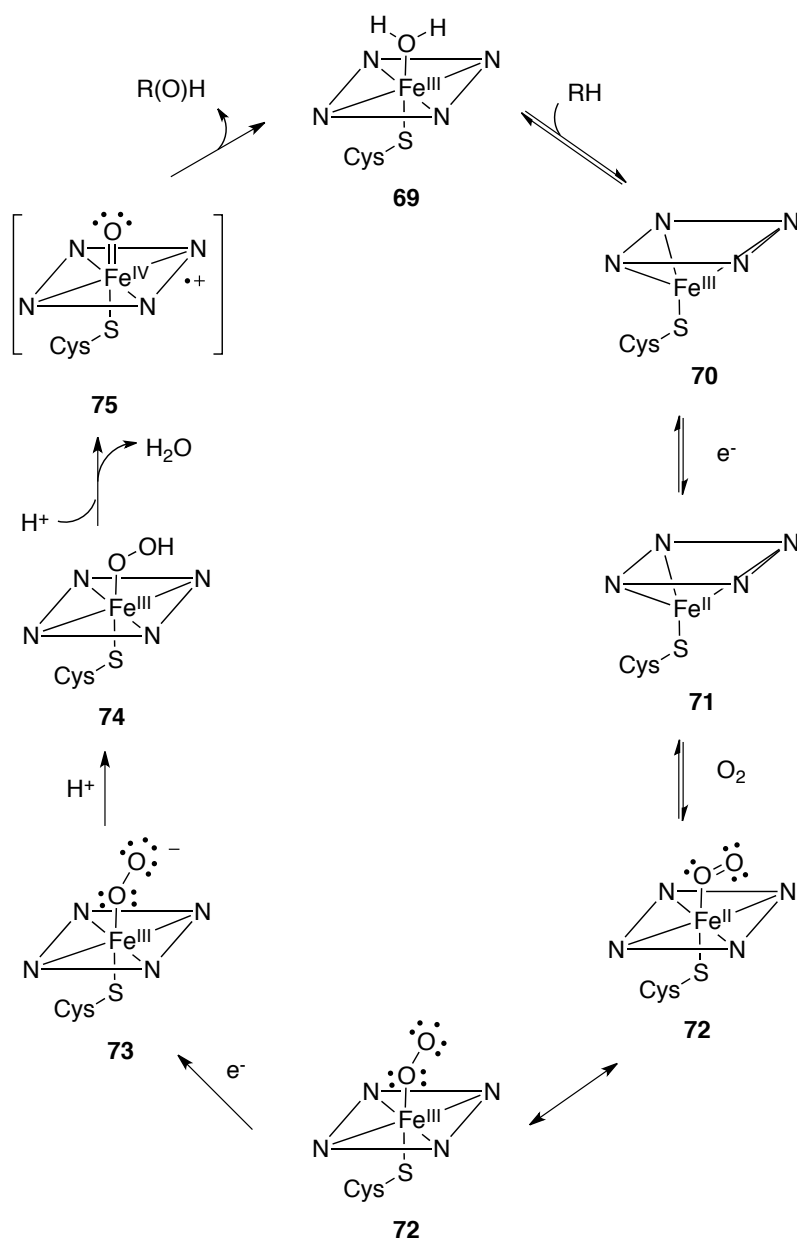
possess at least one transition metal in the enzymatic scaffold as the active sites for oxidation reactions.

The metalloenzymes mainly include cytochrome P-450 alkane hydroxylases (CP-450), integral membrane diiron alkane hydroxylases (AlkB), soluble diiron methane monooxygenases and membrane-bound copper-containing methane monooxygenases (MMOs).<sup>135</sup> In spite of the variety, these enzymes share common characteristics, including the use of molecular oxygen as the oxidant, the presence of a reductant for the reaction to occur, high chemo- and regioselectivity and mild physiological operating conditions.

The cytochromes P450 superfamily is present in most organisms, ranging from microorganisms to fungi and plants, and to animals. The CP-450 enzymes perform various reactions, one of which is alkane hydroxylation. The CP-450 family has been extensively studied and the mechanism of alkane oxidation is established and generally accepted by the field.

The active site of cytochrome P450 consists of a tetradentate porphyrin-supported mononuclear iron complex, which is also coordinated by an axial cysteine residue. The overall oxidation reaction catalyzed by CP-450 consumes protons, electrons, molecular oxygen and alkanes to produce water and, with high selectivity, primary alcohols. The proposed reaction cycle involves the activation of molecular oxygen, oxidation of the alkane, and reduction of the iron center to its low valent ground state (Scheme 2-4).<sup>136</sup> The reactive intermediate is an oxo-ferryl ( $O=Fe^{IV}$ ) porphyrin radical, which abstracts a hydrogen atom from the hydrocarbons. During the cycle, the reduced nicotinamide dinucleotides, abbreviated as NAD(P)H, is required as an electron donor to reduce the intermediate **70** and **72**.

**Scheme 2-4**



Integral membrane diiron alkane hydroxylases (AlkB) are present in *n*-alkane-degrading bacteria.<sup>137</sup> These enzymes have a diiron cluster in the enzymatic scaffold, which

selectively oxidizes the terminal position of linear alkanes. Two types of methane monooxygenase enzymes (MMOs) have been found in methanotrophic bacteria. MMOs that contain diiron centers are soluble in the cell, whereas the copper-containing monooxygenase is membrane-bounded. MMOs also oxidize the alkanes selectively at terminal positions. Due to the multi-component and membrane-bound nature, AlkB and MMOs are still not well understood today.

Enzymes created by nature demonstrate amazing reactivity under mild conditions, but they are very sensitive and unstable outside the living cells. The vulnerability of the enzymes limits in vitro applications as biocatalysts. Molecular protein engineering is a powerful tool to modify enzymes, but current engineered enzymes cannot meet practical standards for productivity.<sup>138</sup> Though direct application of biological metalloenzymes is challenging, the knowledge of enzymes continues to inspire the development of synthetic catalysts.

### *1.2.9 Aerobic alkane oxidation with synthetic catalysts*

Research to develop synthetic catalysts that mimic biological enzymes has also had limited success. The well-known biomimetic “Gif catalyst” system was developed by Barton, et al., to mimic CP-450 and named after the place where it was invented<sup>139</sup>. In the Gif system, oxidation of saturated hydrocarbons is conducted under air at room temperature. Four generations of Gif system have been reported since the initial discovery (Table 2-1).

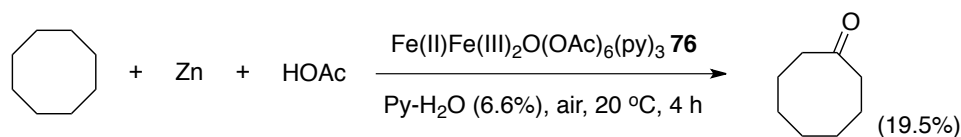
**Table 2-1.** Comparison of four generations of Gif systems

Generation	Catalyst	Electron donor	Proton donor	Additive	Solvent
I	Fe(0)	Fe(0)	HOAc	Na <sub>2</sub> S	Py
II	Fe(0)	Fe(0)	HOAc	H <sub>2</sub> S	Py-H <sub>2</sub> O
III	Fe(0)	Fe(0)	HOAc	-	Py-H <sub>2</sub> O
IV	Fe <sup>II</sup> Fe <sup>III</sup> cluster	Zn	HOAc	-	Py-H <sub>2</sub> O

Fe<sup>II</sup>Fe<sup>III</sup> cluster = Fe<sup>II</sup>Fe<sup>III</sup><sub>2</sub>O(OAc)<sub>6</sub>(py)<sub>3</sub>; Py = Pyridine

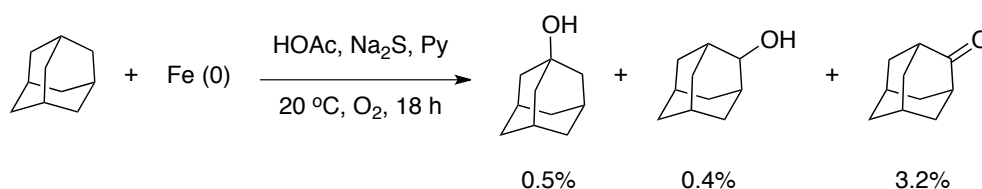
In the first two generations, H<sub>2</sub>S or Na<sub>2</sub>S was added to mimic the cysteine ligand in CP-450.<sup>140</sup> However, control experiments in the absence of sulfur-containing compounds also afford oxygenated products. This result suggests that an Fe-S bond is not essential for the oxidation. The third catalyst generation consists of iron(0) and acetic acid in a solution of pyridine and water. Iron powder serves not only as a precatalyst, but also as an electron donor during the oxidation. Interestingly, a trinuclear organoiron carboxylate cluster was isolated from the reaction mixture. The cluster was characterized as a mixed valent iron complex **76**, Fe<sup>II</sup>Fe<sup>III</sup><sub>2</sub>O(OAc)<sub>6</sub>(py)<sub>3</sub>. In the fourth generation, this iron cluster is utilized as a catalyst and zinc is employed as the stoichiometric electron donor (Eq. 2-23). Further research in Gif chemistry led to the development of new “Gif-Orsay” and generations of “GoAgg” oxidation systems involving Fe(III) or Cu(II) catalysts and H<sub>2</sub>O<sub>2</sub> as an oxidant.<sup>141</sup>

### Equation 2-23



The major products from Gif system are ketones, however alcohols can also be formed as minor products in many reactions. For adamantane oxidation, 2-adamantanone is obtained together with lesser amounts of 1- and 2-adamantanol (Eq. 2-24). Activation of the secondary C–H bond is preferred over both primary and tertiary C–H bonds. The selectivity of C–H bond activation in Gif system is distinct from that involving CY-450 and radical reagents, which prefer the activation of primary and tertiary C–H bonds, respectively. The proposed working hypothesis from Barton involves the formation of Fe oxenoid with unspecified valency as an active intermediate. The activation of hydrocarbons affords the formation of alkyl iron species, which eventually convert to ketones.<sup>142</sup>

### Equation 2-24

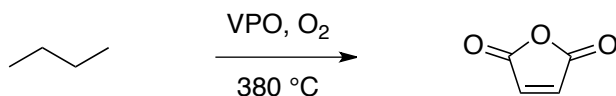


Another important category of biomimetic catalysts capable of alkane oxidation reactions is the metalloporphyrin class. As discussed, CP-450 is an example of a porphyrin complex containing an iron center. Many other transition metals can also be present in the metalloporphyrin complex, including Co, Mn, Cu, Au, Ir, Pd, Pt, etc.<sup>143</sup> Meanwhile, for the

alkane oxidation reactions catalyzed by these complexes, the reducing reagents employed are rather diverse. The most common reagents include molecular hydrogen, metal(0) powders, and aldehydes.

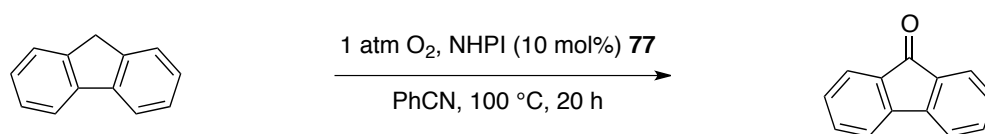
Many heterogeneous catalysts have also been developed for aerobic alkane oxidation.<sup>144</sup> Heterogeneous transition metal catalysts include V, Mo, Mn, Fe, Co, Pd, Au, and Pt, supported variously on silica, metal oxides, polystyrene, montmorillonite K10 and others. Some of these reactions have important industrial applications for fine chemical synthesis. The commercialized *n*-butane oxidation to maleic anhydride using a phosphorus oxide-supported vanadium oxide catalyst (VPO) (Eq. 2-25).<sup>145</sup>

#### Equation 2-25



Though catalysts for aerobic alkane oxidation reactions are predominantly transition-metal complexes, organocatalysts are also known to carry out this task.<sup>146</sup> However, most organocatalysis reactions involve typical radical pathways. These reactions are not as diverse in mechanism as alkane oxidation catalyzed by transition metal complexes. The best-studied organocatalyst is *N*-hydroxyphthalimide (NHPI), which readily oxidizes benzylic methylene groups under oxygen (Eq. 2-26).<sup>147</sup> However, efficient oxidation of alkanes requires the addition of transition metal salts to NHPI **77**, such as  $\text{Co}(\text{OAc})_2$ ,  $\text{Mn}(\text{acac})_2$ , etc.

## Equation 2-26



In conclusion, an appreciable range of catalytic systems have been developed to perform alkane oxidation using molecular oxygen as the oxidizing reagent. Mechanistic research provides valuable insight into understanding and modifying the systems for improved performance. However, the application of alkane oxidation to industrial fine chemical synthesis is still in its early stages. Major challenges include the improvement of catalyst efficiency, the control of partial oxidation processes, and the demonstration of high chemo- and regioselectivity.

## 2.2 Results and Discussion

### 2.2.1 Aerobic alkane oxidation overview

Due to the limitations and drawbacks remaining in alkane oxidation research, developing new catalysts is highly desirable. Here I am presenting my discovery of the aerobic alkane oxidation reactions catalyzed by phosphoranimide-supported nickel and cobalt clusters.

Since the preparation and characterization of these nickel(I) and cobalt(I) clusters, our studies have been exclusively focused on reductive catalysis, including hydrodesulphurization, hydrodeoxygenation, ester hydrogenation, and aldehyde/ketone reduction.<sup>148,149</sup> These reactions are typically conducted under hydrogen. When other reducing reagents, such as silane, are used, the reactions are carried out under inert

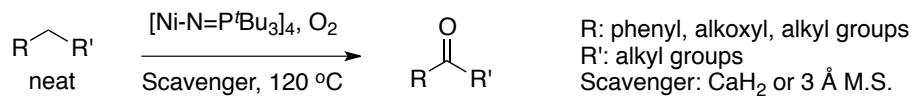
nitrogen atmosphere. Even trace amounts of molecular oxygen leaking into the reaction vessel completely deactivate the cluster and shut down the hydrogenation/hydrogenolysis reactions. Therefore, these highly air-sensitive low valent, low coordinate nickel(I)/cobalt(I) complexes were considered to be unsuitable for catalyzing oxidation reactions.

Interestingly, the exposure of the nickel(I) and cobalt(I) clusters to molecular oxygen or air does not destroy these clusters, as we originally hypothesized.

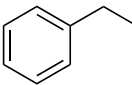
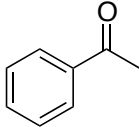
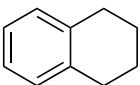
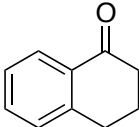
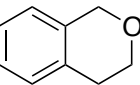
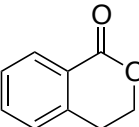
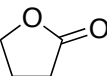
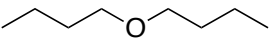
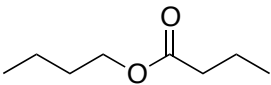
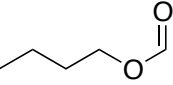
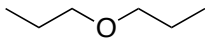
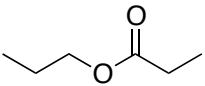
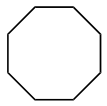
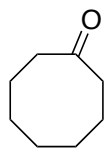
In a failed ketone hydrogenation reaction, a trace amount of solvent, *n*-octane, was oxidized to ketone compounds. Though the air-oxidized clusters are inactive for the hydrogenation and hydrogenolysis reactions, they are surprisingly capable of catalyzing aerobic alkane oxidation reactions at moderately elevated temperatures. Several series of experiments were designed to reveal the hidden oxidation powers of the phosphoranimide-supported nickel and cobalt clusters. This discovery is the first of its kind for oxidation reactions catalyzed by nickel or cobalt clusters.

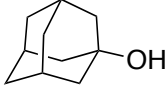
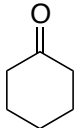
In general, the nickel/cobalt clusters catalyze alkane oxidation with molecular oxygen to afford ketone compounds as the major products (Eq. 2-27). Depending on the substrates and reaction conditions, minor products such as diketones, alcohols, and carboxylic acids may also be obtained. Various hydrocarbon compounds have been tested as substrates for the oxidation reactions, mainly including alkyl arenes, ethers and saturated hydrocarbons as listed in Table 2-2. For ethers and alkyl arenes, the electron-withdrawing group can activate the adjacent methylene groups. As a result, the benzylic C–H bond in alkyl arenes and methylene groups adjacent to ether oxygen can be selectively activated in the oxidation reactions. Non-activated saturated alkanes represents a class of more challenging substrates due to the stronger C–H bonds. In saturated alkanes, tertiary, secondary and primary C–H bonds become progressively more difficult to activate.

### Equation 2-27



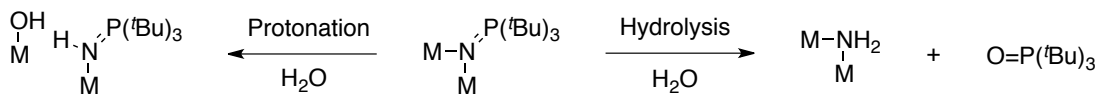
**Table 2-2.** A summary of the aerobic alkane oxidation reactions

Entry	Starting material	Major product	Scavenger	Temperature (°C)	Conversion (%)
1			CaH <sub>2</sub>	120	70
2			CaH <sub>2</sub>	120	40.8
3			3 Å M.S.	120	48.9
4			3 Å M.S.	120	5.3
5			CaH <sub>2</sub>	120	3.6
					4.3
6			CaH <sub>2</sub>	120	5.8
7			CaH <sub>2</sub>	120	8.9

8			3 Å M.S.	120	7.8
9			3 Å M.S.	150	3.3

In aerobic oxidation of alkanes to carbonyl compounds, water is expected to be the final byproduct, containing the hydrogen atoms from the alkane and one oxygen atom from molecular oxygen. However, by protonating and/or hydrolyzing phosphoramidate ligands, water could deactivate the nickel/cobalt cluster (Scheme 2-5). Therefore, a proton scavenger is normally required to maintain the reactivity of our catalysts. Generally,  $\text{CaH}_2$  or 3 Å molecular sieves are used in the experiments discussed to eliminate water from the reaction solutions.

### Scheme 2-5

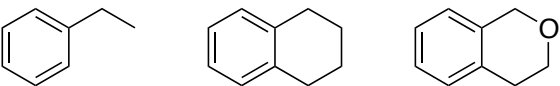
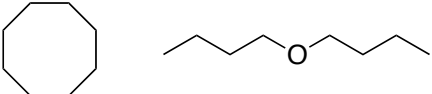


M: Co/ Ni with unspecified valency and ligands

In general, these oxidation reactions are heated to high temperatures (120 °C or above). Since the boiling points of most substrates are higher than 120 °C, the corresponding oxidation reactions can be performed in open Schlenk flasks or other glass reactors. To prevent organic solvent evaporation, a water-cooled condenser is connected to the reaction vessel. However, for substrates with lower boiling points, the reactions cannot be performed in an open system. As an alternative, these reactions were carried out in sealed vessels, which could be pressurized and heated to any desired temperature by immersion

in a thermostated oil bath. Substrates with high and low boiling points are categorized in Table 2-3.

**Table 2-3.** Two categories of substrates that have high or low boiling points

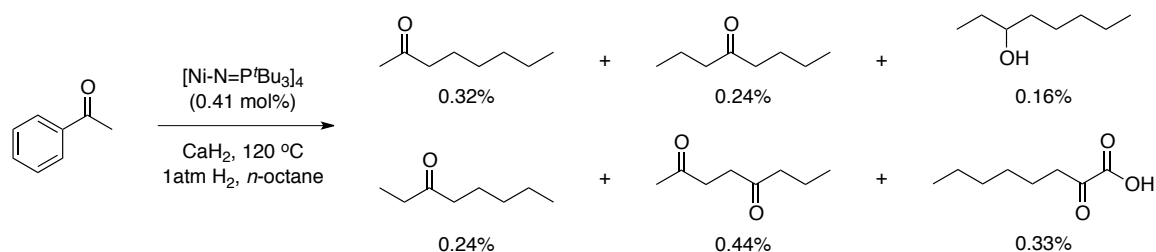
Substrates	Boiling point	Reaction apparatus
	> 120 °C	Open Schlenk flask
		
	< 85 °C	Sealed glass vessel

After conducting a thorough literature search, we find that the phosphoramidite-supported nickel-catalyzed aerobic oxidation reactions are unprecedented. In addition, these reactions possess several unique characteristics that are distinct from the known reactions. First, nickel is not commonly utilized in catalyzing aerobic alkane oxidation, whereas palladium, platinum, iron and copper are much more regularly employed as catalysts. Second, the majority of the reactions catalyzed by biological enzymes and biomimetic catalysts involve the addition of reducing reagents as an electron donor. However such a reducing reagent is *not required* in our nickel-catalyzed reactions. Though proton scavengers are indispensable in our reactions, scavengers normally are not required in literature procedures.

### 2.2.2 The story behind the discovery of the alkane oxidation reactions

Before a detailed discussion of individual oxidation reactions, I will present the interesting story behind this discovery. The discovery of alkane oxidation reactions is related to the study of a failed ketone hydrogenation experiment. While analyzing the reaction mixture of the nickel-catalyzed hydrogenation of acetophenone in octane solvent, we found no alcohol product was obtained. However, interestingly, a trace amount of ketone was discovered among the recovered starting material. A GC-MS analysis of the organic solution was conducted and showed the presence of 2-octanone with 0.32%, 3-octanone with 0.24%, 4-octanone with 0.24% and 2,5-octadione with 0.44% (Eq. 2-28). Based on the experimental observation and analysis, I deduced that the ketone residues were oxidation products of the solvent *n*-octane.

#### Equation 2-28

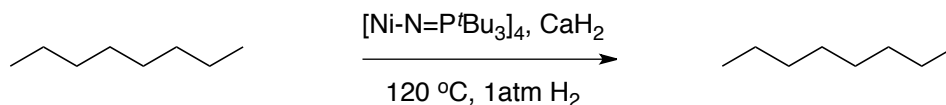


During that failed reaction, a small amount of molecular oxygen presumably leaked into the reaction vessel. After refilling the glass bomb with hydrogen, the color of the solution changed slowly from deep green to light brown. This is a strong indication that air has entered and “destroyed” the catalysts, probably through an error in using the hydrogen line. Not surprisingly, the acetophenone reduction did not afford any 1-phenylethanol as expected, even though that reaction normally proceeds successfully.

A close analysis of the GC-MS spectroscopy results revealed that various octanone isomers were present in the reaction mixture. As octanones were never detected in previous ester hydrogenation reactions, there is no chance of solvent and starting material contamination. In addition, the presence of a series of oxidation products eliminates the possibility of a single source contamination; only a catalytic oxidation reaction of the solvent was left to be the cause. Therefore, we concluded the ketones are the products of a catalytic aerobic oxidation of *n*-octane.

To test the hypothesis that nickel cluster can catalyze alkane oxidation reactions, a similar experiment was conducted to reproduce the result of *n*-octane oxidation. In this reaction, the nickel cluster was added to the *n*-octane solution containing CaH<sub>2</sub> (Eq. 2-29). The hydrogen line was deliberately open to air for a short period of time before fill the reaction vessel with H<sub>2</sub> gas. As observed before, the cluster turned brown after hydrogen gas was introduced. However, this reaction failed to produce the previously observed octanone products.

#### Equation 2-29



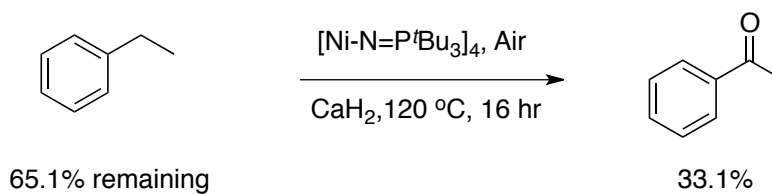
\* hydrogen line was temporarily open to air.

Despite of the failure to reproduce the *n*-octane oxidation, further experiments were carried out to realize a more general oxidation reactions. In place of *n*-octane, ethylbenzene was selected as a better substrate for the following reasons. First, ethylbenzene is oxidized more readily than *n*-octane due to the presence of activated benzylic C–H bonds. Second,

the high boiling point of ethylbenzene (136 °C) renders the reaction amenable to using an open system. Third, the proposed benzylic oxidation and the presence of an ethyl group would result in the formation of a ketone rather than an aldehyde product. Since ketones are more stable than aldehydes, this minimizes the possibility of further oxidation to form more complicated product mixtures.

Ethylbenzene oxidation was conducted with unrestrained exposure to air at elevated temperatures (Eq. 2-30). Calcium hydride was added as a scavenger, as the catalysts were believed to be sensitive to acidic molecules. Acetophenone was expected to be the product and water the only byproduct. A filter filled with desiccating reagent was attached to the reaction vessel to admit dry air. After the reaction was complete, the mixture was analyzed by both <sup>1</sup>H NMR and GC-MS spectroscopy. A significant amount of acetophenone was formed, giving a GC yield of 33.1%. This is the first successful aerobic oxidation reaction catalyzed by nickel cluster.

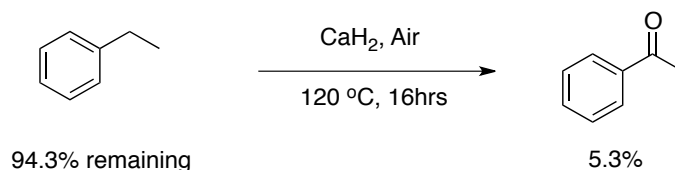
### Equation 2-30



To verify the role of the oxidized nickel cluster as a catalyst for ethylbenzene oxidation, a background experiment was set up at the same time (Eq. 2-31). This reaction was conducted without any nickel catalyst, while the rest of the reaction parameters were kept the same. The GC-MS analysis indicated the presence of 5.3% acetophenone in the product mixture. Though very small amount of acetophenone was observed in the control

experiment; the amount is significantly less than that obtained from the catalyzed reaction. Therefore, the result confirms the catalytic role of the nickel cluster in this oxidation reaction.

### Equation 2-31



#### 2.2.3 Reaction condition optimization using ethylbenzene

After the discovery of the oxidation reaction, ethylbenzene was used as a model compound for more detailed studies. The effect of catalyst, scavenger, temperature, oxidant and solvent has all been scrutinized individually. To obtain a full appreciation of the individual effects, control experiments were carried out carefully for each condition parameter.

In searching for the best catalyst, three experiments were conducted to compare the catalytic reactivity of nickel(I), cobalt(I) and methylnickel(II) clusters (Entry 3-5, Table 2-4).<sup>49,148</sup> The catalyst loading for each metal cluster was controlled in the range of 0.044-0.045 mol%. Meanwhile, an equal excess of molecular sieves was added to each reaction as water scavenger. The reactions were heated to 120 °C and the reactions were performed under a pure oxygen atmosphere. After the indicated reaction period, the organic product mixtures were submitted for GC-MS analysis. As outlined in entries 3-5, the GC results indicated that the nickel cluster catalyzed reaction afforded 51.3% of acetophenone, while the other two reactions did not produce any appreciable amount of ketone product. In

conclusion, nickel cluster is proved to be the only efficient catalyst and was therefore chosen as the catalyst for further oxidation reactions.

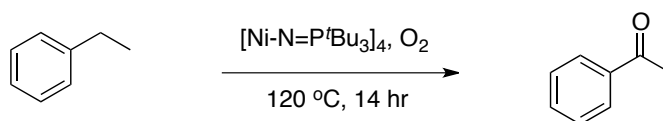
**Table 2-4.** Oxidation of ethylbenzene



Entry	Catalyst	Catalyst Load (mol%)	Scavenger	Oxidant	Reaction time (hr)	Temp (°C)	GC yield (%)
1	-	-	CaH <sub>2</sub>	O <sub>2</sub>	16	120	5.3
2	-	-	3 Å M.S.	O <sub>2</sub>	14	120	0
3	[Ni-N=P <sup>t</sup> Bu <sub>3</sub> ] <sub>4</sub>	0.044	3 Å M.S.	O <sub>2</sub>	14	120	51.3
4	[Me-Co-N=PEt <sub>3</sub> ] <sub>4</sub>	0.044	3 Å M.S.	O <sub>2</sub>	14	120	0
5	[Co-N=P <sup>t</sup> Bu <sub>3</sub> ] <sub>4</sub>	0.044	3 Å M.S.	O <sub>2</sub>	14	120	0
6	[Ni-N=P <sup>t</sup> Bu <sub>3</sub> ] <sub>4</sub>	0.044	CaH <sub>2</sub>	O <sub>2</sub>	14	120	52.6
7	[Ni-N=P <sup>t</sup> Bu <sub>3</sub> ] <sub>4</sub>	0.044	3 Å M.S.	Air	14	120	19.4
8	[Ni-N=P <sup>t</sup> Bu <sub>3</sub> ] <sub>4</sub>	0.025	3 Å M.S.	O <sub>2</sub>	16	100	28.7
9	[Ni-N=P <sup>t</sup> Bu <sub>3</sub> ] <sub>4</sub>	0.050	3 Å M.S.	O <sub>2</sub>	16	80	0.7
10	[Ni-N=P <sup>t</sup> Bu <sub>3</sub> ] <sub>4</sub>	0.040	-	O <sub>2</sub>	17	120	31.0

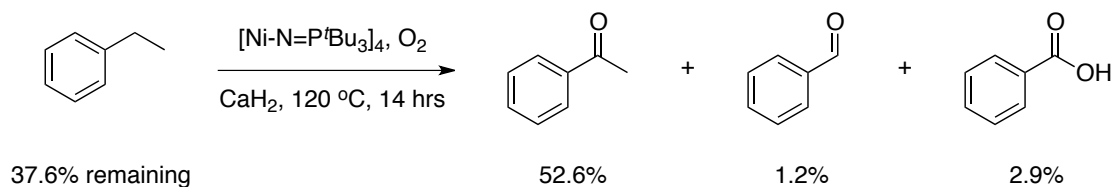
The effects of scavenger have also been studied (entries 3, 6 and 10, Table 2-4). To examine if the scavenger is indispensable, an ethylbenzene oxidation reaction was conducted without scavenger (Eq. 2-32). The reaction surprisingly afforded 31.0% acetophenone from GC-MS analysis. In contrast, the yield increased to 51.3% for the reaction using 3 Å molecular sieves. Therefore, addition of a scavenger is beneficial, but perhaps not essential for the oxidation reaction to occur efficiently.

### Equation 2-32

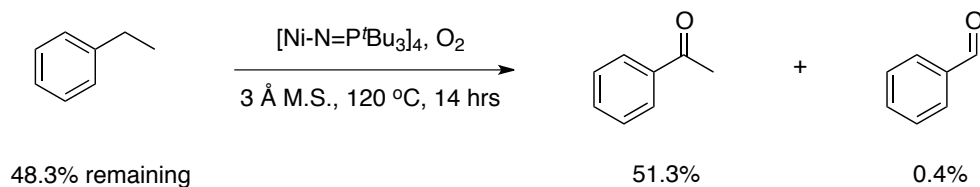


Having proved the benefits of scavenger addition, experiments were set to identify the best scavenger for the reaction. Parallel reactions were conducted to evaluate the relative effectiveness of calcium hydride and 3 Å molecular sieves, in which the rest of the reaction parameters were kept the same. Based on GC-MS analysis, the yield of acetophenone was 52.6% and 51.3% for reactions using calcium hydride and 3 Å molecular sieves, respectively (Eq., 2-34). The result suggests that 3 Å molecular sieves acts similarly comparing to calcium hydride as a scavenger.

### Equation 2-33



### Equation 2-34



The scavenger not only has an impact on the reaction yield, but also affects the product distribution. For the reaction using 3 Å molecular sieves, the minor product was benzaldehyde. For the reaction using calcium hydride, benzoic acid was formed as the major byproduct (Eq. 2-34). More specifically, the formation of both benzoic acid and benzaldehyde involve C–C bond activation; details will be discussed in a separated section. By comparing the minor products, the reaction using 3 Å molecular sieves appears to be cleaner. In the end, 3 Å molecular sieves were selected as the better scavenger based on the higher conversion of acetophenone and reduced byproduct formation.

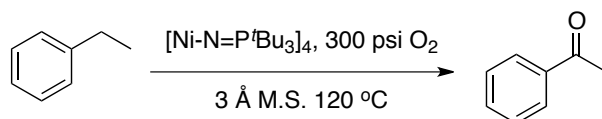
The temperature effect on the oxidation reaction has also been studied. Again, parallel reactions were set, keeping other reaction parameters the same. The ethylbenzene oxidation was conducted at various temperatures, from 120 °C, to 100 °C, to 80 °C (Table 2-4, Entries 3, 8 and 9). The product mixture after reaction was analyzed by <sup>1</sup>H NMR spectroscopy. Based on standard derivation from the <sup>1</sup>H NMR spectrum, the conversion to acetophenone from the reaction at 80 °C was just 0.7%. In comparison, the conversion for the reaction at 100 °C was much higher at 28.7%. The reaction at 120 °C afforded the best conversion, at about 51.3%. In summary, this study indicates that the reaction temperature must be maintained above 100 °C in order to obtain good yields.

Different sources of molecular oxygen were also evaluated to reveal the oxidant influence on the reaction yield. The original reactions were discovered under atmospheric pressure of dry air in which molecular oxygen acts as the oxidizing reagent. A subsequent reaction conducted under a continuous flow of pure oxygen turned out to be successful as well. Two comparative experiments were set up using air and pure molecular oxygen. The reaction using molecular oxygen afforded a much higher yield of acetophenone at the same reaction temperature in the same amount of time. Based on GC-MS analysis, the yield for reaction

under air is 19.4%, while for pure oxygen is 51.3%. Therefore, pure oxygen was selected as the best oxidant for this reaction.

The effects of oxygen pressure have also been studied. The previous reactions were typically performed under a continuous flow of pure oxygen gas. In such an open system, molecular oxygen is at atmospheric pressure. For comparison, an experiment was conducted under higher pressure of oxygen in a steel autoclave (Eq. 2-35). The reaction was carried out at an oxygen pressure of 300 psi, applied before heating, while other reaction parameters remained the same. GC-MS analysis detected 68.3% of the starting ethylbenzene, while the yield of acetophenone was merely 8.1%. The yield of the byproduct 1-phenylethanol increased to 11.4%, which is much higher than in the previous reactions (1-2%). The increase of molecular oxygen pressure thus results in a lower yield of the oxidized products, a rate inhibition similar to that observed under hydrogen in the corresponding reduction reactions mediated by this catalyst.

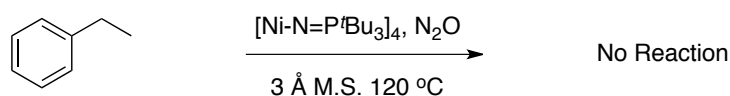
### Equation 2-35



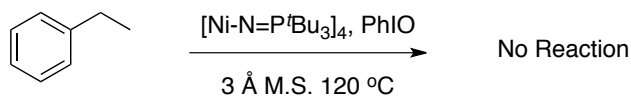
After molecular oxygen was identified as an ideal oxidant, other oxidizing reagents were tested as well, including iodosobenzene and anhydrous nitrous oxide. Due to the gaseous state of nitrous oxide, the corresponding ethylbenzene oxidation reaction was conducted in an open flask under a continuous flow of nitrous oxide (Eq. 2-36). However, after the reaction, ethylbenzene remained and no oxidized products were detected. For the reaction using iodosobenzene as the oxidizing reagent, the ethylbenzene oxidation reaction was conducted in a sealed glass bomb (Eq. 2-37). Unfortunately, the oxidation reaction again

did not occur. Therefore, neither nitrous oxide nor iodosobenzene can be utilized as an alternative oxidant for the oxidation reactions. Under current circumstances, these oxidizing reagents were unable to activate nickel cluster **8**, leaving molecular oxygen the best oxidant for the reaction.

### Equation 2-36

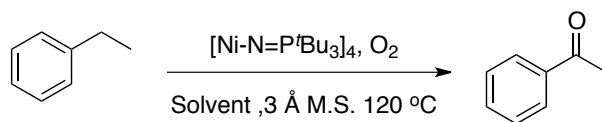


### Equation 2-37



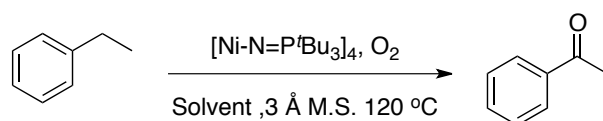
The previous oxidation reactions were all conducted in neat organic substrate as the medium. However, this excludes solid substrates from being oxidized without the introduction of an efficient inert solvent to the system. Therefore solvent effects for this reaction were assessed. Experiments were carried out in which ethylbenzene oxidation reactions were conducted in various solvents, including *n*-octane, toluene, dimethylacetamide (DMA), perfluorohexane, and trifluoromethylbenzene (Eq. 2-38).

### Equation 2-38



The results are presented in Table 2-5; none of the solvents appears to be ideal. The non-polar solvents tested were *n*-octane and toluene, as neither material is oxidized as neat substrates under the reaction conditions. The most polar solvent tested was DMA, which might act as an ancillary donor ligand. Fluorinated solvents are known to dissolve oxygen more readily than hydrocarbons.<sup>150</sup> However, the first fluorinated solvent tested, perfluorohexane, turned out not to be miscible with ethylbenzene. Alternatively, trifluoromethylbenzene could be used to dissolve the substrate, forming a 2.9 M solution. However, the corresponding oxidation reaction afforded a very low GC yield (0.1%) of acetophenone, presumably from the uncatalyzed background reaction. In conclusion, although various solvents have been tested for ethylbenzene oxidation, none of the corresponding reactions proceed satisfactorily.

**Table 2-5.** Solvent optimization for ethylbenzene oxidation<sup>a</sup>



Entry	Solvent	Concentration (M)	Catalyst load (mol%)	Scavenger	Reaction time (hr)	Conversion <sup>b</sup> (%)	TON/TOF
1	<i>n</i> C <sub>8</sub> H <sub>18</sub>	0.6	1.2	CaH <sub>2</sub>	16	0	0/0
2	PhCH <sub>3</sub>	1.0	8.9	CaH <sub>2</sub>	16	0	0/0
3	<i>n</i> -C <sub>6</sub> F <sub>14</sub>	immiscible	2.0	CaH <sub>2</sub>	16	1.4	7/0.43
4	PhCF <sub>3</sub>	2.9	1.8	3 Å M.S.	16	0.1	0.6/0.03
5	DMA	1.4	2.7	3 Å M.S.	17	0	0/0

a. The catalyst is nickel(I) cluster **8**, [Ni-N=P<sup>t</sup>Bu<sub>3</sub>]<sub>4</sub> and reaction conditions are listed in Eq. 2-38

b. GC yield of acetophenone

A series of control experiments has thus provided valuable information on individual reaction parameters. In summary, the phosphoranimide-supported nickel(I) cluster is the most efficient catalyst, although some of the results remain difficult to rationalize. The use of 3 Å molecular sieves, a less aggressive scavenger than calcium hydride, and dry molecular oxygen is the most effective oxidizing reagent. The optimized reaction is conducted under one atm of molecular oxygen in neat organic substrate at temperatures of at least 100 °C.

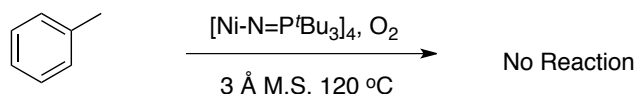
#### *2.2.4 Substrate scope of the oxidation reactions*

The condition optimization study established the basis for further scope exploration. The substrates mainly cover alkyl arenes containing benzylic C–H bond, molecules containing heteroatoms such as ethers and amines, and hydrocarbons consisting of only sp<sup>3</sup> C–C and C–H bonds. The alkyl arenes evaluated include toluene, ethylbenzene, tetralin and isochroman, the latter containing an additional ethereal oxygen.

##### *2.2.4.1. Benzylic oxidation*

Toluene is an attractive substrate for oxidation reaction, as it is readily available on industrial scale. Its oxidized products, benzyl alcohol, benzaldehyde and benzoic acid, are valuable chemicals for the production of pharmaceuticals, dyes, food preservatives, perfumes, etc.<sup>151</sup> The toluene oxidation reaction was performed under optimized conditions (Eq. 2-39). Should benzoic acid be formed, it would be deprotonated by the strongly basic scavenger and precipitate, so the reaction mixture was quenched with dilute hydrochloric acid. The organic solution was then separated out and analyzed by GC-MS spectroscopy. However, to our dismay, the reaction did not afford any oxidation products.

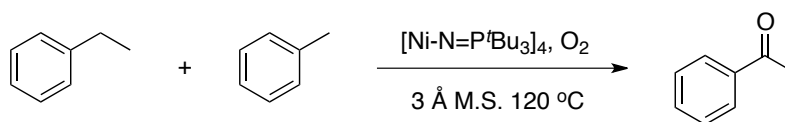
### Equation 2-39



The result is somewhat surprising, as the benzylic C-H bond of toluene is just slightly stronger than that of ethylbenzene. The bond dissociation energy (BDE) for benzylic C-H bond in toluene is about  $88.0 \pm 1.0 \text{ kcal mol}^{-1}$ , while BDE of benzylic C-H bond in ethylbenzene is  $85.4 \pm 1.5 \text{ kcal mol}^{-1}$ .<sup>152</sup> Oxidation of toluene is not expected to be considerably harder than that of ethylbenzene.

Another experiment was conducted in a mixture of toluene and ethylbenzene with 1:1 molar ratio (Eq. 2-40). In that reaction, ethylbenzene is selectively oxidized to acetophenone, whereas toluene remains completely inert. The experiment suggests, inexplicably, that ethylbenzene can be selectively oxidized in the presence of toluene.

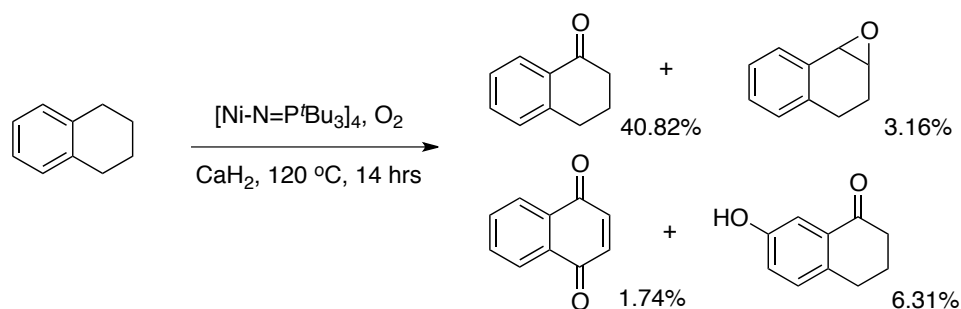
### Equation 2-40



Tetralin was next selected as a substrate. It is structurally similar to ethylbenzene, but contains a cyclic aliphatic ring. As a consequence, the oxidized products could contain “overoxidized” diketone and quinone derivatives. The reaction was conducted in neat tetralin under optimized conditions (Eq. 2-41). The major product was  $\alpha$ -tetralone, formed

in excellent conversion from the oxidation at only one of the two benzylic positions. In addition, minor amounts of epoxide, quinone and phenol derivatives were also detected.

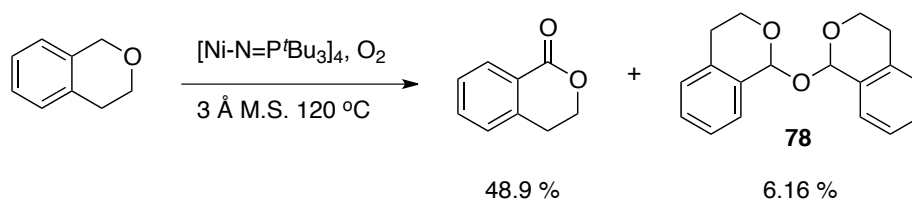
### Equation 2-41



Isochroman oxidation is of great interest, as it not only acts as a new example for the oxidation reaction, but may also produce an interesting lactone for use in the ester hydrogenation reaction. Isochroman has two distinct benzylic positions, one of which is adjacent to an oxygen atom and therefore is doubly activated, at least toward radical oxidation. If the oxidation occurs predominately at the more activated benzylic position, the reaction would selectively afford the lactone, 3,4-dihydroisocoumarin.

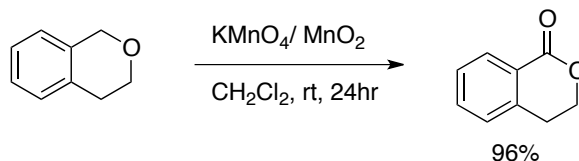
The isochroman oxidation reaction was conducted using 3 Å molecular sieves as a scavenger (Eq. 2-42). Calcium hydride was excluded, as it would be converted to calcium hydroxide inducing lactone hydrolysis. The oxidation reaction afforded 3,4-dihydroisocoumarin in an isolated yield of 48.9% after heating to 120 °C for 16 h. The reaction was conducted neat with a 3.3 g scale and a catalyst loading of  $3.9 \times 10^{-4}$  mol% (10.4 mg). The catalytic reaction was impressively efficient. The turnover number with respect to the tetrametallic nickel cluster is 1250, while the corresponding turnover frequency is  $75.8\text{ h}^{-1}$  at 120 °C.

### Equation 2-42



A control experiment was conducted under the same reaction conditions in the absence of nickel cluster **8**, however no oxidized product was formed. The efficiency of nickel catalyst has been further validated by comparing with literature reactions, in which isochroman oxidation was reported using stoichiometric oxidizing reagents such as the  $\text{KMnO}_4/\text{MnO}_2$  (1: 3) mixture (Eq. 2-43).<sup>153</sup> However, in order to obtain the same amount of lactone product, a substantial 25.0 grams of the  $\text{KMnO}_4/\text{MnO}_2$  mixture is required.

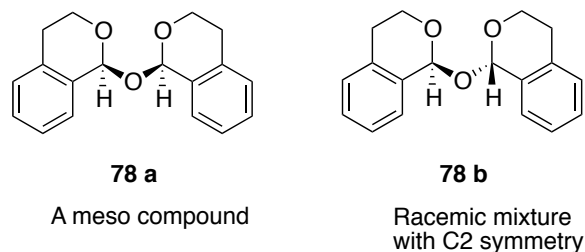
### Equation 2-43



As a byproduct in the isochroman oxidation, 1,1'-oxodiisochromane **78** was obtained in an isolated yield of 6.2%. The compound was characterized by  $^1\text{H}$  and  $^{13}\text{C}$  NMR spectroscopy. Since nine carbon resonances can be clearly identified in the  $^{13}\text{C}$  NMR spectrum, only a single diastereomer must be present. The diastereomer is either a meso compound **78 a** or a racemic mixture **78 b** with  $\text{C}_2$  symmetry (Figure 2-2). The structure of 1,1'-

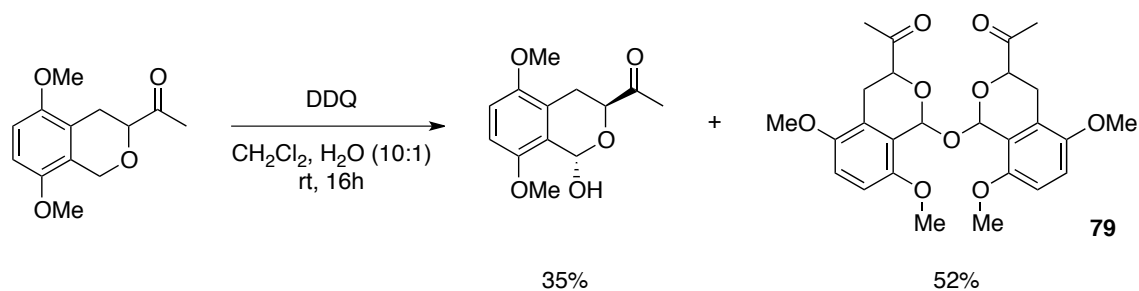
oxodiisochromane **78** was confirmed by comparing to the literature data, indicating that it was the racemic pair **78 b**.

**Figure 2-2.** Diastereomers of 1,1'-oxodiisochromane

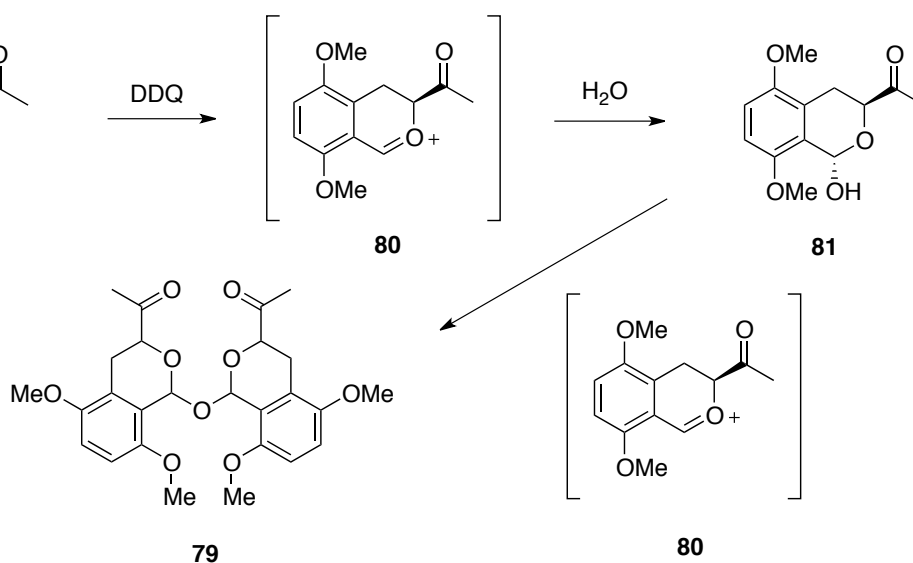


In literature, only two related isochroman oxidation reactions producing 1,1'-oxodiisochromane derivatives have been reported. The first utilizes DDQ as the oxidant and the oxidative coupling product 1,1'-oxodiisochromane derivative **79** was observed as the major product (Eq. 2-44).<sup>154</sup> The formation 1,1'-oxodiisochromane **79** is also diastereoselective, but the detailed stereochemistry remains unclear. In the proposed mechanism,<sup>154</sup> DDQ abstracts a benzylic hydride to form a carbocationic intermediate **80**, which is trapped by water to give a lactol derivative **81**. The lactol **81** then acts as a nucleophile to attack the cation **80**, affording the 1,1'-oxodiisochromane derivative **79** (Scheme 2-6).

### Equation 2-44



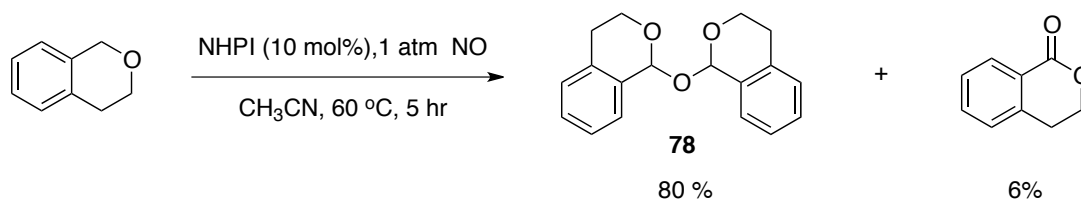
### Scheme 2-6



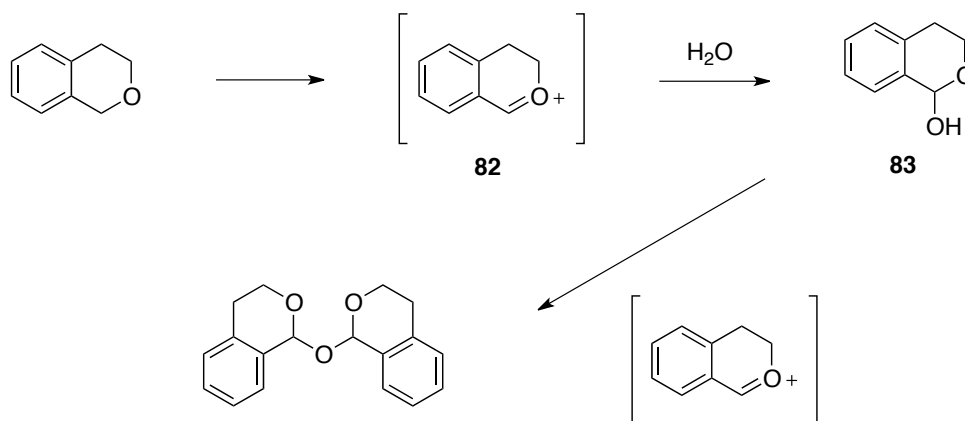
1,1'-oxodihydroisochroman **78** can also be obtained by *N*-hydroxyphthalimide-catalyzed isochroman oxidation using nitric oxide (Eq. 2-45).<sup>155</sup> The reaction is also diastereoselective and the product was determined by X-ray crystallography possessing C<sub>2</sub> symmetry. The proposed mechanism again involves a carbocation intermediate **82** and

lactol **83** and equilibration to the thermodynamically preferred diastereomer **78 b** (Scheme 2-7).

### Equation 2-45



### Scheme 2-7



For nickel-catalyzed isochroman oxidation, it is presumed that the formation of 1,1'-oxodiisochroman **78** involves the same mechanistic pathway. Carbocation intermediate **82** can be formed from a hydride abstraction by the oxygenated nickel cluster. Since water is generated as a byproduct of the lactone formation, it could react with a carbocationic intermediate **82** to form lactol **83**. The lactol further reacts with cation **82** to form the product **78 b**.

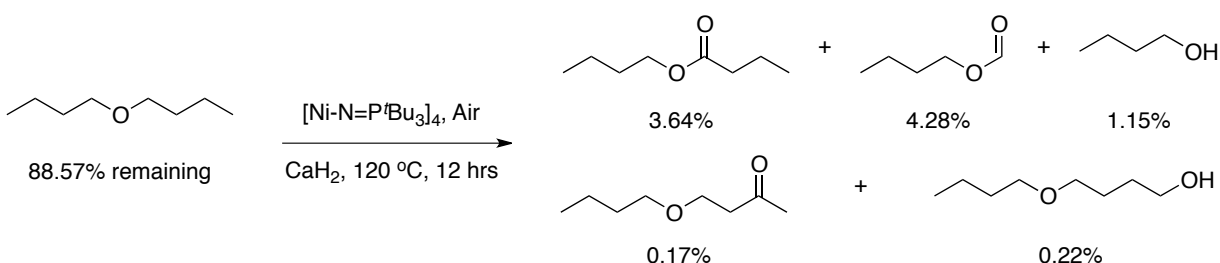
The substrates discussed so far are all alkyl arenes that possess benzylic C–H bond. In general, the oxidation occurs selectively at the benzylic position to afford mainly ketone/lactone derivatives. The substrates that can be readily oxidized include ethylbenzene, tetralin and isochroman, all possessing methylene groups at benzylic positions. However, the oxidation of toluene cannot be realized under current conditions, for reasons that are not at all obvious.

#### *2.2.4.2 Heteroatom-containing hydrocarbon substrates*

Besides the alkylarenes, the oxidation of organic compounds containing nitrogen and oxygen heteroatoms was also explored. Similar to the phenyl group, the heteroatoms in these compounds also possess electron-withdrawing properties, but they can also stabilize radical and carbocationic intermediates via  $n$ -electron donation. The oxidation would thus occur preferably at one of the alpha positions. As a result, formation of ester and amide products is expected from ether and amine oxidation, respectively.

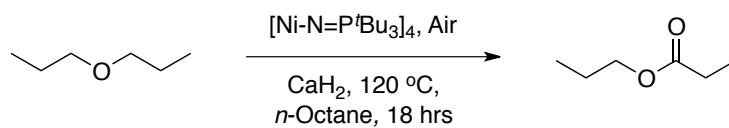
For the ether oxidation reactions, both linear and cyclic ether molecules have been investigated, including di-*n*-butyl ether, di-*n*-propyl ether and tetrahydrofuran. Di-*n*-butylether oxidation was conducted in an open flask (Eq. 2-46). The oxidized mainly include butyl butyrate and butyl formate; however, both were formed in low yields. The formation of the latter product involves an unexpected C-C bond activation and is assumed to be a secondary product.

### Equation 2-46



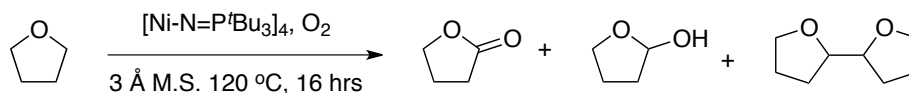
Since di-*n*-propyl ether has a much lower boiling point (90 °C) than di-*n*-butyl ether (142 °C), the oxidation reaction was performed as a solution in *n*-octane (Eq. 2-47). Despite the fact that *n*-octane failed to act as an efficient solvent in ethylbenzene optimization, it appears to be effective in the dipropyl ether oxidation. The reaction afforded a 5.8% yield of *n*-propyl propionate with most ether starting material remaining unreacted.

### Equation 2-47

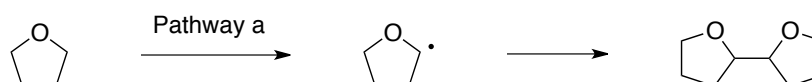


As a cyclic ether and common solvent, THF was also used as a substrate for oxidation. Since THF has a low boiling point (66 °C), the reaction was performed in a sealed glass bomb, degassed and then filled with molecular oxygen (Eq. 2-48). The reaction returned a low conversion, producing  $\gamma$ -butyrolactone and very minor amounts of 2-hydroxyltetrahydrofuran and the dimeric 2,2'-bis ether. It appears that the dimeric product arises from the dimerization of two oxygen-stabilized cyclic radicals, which may reflect intermediates generated in the oxidation process (Scheme 2-8).

### Equation 2-48

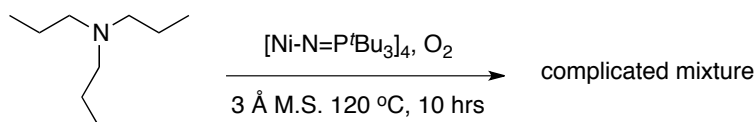


### Scheme 2-8



Tri-*n*-propylamine was also examined for the aerobic oxidation reaction. With a conveniently high boiling point (156 °C), the reaction was performed in an open flask (Eq. 2-49). The organic solution turned reddish during the reaction interval and was submitted for GC-MS analysis. The results showed that the 74.4% of starting material remains and no major product could be conclusively identified in the complicated reaction mixture. Therefore, although the reaction works, it failed to provide any insight into amine oxidation.

### Equation 2-49



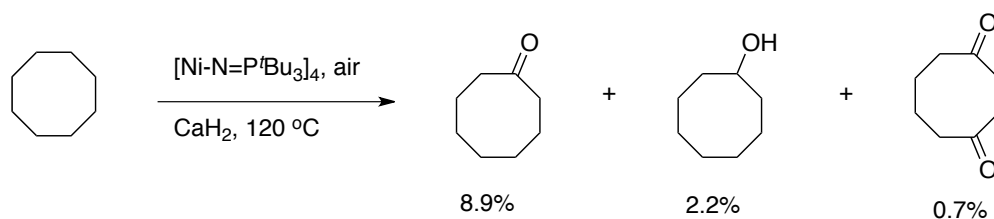
#### 2.2.4.3 Saturated hydrocarbons

The saturated hydrocarbons are more challenging substrates than those containing activating groups, as only  $\text{sp}^3$  C-H and  $\text{sp}^3$  C-C bonds are present. The saturated hydrocarbons investigated include cyclooctane, cyclohexane, adamantane, *n*-octane, 2,5,5-

trimethylpentane and *n*-hexane. Oxidation of the first three aliphatic compounds was successful, whereas the last three remained inactive.

Cyclooctane is the first aliphatic hydrocarbons that can be oxidized efficiently using the nickel catalyst. The oxidation of cyclooctane (149 °C) was conducted in an open flask (Eq. 2-50). After the allotted reaction time, the mixture was analyzed by GC-MS spectroscopy. The results showed that the reaction afforded an 8.9% conversion to cyclooctanone, 2.2% of cyclooctanol, and 0.7% of 1,4-cyclooctadione. The remaining 84% of the mixture was unreacted starting material. Generally speaking, ketones was the major products from cyclooctane oxidation, as observed in alkylarene oxidation.

#### Equation 2-50

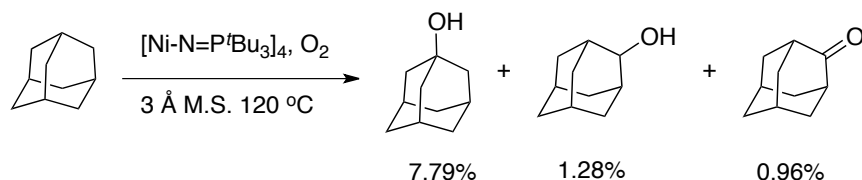


The experiment for adamantane oxidation was technically more challenging. First, adamantane has a very high melting point (270 °C), high above the desired reaction temperature (120 °C). Therefore a solvent was required to dissolve both adamantane and the nickel cluster **8**. Second, adamantane can sublime upon heating, resulting in loss of the starting material. To prevent adamantane sublimation, the reaction was performed in a sealed vessel.

The adamantane oxidation reaction was conducted in a glass bomb filled with pure oxygen (Eq. 2-51). A small amount of hexane was added as a solvent, while activated 3 Å molecular

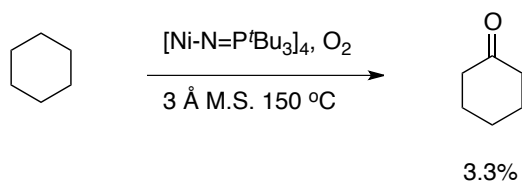
sieves were added as the water scavenger. A GC-MS analysis revealed that about 10% of starting material had been oxidized. The GC yields for 1-adamantanol, 2-adamantanol and 2-adamantanone were 7.8%, 1.3% and 1.0%, respectively. The major product, 1-adamantanol, was derived from tertiary C–H bond activation. On the other hand, both 2-adamantanol and 2-adamantanone were produced via the activation of the secondary C–H bonds. In an adamantane molecule, the number of tertiary C–H bond is four, while secondary sixteen. The preference for activating statistically less abundant tertiary C–H bond strongly suggests the radical character of the reaction.

### Equation 2-51



As a volatile organic liquid, the cyclohexane (80 °C) oxidation was also performed in a sealed glass bomb (Eq. 2-52). The reactor was filled with pure oxygen and 3 Å molecular sieves were added as the scavenger. The external temperature was raised to 150 °C. However, based on the GC-MS analysis, the reaction only afforded 3.3% conversion to cyclohexanone. Though the yield of this reaction is low, it produces ketone as the exclusive product.

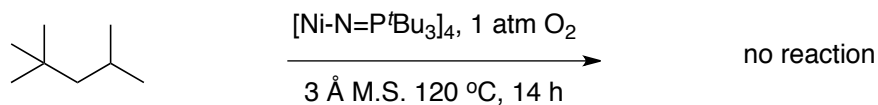
### Equation 2-52



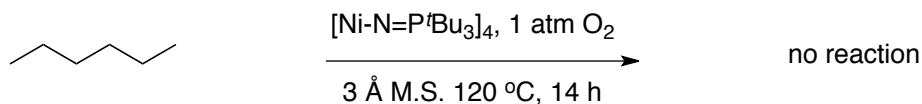
Other aliphatic substrates including *n*-octane, 2,2,4-trimethylpentane and hexane, were more resistant to oxidation. In one *n*-octane oxidation experiment, the reaction temperature was maintained at 150 °C for 14 h. Though the original discovery was inspired by the observation of *n*-octane oxidation, the reaction conditions we developed appear to be incapable of oxidizing *n*-octane.

2,2,4-trimethylpentane was selected as a substrate because it possess primary, secondary and tertiary C–H bonds in a single substrate (Eq. 2-53). Unfortunately, no oxidized products were found in the reaction mixture. Hexane oxidation reactions conducted in a sealed glass bomb also failed to generate any oxygenated products (Eq. 2-54). In conclusion, the catalysts appear to be effective only toward cyclic hydrocarbons and electronically activated aliphatic compounds.

### Equation 2-53



### Equation 2-54

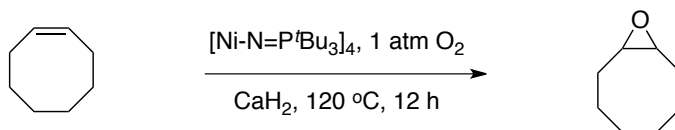


The experimental results suggest that the oxidation of linear hydrocarbons is significantly more challenging than cyclic hydrocarbons. The most significant difference is observed between *n*-octane and cyclooctane: cyclooctane can be readily oxidized whereas *n*-octane remains inert. In general, cyclic alkanes have lower steric hindrance and lower entropy than the corresponding linear alkanes.<sup>156</sup> In terms of bond dissociation energies, secondary C–H bond strengths in both linear and cyclic alkane are rather similar.<sup>152</sup> The preference for cyclic alkane oxidation is more likely to be associated with reaction kinetics, with both steric and entropic contribution to the barrier.

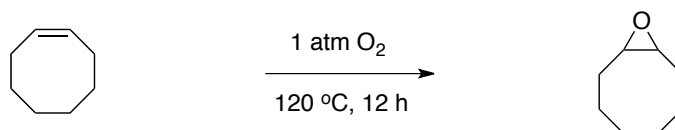
#### 2.2.4.4 Other functionalized substrates

In addition to the alkanes, functionalized compounds that have been studied include alkene, alcohol, and ketone derivatives. For alkene oxidation, the reaction of both ethylene and cyclohexene result in unidentified “decomposition” products. Cyclooctene was oxidized to the corresponding epoxide (Eq. 2-55), but a control experiment showed that the reaction occurs even in the absence of any catalyst (Eq. 2-56).

### Equation 2-55

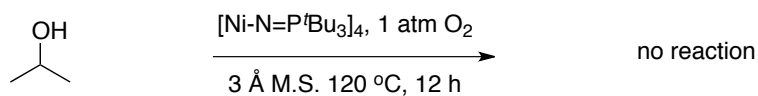


### Equation 2-56



In order to determine whether the alcohol is an intermediate in ketone formation from the alkane, the oxidation of isopropanol was investigated. To prepare for the reaction, isopropanol was carefully desiccated and degassed (see experimental section). The reaction was performed in a sealed glass bomb using 3 Å molecular sieves as the scavenger (Eq. 2-57). The reaction failed to afford acetone, although it is possible that the catalyst decomposed rapidly in neat isopropanol.

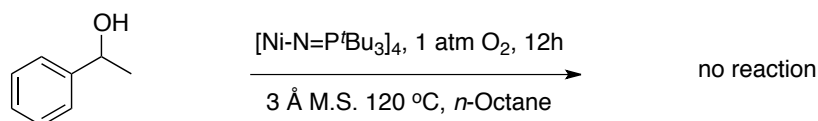
### Equation 2-57



To reduce the possibility of alcohol-induced catalyst decomposition, the second alcohol oxidation was performed in *n*-octane solution. For this reaction, 1-phenylethanol was used as the substrate, as it would be the intermediate in ethylbenzene oxidation (Eq. 2-58). Once again, the reaction failed to produce acetophenone or benzoic acid. During the work-up procedure, hydrochloric acid induced formation of 1-chloroethyl benzene from the recovered alcohol. Overall, the alcohol oxidation to ketones cannot be realized in either

neat substrate or diluted solution. These results support the argument that alcohol is not an intermediate in nickel-catalyzed alkane oxidation.

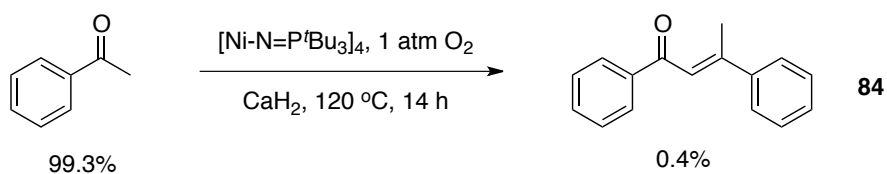
### Equation 2-58



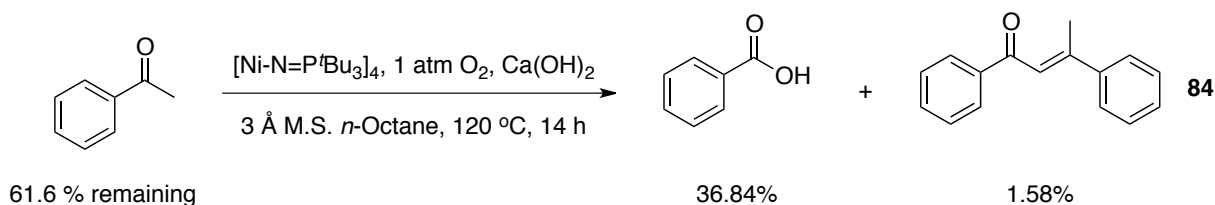
Besides alkenes and alcohols, compounds already containing a ketone group were also selected as substrates. Ketone oxidation might be helpful in understanding the origin of the benzoic acid in the ethylbenzene oxidation, but only when calcium hydride and not 3 Å molecular sieves were used as the scavenger. One of the possibilities we propose is that benzoic acid is formed through an oxidative C–C bond cleavage of acetophenone.

When acetophenone was subjected to catalytic oxidation in the presence of  $\text{CaH}_2$ , no benzoic acid was isolated (Eq. 2-59). 99.3% of the acetophenone was recovered; only 0.40% conversion to an aldol product **84** was detected by GC-MS analysis. To the contrary, when  $\text{Ca}(\text{OH})_2$  was used in place of  $\text{CaH}_2$ , 61.6% of acetophenone remained unreacted, while 36.8% conversion to benzoic acid was observed, along with 1.58% conversion to the enone **84** (Eq. 2-60). The results suggest that  $\text{Ca}(\text{OH})_2$  participates directly in the catalytic C–C bond cleavage of acetophenone.

### Equation 2-59

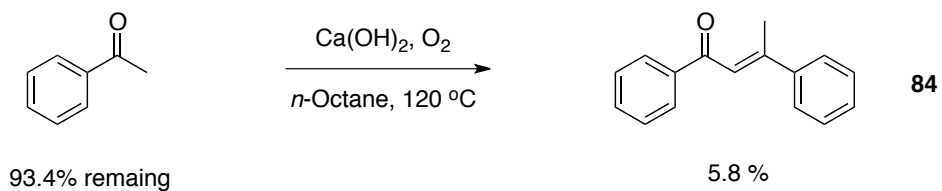


### Equation 2-60



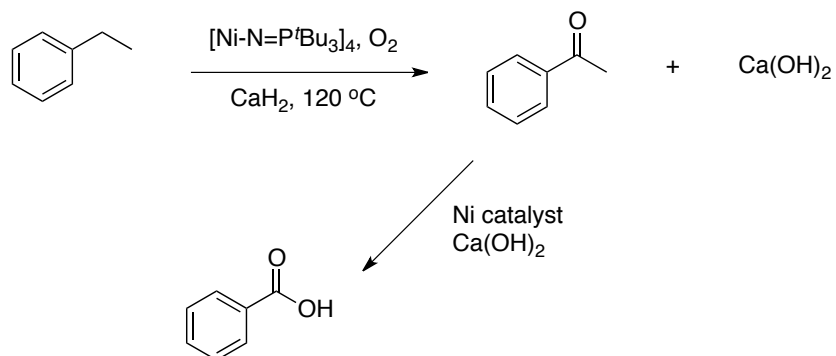
To prove the catalytic role of the nickel cluster **8**, an acetophenone oxidation experiment was performed with the presence of oxygen and  $\text{Ca}(\text{OH})_2$ , but absence of catalyst (Eq. 2-61). The reaction again afforded the enone aldol product, but not benzoic acid. Therefore, acetophenone oxidation to benzoic acid requires the presence of both nickel catalyst and  $\text{Ca}(\text{OH})_2$ . This reaction merits further investigation.

### Equation 2-61



Considering the results of these experiments, the benzoic acid formation in ethylbenzene oxidation reaction using  $\text{CaH}_2$  as the scavenger can be rationalized.  $\text{CaH}_2$  does not participate in the oxidative C–C bond cleavage of acetophenone directly. However, when  $\text{H}_2\text{O}$  is formed as a byproduct from the oxidation reaction, it reacts with  $\text{CaH}_2$  to form  $\text{Ca}(\text{OH})_2$  *in situ*. The presence of  $\text{Ca}(\text{OH})_2$  facilitates the oxidative cleavage of acetophenone and produces benzoic acid as the product (Scheme 2-9).

### Scheme 2-9

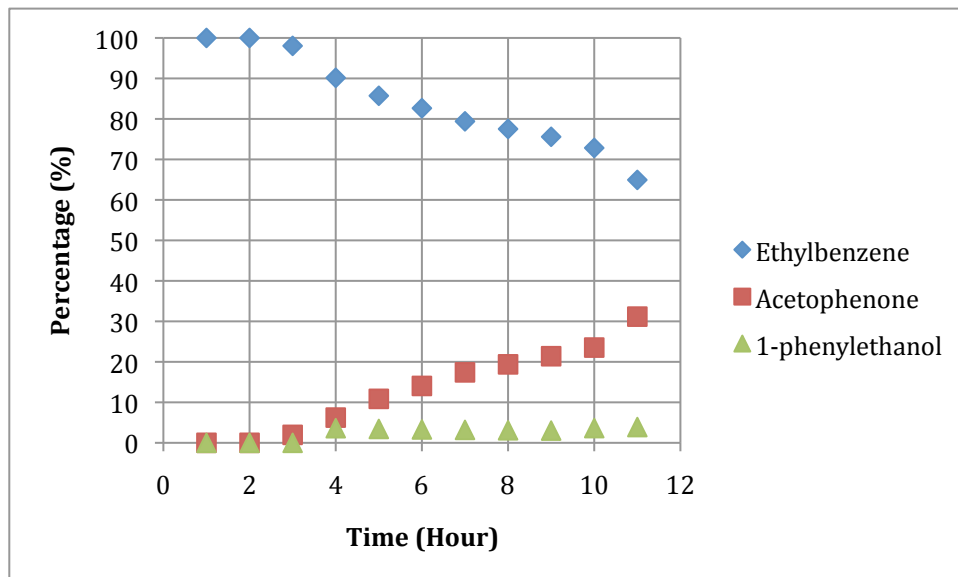


Oxidation of aryl ketones to the corresponding benzoic acids involves C–C bond activation. Such transformations have been reasonably well documented in literature. A variety of conditions have been reported for this oxidative cleavage, including several using molecular oxygen as the oxidant: photooxidation with catalytic  $\text{CBr}_4$ ,<sup>157</sup> oxidation catalyzed by electron-deficient nitroarenes,<sup>158</sup> and aerobic reaction using  $\text{Mn}(\text{NO}_3)_2$  catalyst in combination with  $\text{Co}(\text{NO}_3)_2$  or  $\text{Cu}(\text{NO}_3)_2$ ,<sup>159</sup> among others.

### 2.2.5 Mechanistic studies: the alkane oxidation reaction

The ethylbenzene oxidation was monitored by  $^1\text{H}$  NMR spectroscopy, sampling the reaction mixture every hour. From the  $^1\text{H}$  NMR integration, the conversion of ethylbenzene to acetophenone and 1-phenylethanol can be calculated. The resulting graph of ethylbenzene conversion is plotted with respect to the reaction time (Graph 2-1).

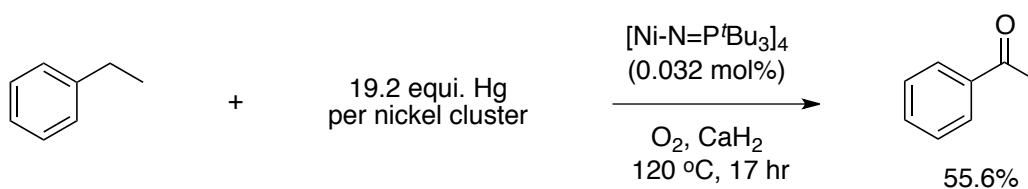
**Graph 2-1. Oxidation of ethylbenzene monitored by  $^1\text{H}$  NMR**



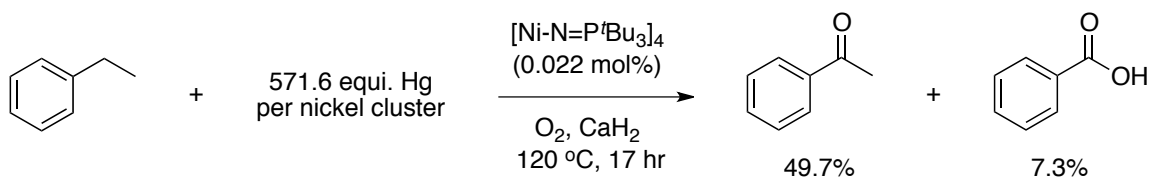
This experiment reveals an induction period for catalyst activation: the oxidation reaction starts roughly two hours after heating and maintains at a steady reaction rate afterwards. Meanwhile, the concentration of 1-phenylethanol remains low without noticeable increase throughout the monitoring period.

Preliminary experiments have also been performed to determine if the active alkane oxidation catalyst is homogeneous or heterogeneous. Two reactions were conducted in the presence of excess elemental mercury.<sup>79</sup> The initial ethylbenzene oxidation was conducted using a ratio of 19.2 : 1.0 mercury : catalyst. The reaction proceeded to acetophenone with a GC yield of 55.6% along with small amount of benzoic acid (Eq. 2-62) A second reaction was performed with significantly increased mercury loading, 571.6 equivalents of mercury with respect to nickel(I) cluster **8** (Eq. 2-63). This reaction again afforded acetophenone and benzoic acid in a GC yield of 49.7% and 7.3%, respectively, very similar to the reaction done in the absence of Hg(0). Furthermore, 2,3-diphenylbutane was also generated in the second reaction, giving a GC yield of 1.8%. Overall, addition of mercury does not suppress the alkane oxidation reaction, but does influence the product distribution. This preliminary result does not prove that the primary alkane oxidation catalyst is heterogeneous. More experiments are needed to determine if the active catalyst is homogeneous or heterogeneous.

### Equation 2-62



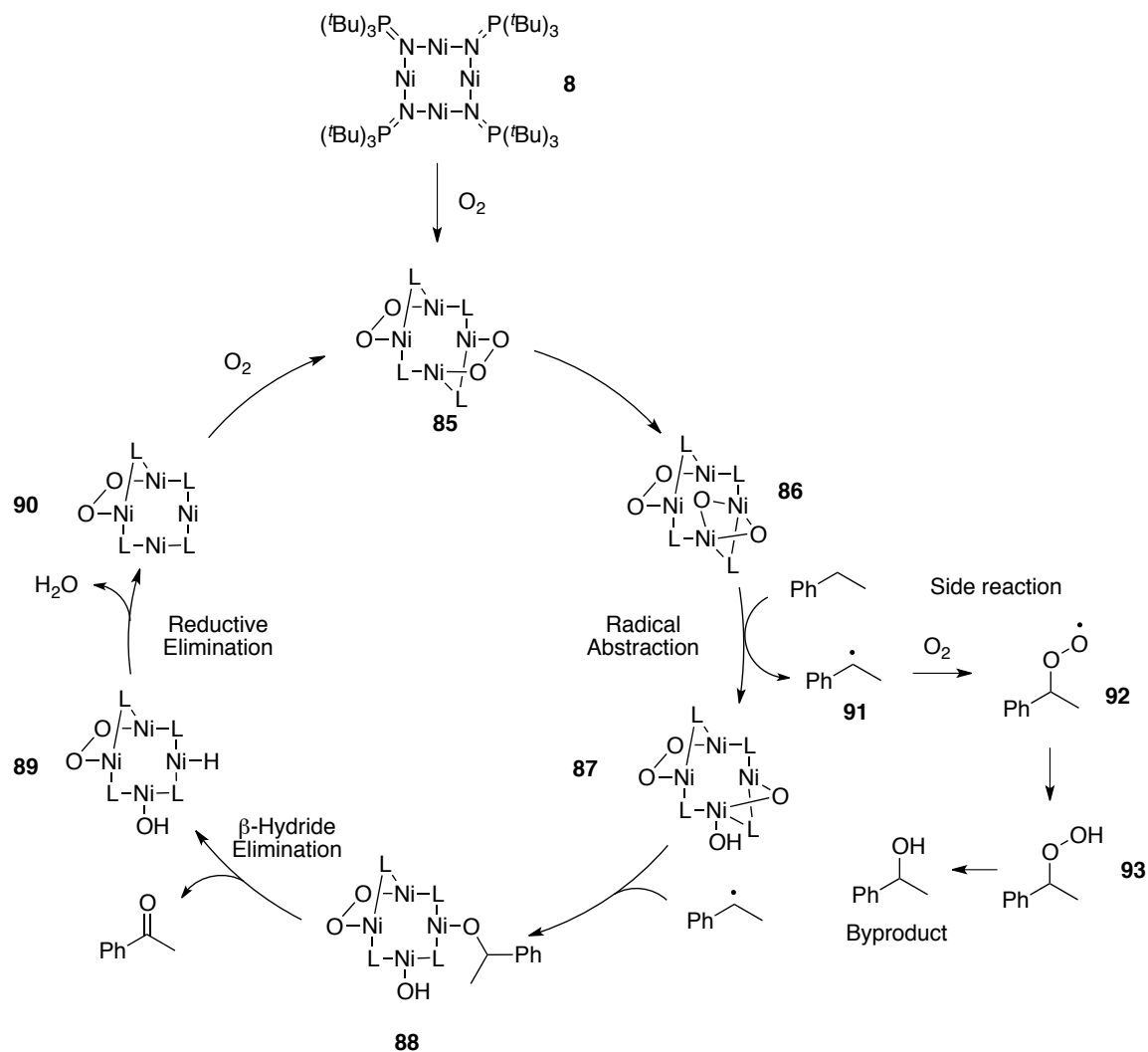
### Equation 2-63



The nickel-catalyzed aerobic oxidation reaction, the mechanism remains undetermined. A working hypothesis is proposed, as a tentative first attempt to frame a more detailed mechanistic investigation (Scheme 2-10). The phosphoranimide-supported nickel(I) cluster **8**, we propose, readily reacts with two equivalents of molecular oxygen to form oxygen-bridged nickel(II) complex **85**. This complex undergoes further rearrangement, breaking the O–O bond to afford the oxo-bridged mixed valent nickel(II)/(III) complex **86**. This high valent species abstracts a benzylic hydrogen atom from ethylbenzene, reducing one nickel(III) center to nickel(II) and at the same time generating a benzyl radical **91**. Before the radical exits the solvent cage, it is immediately captured by the neighboring bridging oxo ligand, reducing the other nickel(III) center. A straightforward  $\beta$ -hydride elimination affords the acetophenone product and a Ni(II) hydride intermediate **89**, which undergoes binuclear reductive elimination to produce water and the mixed valent nickel(I)/(II) complex **90**, which reenters the catalytic cycle after being reoxidized by molecular oxygen.

The formation of 1-phenylethanol can be explained by a side reaction along this pathway. After the benzyl radical **91** is formed, a small amount of it could exit the cage and be trapped by molecular oxygen to form the corresponding hydroperoxide radical **92**. This then abstracts a benzylic hydrogen atom to form the corresponding hydroperoxide **93**, which further decomposes to afford acetophenone and 1-phenylethanol. To support this hypothetical side pathway, the activation of benzylic C–H bonds by hydroperoxide reagents to afford both alcohol and ketone products has been reported even in the absence of catalyst.<sup>160</sup>

## Scheme 2-10



## 2.3 Conclusion

In summary, we have developed aerobic alkane oxidation reactions using  $[\text{Ni}-\text{N}=\text{P}(\text{tBu})_3]_4$  **8** as the precatalyst. These oxidation reactions are unprecedented in literature, as nickel is

rarely used as a catalyst in previously developed oxidation reactions. The reaction was performed with neat substrates, including alkyl arenes, ethers and cyclic alkanes. Addition of a water scavenger, such as  $\text{CaH}_2$  or 3 Å molecular sieves, is found to be beneficial to the reaction. However, at this stage, the real active catalyst in the oxidation reaction and detailed mechanism remain unknown.

## 2.4 Future work

The main focus for our future work is the isolation and characterization of the oxidized nickel cluster or clusters responsible for the oxidation reaction. Obtaining an X-ray crystal structure of any nickel cluster containing oxygen is also of high priority. This might prove difficult, since the oxidized nickel cluster may not be a single species and may be only metastable. Various nickel species may exist, depending on the coordination mode of the molecular oxygen and the nuclearity of the active catalyst(s). The isolation of oxygenated nickel clusters has been attempted; however, part of the oxidized nickel complexes can be dissolved in diethyl ether while the remaining residue is only soluble in THF. Further investigation is needed to evaluate the selectivity of other oxidizing reagents that might afford a stable oxonickel cluster.

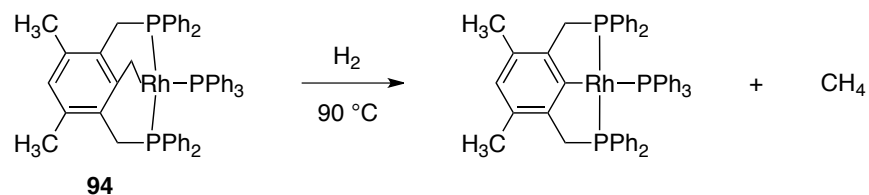
A more detailed mechanistic study of the alkane oxidation is also necessary. Applying the rapid kinetic techniques during the oxidation reaction may provide more information on the nature of the active catalyst and reaction intermediates. A better understanding of the mechanism will assist in further optimizing the catalyst and reaction conditions and generalizing the substrate scope. More generally, other oxidation catalysts bearing novel ligands or different metals such as iron or copper need to be developed. For us, the ultimate challenge is the selective oxidation of methane, from which methanol, formaldehyde, methylformate or formic acid will be produced.

## Part II: Toward Cobalt- and Iron-Mediated [5+2] Ring-Expansion Reactions

The activation of C–C  $\sigma$ -bonds remains one of the most challenging subjects in organic chemistry. Among recent developments, it has been demonstrated that transition metal complexes can act as useful tools to facilitate C–C  $\sigma$ -bond activation. However, in those metal-mediated reactions, two generally weak alkyl-metal bonds (20–30 kcal mol<sup>-1</sup> per bond) are formed at the expense of a strong C–C  $\sigma$ -bond (~90 kcal mol<sup>-1</sup>).<sup>161</sup> Therefore, transition metal-mediated C–C  $\sigma$ -bond activation is generally a thermodynamically endergonic process.<sup>162</sup> Furthermore, C–C  $\sigma$ -bonds are normally shielded by multiple C–H bonds nearby and therefore sterically less accessible. Thus, in terms of kinetics, C–C bond activation is also less favored than C–H bond activation.<sup>162</sup>

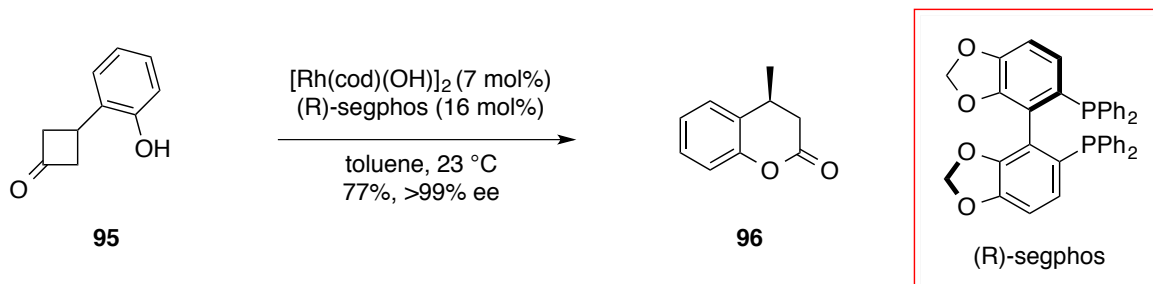
Despite the challenges, a considerable number of reactions have been developed aiming to achieve C–C  $\sigma$ -bond activation. Among these, one important strategy is the direct oxidative addition of a low valent late transition metal complex into various types of C–C  $\sigma$ -bonds. Many of these reactions succeeded by taking advantage of additional thermodynamic driving force(s), including ring strain release, aromatic product formation, etc.<sup>163,164</sup> More significantly, C–C  $\sigma$ -bond activation in certain non-activated substrates has also been realized. One important example was reported by Milstein et al., in which an intermolecular C–C bond activation was observed in a rhodium pincer complex **94** (Eq. I2-1).<sup>165</sup> Besides oxidative addition, other strategies adopted for the activation of C–C  $\sigma$  bonds include  $\beta$ -carbon elimination, activation/decarbonylation, and radical activation reactions.<sup>162</sup>

### Equation I2-1



In addition to such stoichiometric reactions, catalytic C–C bond activation processes have also been developed. Thermodynamic driving forces such as the release of ring strains are still necessary in order for many catalytic reactions to proceed.<sup>166</sup> In one more recent development, an enantioselective catalytic C–C bond activation was reported in which a rhodium-catalyzed isomerization of substituted cyclobutanols **95** affords enantiopure dihydrocoumarin derivatives **96** (Eq. I2-2).<sup>167</sup>

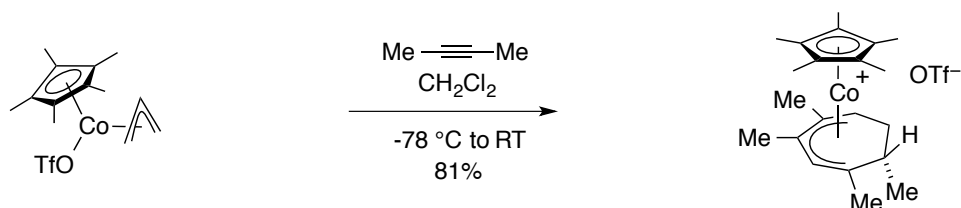
### Equation I2-2



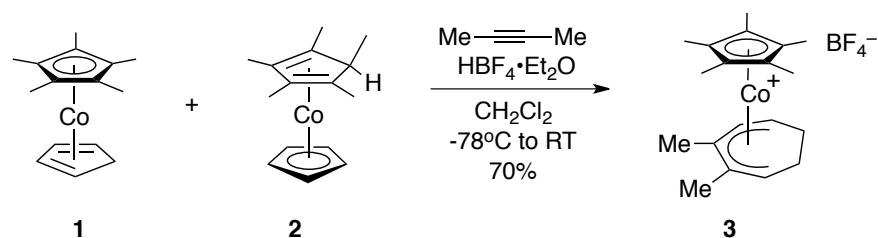
Our group has also contributed to the development of novel stoichiometric reactions involving C–C bond activation. During our study into cobalt-mediated [3+2+2] cycloaddition reactions, an unexpected C–C  $\sigma$ -bond activation was observed (Eq. I2-3),<sup>168</sup> leading to the independent development of an unprecedented cobalt-mediated [5+2] ring-expansion reaction (Eq. I2-4).<sup>169</sup> Unlike previously reported reactions, where precious

metals such as rhodium, iridium and platinum were used,<sup>162</sup> these newly discovered reactions appear particularly attractive, as they accomplish a ring-opening C–C bond activation using relatively inexpensive first-row metal, cobalt. These cobalt-mediated reactions could provide a new method for the construction of synthetically challenging seven-membered ring structures.<sup>170</sup>

### Equation I2-3



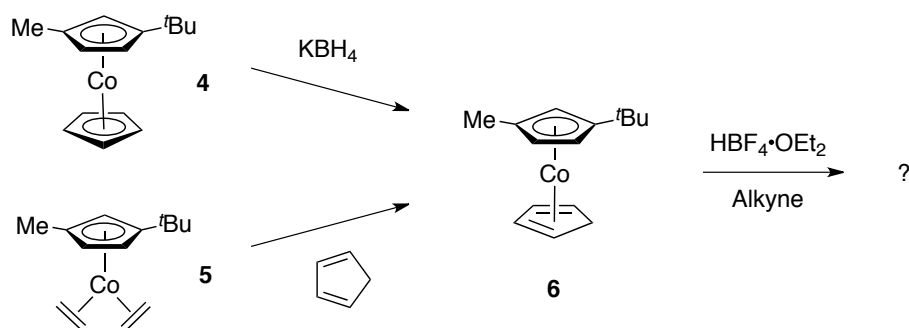
### Equation I2-4



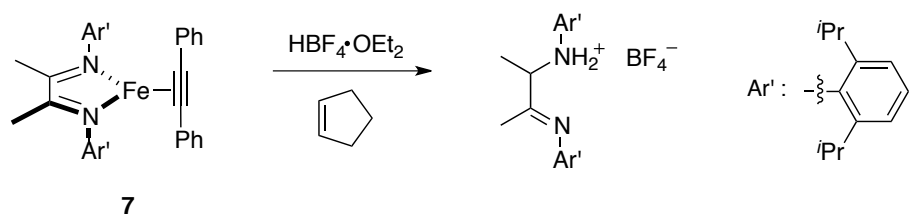
The second part of this dissertation focuses on the continued development of first-row transition-metal mediated [5+2] ring-expansion reactions. More specifically, Chapter 3 discussed research conducted for the improvement of cobalt-mediated [5+2] ring-expansion reactions, involving the synthesis of  $\eta^4$ -cyclopentadiene cobalt(I) complexes **3** and the corresponding ring-expansion reactions triggered by protonation (Scheme I2-1). In Chapter 4, a new strategy for [5+2] ring-expansion reactions is briefly presented. This

strategy was developed based on DFT calculations on potential reaction mechanisms, suggesting that the [5+2] ring-expansion reactions can be performed starting from low-valent metal alkyne complexes. For the ring-expansion reactions we attempted (Eq. I2-5), diimine iron(0) alkyne complex **7**<sup>171</sup> was used as the starting material.

### Scheme I2-1



### Equation I2-5



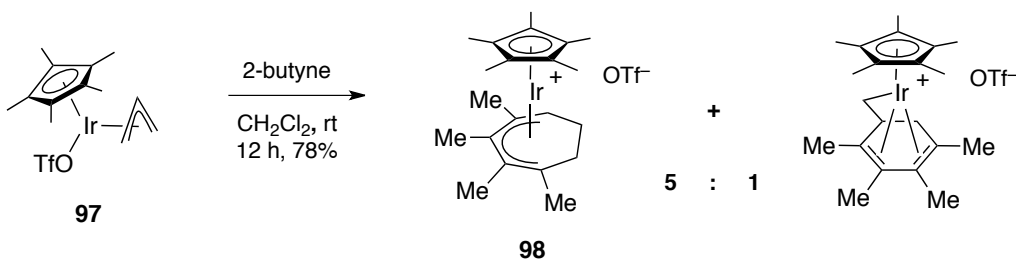
## Chapter 3. Toward cobalt-mediated [5+2] ring-expansion reactions

### 3.1 Introduction

Transition metal-mediated cycloaddition reactions are valuable synthetic tools for the construction of cyclic/polycyclic organic compounds.<sup>172,173</sup> The developed methods provide access to small and medium ring structures, mainly involving three to eight-membered rings.<sup>173</sup> Among these molecules, seven-membered ring structures are synthetically challenging and only few general methods have been established to achieve their synthesis.

Our group has previously developed several transition metal-mediated reactions for the construction of seven-membered rings. The first strategy developed was the iridium-mediated [3+2+2] allyl/alkyne cycloaddition reaction (Eq. 3-1),<sup>174</sup> in which one equivalent of  $\eta^3$ -allyl iridium complex **97** incorporates two equivalents of various internal alkynes to afford the corresponding  $\eta^5$ -cycloheptadienyl iridium complexes **98** (illustrate with 2-butyne).

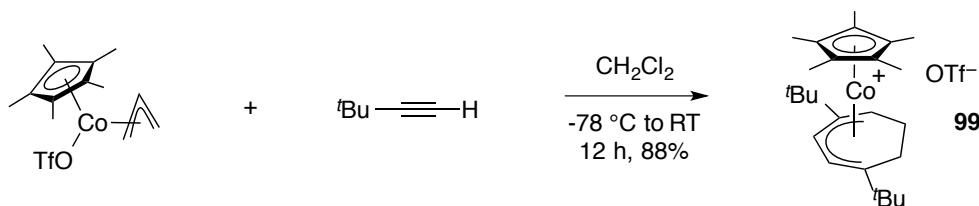
#### Equation 3-1



Subsequently, analogous cobalt-mediated [3+2+2] allyl/alkyne cycloaddition reactions were also developed (Eq. 3-2), demonstrating that the reaction could be conducted using a

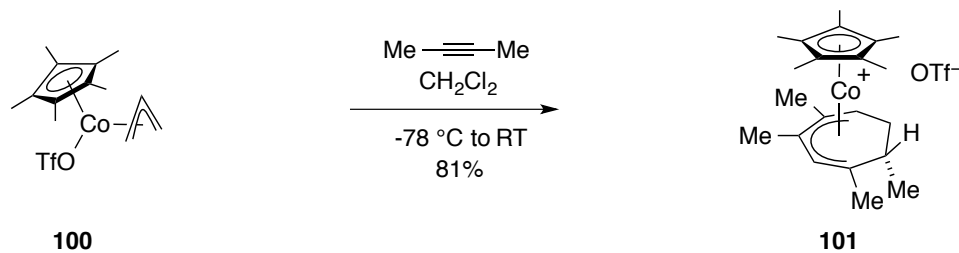
much less expensive reagent metal.<sup>175</sup> This cobalt-mediated three-component cycloaddition is generally applicable, working well with various allyl components and alkyne substrates. Moreover, when highly differentiated unsymmetrical alkynes are used (e.g., *tert*-butylacetylene), the reactions are regioselective, affording only one major product **99**.

### Equation 3-2

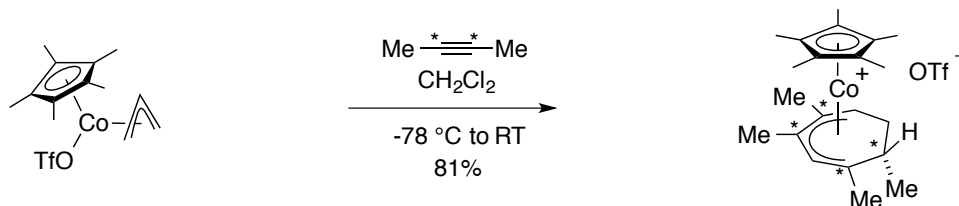


During the study of cobalt-mediated [3+2+2] cycloaddition reactions, unexpected products generated as a result of C–C bond activation were isolated (e.g., Eq. 3-3).<sup>168</sup> When electrophilic  $\eta^3$ -allyl cobalt(III) complex **100** reacted with 2-butyne, the allyl component is cleaved and its carbon atoms become separated in the final  $\eta^5$ -cycloheptadienyl cobalt product **101**. Further investigation using doubly  $^{13}\text{C}$ -labelled 2-butyne confirmed that a C–C  $\sigma$ -bond in the allyl ligand had been activated and the corresponding carbon atoms in the product are indeed ‘relocated’ (Eq. 3-4).

### Equation 3-3

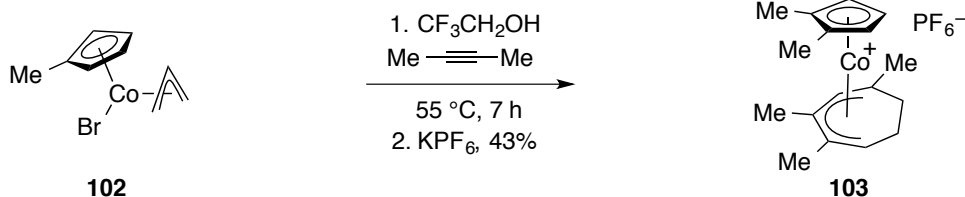


### Equation 3-4



Further investigation into the “anomalous” [3+2+2] cycloaddition revealed a second reaction with a C–C  $\sigma$ -bond activation embedded into it (Eq. 3-5). When the  $\eta^3$ -allyl cobalt complex **102** was treated with an excess of 2-butyne, an unexpected ring expansion of the ancillary  $\eta^5$ -methylcyclopentadienyl ligand occurred, affording  $\eta^5$ -*trimethylcycloheptadienyl* cobalt(III) product **103** from alkyne insertion. Meanwhile, a new  $\eta^5$ -dimethylcyclopentadienyl ligand was produced from the [3+2] cycloaddition reaction between the  $\eta^3$ -allyl ligand and 2-butyne. Therefore, this second reaction clearly demonstrated the occurrence of an unprecedented [5+2] ring-expansion process.

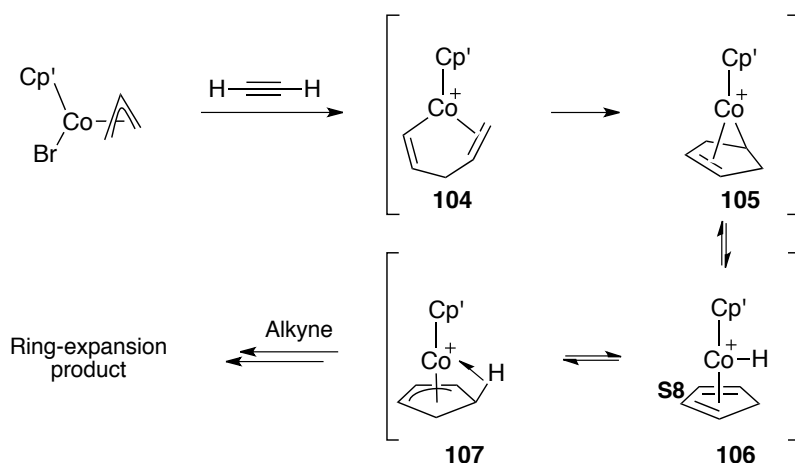
### Equation 3-5



Observation of C–C bond activation in the cobalt-mediated [3+2+2] cycloaddition prompted further investigation into [5+2] ring-expansion reactions. The detailed mechanism for the ring-expansion process in [3+2+2] reaction remains undetermined. However, a hypothesis was proposed, involving the formation of an agostic  $\eta^3$ -

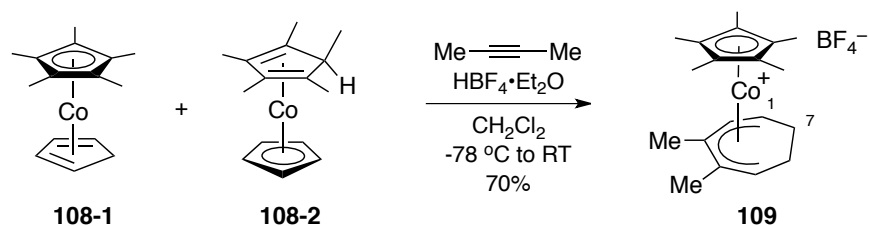
cyclopentenyl intermediate **107** (Scheme 3-1).<sup>168</sup> Alternatively, the same intermediate could be generated by the protonation of cyclopentadiene cobalt(I) complex, serving as a second way to generate the intermediate **106**. Furthermore, the novel [5+2] ring-expansion reactions might be accessible by protonating a substituted  $\eta^5$ -cyclopentadienyl cobalt(I)  $\eta^4$ -cyclopentadiene complex in the presence of alkynes.

**Scheme 3-1**

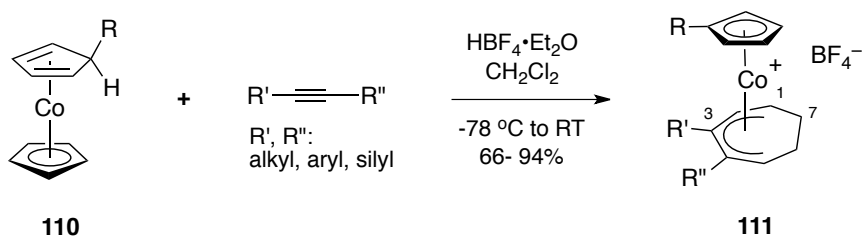


Thus, a rationally designed [5+2] ring-expansion reaction was developed.<sup>169</sup> In these reactions,  $\eta^5$ -cycloheptadienyl cobalt complexes **109** and **111** were produced from either cyclopentadiene or cyclopentadienyl ligand expansion (Eq. 3-6, 7), depending on the substituents present on either ring. These results indicate clearly that in addition to  $\eta^3$ -allyl cobalt(III) complexes,  $\eta^4$ -cyclopentadiene cobalt(I) complexes can also be used as starting materials for the [5+2] ring-expansion.

### Equation 3-6



### Equation 3-7

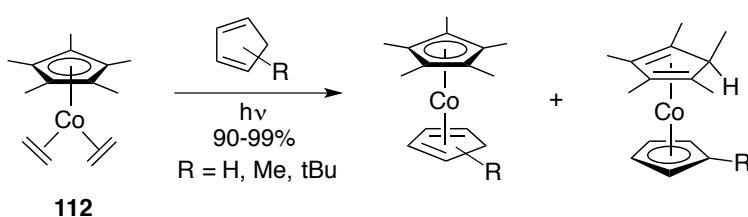


The [5+2] ring-expansion reactions were generalized from two types of  $\eta^4$ -cyclopentadiene cobalt(I) precursors, complexes **108** and **110**, which contain either a pentamethylcyclopentadienyl or a monosubstituted cyclopentadienyl ligand. In these reactions, the two types of complexes were prepared using two distinct synthetic methods.

( $\eta^5$ -Me<sub>5</sub>Cp)Co(I)( $\eta^4$ -CpH) **108-1** was prepared by photolysis of ( $\eta^5$ -Me<sub>5</sub>Cp)Co(I)( $\eta^2$ -C<sub>2</sub>H<sub>4</sub>)<sub>2</sub> **112** in the presence of cyclopentadiene, a reaction in which both ethylene ligands were eventually substituted (Eq. 3-8).<sup>169</sup> However, in addition to ( $\eta^5$ -Me<sub>5</sub>Cp)Co(I)( $\eta^4$ -CpH) **108-1**, an unexpected isomer, ( $\eta^5$ -Cp)Co(I)( $\eta^4$ -Me<sub>5</sub>CpH) **108-2** was also obtained. The isomerization can be attributed to the photo-induced hydride migration between the two cyclopentadienyl rings, a reaction that does not happen thermally. Protonation of the isomeric cobalt(I) mixture in the presence of 2-butyne affords only  $\eta^5$ -cycloheptadienyl

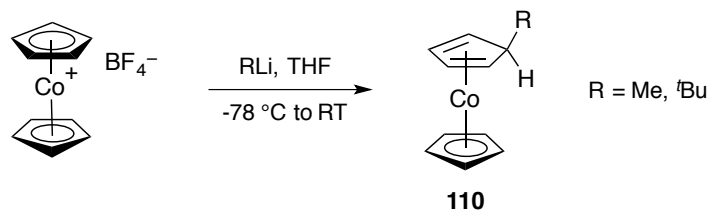
cobalt complexes **109**, the ring-expansion product of the unsubstituted ring. Upon protonation, cobalt(I) complexes **108** equilibrate, converging on a pentamethylcyclopentadienyl ligand and incorporating the 2-butyne into the less substituted ring, probably due to the steric hindrance imposed by the bulky ligand.

### Equation 3-8



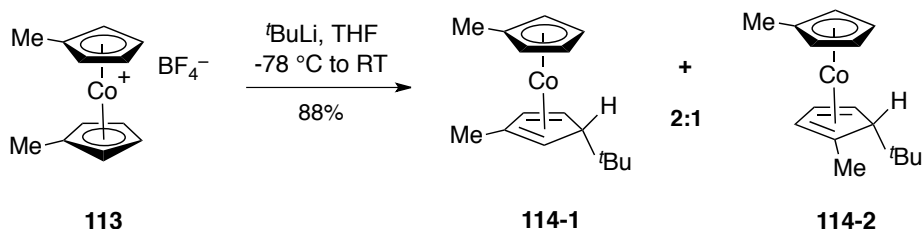
Cyclopentadienyl cobalt(I) complexes **110** possessing a monosubstituted cyclopentadiene ligand were expected to be more sterically accessible during alkyne incorporation. These complexes were produced from the alkylative reduction of cobaltocenium compounds using strong alkyl anions (Eq. 3-9)<sup>176</sup> and used for [5+2] ring-expansion reactions, affording  $\eta^5$ -cycloheptadienyl cobalt complexes **111** in good to excellent yields. In the latter reactions, the cyclopentadienyl ligand is exclusively activated, whereas the monosubstituted cyclopentadiene remains unactivated, transforming into the corresponding anionic ligand in the products. More importantly, in these ring expansion reactions, both terminal and internal alkynes can be incorporated into the products, including 2-butyne, diphenylacetylene and *tert*-butylacetylene.

### Equation 3-9



To further study the effect of the cyclopentadienyl ring substitution pattern on the ring-expansion reactions, cobalt(I) complexes bearing disubstituted cyclopentadienyl were also examined, albeit briefly and in preliminary form. Prepared from 1,1'-dimethylcobaltocenium **113**, an isomeric mixture of cobalt(I) complexes **114** was obtained (Equation 3-10).<sup>177</sup> This is because the addition of alkyl group toward the cyclopentadienyl ring is not highly regioselective, leading to both 1,3- and 1,2-disubstituted cobalt(I) complexes **114-1** and **114-2** in a 2:1 ratio, respectively.

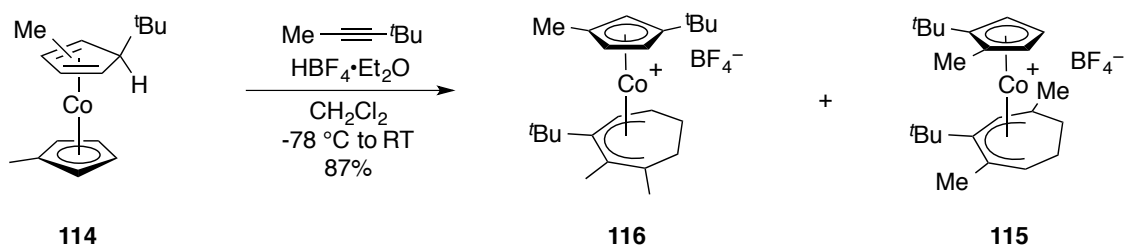
### Equation 3-10



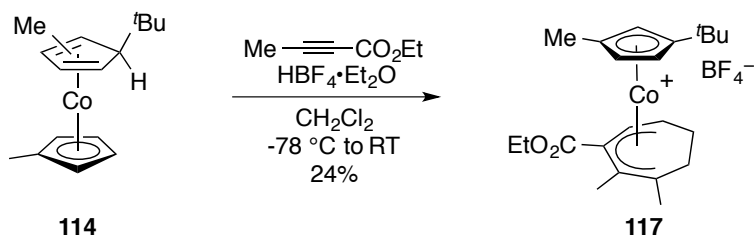
The mixture of isomeric complexes **114** was then subjected to protonation and the subsequent [5+2] ring-expansion reactions (Eq. 3-11). The purification and characterization of individual products from the resultant complex mixture turned out to be very difficult. Despite the fact that the starting material is limited to a disubstituted isomeric mixture, the alkyne scope for this system appears even more general than the previous reaction using monosubstituted cobalt(I) complexes. For the first time, an alkyne bearing an electron-withdrawing ester functional group was incorporated into the  $\eta^5$ -

cycloheptadienyl cobalt product **117**, albeit in low yield (Eq. 3-12). This introduction of ester and related carbonyl functionality is invaluable for further functionalization of the seven-membered ring after demetallation.

### Equation 3-11



### Equation 3-12



## 3.2 Results and Discussion

Trevor Dzwiniel discovered that disubstituted cyclopentadienyl cobalt(I) complexes demonstrated promising and unique reactivity toward ring-expansion reactions.<sup>177</sup> However, to prepare these individual cobalt(I) complexes both efficiently and cleanly remained a challenging task. It was therefore necessary to develop a new method for the

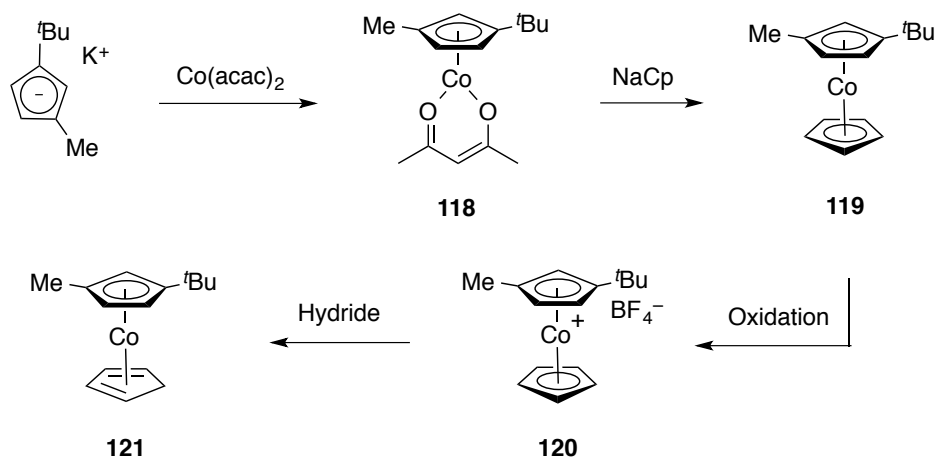
synthesis of 1,2- and/or 1,3-disubstituted cyclopentadienyl cobalt(I) complexes for the benefit of further investigation into [5+2] ring-expansion reactions.

Different strategies for the synthesis of cyclopentadiene cobalt(I) complexes have been explored by previous group members. Chan focused on the [5+2] ring-expansion reactions using a cobalt complex bearing 1,3-di-*tert*-butylcyclopentadienyl ligand. The corresponding cobalt(I) cyclopentadiene complex was prepared from  $\text{Co}(\text{acac})_2$ . Prior to Chan's investigation, Trevor prepared cobalt(I) cyclopentadiene complex from the corresponding bisethylene complex by ligand replacement. Both Chan and Trevor's method have been tested for the preparation of individual disubstituted cobalt(I) cyclopentadiene complexes, as discussed in details below. However, in Chan's method, an unexpected disproportionation problem of 1-methyl-3-*tert*-butylCpCo(II)Cp to cobaltocene prevent further application of this method. While adopting Trevor's preparation procedure, (1-methyl-3-*tert*-butylcyclopentadienyl) cobalt(I) bisethylene complexes were found highly unstable. Therefore, this method had to be abandoned eventually.

### *3.2.1 Acac-based approach to Cp'Co(I) templates.*

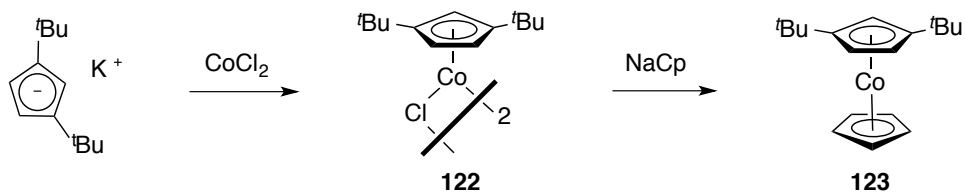
The first strategy for preparing the desired disubstituted cyclopentadienyl cobalt(I) complexes was to first generate the unsymmetrical cobaltocene complex **119** from  $\text{Co}(\text{acac})_2$ , followed by oxidation to the cobaltocenium derivative **120** and a subsequent reduction with hydride reagents (Scheme 3-2). This strategy was developed by Dr. Bryan Chan for the synthesis of the unsymmetrical cobaltocene, (1,3-di-*t*BuCp)Co(Cp) **123**, after adapting literature methods for the synthesis of the corresponding bis(ethylene) complex failed to produce isolable material.<sup>178</sup>

### Scheme 3-2

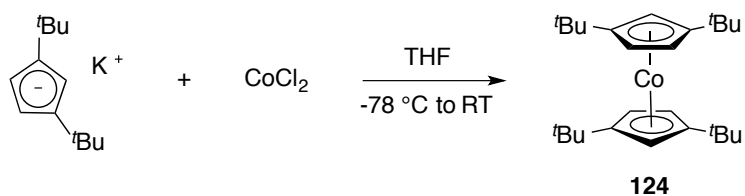


Prior to using  $\text{Co}(\text{acac})_2$  as the starting material, Chan first tried to adapt a preparation for making unsymmetrical cobaltocenes starting from cobalt(II) chloride.  $\text{CoCl}_2$  was used, reacting with 1,3-di-*tert*-BuCpLi to produce a chloro-bridged dimer,  $[(1,3\text{-di-}^t\text{BuCp})\text{CoCl}]_2$  **122**, to which CpNa could be subsequently added, generating the mixed cobaltocene, (1,3-di-*tert*-BuCp)Co(Cp) **123** (Scheme 3-3). However, to Chan's dismay, the reaction between  $\text{CoCl}_2$  and 1,3-di-*tert*-butylcyclopentadienyl anion afforded mostly the symmetrical cobaltocene, (1,3-di-*tert*-BuCp) $_2$ Co **124** (Eq. 3-13). From the reaction, it was clear that the chloride ligand is too labile to prevent the disproportionation of  $[(1,3\text{-di-}^t\text{BuCp})\text{CoCl}]_2$  **122**, in contrast to the indefinitely stable Cp\* analogues.<sup>179</sup> A cobalt precursor possessing a stronger coordinating ligand or ligands is required.

### Scheme 3-3



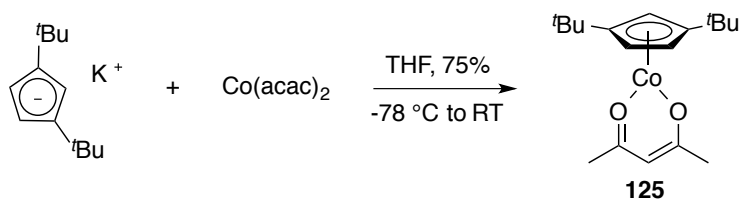
### Equation 3-13



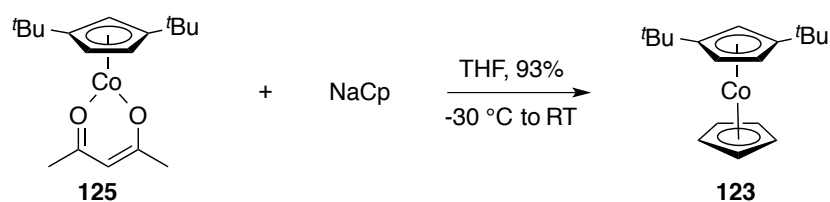
In so far as acetylacetonate is a bidentate ligand which provides for stronger coordination,  $Co(acac)_2$  was then used to prepare unsymmetrical cobaltocene **123**. Reaction between 1,3-di-*t*BuCpLi and  $Co(acac)_2$  afforded (1,3-di-*t*BuCp)Co(acac) **125** successfully (Eq. 3-14), which was stable indefinitely in monomeric form. Further replacement of the acetylacetonate ligand by cyclopentadienyl anion produced the unsymmetrical cobaltocene **123** in excellent yield (Eq. 3-15).

This now precedented route was therefore applied toward the synthesis of the analogous disubstituted unsymmetrical cobaltocene **119** that bears a *tert*-butyl and methyl group on the cyclopentadienyl ligand, substituted in a 1,3-relationship (Scheme 3-4).

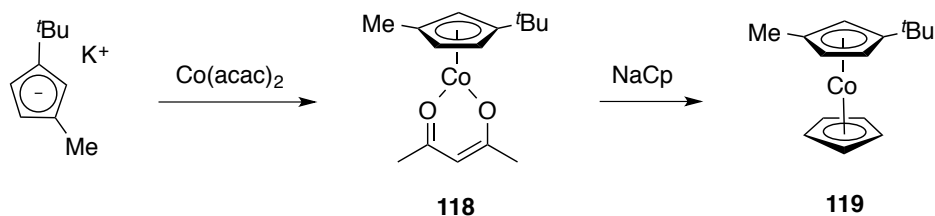
### Equation 3-14



### Equation 3-15

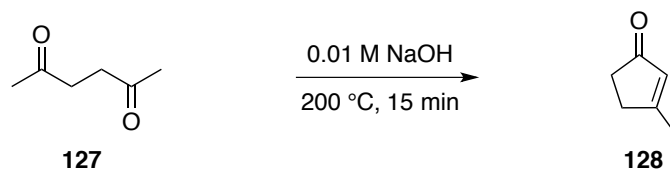


### Scheme 3-4

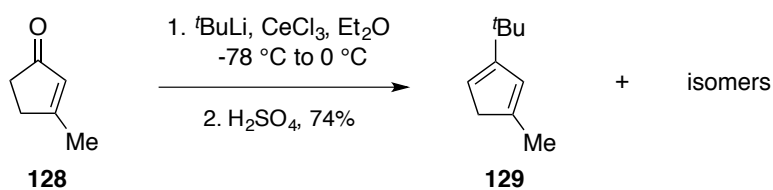


To prepare the unsymmetrical cobaltocene **119**, the corresponding anionic cyclopentadienyl ligand, 1-Me-3-*t*BuCpK **126**, was first synthesized starting from 2,5-hexadione **127**. Under basic conditions, 2,5-hexadione undergoes an intramolecular aldol condensation, producing 3-methyl-2-cyclopente-1-one **128** in good yield after purification by distillation (Eq. 3-16).<sup>180</sup> Then, 1-methyl-3-*tert*-butylcyclopentadiene **129** was prepared by 1,2-addition of an *in situ* generated *tert*-butylcerium reagent to 3-methyl-2-cyclopente-1-one **128**, and subsequent acid-catalyzed alcohol dehydration reaction (Eq. 3-17).<sup>181</sup> The disubstituted cyclopentadiene **129** undergoes sequential [1,5] shifts readily at room temperature to give an equilibrium isomeric mixture.<sup>182</sup> Eventually, deprotonation using potassium hydride afforded the single anionic ligand, 1-Me-3-*t*BuCpK **126** (Eq. 3-18).

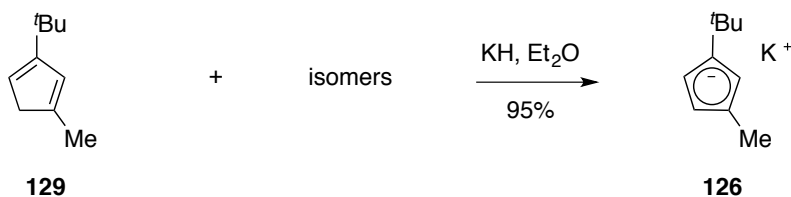
### Equation 3-16



### Equation 3-17



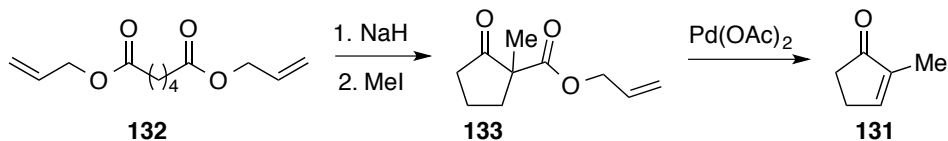
### Equation 3-18



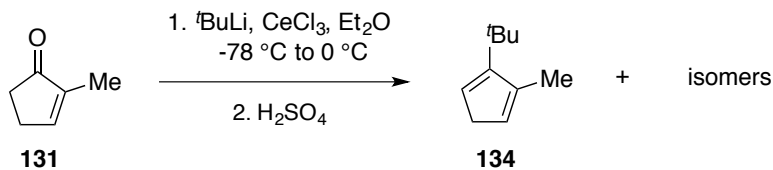
The corresponding 1-Me-2-<sup>t</sup>BuCpK **130** was prepared using essentially the same synthetic route, starting from the corresponding cyclopentenone substrate. The preparation of 2-methyl-2-cyclopentenone **131** was adapted from the literature and required more steps (Scheme 3-5). This synthesis was carried out on a large scale by Devin Reaugh as an undergraduate project. The bis(allyl ester) **132** was first generated from a Fischer esterification between adipic acid and allyl alcohol. The ester **132** was then converted to β-ketoester **133** by Dieckman condensation, followed by a subsequent methylation. Finally, an oxidative elimination reaction catalyzed by Pd(OAc)<sub>2</sub> was carried out and the desired 2-

methyl-2-cyclopent-1-one **131** was obtained.<sup>183</sup> Accordingly, this enone **131** was used to synthesize 1-Me-2-*t*BuCpH **134** (Eq. 3-19). In contrast to 1-Me-3-*t*BuCpH **129**, however, 1-Me-2-*t*BuCpH **134** undergoes Diels-Alder reactions readily, forming a mixture of dimers in hours at room temperature. Therefore, to maximize the reaction yield, the subsequent 1-Me-2-*t*BuCpH purification and deprotonation steps were conducted as fast as possible (Eq. 3-20)

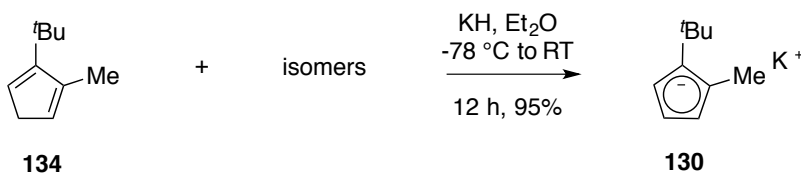
### Scheme 3-5



### Equation 3-19



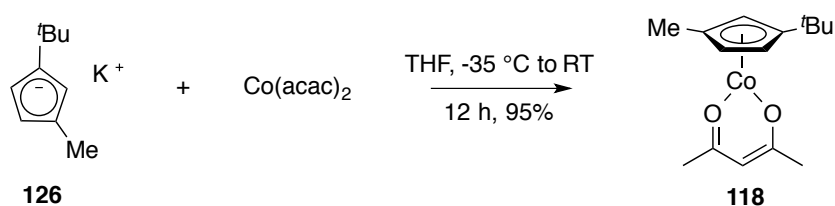
### Equation 3-20



With 1-Me-3-*t*BuCpK **126** in hand, the synthesis of unsymmetrical cobaltocene **119** begins with the addition of 1-Me-3-*t*BuCpK **126** to Co(acac)<sub>2</sub> (Eq. 3-21). The reaction produced a

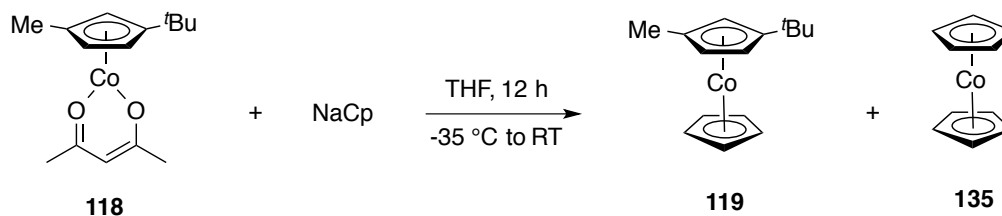
pentane-soluble oily product together with the formation of a pink precipitate. Since potassium acetylacetonate is a THF-insoluble solid, this observation indicates that a ligand replacement occurs. Due to the paramagnetic nature of the cobalt(II) product, NMR spectroscopy was not a viable technique for compound identification. The product was determined by HRMS to be the desired cobalt(II) complex **118**.

### Equation 3-21



Half-sandwich cobalt complex **118** was then subjected to substitution reaction using recrystallized CpNa (Eq. 3-22), generating a pink solid and brownish oily compound that was again analyzed by HRMS. The pink solid proved to be Na(acac) and the brownish oily fraction contained both unsymmetrical cobaltocene **119** and the unsubstituted cobaltocene **135**. The observation of the undesired byproduct raised concern that the targeted unsymmetrical cobaltocene **119** might not be stable toward disproportionation to form cobaltocene **135**.

### Equation 3-22



This disproportionation problem was confirmed after subjecting the oily residue to oxidation using  $[\text{Cp}_2\text{Fe}][\text{PF}_6]$ . In accordance with the assumption, the reaction afforded two cobaltocenium compounds: unsymmetrical cobaltocenium complex **120** and the known cobaltocenium tetrafluoroborate **136**<sup>184</sup> were isolated (Eq. 3-23). Separation was performed by using column chromatography on the benchtop, giving nearly equal amounts of each complex, **120** : **136** = 1.2 : 1. Alternatively, when iodine or bromine was used as the oxidizing reagent, the ratio of the two cobaltocenium derivatives varied depending on the reaction temperature (Table 3-1). A reaction conducted at  $-78\text{ }^\circ\text{C}$  afforded the lowest yield (10%) of unsymmetrical cobaltocenium compound **120** as listed in entry 3, Table 3-1.

### Equation 3-23

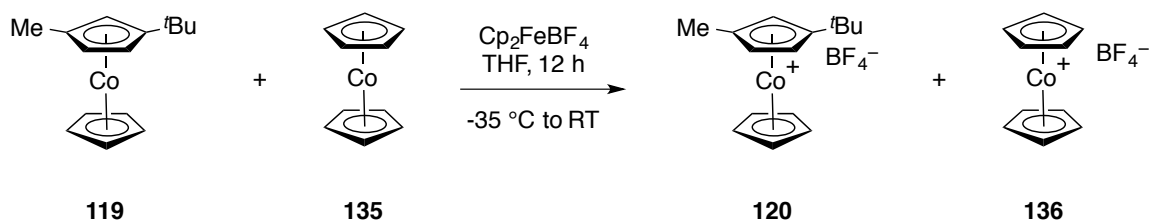
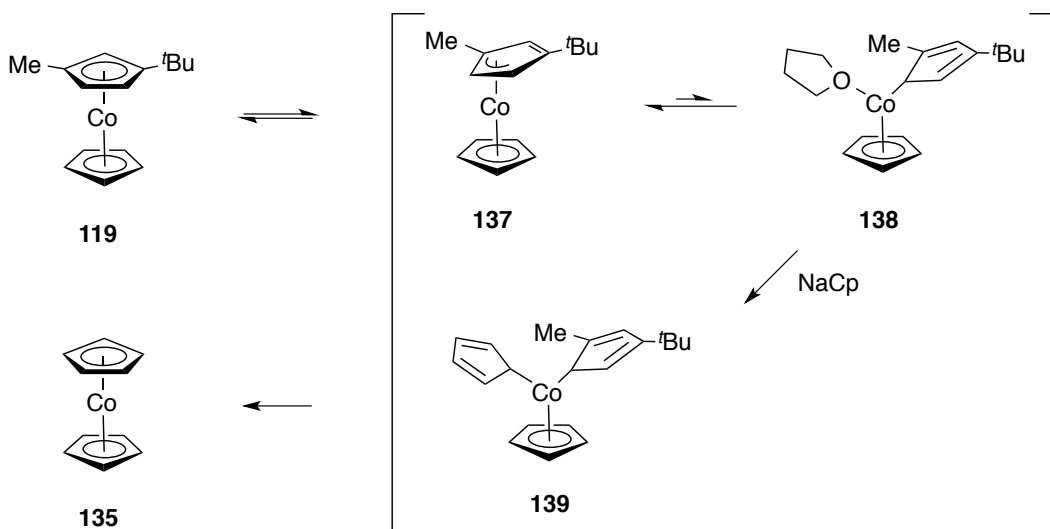


**Table 3-1.** A summary of cobaltocene derivatives oxidation using halogens

Entry	Oxidant	Equivalence	Temperature ( $^\circ\text{C}$ )	Yield (%)	Ratio of <b>120</b> : <b>136</b>
1	$\text{I}_2$	1.0	25	75	1:1
2	$\text{I}_2$ in ether	0.5	25	50	1:2
3	$\text{I}_2$ in ether	0.5	$-78$	60	1:5
4	$\text{Br}_2$	0.5	25	75	2:3

The isolation of cobaltocenium compound **136** provides evidence that supports the rapid disproportionation of unsymmetrical cobaltocene **119** (Scheme 3-6). Though complex **119** possesses 19 valence electrons, as the coordination status of 1-Me-3-*t*BuCp changes from  $\eta^5$  to  $\eta^3$ , 17-electron cobalt complex **137** could be easily produced. Furthermore, either solvent molecules or iodide/bromide anions might also participate in assisting the ligand-slip process, leading to an  $\eta^1$ -coordination mode. Subsequently, an intermolecular cyclopentadienyl transfer replaces the  $\eta^1$ -1-Me-3-*t*BuCp ligand to afford cobaltocene **135**.

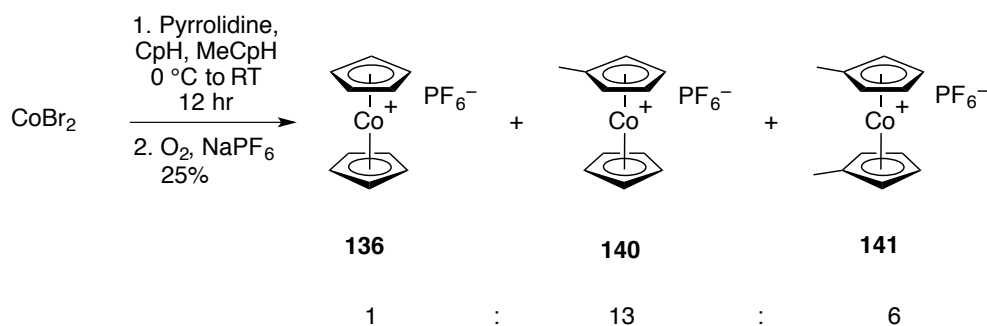
**Scheme 3-6**



This unexpected disproportionation of the unsymmetrical cobaltocene significantly decreases the yield of the desired product. It then became our goal to develop new and more direct methodology for the synthesis of the unsymmetrical cobaltocenium complexes. To the best of our knowledge, few precedents are available in the literature for synthesizing unsymmetrical cobaltocenium compounds.

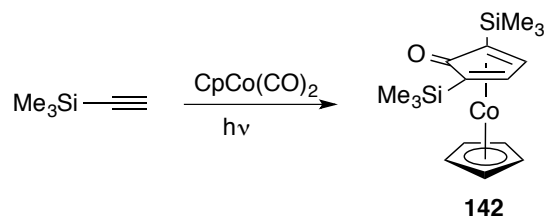
In 1970, a synthesis of monosubstituted cobaltocenium compound **140** was reported by Sheats.<sup>185</sup> In this reaction, both cyclopentadiene and methylcyclopentadiene were added into  $\text{CoBr}_2$  to form cobaltocene derivatives, which were then oxidized by molecular oxygen (Eq. 3-24). Unfortunately, this reaction gives a mixture of three cobaltocenium complexes, with the desired mixed cobaltocenium **140** in a low yield (16%).

### Equation 3-24

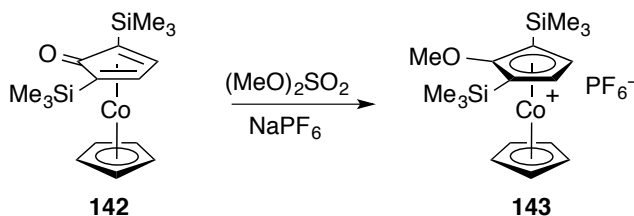


The cyclopentadienone cobalt(I) complex **142** was prepared by Vollhardt and coworkers (Eq. 3-25).<sup>186</sup> They discovered that the addition of dimethyl sulfate afforded a methylated adduct, the desired trisubstituted cobaltocenium compound **143** (Eq. 3-26). However, due to the limited scope, this methodology is not practical for the synthesis of disubstituted mixed cobaltocenium complexes.

### Equation 3-25



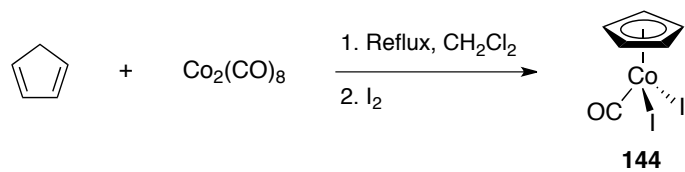
### Equation 3-26



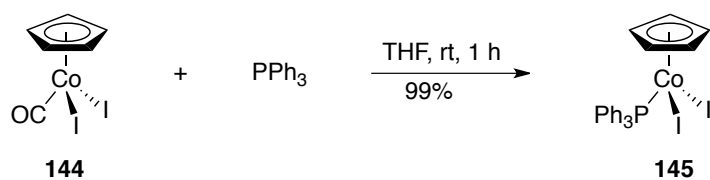
The lack of literature and our fundamental interest in such complexes then prompted us to develop a more general method for the preparation of unsymmetrical cobaltocenium compounds. Our first attempt was made by substituting the labile ligands in various cyclopentadienyl cobalt(III) precursors with a disubstituted cyclopentadienyl ligand. The cobalt(III) compounds examined in this method include CpCoI<sub>2</sub>CO **144**, CpCoI<sub>2</sub>PPh<sub>3</sub> **145**, and [CpCoI<sub>2</sub>]<sub>2</sub> **146**, each readily available by literature methods.<sup>187,188</sup>

CpCoI<sub>2</sub>CO **144** was made in two steps using a one-pot procedure. First, CpCo(CO)<sub>2</sub> **147** was synthesized by the reaction of Co<sub>2</sub>(CO)<sub>8</sub> with cyclopentadiene. The product was then subjected to oxidation with iodine *in situ* (Eq. 3-27).<sup>189</sup> Addition of triphenylphosphine to CpCoI<sub>2</sub>CO **144** affords the substitution product, CpCoI<sub>2</sub>PPh<sub>3</sub> **145** (Eq. 3-28) in excellent yield and refluxing CpCoI<sub>2</sub>CO **144** in *n*-octane under a continuous purge of nitrogen gas leads to the formation of dimeric compound [CpCoI<sub>2</sub>]<sub>2</sub> **146** (Eq. 3-29). Despite the purity of the starting materials, however, reactions of all three cyclopentadienyl cobalt(III) complexes, **144-146**, with 1-Me-3-*t*-BuCpK **126** resulted only in intractable decompositions (Eq. 3-30, 31, 32).

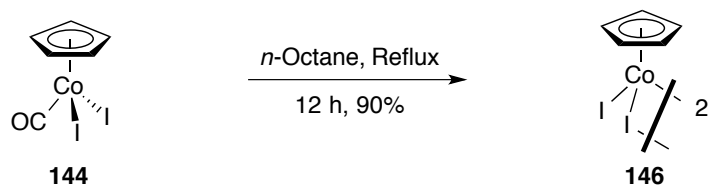
### Equation 3-27



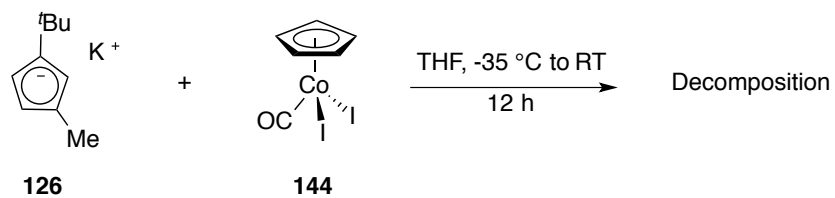
### Equation 3-28



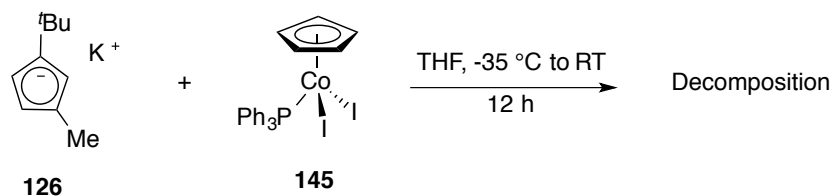
### Equation 3-29



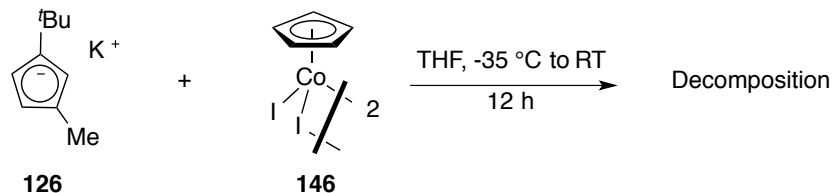
### Equation 3-30



### Equation 3-31

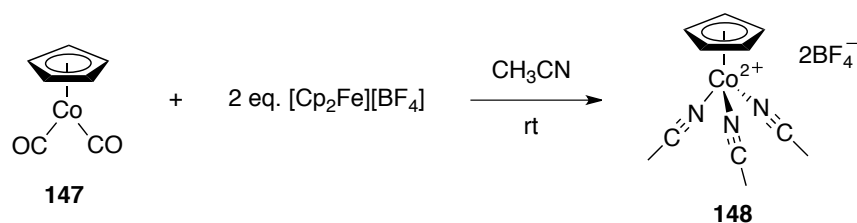


### Equation 3-32

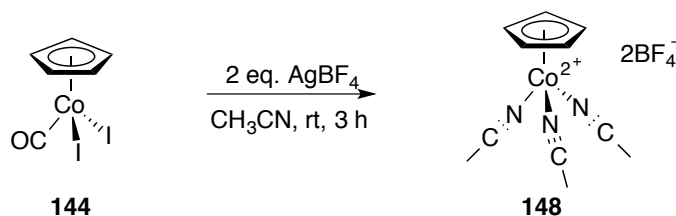


A new strategy was adopted, attempting to trap dicationic cobalt(III) tris(acetonitrile) complex **148** with a disubstituted cyclopentadienyl anion. This was deemed possible because acetonitrile is a labile neutral ligand that can be replaced more readily than an iodide ligand. It was previously reported by Kuhn that dicationic complexes were prepared from the oxidation of  $\text{CpCo}(\text{CO})_2$  **147** in the presence of acetonitrile (Eq. 3-33).<sup>190</sup> In our case,  $\text{CpCoI}_2\text{CO}$  **144** is both air-stable and easy enough to purify that a new reaction was developed, generating dicationic cobalt(III) acetonitrile complex **148** directly from  $\text{CpCoI}_2\text{CO}$  (Eq. 3-34) by assisted ionization. The reaction was realized by adding silver tetrafluoroborate to remove the iodide ligands, giving the reddish dicationic cobalt(III) complex **148**, which was generated *in situ* and trapped with 1-Me-3-*t*-BuCpK **126** afterwards.

### Equation 3-33



### Equation 3-34



The above procedure indeed resulted in the generation of the unsymmetrical cobaltocenium compound  $[(1\text{-Me-3-}^t\text{BuCp})\text{Co}(\text{Cp})][\text{BF}_4]$  **120**. However, when the reaction was conducted at  $-78\text{ }^\circ\text{C}$ , **120** was obtained in a yield of only 30%. Fortunately, a second reaction performed at  $-20\text{ }^\circ\text{C}$  gave a higher yield of the desired product at 68% (Eq. 3-35). The unsymmetrical cobaltocenium compound was characterized by X-ray crystallography in Appendix 1 (Fig. 3-1).

### Equation 3-35

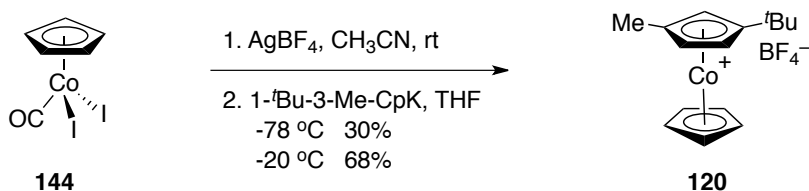
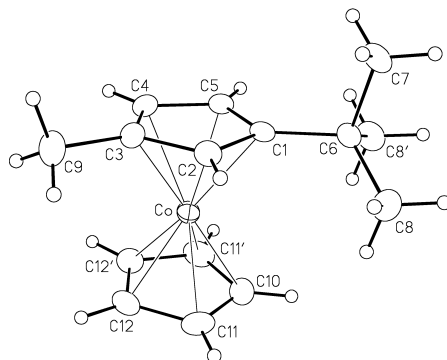


**Figure 3-1.** X-ray crystal structure of  $[(1\text{-Me-3-}t\text{BuCp})\text{Co}(\text{Cp})][\text{BF}_4]$



Perspective view of the  $[(\eta^5\text{-1-}t\text{-butyl-3-methylcyclopentadienyl})\text{CoCp}]^+$  complex ion showing the atom labelling scheme. Non-hydrogen atoms are represented by Gaussian ellipsoids at the 20% probability level. Hydrogen atoms are shown with arbitrarily small thermal parameters.  $R_1 = 0.0318$ ,  $R(w) = 0.0850$

With the unsymmetrical cobaltocenium compound **120** in hand, reduction to the corresponding cobalt(I) cyclopentadiene complexes was investigated. According to Vollhardt's study on the reduction of substituted cobaltocenium complexes (Eq. 3-36),<sup>191</sup> various alkyllithium and hydride reagents can be used, as listed in Table 3-2. For many sterically unhindered alkyllithium reagents, addition toward the more substituted cyclopentadienyl ring is favored. Only the sterically bulky *tert*-butyllithium exclusively added to the less substituted cyclopentadienyl ring. More specifically, reduction using LiH afforded a 3 : 1 mixture of compounds **149** and **150**, respectively, suggesting that hydride addition to the more substituted cyclopentadienyl ring is preferred (Entry 11, Table 3-2).

### Equation 3-36

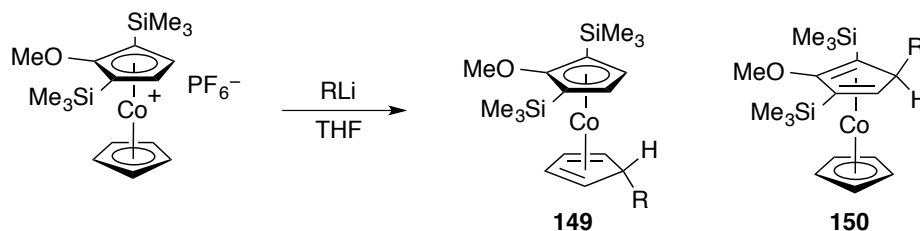


**Table 3-2.** Reduction of substituted cobaltocenium compounds with alkyllithium

Entry	R group in alkyllithium	Ratio between <b>149</b> and <b>150</b>	Yield (%)
1	<i>t</i> Bu	0 : 100	84
2	Me	29 : 71	98
3	<i>n</i> C <sub>6</sub> H <sub>13</sub> -C=CH ( <i>trans</i> )	55 : 45	85
4	<i>n</i> C <sub>6</sub> H <sub>13</sub> -C=CH ( <i>cis</i> )	19 : 81	80
5	<i>n</i> C <sub>6</sub> H <sub>13</sub> -C≡C	73 : 27	95
6	Me <sub>3</sub> Si-C≡C	80 : 20	83
7	CH <sub>3</sub> O-C≡C	74 : 26	92
8	<i>t</i> BuO-C≡C	69 : 31	94
9	C <sub>6</sub> H <sub>5</sub> S-C≡C	75 : 25	89
10	Cl-C≡C	74 : 26	79
11	H	75 : 25	100

In our case, hydride reagents are required to produce the disubstituted cobalt(I) precursors for [5+2] ring-expansion reactions. Based on Vollhardt's study, hydride addition was expected to be selective for the 1-Me-3-*t*BuCp ring. However as the disubstituted cyclopentadienyl ring possesses five distinct hydride addition sites, we therefore anticipated obtaining a mixture of six isomers from the cobaltocenium complex **120** (Fig. 3-

2). Indeed, after treatment with excess  $\text{KBH}_4$ , a complicated mixture of cobalt(I) complexes **151** was produced based on  $^1\text{H}$  NMR spectroscopy (Eq. 3-37), but no further information was revealed on either the amount or identity of each isomer.

**Equation 3-37**

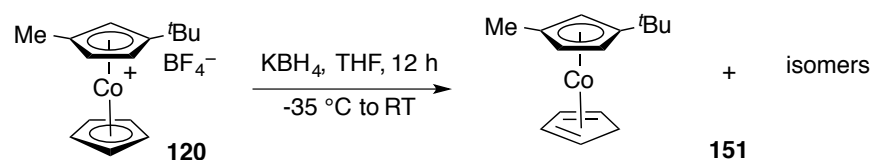
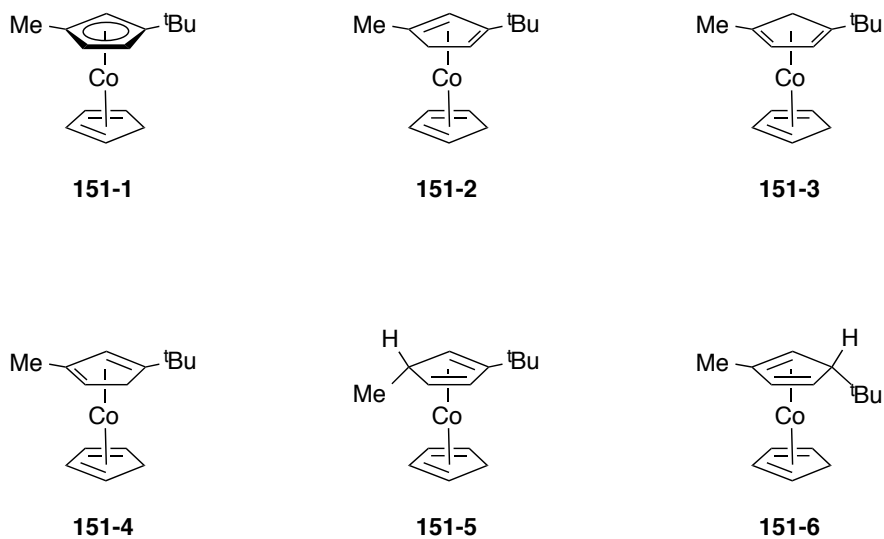


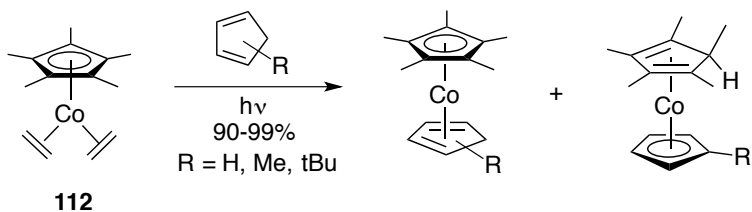
**Figure 3-2.** Isomeric structures of cyclopentadiene cobalt(I) complexes



During Trevor's study on  $\eta^5$ -pentamethylcycloheptadienyl cobalt(I) complex **108**, he observed hydride migration between two cyclopentadienyl rings under photolysis, but not thermolysis, conditions (Eq. 3-38).<sup>169</sup> In an attempt to equilibrate the mixture of isomers to

a major thermodynamic product, both thermal and photochemical reactions were investigated. Neither reaction, however, produced tractable product(s), both apparently leading to the decomposition (Eq. 3-39, 40).

**Equation 3-38**



**Equation 3-39**



**Equation 3-40**



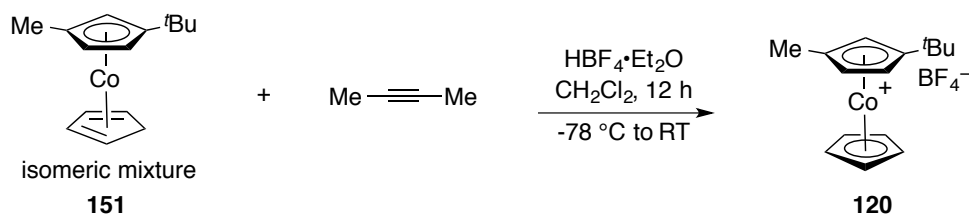
Other nucleophilic hydride reagents were also tested for selectivity in the reduction of unsymmetrical cobaltocenium compound **120**, including LiAlH<sub>4</sub>, Super Hydride (LiEt<sub>3</sub>BH), Li(<sup>t</sup>BuO)<sub>3</sub>AlH and Na(MeO)<sub>3</sub>BH. Na(MeO)<sub>3</sub>BH was initially used because we believe its

milder reducing ability would result in a better product selectivity. However, among these reducing reagents, only  $\text{LiAlH}_4$ , Super Hydride, and  $\text{Li}(\text{tBuO})_3\text{AlH}$  are capable of reducing compound **120**. Unfortunately, these reactions also show poor regioselectivity, producing similar isomeric cobalt(I) mixtures.

Prior investigation of the [5+2] ring-expansion reactions revealed that upon protonation, mixtures of cyclopentadiene/cyclopentadienyl isomers equilibrated rapidly and the less substituted five-membered ring was predominately activated, regardless of the starting derivative. It was therefore expected that under the same reaction conditions, the cyclopentadienyl ligands in isomers from **151-2** to **151-6** are expected to equilibrate, and only the unsubstituted cyclopentadiene ligand of isomer **151-1** is anticipated to undergo ring-expansion. After ring-expansion, a single product, (1-Me-3-*t*Bu-cyclopentadienyl) cobalt(III) cycloheptadienyl derivative **152** would be obtained.

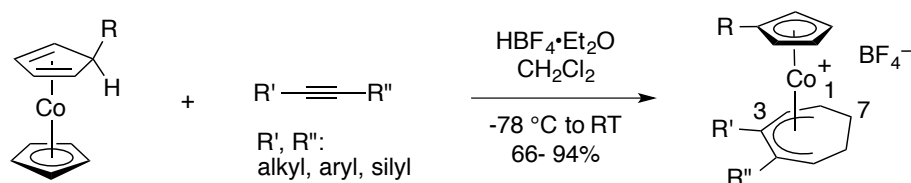
Therefore, the cobalt(I) mixture was used directly as the starting material for studying [5+2] ring-expansion reactions (Eq. 3-41). Following Dzwiniel's procedure, the cobalt(I) mixture was dissolved in dichloromethane and cooled to  $-78\text{ }^\circ\text{C}$  in a dry ice/acetone bath. Fluoroboric acid and the alkyne substrate were then added in sequence. The reaction mixture was left in the cold bath which warms back to room temperature gradually overnight. Using this procedure, the reaction of 2-butyne, *tert*-butyl acetylene, and phenyl acetylene were investigated. However, the reactions failed to produce any ring-expansion products, and only the unsymmetrical cobaltocenium compounds **120** could be isolated after the reaction, in a yield of roughly 20-40%.

### Equation 3-41



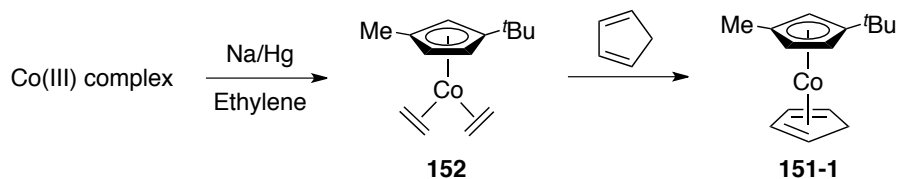
The presence of **151-5** and **151-6** as principal components of the cobalt(I) mixture may be responsible for the failed [5+2] ring-expansion reactions. As discussed, it is the less substituted five-membered ring that undergoes irreversible ring-expansion; therefore, with the readily available cyclopentadiene already embedded in its structure, **151-1** is expected to undergo the ring-expansion reaction directly and efficiently. Similar to the monosubstituted cyclopentadiene cobalt(I) complexes (Eq. 3-42), it is expected that the protonated cobalt(I) complexes first isomerize to the same intermediate obtained by protonation of **151-1**, via hydride migration from  $\eta^4$ -1-methyl-3-*tert* butyl-cyclopentadiene to the cyclopentadienyl ligand before the reaction with alkyne and ring-expansion could occur. However, with the  $\text{sp}^3$ -hydrogen substituents pointing outward (away) from the cobalt center, hydride migrations in isomers **151-5** and **151-6** cannot occur by an intramolecular pathway and may be very slow, if it proceeds at all. As a consequence, these two cobalt(I) isomers would demonstrate no reactivity toward the [5+2] ring-expansion reactions and presumably divert along the other reaction paths.

### Equation 3-42



Since inseparable mixture obtained from the unsymmetrical cobaltocenium reduction does not undergo [5+2] ring-expansion, a new synthetic preparation leading to the synthesis of clean ( $\eta^4$ -cyclopentadiene) cobalt(I) complexes was required. Thus we explored ethylene/cyclopentadiene ligand exchange using 1-methyl-3-*tert* butyl cobalt(I) bis(ethylene) complex **152**, an unknown complex (Scheme 3-7).

### Scheme 3-7

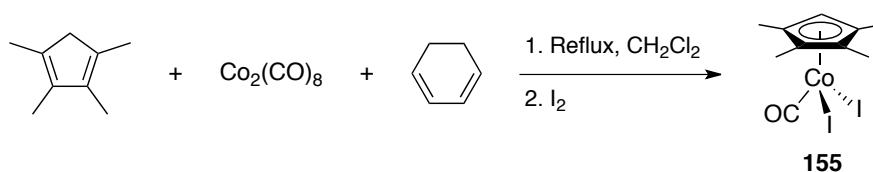


Dzwiniel previously demonstrated that  $\eta^5$ -Cp\*Co(I)CpH **108** could be prepared from ( $\eta^5$ -pentamethylcyclopentadienyl) cobalt(I) bis(ethylene) **112**,<sup>169</sup> although this ethylene exchange strategy might not be applicable to the synthesis of this particular series of  $\eta^4$ -cyclopentadiene cobalt(I) complexes. This is because the stability of cobalt(I) bis(ethylene) complexes depends largely on the substitution pattern of the cyclopentadienyl ligand and the range of the known analogues is quite limited.<sup>192</sup> More specifically, Cp\*Co(ethylene)<sub>2</sub> **112** is stable at room temperature,<sup>193</sup> whereas the Jonas reagent **153**, CpCo(ethylene)<sub>2</sub>, is

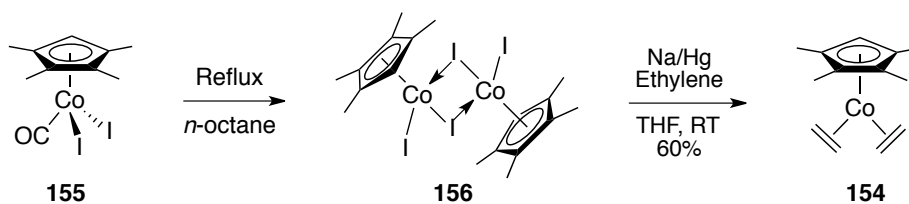
only persistent at a low temperature.<sup>194</sup> Accordingly, the stability of disubstituted cyclopentadienyl cobalt(I) bis(ethylene) complex **152** cannot be predicted in advance.

To gain better insight into the stability problem, tetramethylcyclopentadienyl cobalt(I) bis(ethylene) **154** was first prepared to test this strategy before the riskier disubstituted cyclopentadienyl cobalt(I) bis(ethylene) was attempted. The preparation of compound **154** follows the standard three-step procedure (Scheme 3-8).  $(\text{Me}_4\text{Cp})\text{CoI}_2\text{CO}$  **155** was first prepared the same way in which  $\text{CpCoI}_2\text{CO}$  was synthesized (Eq. 3-43).<sup>190</sup> Heating compound **155** to reflux in *n*-octane results in the release of carbon monoxide and formation of iodine-bridged dimer  $[(\text{Me}_4\text{Cp})\text{CoI}_2]_2$  **156**. Subsequently, sodium amalgam reduction of complex **156** in the presence of ethylene affords reddish  $(\text{Me}_4\text{Cp})\text{Co}(\text{ethylene})_2$  **154**, with an isolated yield of 60% after filtration through Celite using pentane.

### Equation 3-43

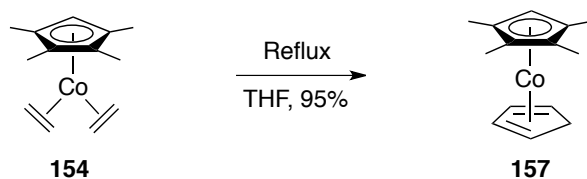


### Scheme 3-8



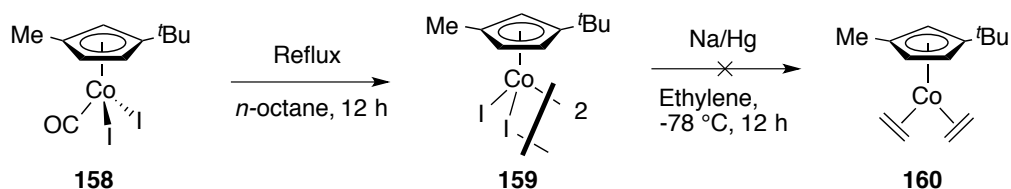
The cobalt(I) bis(ethylene) complex **154** is stable in solution at room temperature for at least an hour and can be stored in a freezer (-35 °C) for weeks without noticeable decomposition. Heating this material to reflux in THF in the presence of excess cyclopentadiene afforded the desired complex, (Me<sub>4</sub>Cp)CoCpH **157**, as a single compound in an isolated yield of 95% (Eq. 3-44). Compared to the Dzwiniel preparation of Cp\*CoCpH by a similar exchange, which requires photolysis, this ethylene exchange reaction was conducted under mild thermal conditions. No hydride migration from (Me<sub>4</sub>Cp)CoCpH to form CpCo(Me<sub>4</sub>CpH) has been observed, consistent with expectations.

#### Equation 3-44



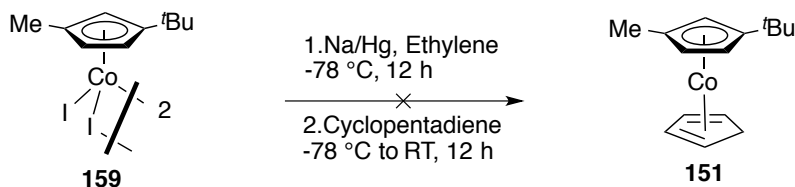
With the successful synthesis of (tetramethylcyclopentadienyl) cobalt(I) bis(ethylene) **154**, the strategy was then applied to the synthesis of (1-Me-3-*t*BuCp)CoCpH **151-1** (Scheme 3-9). Following the same procedures, after (1-Me-3-*t*BuCp)CoI<sub>2</sub>CO **158** was prepared and characterized, the complex was heated to reflux in *n*-octane, affording a black solid **159**. However, characterization of this material proved to be difficult, as it decomposes in coordinating solvents such as THF and is insoluble in non-coordinating solvents. Furthermore, the reduction of crude complex **159** under a continuous flow of ethylene did not afford any of the desired bis(ethylene) product **160**.

### Scheme 3-9



We initially believed that the failure to synthesize cobalt(I) bis(ethylene) complex **160** could be attributed to its thermal instability. Therefore, one remedy that was considered was to use cyclopentadiene to trap complex **160**, as generated *in situ*. The uncharacterized black solid from thermolysis of (1-Me-3-*t*-BuCp)CoI<sub>2</sub>CO **158** was reduced by sodium amalgam in the presence of ethylene, with excess cyclopentadiene added subsequently but without isolation of any intermediates. The solution was allowed to warm slowly to room temperature (Eq.3-45). Unfortunately, none of the desired cyclopentadiene cobalt(I) complex **151** was obtained, unless it was a minor component of the intractable product mixture, as judged by <sup>1</sup>H NMR spectroscopy.

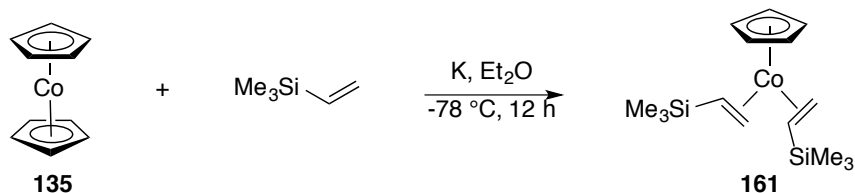
### Equation 3-45



The failure to obtain the desired cobalt(I) cyclopentadiene complex may be associated with the difficulty in promoting ethylene displacement. The use of a more reactive cobalt(I) bis(olefin) complex, CpCo(H<sub>2</sub>C=CHSiMe<sub>3</sub>)<sub>2</sub> **161**, was attempted, prepared *in situ* from the reduction of cobaltocene in the presence of trimethylvinylsilane at -78 °C (Eq. 3-46).<sup>195</sup> A

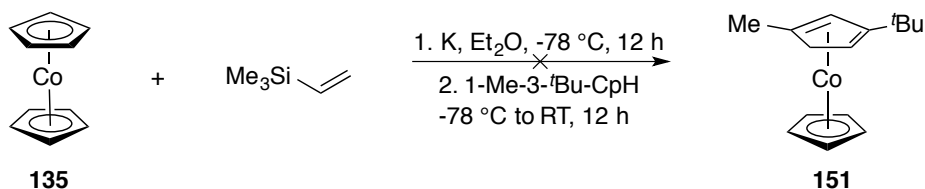
thermally sensitive product was obtained; low-temperature NMR studies suggest that once the temperature rises above  $-30\text{ }^{\circ}\text{C}$ , complex **161** starts to decompose. In contrast, the Jonas reagent shows greater stability, as it stays intact even at  $0\text{ }^{\circ}\text{C}$ .<sup>194</sup> Therefore, it was apparent that complex **161** could be used as a highly reactive starting material for ligand replacement by cyclopentadiene.

### Equation 3-46

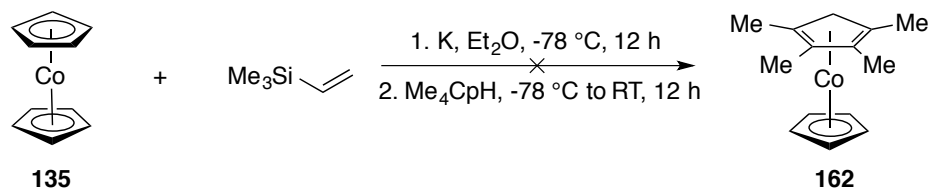


The reaction was set up by preparing the reddish bis(olefin) complex **161** at  $-78\text{ }^{\circ}\text{C}$ , with the disubstituted cyclopentadiene ligand subsequently added into the solution (Eq. 3-47). The reaction mixture was then left to warm slowly to room temperature. However, to our dismay, the reaction failed to generate cyclopentadiene complex **151**. A second reduction was conducted, substituting tetramethylcyclopentadiene in place of the disubstituted cyclopentadiene (Eq. 3-48). However, this treatment also resulted in a complicated product mixture that we were unable to characterize.

### Equation 3-47

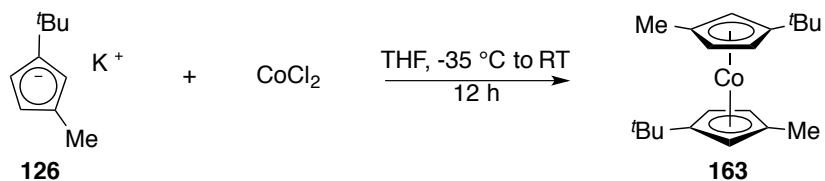


### Equation 3-48

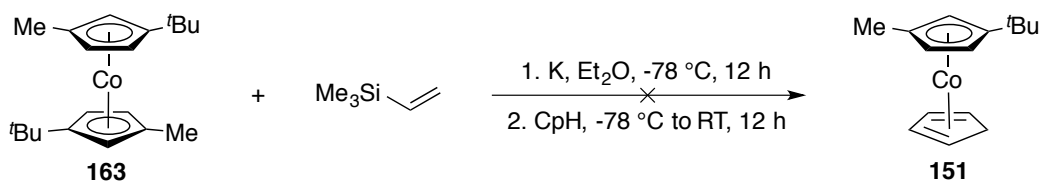


To gain a fuller appreciation of the ethylene replacement method, the reverse strategy was also attempted. This route involves the synthesis of the disubstituted cyclopentadienyl cobalt(I) bis(trimethylvinylsilane) intermediate, with subsequent exchange trapping by cyclopentadiene. The substituted cobaltocene **163** was prepared from cobalt(II) chloride and two equivalents of 1-Me-3-*t*BuCpK **126** (Eq. 3-49). Reduction of cobaltocene **163** in the presence of trimethylvinylsilane produced a promising reddish solution (Eq. 3-50). While the solution was maintained at  $-78\text{ }^\circ\text{C}$ , cyclopentadiene was added to replace the labile trimethylvinylsilane ligands. However, in the end, the reaction again afforded an intractable mixture.

### Equation 3-49



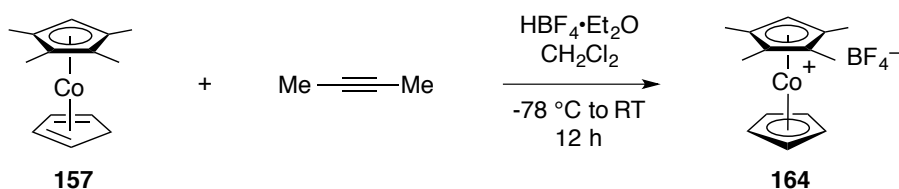
### Equation 3-50



These results confirm that the ethylene replacement strategy is not successful in producing (1-methyl-3-*tert*-butyl cyclopentadienyl)cobalt(I)cyclopentadiene **151** and/or its corresponding isomers. One assumption to account for the failed reaction might be due to a slipping of the disubstituted ligand in order to relieve steric hindrance on *tert*-butyl group. This may lead to the  $\eta^1$ -Cp coordination mode of the Cp carbon atom bearing the methyl substituent and further  $\beta$ -hydride elimination. Therefore, a complicated mixture could be generated without desired results.

We then turned to the use of (Me<sub>4</sub>Cp)CoCpH **157** directly for [5+2] ring-expansion reactions (Eq. 3-51), giving up completely on the notion of a disubstituted ancillary ligand. However, upon protonation, only loss of hydrogen was observed, producing 1,2,3,4-tetramethylcyclopentadienyl cobaltocenium **164** without detection of any (cycloheptadienyl)cobalt(III) ring-expansion product.

### Equation 3-51



In conclusion, the new cobalt(I) cyclopentadiene complexes could not undergo [5+2] ring-expansion reactions. In the presence of alkyne substrates, loss of H<sub>2</sub> remains a competitive reaction pathway to afford the corresponding cobaltocenium compounds. Though the tetramethylcyclopentadienyl cobalt(I)  $\eta^4$ -cyclopentadiene is structurally similar to Trevor's cobalt(I) complex bearing a pentamethylcyclopentadienyl ligand, their reactivities toward [5+2] ring-expansion reactions appears vastly different. The result suggests that the ring-expansion reactivity is highly sensitive toward the substitution pattern of the cyclopentadienyl ligand. The detailed mechanism remains unclear, but DFT calculations from Dr. Ammal provides interesting insight, leading to a new strategy as discussed in Chapter 4.

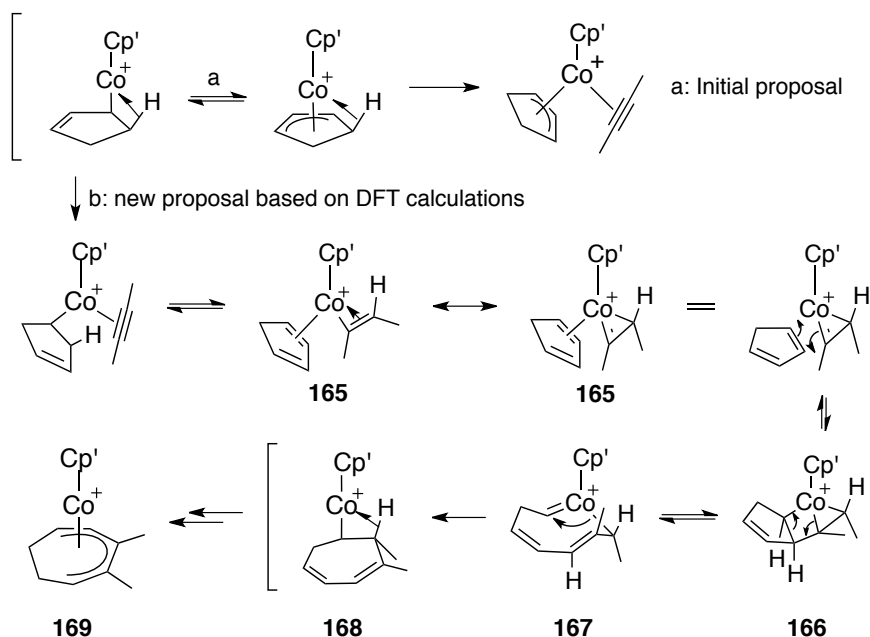
## Chapter 4. Towards an iron-mediated [5+2] ring-expansion reaction

### 4.1 Introduction

As the current methodology proved incapable of producing  $\eta^4$ -cyclopentadiene cobalt(I) complexes, a new strategy for [5+2] ring-expansion reactions was proposed. The suggested mechanism for the reaction involves the formation of an agostic  $\eta^3$ -cyclopentenyl cobalt(III) complex **107** as the key intermediate for the ring-expansion reaction. However, in contrast to our working hypothesis, which posited alkyne coordination and migration, DFT calculations revealed a hidden and novel mechanistic pathway.

Our collaborators at the University of Tokyo, Dr. Salai Ammal and Prof. Eiichi Nakamura, determined computationally that it is the  $\eta^2$ -vinyl cobalt(III) complex **165** that acts as the reactive intermediate for the [5+2] ring-expansion reactions (Scheme 4-1).<sup>196</sup> After the addition of  $\text{HBF}_4$ , the alkyne substrate becomes protonated to form an  $\eta^2$ -vinyl cobalt(III) complex **165**, which electronically resembles a cobalt alkylidene fragment. This then undergoes a [2+2] cycloaddition with a  $\eta^2$ -coordinated cyclopentadiene. A [2+2] cycloreversion cleaves the cyclopentene C–C  $\sigma$ -bond and affords an eight-membered metallacyclic alkylidene **167**. 1,2-migration of the alkyl carbon yields an agostic cycloheptadienyl cobalt(III) complex **168**, which undergoes further isomerization to afford the observed  $\eta^5$ -cycloheptadienyl cobalt(III) complex **169**.

### Scheme 4-1

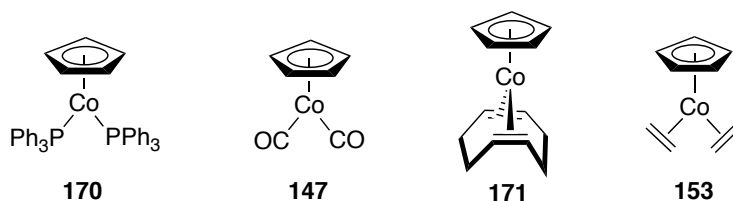


Inspired by the DFT calculations, a new entry into [5+2] ring-expansion reactions was devised. As the mechanism suggests, it is to the coordinated alkyne that the proton migrates instead of to the cyclopentadiene ligand, therefore, the reactions could be performed starting from a metal alkyne precursor, with the addition of acid and a free diene. In addition, based on Salai's calculations, only one double bond in cyclopentadiene is subject to the metathesis during the ring-expansion process. Thus, the use of cyclopentadiene is no longer necessary and often unstable cyclopentadiene component can be replaced by a simple cyclopentene. In summary, the new strategy for the ring-expansion reaction became protonation of the metal alkyne complex in the presence of cyclopentene.

To the best of our knowledge, isolable cyclopentadienyl cobalt(I) alkyne complexes have never been reported in literature and many precursors are efficient catalysts for alkyne

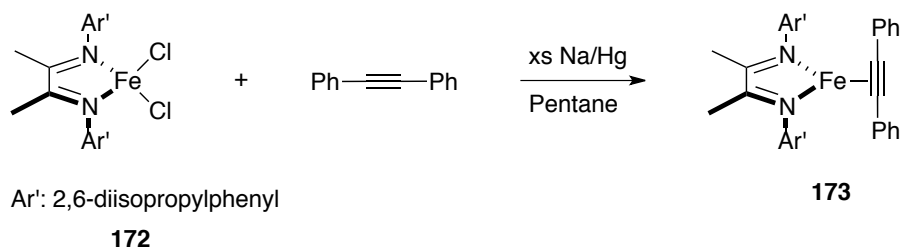
trimerization, including  $\text{CpCo}(\text{CO})_2$  **147**,  $\text{CpCo}(\text{PPh}_3)_2$  **170** and  $\text{CpCo}(\text{olefin})_2$  complexes **171** and **153** (Figure 4-1).<sup>195</sup> On the whole, alkyne trimerization is a thermodynamically favored exothermic reaction that involves the formation of three new C–C  $\sigma$  bonds and an aromatic  $\pi$ -system.<sup>197</sup> Therefore, the preparation of cobalt(I) alkyne complexes is tremendously challenging and another metal system was sought.

**Figure 4-1.** Structures of cobalt(I) complexes



Iron(0) alkyne complexes have been previously reported by Chirik, *et al.*, to be active alkene hydrogenation catalysts.<sup>171</sup> Reduction of diimine iron(II) chloride **172** in the presence of the corresponding alkyne afforded iron(0) alkyne complexes (Eq. 4-1). As reported, the iron(0) diphenylacetylene complex **173** could be purified by recrystallization, whereas the analogous iron(0) 2-butyne complex **174** remained oily and resisted purification. The [5+2] ring-expansion reaction was thus developed using known iron(0) diphenylacetylene complex **173**.

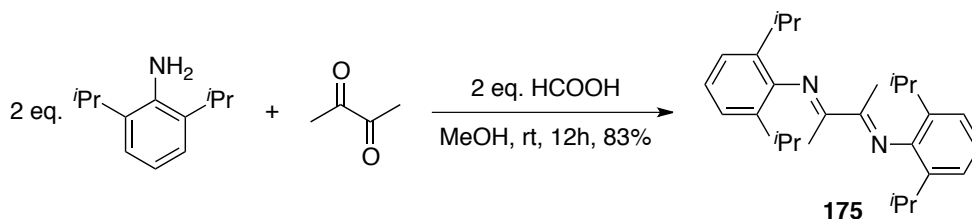
**Equation 4-1**



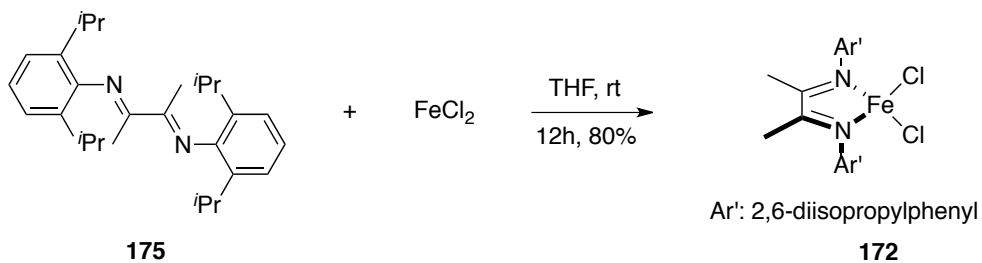
## 4.2 Results and discussion

Before conducting [5+2] ring-expansion experiments, iron(0) alkyne complex **173** was first prepared. Diimine **175** was obtained from 2,6-diisopropylaniline and 2,3-butadione condensation (Eq. 4-2).<sup>198</sup> Subsequently, the addition of diimine to ferrous chloride generated the iron(II) complex **172** (Eq. 4-3).<sup>199</sup> Following the reduction of iron(II) complex **172** as previously described, iron(0) alkyne complex **173** was produced and purified by recrystallization from pentane.

### Equation 4-2



### Equation 4-3

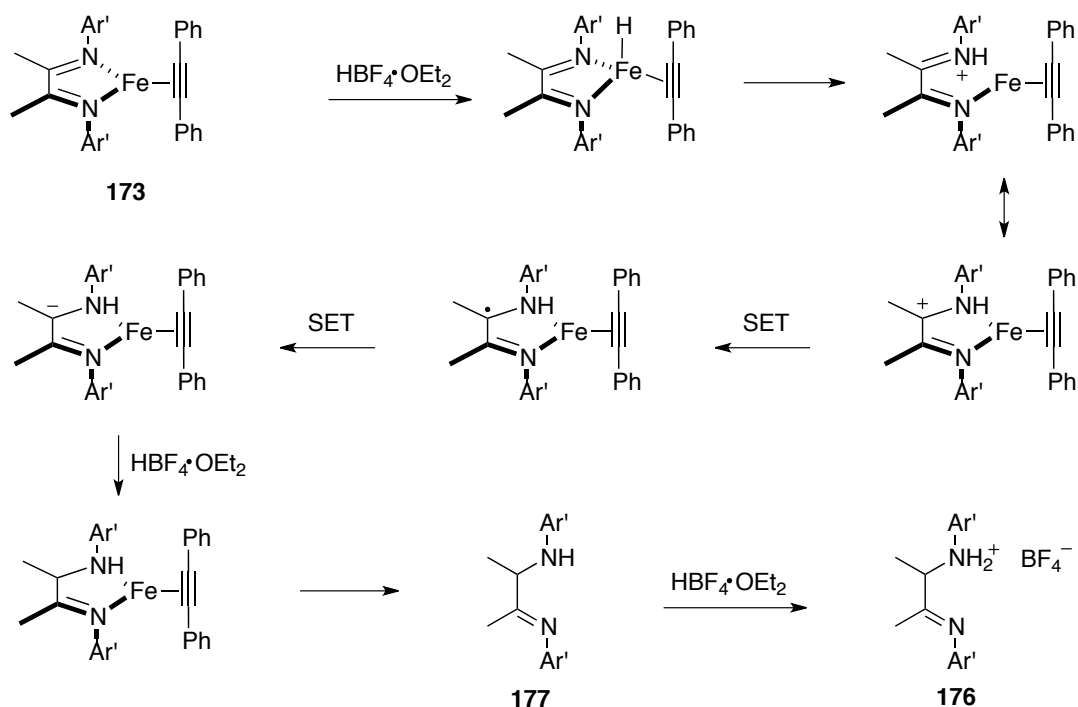


With iron(0) alkyne complex **173** in hand, the new [5+2] ring-expansion reaction could be investigated. To a solution containing iron(0) complex **173**, excess cyclopentene and one equivalent fluoroboric acid were subsequently added at -78 °C (Eq. 4-4). The solution



yield of 25% crystallized ammonium **176** represents a high conversion, suggesting the proposed mechanism is the dominant reaction pathway.

#### Scheme 4-2



#### Part II. Conclusion

In summary, the attempted [5+2] ring-expansion reactions failed to undergo C–C bond activation to afford the desired products. The preparation of ( $\eta^5$ -1-methyl-3-*tert*butylcyclopentadienyl)cobalt(I)- $\eta^4$ -cyclopentadiene appears to be very challenging. Two synthetic routes were examined, including the reduction of corresponding cobaltocenium compound and replacement of ethylene ligands with cyclopentadiene starting from the cobalt(I) bis(ethylene) complex. However, the  $\eta^4$ -cyclopentadiene

cobalt(I) complexes that were prepared followed an undesired pathway to afford the corresponding cobaltocenium compounds.

Inspired by DFT calculations from a collaborator, our second strategy for ring-expansion reaction now involves the protonation of iron(0) alkyne complex in the presence of cyclopentene. However, using the bis(imine) iron(0) complex reported in the literature, this reaction instead involves the reduction of the imine ligand. The product from C–C bond activation was not formed. In conclusion, ring-expansion reactions could not be achieved from either  $\eta^4$ -cyclopentadiene cobalt(I) or iron(0) alkyne complexes and this phase of the project was abandoned.

## **Part II. Future work**

With the development of trialkylphosphoranimide-supported first-row transition metal clusters in our group, a new opportunity for exploring [5+2] ring-expansion reactions has become available. Since phosphoranimide-supported nickel(I) and cobalt(I) clusters are coordinately unsaturated, the compounds may mediate a range of novel organometallic reactions. It may be possible to prepare and isolate the corresponding cobalt(I)/nickel(I) cyclopentene or cyclopentadiene complexes. Protonation of such complexes in the presence of alkynes could lead to the formation of ring-expansion products.

## Chapter 5: Experimental information

### Reagents and methods

All manipulations of air sensitive compounds were conducted under a nitrogen atmosphere using standard Schlenk techniques, or in an mBraun Labmaster drybox equipped with a -35 °C freezer. Tetrahydrofuran, diethyl ether, hexane, pentane, benzene and toluene were distilled from sodium benzophenone ketyl (THF, Et<sub>2</sub>O, PhH), potassium benzophenone ketyl (pentane, hexane), or molten sodium (PhMe) respectively under nitrogen.

Dichloromethane, *n*-octane, ethylbenzene and other solvents/liquid reagents were dried over calcium hydride and degassed by three freeze-pump-thaw cycles at high vacuum (10<sup>-5</sup> mm Hg). Solid chemicals were directly transferred into the drybox as received. The precatalyst complexes [Ni-N=P<sup>t</sup>Bu<sub>3</sub>]<sub>4</sub> (**8**), [Co-N=P<sup>t</sup>Bu<sub>3</sub>]<sub>4</sub> (**9**), [Me-Co-N=PEt<sub>3</sub>]<sub>4</sub> and [Me-Co-N=PEt<sub>3</sub>]<sub>4</sub>[BF<sub>4</sub>] were prepared as previously described.<sup>49,148</sup> 3 Å molecular sieves were stored in a 120 °C oven for at least two days before being transferred into the dry box. Both calcium hydride and 3 Å molecular sieves were crushed to fine powders using a pestle and mortar and kept in drybox for storage. All glassware were dried in a 120 °C oven overnight prior to use.

### Further Note on Spectroscopic Methods

<sup>1</sup>H NMR and <sup>13</sup>C NMR spectra were recorded on either a Varian Unity-Inova 300 (<sup>1</sup>H 300 MHz) or a Varian Unity-Inova 400 (<sup>1</sup>H 400 MHz; <sup>13</sup>C 100 MHz) spectrometer. Chemical shifts for <sup>1</sup>H NMR spectra are reported in ppm and referenced against the residual protonated NMR solvent peaks. Gas chromatograph-mass spectrometry was performed using a Hewlett Packard GCD series G1800A GC-MS in the Analytical and Instrumentation Laboratories. High-resolution electron impact mass spectra were obtained from a Kratos

Analytical MS-50G Mass Spectrometry. Elemental analysis was performed with a Carlo Erba EA1108 Elemental Analyzer in Analytical and Instrumentation Laboratory. X-Ray structural data were collected on a Bruker Platform diffractometer with a SMART 1000 CCD area detector and analyzed by Dr. Robert McDonald and Dr. Micheal J. Ferguson for structural resolution and refinement in the X-Ray Crystallography Laboratory.

## **Experimental section of Chapter 1**

### **General Procedures**

Unless stated otherwise, all hydrogenation reactions were performed in cylindrical thick-walled Pyrex glass vessels equipped with Teflon vacuum stopcocks, referred to as glass bombs. The Schlenk line was purged with a continuous flow of hydrogen for at least 30 minutes before conducting hydrogenation reactions. The glass bomb was kept under vacuum for at least 10 minutes while immersed in liquid nitrogen bath to freeze reaction mixture. Afterwards the glass bomb was back-filled with hydrogen, sealed and warmed to room temperature. The entire glassware was immersed in an oil bath at 120 °C or temperatures otherwise stated behind a safety shield. The reaction mixture was stirred at a speed of 1500 rpm, unless stated otherwise.

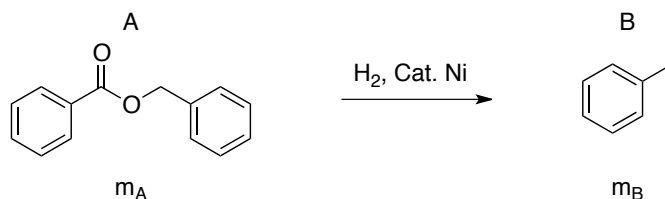
#### *Standardization of GC yield*

Many ester hydrogenation reactions involve the generation of volatile products, such as toluene and hexane in previous examples. Since the quantitative isolation of these organic liquids is technically impractical, GC-MS analysis provides an alternative method to probe the reactions. However, GC yield is based on the relative intensity of detected signal and

might deviate from actual reaction yield. Therefore it is essential to standardize GC yield to actual yield of the final product.

A calibration graph reflecting the relationship between GC and actual yield is plotted, in which x- and y-axis represents GC and actual yield, respectively. To plot this graph, a series of solutions containing starting material and product with various molar ratios are prepared. Each solution contributes to one point on the graph, which is represented as (x, y). The x-value is obtained from GC-MS analysis and y-value calculated based on moles of the compounds. (Figure 5-1) After drawing a series of points on the graph, a smooth trendline is generated to fit the dots. Eventually, the graph can be utilized to convert GC yield of any reaction to corresponding actual yield.

**Figure 5-1.** Calculation of toluene yield (y-value)



For A+B solution preparation,  $m_A$  and  $m_B$  are measured.

$$\begin{array}{ccc}
 m_A & \xrightarrow{\text{mol} = m / \text{M.W.}} & \text{mol}_A \\
 m_B & & \text{mol}_B
 \end{array}
 \xrightarrow{\text{B mol\%} = \text{mol}_B / (\text{mol}_A + \text{mol}_B)}
 \text{B mol\%, which is y-value}$$

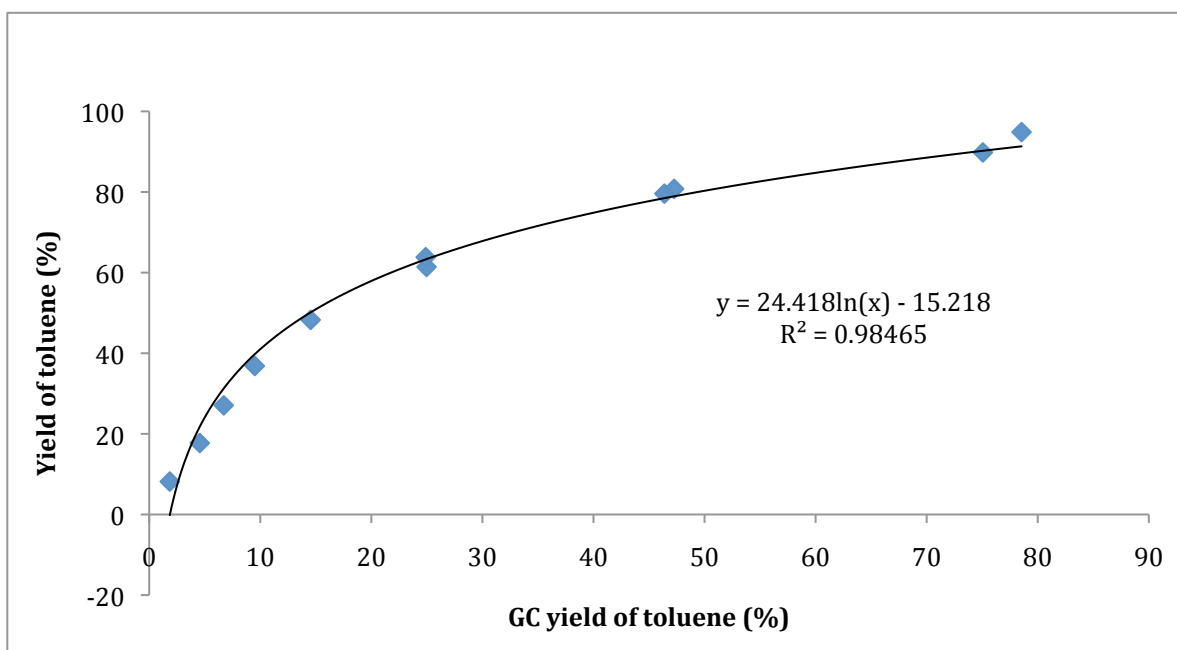
Benzyl benzoate hydrogenation reactions were repeatedly conducted for condition optimization. The calibration graph for toluene GC yield is valuable for the estimation of the actual yield. The graph is plotted based on the preparation of a series of diethyl ether solutions containing known concentrations of toluene and benzyl benzoate. The detailed calculation for toluene molar percent is provided in Figure 5-1. On the other hand, GC yield

for the samples are obtained from GC-MS analysis. A summary about GC and molar percent of toluene is shown in Table 5-1. Based on these data, eleven points are plotted on the Graph 5-1. A logarithmic trendline is generated that has the best fit to the data. The corresponding formula is also provided, which is  $y=24.418\ln(x)-15.218$ .

**Table 5-1.** A summary of GC and mol percent for toluene in prepared diethyl ether solutions

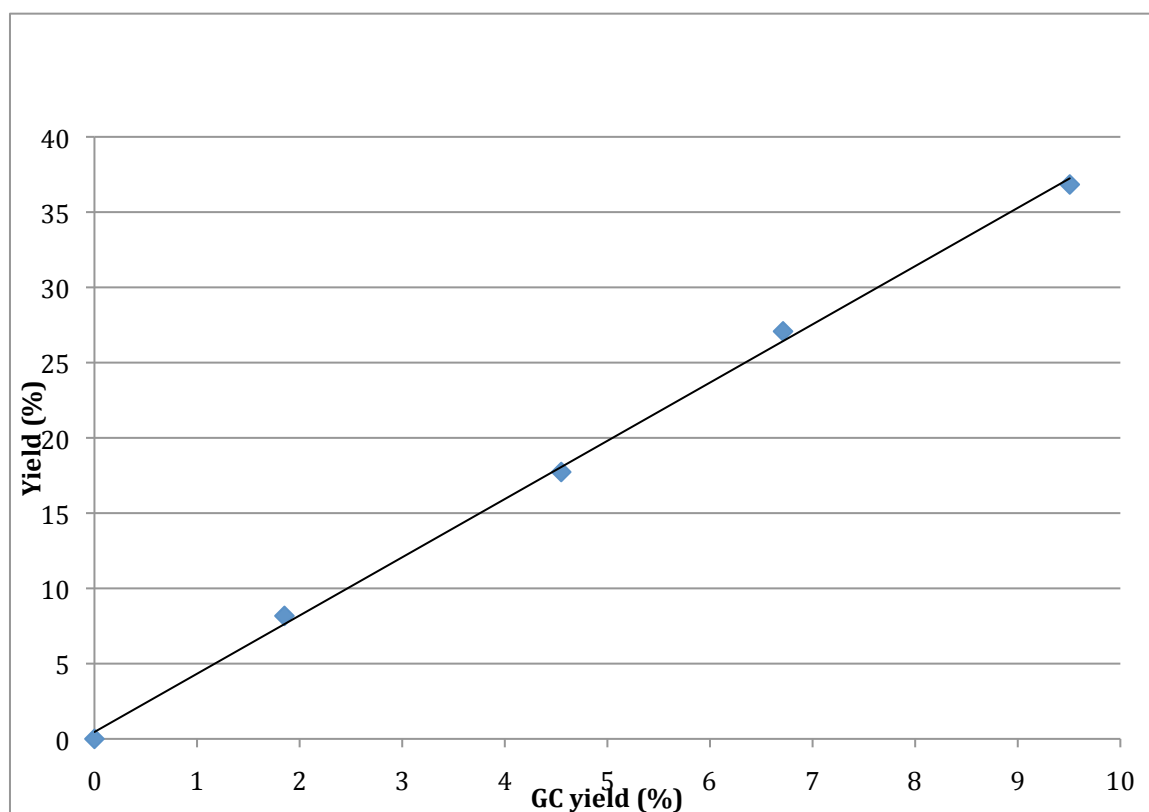
Sample	1	2	3	4	5	6
x-value: GC %	1.9	4.6	6.7	9.5	14.5	25.0
y-value: mol%	8.2	17.7	27.1	36.8	48.3	61.4
Sample	7	8	9	10	11	
x- value: GC %	24.9	47.3	46.4	75.1	78.5	
y- value: mol%	63.8	80.8	79.6	89.8	94.9	

**Graph 5-1.** Standardization of GC Yield for Benzyl Benzoate Reduction to Toluene.



The logarithmic curve appears to fit the data reasonably well, as the dots are located closely to the curve and distributed evenly on both sides as well. For the graph, r-squared value equals 0.98465, which also suggests the regression line fits the data well. If the first four sets of data in graph 5-1 were examined more closely, they appear quite linear as shown in graph 5-2.

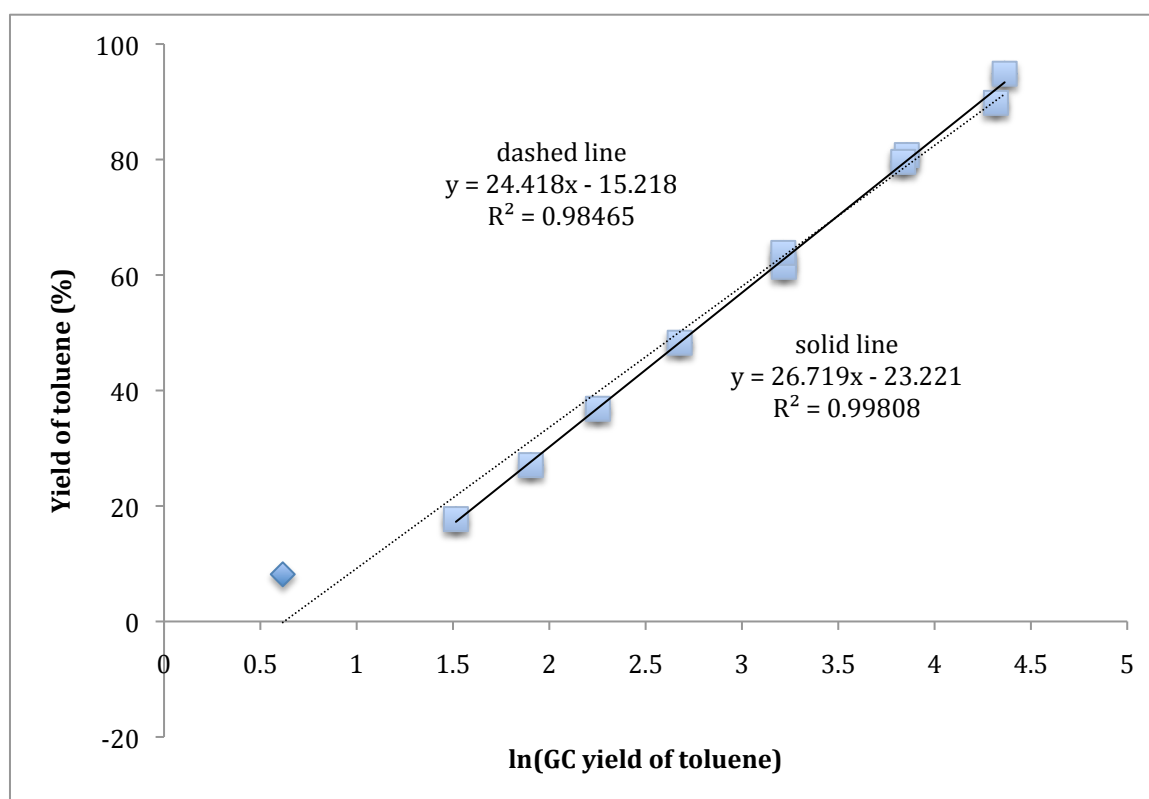
**Graph 5-2.** Plotting of the first four sets of data in graph 5-1.



Based on the formula related to logarithmic curve, the relationship between molar percent and  $\ln(\text{GC } \%)$  is anticipated to be linear. The graph containing  $\ln(\text{GC } \%)$  as x-axis is also plotted and the formula for the line is  $y=24.418x-15.218$  with r-squared value equals

0.98465. Most of the points appear close to the straight line except the first data point. Therefore, a new graph that neglects the first dot is plotted as shown in Graph 5-3, which appears to fit the data nicely. R-squared value increases to 0.99808. The formula for the new line is  $y = 26.719x - 23.221$ .

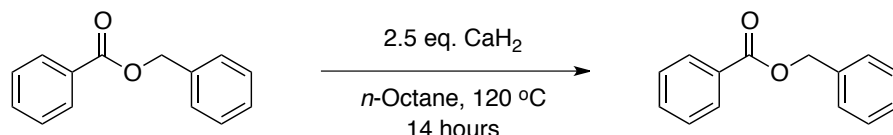
**Graph 5-3.** Standardization of GC Yield for Benzyl Benzoate Reduction to Toluene



In conclusion, the relationship between GC yield and actual yield appears to be a logarithmic curve in Graph 5-1. The formula relating to the curve provides a good estimation of the actual yield based on the GC yield from measurement.

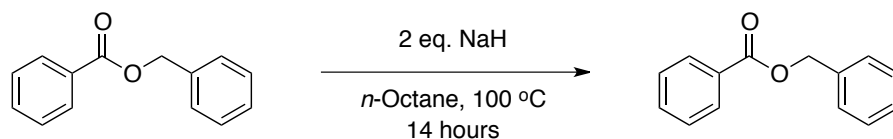
## Detailed Experimental Procedures for Chapter 2

*Control experiment: reaction of CaH<sub>2</sub> with benzyl benzoate*



Benzyl benzoate (68.4 mg, 0.32 mmol) was weighed into a glass vial and dissolved in 1.0 ml *n*-octane. The solution was transferred to a glass bomb equipped with a stir bar and rinsed with another 0.5 ml *n*-octane. Calcium hydride (33.9 mg, 0.81 mmol, 2.5 equiv) was added to the glass bomb. The vessel was heated to 120 °C for 14 h. Water (0.1 ml) and 0.5M HCl solution (2 ml) were added in sequence dropwise to the reaction mixture. After separation of the organic phase, diethyl ether was used to extract the organic compounds from aqueous layer three times. GC-MS analysis of the combined organic solution indicated that benzyl benzoate and solvents are the only compounds present.

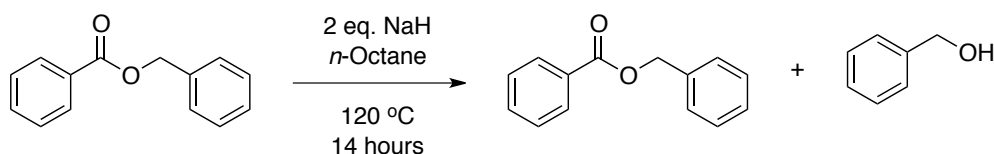
*Control experiment: reaction of NaH with benzyl benzoate at 100 °C*



Benzyl benzoate (70.2 mg, 0.33 mmol) was weighed into a glass vial and dissolved in 1.0 ml *n*-octane. The solution was transferred to a glass bomb equipped with a stir bar and rinsed with another 0.5 ml *n*-octane. Sodium hydride (15.9 mg, 0.66 mmol, 2.0 equiv) was added to the glass bomb. The vessel was heated to 100 °C for 14 h. Water (0.1 ml) and 0.5M HCl

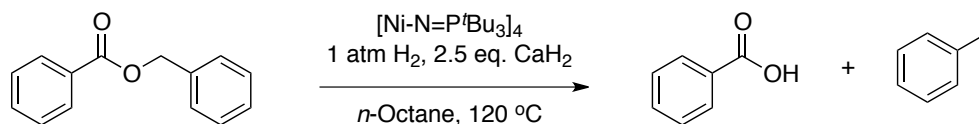
solution (2 ml) were added dropwise in sequence to quench the reaction mixture. After separation of the organic phase, diethyl ether was used to extract the organic compounds from aqueous layer three times. GC-MS analysis of the combined organic solution indicated that benzyl benzoate and solvents are the only compounds present.

*Control experiment: reaction of NaH with benzyl benzoate at 120 °C*

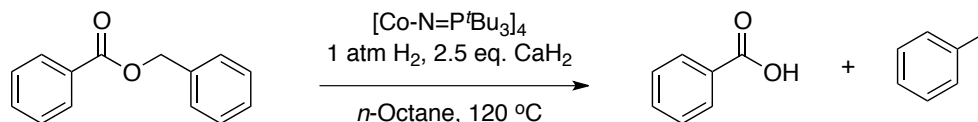


Benzyl benzoate (67.8 mg, 0.32 mmol) was weighed into a glass vial and dissolved in 1.0 ml *n*-octane. The solution was transferred to a glass bomb equipped with a stir bar and rinsed with another 0.5 ml *n*-octane. Sodium hydride (15.3 mg, 0.64 mmol, 2.0 equiv) was added to the glass bomb. The vessel was heated to 120 °C for 14 h. Water (0.1 ml) and 0.5M HCl solution (2 ml) were added dropwise in sequence to quench the reaction mixture. After separation of the organic phase, diethyl ether was used to extract the organic compounds from aqueous layer three times. GC-MS analysis of the combined organic solution indicated the presence of benzyl alcohol (3.2%) and benzyl benzoate (96.8%) in addition to the solvents.

*Comparison of precatalysts for benzyl benzoate reduction*

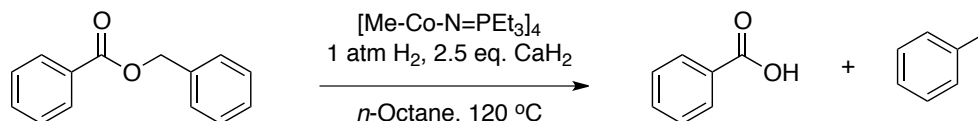


In a drybox, **8** (9.1 mg,  $8.3 \times 10^{-3}$  mmol, 2.0 mol% per cluster) and benzyl benzoate (87.9 mg, 0.41 mmol) were weighed into glass vials separately and dissolved in 0.5 ml *n*-octane. The solutions were transferred to a glass bomb equipped with a stir bar and rinsed with another 0.5 ml *n*-octane. Calcium hydride (43.1 mg, 1.03 mmol, 2.5 equiv) was added to the glass bomb. The content of glass bomb was put under hydrogen atmosphere using the Schlenk line as discussed. The vessel was heated to 120 °C for 14 h during which white solids precipitated. The *n*-octane soluble fraction was filtered through Celite and rinsed with diethyl ether. GC-MS analysis of the *n*-octane soluble fraction indicated that toluene and solvents are the only compounds present. Water (0.1 ml) and 0.5M HCl solution (2 ml) were added in sequence dropwise to the remaining solid. Diethyl ether was used to extract the organic compounds from aqueous layer three times. The organic layer was dried over  $\text{Na}_2\text{SO}_4$  and the diethyl ether was removed *in vacuo* to afford a white solid (51.0 mg, 100%).  $^1\text{H}$  NMR spectrum was obtained to identify the solid as benzoic acid.

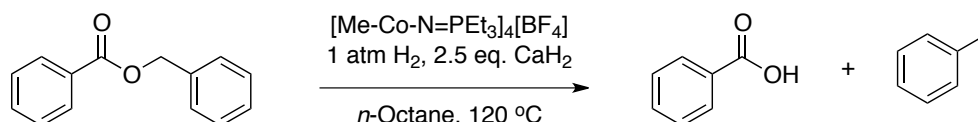


In a drybox, **9** (9.1 mg,  $8.3 \times 10^{-3}$  mmol, 2.0 mol% per cluster) and benzyl benzoate (87.4 mg, 0.41 mmol) were weighed into glass vials separately and dissolved in 0.5 ml *n*-octane. The solutions were transferred to a glass bomb equipped with a stir bar and rinsed with another 0.5 ml *n*-octane. Calcium hydride (43.3 mg, 1.03 mmol, 2.5 equiv) was added to the glass bomb. The content of glass bomb was put under hydrogen atmosphere using the Schlenk line as discussed. The vessel was heated to 120 °C for 14 h during which white solids precipitated. The *n*-octane soluble fraction was filtered through Celite and rinsed with diethyl ether. GC-MS analysis of the *n*-octane soluble fraction indicated that the presence of benzyl benzoate (97.6%) and toluene (2.4%). Water (0.1 ml) and 0.5M HCl solution (2 ml) were added in sequence dropwise to the remaining solid. Diethyl ether was

used to extract the organic compounds from aqueous layer three times. The organic layer was dried over  $\text{Na}_2\text{SO}_4$  and the diethyl ether was removed *in vacuo* to afford a white solid (0.3 mg, 0.6%).  $^1\text{H}$  NMR spectrum was obtained and the solid was identified as benzoic acid.



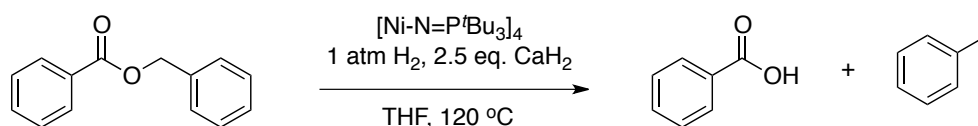
In a drybox,  $[\text{Me-Co-N=PEt}_3]_4$  (6.9 mg,  $8.4 \times 10^{-3}$  mmol, 2.0 mol% per cluster) and benzyl benzoate (88.1 mg, 0.42 mmol) were weighed into glass vials separately and dissolved in 0.5 ml *n*-octane. The solutions were transferred to a glass bomb equipped with a stir bar and rinsed with another 0.5 ml *n*-octane. Calcium hydride (43.6 mg, 1.04 mmol, 2.5 equiv) was added to the glass bomb. The content of glass bomb was put under hydrogen atmosphere using the Schlenk line as discussed. The vessel was heated to 120 °C for 14 h. The *n*-octane soluble fraction was filtered through Celite and rinsed with diethyl ether. GC-MS analysis of the *n*-octane soluble fraction indicated that only benzyl benzoate and solvent was present.



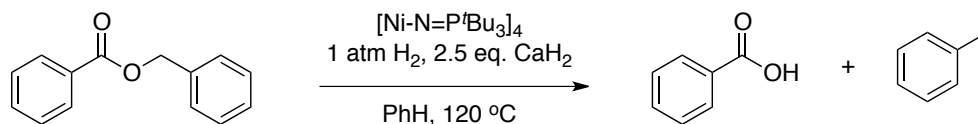
In a drybox,  $[\text{Me-Co-N=PEt}_3]_4[\text{BF}_4]$  (8.8 mg,  $8.0 \times 10^{-3}$  mmol, 2.0 mol% per cluster) and benzyl benzoate (85.2 mg, 0.40 mmol) were weighed into glass vials separately and dissolved in 0.5 ml *n*-octane. The solutions were transferred to a glass bomb equipped with a stir bar and rinsed with another 0.5 ml *n*-octane. Calcium hydride (42.0 mg, 1.0 mmol, 2.5 equiv) was added to the glass bomb. The content of glass bomb was put under hydrogen

atmosphere using the Schlenk line as discussed. The vessel was heated to 120 °C for 14 h. The *n*-octane fraction was filtered through Celite and rinsed with diethyl ether. GC-MS analysis of the *n*-octane soluble fraction indicated that the only presence of benzyl benzoate and solvents.

#### *Solvent screen for benzyl benzoate reduction*

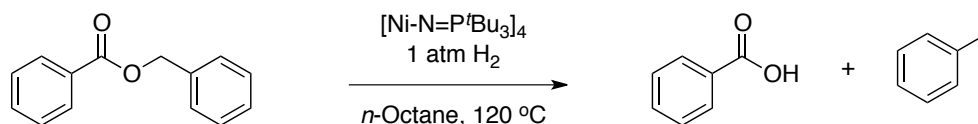


In a drybox, **8** (6.2 mg,  $5.6 \times 10^{-3}$  mmol, 2.0 mol% per cluster) and benzyl benzoate (59.0 mg, 0.28 mmol) were weighed into glass vials separately and dissolved in 0.5 ml THF. The solutions were transferred to a glass bomb equipped with a stir bar and rinsed with another 0.5 ml THF. Calcium hydride (29.3 mg, 0.69 mmol, 2.5 equiv) was added to the glass bomb. The content of glass bomb was put under hydrogen atmosphere using the Schlenk line as discussed. The vessel was heated to 120 °C for 14 h during which white solids precipitated. The THF soluble fraction was filtered through Celite and rinsed with diethyl ether. GC-MS analysis of the *n*-octane soluble fraction indicated the presence of toluene (85.8%) and benzyl benzoate (14.2%). Water (0.1 ml) and 0.5M HCl solution (2 ml) were added in sequence dropwise to the remaining solid. Diethyl ether was used to extract the organic compounds from aqueous layer three times. The organic layer was dried over  $\text{Na}_2\text{SO}_4$  and the diethyl ether was removed *in vacuo* to afford a white solid (31.7 mg, 93.4%).  $^1\text{H}$  NMR spectrum was obtained to identify the solid as benzoic acid.



In a drybox, **8** (6.1 mg,  $5.5 \times 10^{-3}$  mmol, 2.0 mol% per cluster) and benzyl benzoate (58.8 mg, 2.8 mmol) were weighed into glass vials separately and dissolved in 0.5 ml benzene. The solutions were transferred to a glass bomb equipped with a stir bar and rinsed with another 0.5 ml benzene. Calcium hydride (30.3 mg, 0.72 mmol, 2.5 equiv) was added to the glass bomb. The content of glass bomb was put under hydrogen atmosphere using the Schlenk line as discussed. The vessel was heated to 120 °C for 14 h during which white solids precipitated. The benzene soluble fraction was filtered through Celite and rinsed with diethyl ether. GC-MS analysis of the benzene soluble fraction indicated the presence of toluene (55.7%) and benzyl benzoate (44.3%). Water (0.1 ml) and 0.5M HCl solution (2 ml) were added dropwise in sequence to quench the remaining solid. Diethyl ether was used to extract the organic compounds from aqueous layer three times. The organic layer was dried over  $\text{Na}_2\text{SO}_4$  and the diethyl ether was removed *in vacuo* to afford a white solid (28.5 mg, 83.3%).  $^1\text{H}$  NMR spectrum was obtained to identify the solid as benzoic acid.

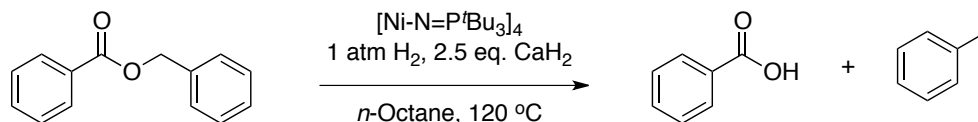
#### *Benzyl benzoate reduction without base scavenger*



In a drybox, **8** (5.5 mg,  $5.0 \times 10^{-3}$  mmol, 2.0 mol% per cluster) and benzyl benzoate (52.7 mg, 24.8 mmol) were weighed into glass vials separately and dissolved in 0.5 ml *n*-octane. The solutions were transferred to a glass bomb equipped with a stir bar and rinsed with another 0.5 ml *n*-octane. The content of glass bomb was put under hydrogen atmosphere

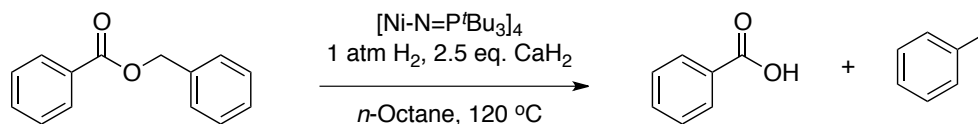
using the Schlenk line as discussed. The vessel was heated to 120 °C for 14 h during which white solids precipitated. The *n*-octane soluble fraction was filtered through Celite and rinsed with diethyl ether. GC-MS analysis of the *n*-octane soluble fraction indicated the presence of toluene (7%) and benzyl benzoate (93%). Water (0.1 ml) and 0.5M HCl solution (2 ml) were added dropwise in sequence to quench the remaining solid. Diethyl ether was used to extract the organic compounds from aqueous layer three times. The organic layer was dried over Na<sub>2</sub>SO<sub>4</sub> and the diethyl ether was removed *in vacuo* to afford a white solid. <sup>1</sup>H NMR spectrum was obtained to identify the solid as benzoic acid.

*Benzyl benzoate reduction at longer reaction time*



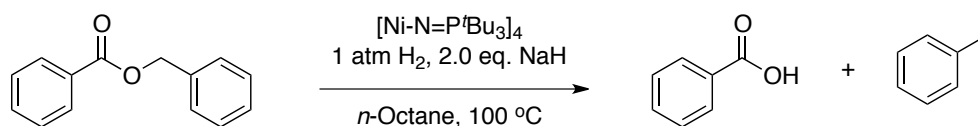
In a drybox, **8** (2.9 mg, 2.6×10<sup>-3</sup> mmol, 1.0 mol% per cluster) and benzyl benzoate (56.0 mg, 0.26 mmol) were weighed into glass vials separately and dissolved in 0.4 ml *n*-octane. The solutions were transferred to a glass bomb equipped with a stir bar and rinsed with another 0.4 ml *n*-octane. Calcium hydride (27.7 mg, 0.66 mmol, 2.5 equiv) was added to the glass bomb. The content of glass bomb was put under hydrogen atmosphere using the Schlenk line as discussed. The vessel was heated to 120 °C for 14 h during which white solids precipitated. The *n*-octane soluble fraction was filtered through Celite and rinsed with diethyl ether. GC-MS analysis of the *n*-octane soluble fraction indicated the presence of toluene (59.3%) and benzyl benzoate (40.7%) besides solvents. Water (0.1 ml) and 0.5M HCl solution (2 ml) were added dropwise in sequence to quench the remaining solid. Diethyl ether was used to extract the organic compounds from aqueous layer three times. The organic layer was dried over Na<sub>2</sub>SO<sub>4</sub> and the diethyl ether was removed *in vacuo* to

afford a white solid.  $^1\text{H}$  NMR spectrum was obtained to identify the solid as benzoic acid (28.0 mg, 86.9%).

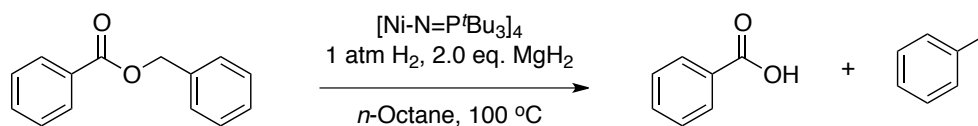


In a drybox, **8** (3.5 mg,  $3.2 \times 10^{-3}$  mmol, 1.0 mol% per cluster) and benzyl benzoate (68.4 mg, 0.32 mmol) were weighed into glass vials separately and dissolved in 0.5 ml *n*-octane. The solutions were transferred to a glass bomb equipped with a stir bar and rinsed with another 0.5 ml *n*-octane. Calcium hydride (33.8 mg, 0.81 mmol, 2.5 equiv) was added to the glass bomb. The content of glass bomb was put under hydrogen atmosphere using the Schlenk line as discussed. The vessel was heated to 120 °C for 28 h during which white solids precipitated. The *n*-octane soluble fraction was filtered through Celite and rinsed with diethyl ether. GC-MS analysis of the *n*-octane soluble fraction indicated that toluene and solvents are the only compounds present. Water (0.1 ml) and 0.5M HCl solution (2 ml) were added dropwise in sequence to quench the remaining solid. Diethyl ether was used to extract the organic compounds from aqueous layer three times. The organic layer was dried over  $\text{Na}_2\text{SO}_4$  and the diethyl ether was removed *in vacuo* to afford a white solid (40.3 mg, 100%).  $^1\text{H}$  NMR spectrum was obtained to identify the solid as benzoic acid.

#### Comparison of base scavengers for benzyl benzoate reduction

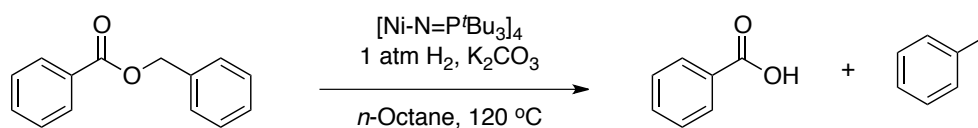


In a drybox, **8** (3.6 mg,  $3.2 \times 10^{-3}$  mmol, 1.0 mol% per cluster) and benzyl benzoate (68.7 mg, 0.32 mmol) were weighed into glass vials separately and dissolved in 0.5 ml *n*-octane. The solutions were transferred to a glass bomb equipped with a stir bar and rinsed with another 0.5 ml *n*-octane. Sodium hydride (15.5 mg, 0.65 mmol, 2.0 equiv) was added to the glass bomb. The content of glass bomb was put under hydrogen atmosphere using the Schlenk line as discussed. The vessel was heated to 100 °C for 14 h during which white solids precipitated. The *n*-octane soluble fraction was filtered through Celite and rinsed with diethyl ether. GC-MS analysis of the *n*-octane soluble fraction indicated that toluene and solvents are the only compounds present. Water (0.1 ml) and 0.5M HCl solution (2 ml) were added dropwise in sequence to quench the remaining solid. Diethyl ether was used to extract the organic compounds from aqueous layer three times. The organic layer was dried over Na<sub>2</sub>SO<sub>4</sub> and the diethyl ether was removed *in vacuo* to afford a white solid (40.2 mg, 100%). <sup>1</sup>H NMR spectrum was obtained to identify the solid as benzoic acid. <sup>1</sup>H NMR (300 MHz, CDCl<sub>3</sub>) δ 8.12 (m, 2H); 7.62 (m, 1H); 7.45 (m, 2H).

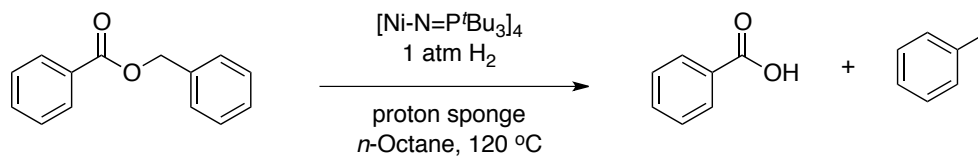


In the dry box, **8** (3.5 mg,  $3.2 \times 10^{-3}$  mmol, 1.0 mol% per cluster) and benzyl benzoate (68.4 mg, 0.32 mmol) were weighed into glass vials separately and dissolved in 0.5 ml *n*-octane. The solutions were transferred to a glass bomb equipped with a stir bar and rinsed with another 0.5 ml *n*-octane. Magnesium hydride (17.0 mg, 0.64 mmol, 2.0 equiv) was added to the glass bomb. The content of glass bomb was put under hydrogen atmosphere using the Schlenk line as discussed. The vessel was heated to 100 °C for 14 h during which white solids precipitated. The *n*-octane soluble fraction was filtered through Celite and rinsed with diethyl ether. GC-MS analysis of the *n*-octane soluble fraction indicated the presence of

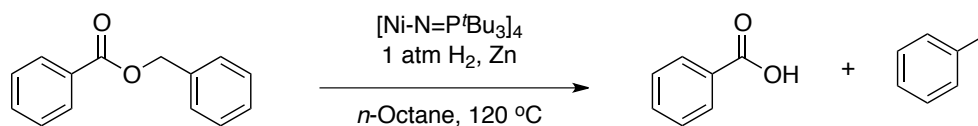
toluene (20.2%) and benzyl benzoate (79.8%) besides solvents. Water (0.1 ml) and 0.5M HCl solution (2 ml) were added dropwise in sequence to quench the remaining solid. Diethyl ether was used to extract the organic compounds from aqueous layer three times. The organic layer was dried over Na<sub>2</sub>SO<sub>4</sub> and the diethyl ether was removed *in vacuo* to afford a white solid (17.2 mg, 43.7%). <sup>1</sup>H NMR spectrum was obtained to identify the solid as benzoic acid.



In a drybox, **8** (5.1 mg, 4.6×10<sup>-3</sup> mmol, 2.0 mol% per cluster) and benzyl benzoate (47.3 mg, 0.22 mmol) were weighed into glass vials separately and dissolved in 0.5 ml *n*-octane. The solutions were transferred to a glass bomb equipped with a stir bar and rinsed with another 0.5 ml *n*-octane. Potassium carbonate (87.2 mg, 0.63 mmol) was added to the glass bomb. The content of glass bomb was put under hydrogen atmosphere using the Schlenk line as discussed. The vessel was heated to 120 °C for 14 h during which white solids precipitated. The *n*-octane soluble fraction was filtered through Celite and rinsed with diethyl ether. GC-MS analysis of the *n*-octane soluble fraction indicated the presence of toluene (9%) and benzyl benzoate (90%) besides solvents. Water (0.1 ml) and 0.5M HCl solution (2 ml) were added dropwise in sequence to quench the remaining solid. Diethyl ether was used to extract the organic compounds from aqueous layer three times. The organic layer was dried over Na<sub>2</sub>SO<sub>4</sub> and the diethyl ether was removed *in vacuo* to afford a white solid. <sup>1</sup>H NMR spectrum was obtained to identify the solid as benzoic acid.



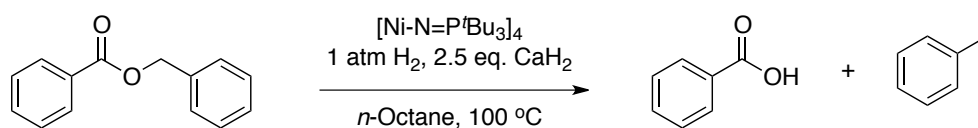
In a drybox, **8** (6.5 mg,  $5.9 \times 10^{-3}$  mmol, 2.0 mol% per cluster) and benzyl benzoate (62.8 mg, 0.30 mmol) were weighed into glass vials separately and dissolved in 0.5 ml *n*-octane. The solutions were transferred to a glass bomb equipped with a stir bar and rinsed with another 0.5 ml *n*-octane. 1,8-bis(dimethylamino)naphthalene (88.9 mg, 0.41 mmol, 1.4 equiv), known as proton sponge, was added to the glass bomb. The content of glass bomb was put under hydrogen atmosphere using the Schlenk line as discussed. The vessel was heated to 120 °C for 14 h during which brown solids precipitated. The *n*-octane soluble fraction was filtered through Celite and rinsed with diethyl ether. GC-MS analysis of the *n*-octane soluble fraction indicated the presence of toluene (8.3%) and benzyl benzoate (91.7%) besides solvents and proton sponge.



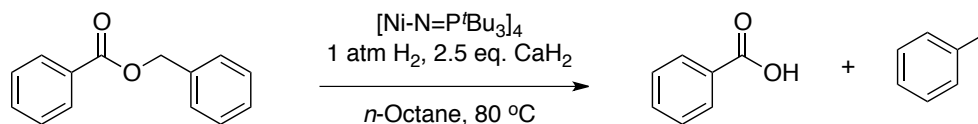
In a drybox, **8** (4.3 mg,  $3.9 \times 10^{-3}$  mmol, 2.0 mol% per cluster) and benzyl benzoate (41.1 mg, 0.19 mmol) were weighed into glass vials separately and dissolved in 0.3 ml *n*-octane. The solutions were transferred to a glass bomb equipped with a stir bar and rinsed with another 0.3 ml *n*-octane. Rieke zinc (6.3 mg, 0.096 mmol, 0.5 equiv) was added to the glass bomb.<sup>200</sup> The content of glass bomb was put under hydrogen atmosphere using the Schlenk line as discussed. The vessel was heated to 120 °C for 14 h during which white solids precipitated. The *n*-octane soluble fraction was filtered through Celite and rinsed with diethyl ether. GC-MS analysis of the *n*-octane soluble fraction indicated the presence of

toluene (9.4%) and benzyl benzoate (90.6%) besides solvents. Water (0.1 ml) and 0.5M HCl solution (2 ml) were added dropwise in sequence to quench the remaining solid. Diethyl ether was used to extract the organic compounds from aqueous layer three times. The organic layer was dried over Na<sub>2</sub>SO<sub>4</sub> and the diethyl ether was removed *in vacuo* to afford a white solid (6.3 mg, 26.7%). <sup>1</sup>H NMR spectrum was obtained to identify the solid as benzoic acid.

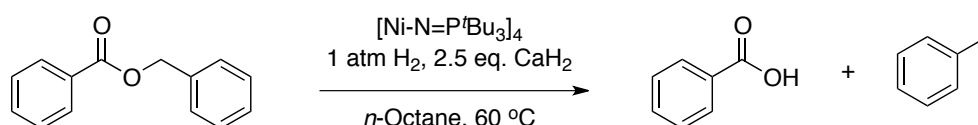
*Effect of reaction temperature for the benzyl benzoate reduction*



In a drybox, **8** (7.7 mg, 7.0×10<sup>-3</sup> mmol, 2.0 mol% per cluster) and benzyl benzoate (74.2 mg, 0.35 mmol) were weighed into glass vials separately and dissolved in 0.5 ml *n*-octane. The solutions were transferred to a glass bomb equipped with a stir bar and rinsed with another 0.5 ml *n*-octane. Calcium hydride (36.8 mg, 0.88 mmol, 2.5 equiv) was added to the glass bomb. The content of glass bomb was put under hydrogen atmosphere using the Schlenk line as discussed. The vessel was heated to 100 °C for 14 h during which white solids precipitated. The *n*-octane soluble fraction was filtered through Celite and rinsed with diethyl ether. GC-MS analysis of the *n*-octane soluble fraction indicated the presence of toluene (74.9%) and benzyl benzoate (25.1%) besides solvents. Water (0.1 ml) and 0.5M HCl solution (2 ml) were added dropwise in sequence to quench the remaining solid. Diethyl ether was used to extract the organic compounds from aqueous layer three times. The organic layer was dried over Na<sub>2</sub>SO<sub>4</sub> and the diethyl ether was removed *in vacuo* to afford a white solid (38.5 mg, 90.2%). <sup>1</sup>H NMR spectrum was obtained to identify the solid as benzoic acid.



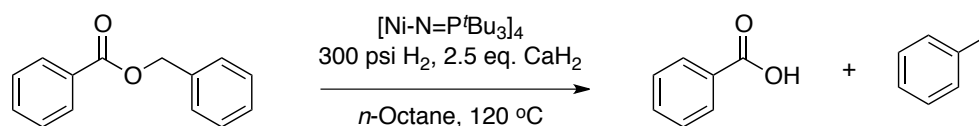
In a drybox, **8** (8.2 mg,  $7.5 \times 10^{-3}$  mmol, 2.0 mol% per cluster) and benzyl benzoate (78.7 mg, 0.37 mmol) were weighed into glass vials separately and dissolved in 0.5 ml *n*-octane. The solutions were transferred to a glass bomb equipped with a stir bar and rinsed with another 0.5 ml *n*-octane. Calcium hydride (39.0 mg, 0.93 mmol, 2.5 equiv) was added to the glass bomb. The content of glass bomb was put under hydrogen atmosphere using the Schlenk line as discussed. The vessel was heated to 80 °C for 14 h during which white solids precipitated. The *n*-octane soluble fraction was filtered through Celite and rinsed with diethyl ether. GC-MS analysis of the *n*-octane soluble fraction indicated the presence of toluene (21.0%) and benzyl benzoate (79.0%) besides solvents. Water (0.1 ml) and 0.5M HCl solution (2 ml) were added dropwise in sequence to quench the remaining solid. Diethyl ether was used to extract the organic compounds from aqueous layer three times. The organic layer was dried over Na<sub>2</sub>SO<sub>4</sub> and the diethyl ether was removed *in vacuo* to afford a white solid. <sup>1</sup>H NMR spectrum was obtained to identify the solid as benzoic acid.



In a drybox, **8** (6.4 mg,  $5.8 \times 10^{-3}$  mmol, 2.0 mol% per cluster) and benzyl benzoate (61.9 mg, 0.29 mmol) were weighed into glass vials separately and dissolved in 0.5 ml *n*-octane. The solutions were transferred to a glass bomb equipped with a stir bar and rinsed with another 0.5 ml *n*-octane. Calcium hydride (30.7 mg, 0.73 mmol, 2.5 equiv) was added to the glass bomb. The content of glass bomb was put under hydrogen atmosphere using the Schlenk line as discussed. The vessel was heated to 60 °C for 14 h during which white solids

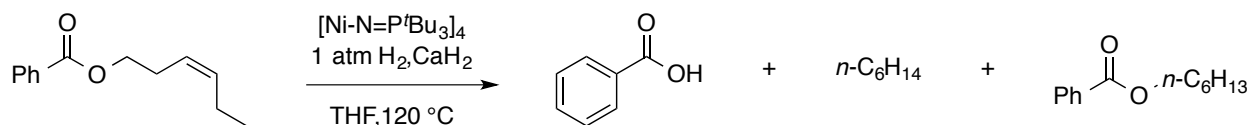
precipitated. The *n*-octane soluble fraction was filtered through Celite and rinsed with diethyl ether. GC-MS analysis of the *n*-octane soluble fraction indicated the presence of toluene (8.0%) and benzyl benzoate (92.0%) besides solvents. Water (0.1 ml) and 0.5M HCl solution (2 ml) were added dropwise in sequence to quench the remaining solid. Diethyl ether was used to extract the organic compounds from aqueous layer three times. The organic layer was dried over Na<sub>2</sub>SO<sub>4</sub> and the diethyl ether was removed *in vacuo* to afford a white solid. <sup>1</sup>H NMR spectrum was obtained to identify the solid as benzoic acid.

*Effect of hydrogen pressure to the benzyl benzoate reduction*

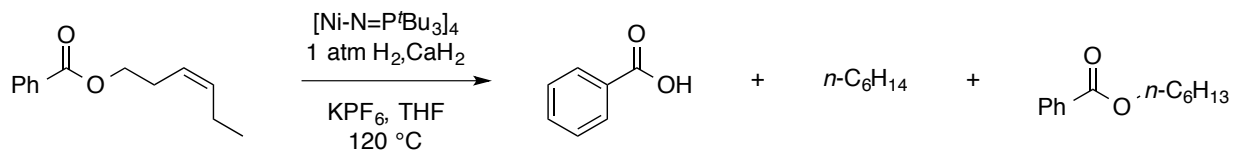


In the drybox, **8** (3.4 mg, 3.1×10<sup>-3</sup> mmol, 1.0 mol% per cluster) and benzyl benzoate (65.9 mg, 0.31 mmol) were weighed into glass vials separately and dissolved in 0.5 ml *n*-octane. The solutions were transferred to a glass container equipped with a stir bar and rinsed with another 0.5 ml *n*-octane. Calcium hydride (32.7 mg, 0.78 mmol, 2.5 equiv) was added to the glass container. A high-pressure steel reactor was assembled inside the drybox and pressured to 300 psi hydrogen gas before conducting the reaction. The reactor was heated to 120 °C for 14 h during which white solids precipitated. The *n*-octane soluble fraction was filtered through Celite and rinsed with diethyl ether. GC-MS analysis of the *n*-octane soluble fraction indicated the presence of toluene (17.4%) and benzyl benzoate (82.6%) besides solvents. Water (0.1 ml) and 0.5M HCl solution (2 ml) were added dropwise in sequence to quench the remaining solid. Diethyl ether was used to extract the organic compounds from aqueous layer three times. The organic layer was dried over Na<sub>2</sub>SO<sub>4</sub> and the diethyl ether was removed *in vacuo* to afford a white solid. <sup>1</sup>H NMR spectrum was obtained to identify the solid as benzoic acid.

Study of cation effect of sodium/ potassium to 3-hexenyl benzoate reduction

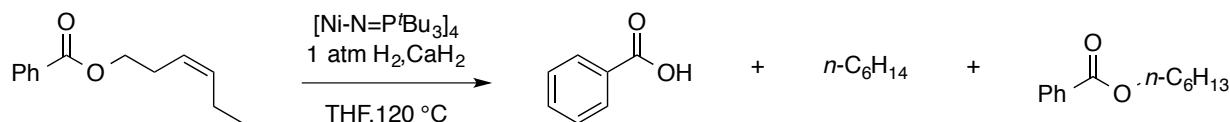


In a drybox, **8** (6.0 mg,  $5.6 \times 10^{-3}$  mmol, 2.0 mol% per cluster) and 3-hexenyl benzoate (56.9 mg, 0.28 mmol) were weighed into glass vials separately and dissolved in 0.5 ml THF. The solutions were transferred to a glass bomb equipped with a stir bar and rinsed with another 0.5 ml THF. Calcium hydride (170.2 mg, 4.04 mmol, 14.4 equiv) was added to the glass bomb. The content of glass bomb was put under hydrogen atmosphere using the Schlenk line as discussed. The vessel was heated to 120 °C for 14 h during which white solids precipitated. The *n*-octane soluble fraction was filtered through Celite and rinsed with diethyl ether. GC-MS analysis of the THF soluble fraction indicated the presence of hexane (1.4%) and hexyl benzoate (98.6%) besides solvents. Water (0.1 ml) and 0.5M HCl solution (2 ml) were added dropwise in sequence to quench the remaining solid. Diethyl ether was used to extract the organic compounds from aqueous layer three times. The organic layer was dried over Na<sub>2</sub>SO<sub>4</sub> and the diethyl ether was removed *in vacuo* to afford a white solid (4.7 mg, 13.6%). <sup>1</sup>H NMR spectrum was obtained to identify the solid as benzoic acid.



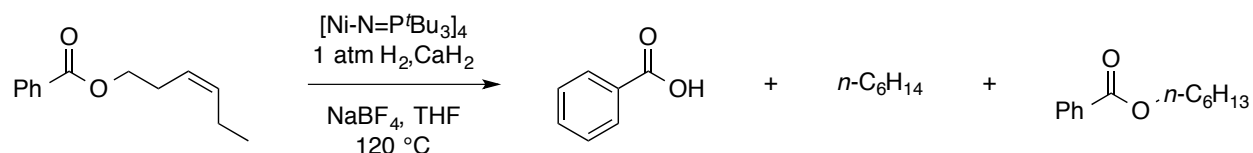
In a drybox, **8** (6.0 mg,  $5.6 \times 10^{-3}$  mmol, 2.0 mol% per cluster) and 3-hexenyl benzoate (56.9 mg, 0.28 mmol) were weighed into glass vials separately and dissolved in 0.5 ml THF. The solutions were transferred to a glass bomb equipped with a stir bar and rinsed with

another 0.5 ml THF. Calcium hydride (170.3 mg, 4.04 mmol, 14.4 equiv) and potassium hexafluorophosphate (90.8 mg, 0.49 mmol, 1.8 equiv) were added to the glass bomb. The content of glass bomb was put under hydrogen atmosphere using the Schlenk line as discussed. The vessel was heated to 120 °C for 14 h during which white solids precipitated. The THF soluble fraction was filtered through Celite and rinsed with diethyl ether. GC-MS analysis of the THF soluble fraction indicated the presence of hexane (1.3%) and hexyl benzoate (98.7%) besides solvents. Water (0.1 ml) and 0.5M HCl solution (2 ml) were added dropwise in sequence to quench the remaining solid. Diethyl ether was used to extract the organic compounds from aqueous layer three times. The organic layer was dried over Na<sub>2</sub>SO<sub>4</sub> and the diethyl ether was removed *in vacuo* to afford a white solid (5.9 mg, 17.4%). <sup>1</sup>H NMR spectrum was obtained to identify the solid as benzoic acid.



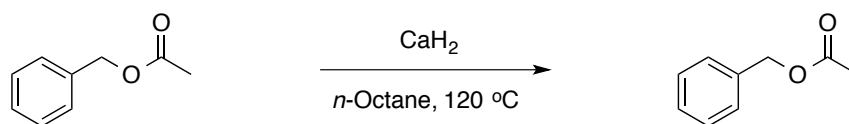
In a drybox, **8** (9.2 mg, 8.4×10<sup>-3</sup> mmol, 2.0 mol% per cluster) and 3-hexenyl benzoate (85.5 mg, 0.42 mmol) were weighed into glass vials separately and dissolved in 0.5 ml THF. The solutions were transferred to a glass bomb equipped with a stir bar and rinsed with another 0.5 ml THF. Calcium hydride (200.0 mg, 4.75 mmol, 11.3 equiv) was added to the glass bomb. The content of glass bomb was put under hydrogen atmosphere using the Schlenk line as discussed. The vessel was heated to 120 °C for 14 h during which white solids precipitated. Water (0.1 ml) and 0.5M HCl solution (2 ml) were added dropwise in sequence to quench the reaction mixture. Diethyl ether was used to extract the organic compounds from aqueous layer three times. The organic fraction was dried over Na<sub>2</sub>SO<sub>4</sub> and submitted for GC-MS analysis. The GC-MS result indicated the presence of hexane (1.1%), benzoic acid (5.5%) and hexyl benzoate (93.4%) besides solvents. In principle, the

molar amounts of hexane and benzoic acid generated were equivalent. However, the GC yield only reflects the relative strength of the detected signal, it deviates from the actual yield.



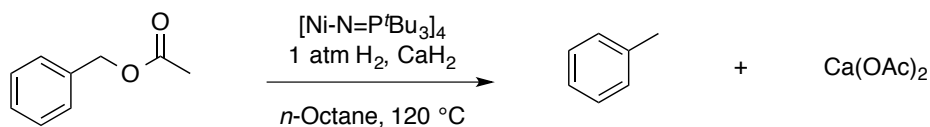
In a drybox, **8** (9.2 mg,  $8.4 \times 10^{-3}$  mmol, 2.0 mol% per cluster) and 3-hexenyl benzoate (85.5 mg, 0.42 mmol) were weighed into glass vials separately and dissolved in 0.5 ml THF. The solutions were transferred to a glass bomb equipped with a stir bar and rinsed with another 0.5 ml THF. Calcium hydride (200.0 mg, 4.75 mmol, 11.3 equiv) and sodium tetrafluoroborate (103.5 mg, 0.94 mmol, 2.2 equiv) were added to the glass bomb. The content of glass bomb was put under hydrogen atmosphere using the Schlenk line as discussed. The vessel was heated to 120 °C for 14 h during which white solids precipitated. Water (0.1 ml) and 0.5M HCl solution (2 ml) were added dropwise in sequence to quench the reaction mixture. Diethyl ether was used to extract the organic compounds from aqueous layer three times. The organic fraction was dried over  $\text{Na}_2\text{SO}_4$  and submitted for GC-MS analysis. The GC-MS result indicated the presence of hexane (0.8%), benzoic acid (4.1%) and hexyl benzoate (95.1%) besides solvents.

#### *Control experiment for benzyl acetate reduction*



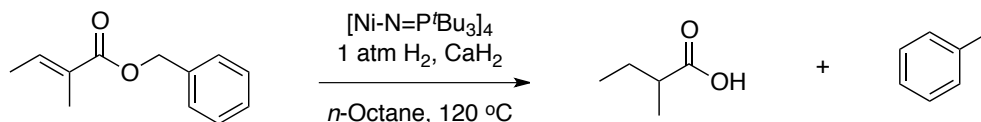
In a drybox, benzyl acetate (34.3 mg, 0.23 mmol) were weighed into glass vials and dissolved in 0.5 ml *n*-octane. The solution was transferred to a glass bomb equipped with a stir bar and rinsed with another 0.5 ml *n*-octane. Calcium hydride (24.0 mg, 0.57 mmol, 2.5 equiv) was added to the glass bomb. The vessel was heated to 120 °C for 14 h. Water (0.1 ml) and 0.5M HCl solution (2 ml) were added dropwise in sequence to quench the reaction mixture. The *n*-octane soluble fraction was filtered through Celite and extracted by diethyl ether. GC-MS analysis of the combined organic fraction indicated that only benzyl acetate (100%) and solvents were present in the solution.

*Substrate scope extension using the optimized condition: benzyl acetate reduction*



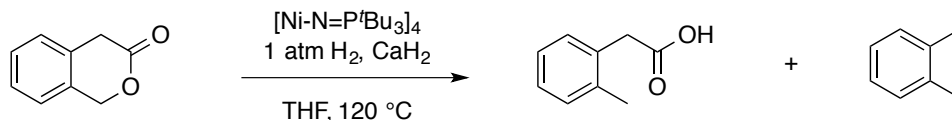
In a drybox, **8** (7.8 mg,  $7.1 \times 10^{-3}$  mmol, 2.0 mol% per cluster) and benzyl acetate (53.5 mg, 0.36 mmol) were weighed into glass vials separately and dissolved in 0.5 ml *n*-octane. The solutions were transferred to a glass bomb equipped with a stir bar and rinsed with another 0.5 ml *n*-octane. Calcium hydride (37.5 mg, 0.89 mmol, 2.5 equiv) was added to the glass bomb. The content of glass bomb was put under hydrogen atmosphere using the Schlenk line as discussed. The vessel was heated to 120 °C for 14 h during which white solids precipitated. The *n*-octane soluble fraction was filtered through Celite and rinsed with diethyl ether. GC-MS analysis of the *n*-octane soluble fraction indicated that the toluene is the only product along with solvents. The remaining solid was dissolved in D<sub>2</sub>O and analyzed by <sup>1</sup>H and <sup>13</sup>C NMR spectroscopy. The solid was identified as calcium acetate. Due to the presence of CaH<sub>2</sub> and/or Ca(OH)<sub>2</sub>, the weight of Ca(OAc)<sub>2</sub> cannot be determined. <sup>1</sup>H NMR (300 MHz, D<sub>2</sub>O) δ 1.86 (s, 1H); <sup>13</sup>C NMR (400 MHz, D<sub>2</sub>O) δ 181.6 (C=O); 27.8 (CH<sub>3</sub>).

### Benzyl tiglate reduction



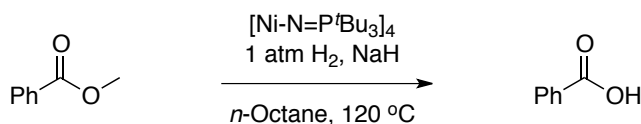
In a drybox, **8** (8.8 mg,  $8.0 \times 10^{-3}$  mmol, 2.0 mol% per cluster) and benzyl tiglate (76.5 mg, 0.40 mmol) were weighed into glass vials separately and dissolved in 0.5 ml  $n$ -octane. The solutions were transferred to a glass bomb equipped with a stir bar and rinsed with another 0.5 ml  $n$ -octane. Calcium hydride (42.2 mg, 1.0 mmol, 2.5 equiv) was added to the glass bomb. The content of glass bomb was put under hydrogen atmosphere using the Schlenk line as discussed. The vessel was heated to 120 °C for 14 h during which white solids precipitated. The  $n$ -octane soluble fraction was filtered through Celite and rinsed with diethyl ether. GC-MS analysis of the  $n$ -octane soluble fraction indicated that the toluene is the only product along with solvents. The remaining solid was dissolved in  $\text{D}_2\text{O}$  and analyzed by  $^1\text{H}$  and  $^{13}\text{C}$  NMR spectroscopy. The solid was identified as calcium 2-methylbutanoate. Due to the presence of  $\text{CaH}_2$  and/or  $\text{Ca}(\text{OH})_2$  in the remaining solid, the weight of calcium 2-methylbutanoate cannot be determined.  $^1\text{H}$  NMR (300 MHz,  $\text{D}_2\text{O}$ )  $\delta$  2.15 (ddt,  $J=10.4, 7.0, 7.0$  Hz, 1H); 1.45 (m, 1H); 1.33 (m, 1H); 1.00 (d,  $J=7.0$  Hz, 3H); 0.81 (t,  $J=7.4$  Hz, 3H).

### 3-isochromanone reduction



In a drybox, **8** (8.4 mg,  $7.6 \times 10^{-3}$  mmol, 2.0 mol% per cluster) and 3-isochromanone (56.4 mg, 0.38 mmol) were weighed into glass vials separately and dissolved in 0.5 ml THF. The solutions were transferred to a glass bomb equipped with a stir bar and rinsed with another 0.5 ml THF. Calcium hydride (40.1 mg, 0.95 mmol, 2.5 equiv) was added to the glass bomb. The content of glass bomb was put under hydrogen atmosphere using the Schlenk line as discussed. The vessel was heated to 120 °C for 14 h during which white solids precipitated. The THF soluble fraction was filtered through Celite and rinsed with diethyl ether. GC-MS analysis of the THF soluble fraction indicated that the presence of *o*-xylene (14.9%) and 3-isochromanone (85.1%) along with solvents. The solid was added with water (0.1 ml) and dilute HCl (2 ml) subsequently. The organic fraction was extracted with diethyl ether. After evaporation, the solid (31.3 mg, 54.7%) was dissolved in CDCl<sub>3</sub> and analyzed by <sup>1</sup>H and <sup>13</sup>C NMR spectroscopy. The solid was identified as *o*-tolylacetic acid. <sup>1</sup>H NMR (300 MHz, CDCl<sub>3</sub>) δ 7.17 (m, 4H); 3.65 (s, 2H); 2.31 (s, 3H). <sup>13</sup>C NMR (400 MHz, CDCl<sub>3</sub>) δ 178.4 (C=O); 136.9 (Ar); 132.0 (Ar); 130.4 (Ar); 130.3 (Ar); 127.7 (Ar); 126.19 (Ar); 38.9 (CH<sub>2</sub>); 19.5 (CH<sub>3</sub>).

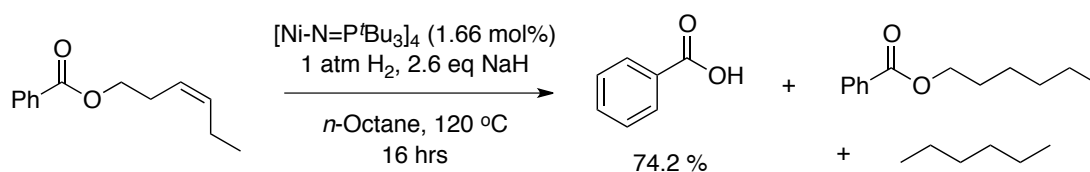
#### *Methyl benzoate reduction*



In a drybox, **8** (9.7 mg,  $8.8 \times 10^{-3}$  mmol, 2.0 mol% per cluster) and methyl benzoate (60.0 mg, 0.44 mmol) were weighed into glass vials separately and dissolved in 0.5 ml *n*-octane. The solutions were transferred to a glass bomb equipped with a stir bar and rinsed with another 0.5 ml *n*-octane. Sodium hydride (21.1 mg, 0.88 mmol, 2.0 equiv) was added to the glass bomb. The content of glass bomb was put under hydrogen atmosphere using the

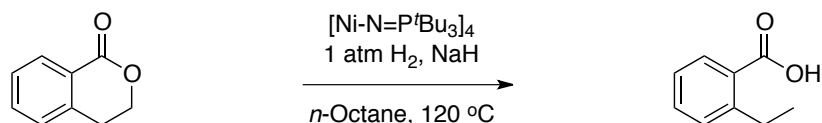
Schlenk line as discussed. The vessel was heated to 120 °C for 14 h during which white solids precipitated. The *n*-octane soluble fraction was filtered through Celite and rinsed with diethyl ether. The remaining solid was acidified by adding dilute HCl (2 ml) and extracted with diethyl ether. After evaporation, the solid was isolated (43.1 mg, 72%). The solid was dissolved in CDCl<sub>3</sub> and analyzed by <sup>1</sup>H and <sup>13</sup>C NMR spectroscopy. The solid was identified as benzoic acid. <sup>1</sup>H NMR (300 MHz, CDCl<sub>3</sub>) δ 8.12 (m, 2H); 7.62 (m, 1H); 7.45 (m, 2H).

#### *cis*-3-hexenyl benzoate reduction



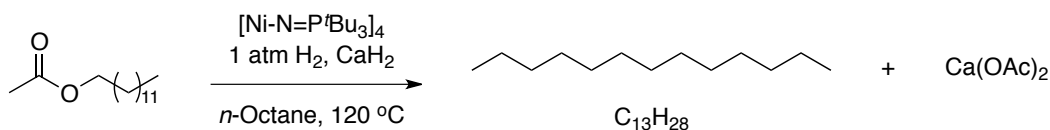
In a drybox, **8** (6.8 mg, 6.2×10<sup>-3</sup> mmol, 1.7 mol% per cluster) and *cis*-3-hexenyl benzoate (76.2 mg, 0.37 mmol) were weighed into glass vials separately and dissolved in 0.5 ml *n*-octane. The solutions were transferred to a glass bomb equipped with a stir bar and rinsed with another 0.5 ml *n*-octane. Sodium hydride (23.1 mg, 0.96 mmol, 2.6 equiv) was added to the glass bomb. The content of glass bomb was put under hydrogen atmosphere using the Schlenk line as discussed. The vessel was heated to 120 °C for 16 h during which white solids precipitated. The *n*-octane soluble fraction was filtered through Celite and rinsed with diethyl ether. The remaining solid was acidified by adding dilute HCl (2 ml) and extracted with diethyl ether. After evaporation, the solid was dissolved in CDCl<sub>3</sub> and analyzed by <sup>1</sup>H NMR spectroscopy. The solid was identified as benzoic acid (33.8 mg, 74.2%). <sup>1</sup>H NMR (300 MHz, CDCl<sub>3</sub>) δ 8.12 (m, 2H); 7.62 (m, 1H); 7.45 (m, 2H).

### 3,4-dihydroisocoumarin reduction



In a drybox, **8** (9.2 mg,  $8.4 \times 10^{-3}$  mmol, 2.0 mol% per cluster) and 3,4-dihydroisocoumarin (62.2 mg, 0.42 mmol) were weighed into glass vials separately and dissolved in 0.5 ml *n*-octane. The solutions were transferred to a glass bomb equipped with a stir bar and rinsed with another 0.5 ml *n*-octane. Sodium hydride (20.2 mg, 0.84 mmol, 2.0 equiv) was added to the glass bomb. The content of glass bomb was put under hydrogen atmosphere using the Schlenk line as discussed. The vessel was heated to 120 °C for 14 h during which white solids precipitated. The *n*-octane soluble fraction was filtered through Celite and rinsed with diethyl ether. The remaining solid was acidified by dilute HCl (2 ml) and extracted with diethyl ether. After evaporation, the solid was dissolved in CDCl<sub>3</sub> and analyzed by <sup>1</sup>H and <sup>13</sup>C NMR spectroscopy. The solid was identified as *o*-ethylbenzoic acid (61.2 mg, 97%). <sup>1</sup>H NMR (300 MHz, CDCl<sub>3</sub>) δ 8.06 (m, 1H), 7.51 (m, 1H), 7.33 (m, 1H), 7.29 (m, 1H), 3.10 (q, *J* = 7.5 Hz, 2H), 1.25 (t, *J* = 7.5 Hz, 3H).

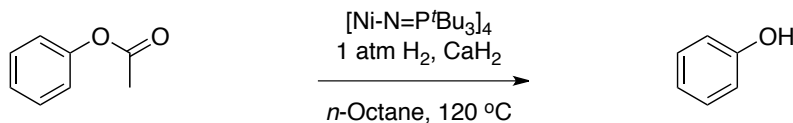
### Tridecyl acetate reduction



In a drybox, **8** (11.0 mg, 0.01 mmol, 2.0 mol% per cluster) and tridecyl acetate (92.4 mg, 0.50 mmol) were weighed into glass vials separately and dissolved in 0.5 ml *n*-octane. The

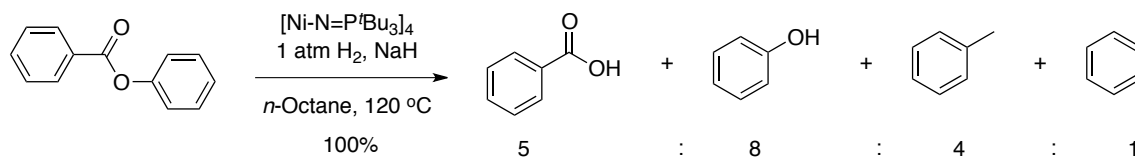
solutions were transferred to a glass bomb equipped with a stir bar and rinsed with another 0.5 ml *n*-octane. Calcium hydride (52.6 mg, 1.25 mmol, 2.5 equiv) was added to the glass bomb. The content of glass bomb was put under hydrogen atmosphere using the Schlenk line as discussed. The vessel was heated to 120 °C for 14 h during which white solids precipitated. The *n*-octane soluble fraction was filtered through Celite and rinsed with diethyl ether. GC-MS analysis of the *n*-octane soluble fraction indicated the presence of tridecane (0.75%) and tridecyl acetate (99.2%) along with solvents.

#### *Phenyl acetate reduction*



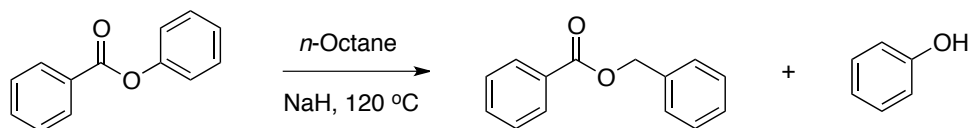
In a drybox, **8** (10.9 mg,  $9.9 \times 10^{-3}$  mmol, 2.0 mol% per cluster) and phenyl acetate (67.2 mg, 0.49 mmol) were weighed into glass vials separately and dissolved in 0.5 ml *n*-octane. The solutions were transferred to a glass bomb equipped with a stir bar and rinsed with another 0.5 ml *n*-octane. Calcium hydride (51.8 mg, 1.23 mmol, 2.5 equiv) was added to the glass bomb. The content of glass bomb was put under hydrogen atmosphere using the Schlenk line as discussed. The vessel was heated to 120 °C for 14 h during which white solids precipitated. Water (0.1 ml) and diluted HCl (2 ml) were subsequently added to the reaction mixture. The organic fraction was extracted with diethyl ether and submitted for GC-MS analysis. The GC result indicated the presence of both phenol (100%) and solvents.

### Phenyl benzoate reduction



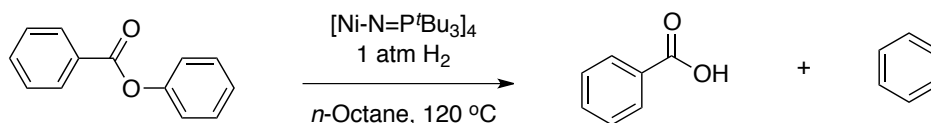
In a drybox, **8** (9.8 mg,  $8.9 \times 10^{-3}$  mmol, 4.0 mol% per cluster) and phenyl benzoate (42.6 mg, 0.21 mmol) were weighed into glass vials separately and dissolved in 0.5 ml *n*-octane. The solutions were transferred to a glass bomb equipped with a stir bar and rinsed with another 0.5 ml *n*-octane. Sodium hydride (10.1 mg, 0.42 mmol, 2.0 equiv) was added to the glass bomb. The content of glass bomb was put under hydrogen atmosphere using the Schlenk line as discussed. The vessel was heated to 120 °C for 14 h during which white solids precipitated. The *n*-octane soluble fraction was filtered through Celite and rinsed with diethyl ether. The organic fraction was submitted for GC-MS analysis. The result indicated the presence of benzene (15.7%) and toluene (84.3%). The remaining solid was acidified by adding dilute HCl (2 ml) and extracted with diethyl ether. After evaporation, the remaining oily residue was dissolved in  $\text{CDCl}_3$  and analyzed by  $^1\text{H}$  and  $^{13}\text{C}$  NMR spectroscopy.  $^1\text{H}$  NMR analysis shows the product contains both benzoic acid and phenol with 1:1.6 (benzoic acid : phenol) ratio.

### Control experiment for phenyl benzoate reduction



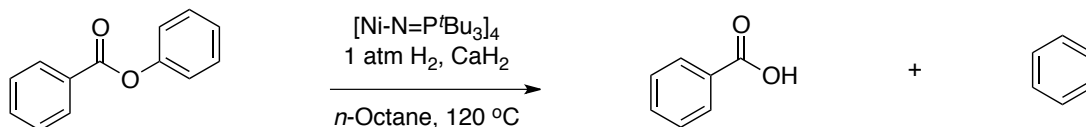
In a drybox, phenyl benzoate (62.3 mg, 0.46 mmol) was weighed into glass vials and dissolved in 0.5 ml *n*-octane. The solution was transferred to a glass bomb equipped with a stir bar and rinsed with another 0.5 ml *n*-octane. Sodium hydride (22.0 mg, 0.92 mmol, 2.0 equiv) was added to the glass bomb. The vessel was heated to 120 °C for 14 h during which white solids precipitated. The organic fraction was filtered through Celite and submitted for GC-MS. The result indicated the presence of toluene (9.4%) and benzyl benzoate (90.6%). The remaining solid was acidified by dilute HCl (2 ml), and extracted with diethyl ether. After removing solvent, the residue was identified as phenol by <sup>1</sup>H NMR.

*Phenyl benzoate reduction with 25 mol% nickel cluster*



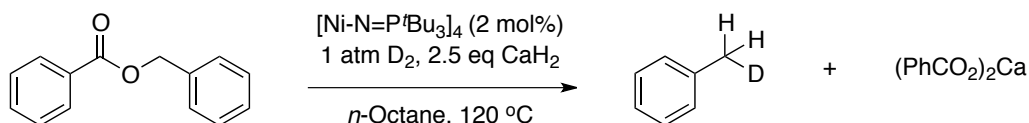
In a drybox, **8** (43.0 mg, 0.039 mmol, 25.0 mol% per cluster) and phenyl benzoate (31.0 mg, 0.16 mmol) were weighed into glass vials separately and dissolved in 0.5 ml *n*-octane. The solutions were transferred to a glass bomb equipped with a stir bar and rinsed with another 0.5 ml *n*-octane. The content of glass bomb was put under hydrogen atmosphere using the Schlenk line as discussed. The vessel was heated to 120 °C for 14 h during which white solids precipitated. The *n*-octane soluble fraction was filtered through Celite and rinsed with diethyl ether. The organic fraction was submitted for GC-MS analysis and identified as benzene (52.8%) and phenyl benzoate (47.2%). The remaining solid was acidified by dilute HCl (2 ml) and extracted with diethyl ether. After evaporation, the solid was dissolved in  $\text{CDCl}_3$  and analyzed by <sup>1</sup>H NMR spectroscopy. The solid was identified as benzoic acid. <sup>1</sup>H NMR (300 MHz,  $\text{CDCl}_3$ )  $\delta$  8.12 (m, 2H); 7.62 (m, 1H); 7.45 (m, 2H).

### Phenyl benzoate reduction with 5 mol% nickel cluster



In a drybox, **8** (3.1 mg,  $2.8 \times 10^{-3}$  mmol, 5.0 mol% per cluster) and phenyl benzoate (28.2 mg, 0.14 mmol) were weighed into glass vials separately and dissolved in 0.5 ml *n*-octane. The solutions were transferred to a glass bomb equipped with a stir bar and rinsed with another 0.5 ml *n*-octane. Calcium hydride (15.2 mg, 0.36 mmol, 2.5 equiv) was added to the glass bomb. The content of glass bomb was put under hydrogen atmosphere using the Schlenk line as discussed. The vessel was heated to 120 °C for 14 h during which white solids precipitated. The *n*-octane soluble fraction was filtered through Celite and submitted for GC-MS. The GC result indicated the presence of benzene (33.8%) and phenyl benzoate (67.2%). The remaining solid was acidified by dilute HCl (2 ml) and extracted with diethyl ether. After evaporation, the solid was dissolved in  $\text{CDCl}_3$  and analyzed by  $^1\text{H}$  NMR spectroscopy. The solid was identified as benzoic acid.  $^1\text{H}$  NMR (300 MHz,  $\text{CDCl}_3$ )  $\delta$  8.12 (m, 2H); 7.62 (m, 1H); 7.45 (m, 2H).

### Deuterium labeling experiment for the benzyl benzoate reduction

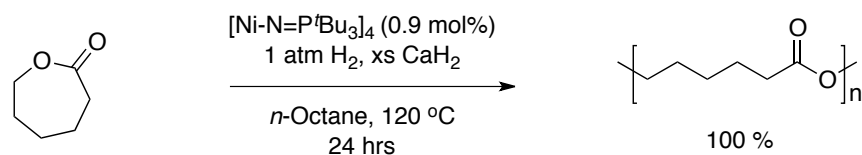


In a drybox, **8** (6.0 mg,  $5.5 \times 10^{-3}$  mmol, 2.0 mol% per cluster) and benzyl benzoate (56.2 mg, 0.26 mmol) were weighed into glass vials separately and dissolved in 0.5 ml *n*-octane. The solutions were transferred to a glass bomb equipped with a stir bar and rinsed with



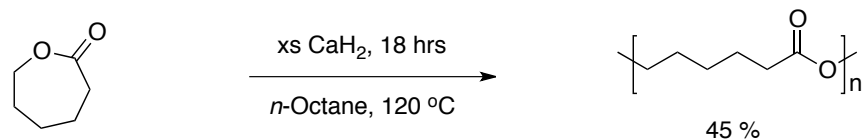
The organic layer was dried over Na<sub>2</sub>SO<sub>4</sub> and then filtered through Celite. GC-MS analysis of the organic fraction indicated the presence of chroman (79%) and dihydrocoumarin (21%) besides solvents. The compounds were isolated by column chromatography. <sup>1</sup>H NMR spectrum was obtained to identify the solid as chroman and dihydrocoumarin. <sup>1</sup>H NMR (300 MHz, CDCl<sub>3</sub>) δ 7.05 (m, 2H), 6.80 (m, 2H), 4.18 (t, *J*= 5.1 Hz, 2H), 2.79 (t, *J*= 6.5 Hz, 2H), 2.00 (m, 2H).

#### *Polymerization of ε-caprolactone*



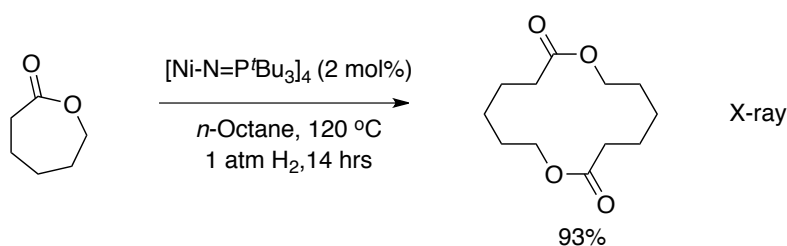
In a drybox, **8** (4.7 mg,  $4.3 \times 10^{-3}$  mmol, 2.0 mol% per cluster) and ε-caprolactone (35.5 mg, 0.31 mmol) were weighed into glass vials separately and dissolved in 0.5 ml *n*-octane. The solutions were transferred to a glass bomb equipped with a stir bar and rinsed with another 0.5 ml *n*-octane. Calcium hydride (32.6 mg, 0.78 mmol, 2.5 equiv) was added to the glass bomb. The content of glass bomb was put under hydrogen atmosphere using the Schlenk line as discussed. The vessel was heated to 120 °C for 14 h during which white solids precipitated. The *n*-octane soluble fraction was filtered through Celite and rinsed with diethyl ether. GC-MS analysis of the *n*-octane soluble fraction indicated that only solvents were present. The remaining solid was dissolved in CDCl<sub>3</sub> and analyzed by <sup>1</sup>H and <sup>13</sup>C NMR spectroscopy. The solid was identified as ε-caprolactone polymer. The solid was also submitted for HR-MS analysis, demonstrating the highest  $[m+Na]/z$  at 7644. <sup>1</sup>H NMR (300 MHz, CDCl<sub>3</sub>) δ 4.06 (t, *J*=6.0 Hz, 2H); 2.30 (t, *J*=7.2 Hz, 2H); 1.64 (m, 4H); 1.40 (m, 2H). <sup>13</sup>C NMR (400 MHz, CDCl<sub>3</sub>) δ 173.1 (C=O); 63.8 (CH<sub>2</sub>-O); 33.7 (CH<sub>2</sub>-C=O); 28.0 (CH<sub>2</sub>); 25.1 (CH<sub>2</sub>); 24.2 (CH<sub>2</sub>).

*Control experiment for  $\epsilon$ -caprolactone polymerization with  $\text{CaH}_2$  only*



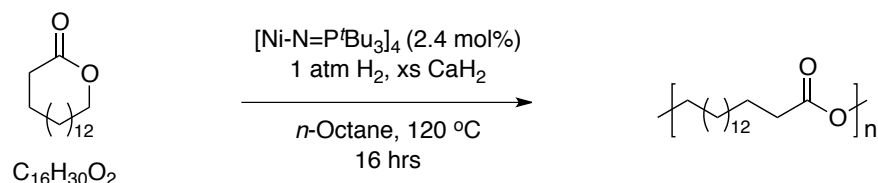
$\epsilon$ -caprolactone (129.6 mg, 1.1 mmol) was weighed into a glass vial and dissolved in 0.5 ml  $n$ -octane. The solution was transferred to a glass bomb equipped with a stir bar and rinsed with another 0.5 ml  $n$ -octane. Calcium hydride (119.5 mg, 2.8 mmol, 2.5 equiv) was added to the glass bomb. The vessel was heated to 120 °C for 18 h during which white solids precipitated. The  $n$ -octane soluble fraction was filtered through Celite and rinsed with diethyl ether. GC-MS analysis of the  $n$ -octane soluble fraction indicated that both  $\epsilon$ -caprolactone and solvents were present. The remaining solid (45.3 mg) was identified as  $\epsilon$ -caprolactone polymer by  $^1\text{H}$  and  $^{13}\text{C}$  NMR spectroscopy.  $^1\text{H}$  NMR (300 MHz,  $\text{CDCl}_3$ )  $\delta$  4.06 (t,  $J=6.0$  Hz, 2H); 2.30 (t,  $J=7.2$  Hz, 2H); 1.64 (m, 4H); 1.40 (m, 2H).  $^{13}\text{C}$  NMR (400 MHz,  $\text{CDCl}_3$ )  $\delta$  173.1 (C=O); 63.8 ( $\text{CH}_2\text{-O}$ ); 33.7 ( $\text{CH}_2\text{-C=O}$ ); 28.0 ( $\text{CH}_2$ ); 25.1 ( $\text{CH}_2$ ); 24.2 ( $\text{CH}_2$ ).

*Control experiment for  $\epsilon$ -caprolactone polymerization with precatalyst only*



In a drybox, **8** (7.0 mg,  $6.4 \times 10^{-3}$  mmol, 2.0 mol% per cluster) and  $\epsilon$ -caprolactone (26.4 mg, 0.32 mmol) were weighed into glass vials separately and dissolved in 0.5 ml *n*-octane. The solutions were transferred to a glass bomb equipped with a stir bar and rinsed with another 0.5 ml *n*-octane. The content of glass bomb was put under hydrogen atmosphere using the Schlenk line as discussed. The vessel was heated to 120 °C for 14 h during which white solids sublimed to the top of glass bomb. The *n*-octane soluble fraction was filtered through Celite and rinsed with diethyl ether. GC-MS analysis of the *n*-octane soluble fraction indicated that only solvents were present. A crystal grew from the *n*-octane/diethyl ether solution with 93% yield and was identified as a dimer by X-ray diffraction. The compound has the same structure as reported in literature.<sup>201</sup>

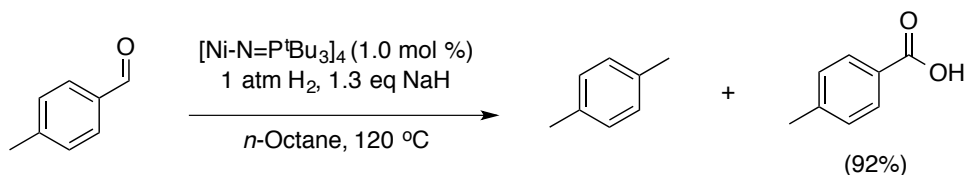
#### Polymerization of 16-hexadecanalide



In a drybox, **8** (5.5 mg,  $5.0 \times 10^{-3}$  mmol, 2.0 mol% per cluster) and 16-hexadecanalide (63.4 mg, 0.25 mmol) were weighed into glass vials separately and dissolved in 0.5 ml *n*-octane. The solutions were transferred to a glass bomb equipped with a stir bar and rinsed with another 0.5 ml *n*-octane. Calcium hydride (26.3 mg, 0.63 mmol, 2.5 equiv) was added to the glass bomb. The content of glass bomb was put under hydrogen atmosphere using the Schlenk line as discussed. The vessel was heated to 120 °C for 14 h during which white solids precipitated. The *n*-octane soluble fraction was filtered through Celite and rinsed with diethyl ether. GC-MS analysis of the *n*-octane soluble fraction indicated that only 16-hexadecanalide and solvents were present. The remaining solid was dissolved in  $\text{CDCl}_3$  and

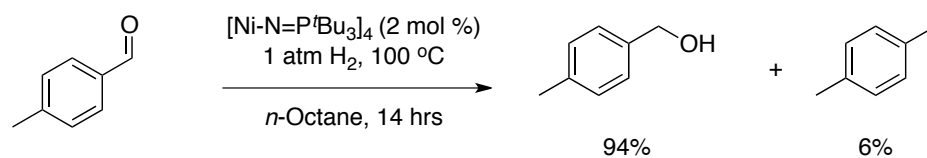
analyzed by  $^1\text{H}$  NMR spectroscopy.  $^1\text{H}$  NMR (300 MHz,  $\text{CDCl}_3$ )  $\delta$  4.08 (m, 2H), 2.29 (m, 2H), 1.60 (m, 2H), 1.26 (m, 44H). The solid was also submitted for HR-MS analysis. HR-MS (DCTB+Na) 3718.8.

*Hydrogenation of p-methylbenzaldehyde: Tishchenko reaction and ester hydrogenolysis in one-pot*



In a drybox, **8** (5.2 mg,  $4.7 \times 10^{-3}$  mmol, 1.0 mol% per cluster) and p-methylbenzaldehyde (56.7 mg, 0.47 mmol) were weighed into glass vials separately and dissolved in 0.5 ml n-octane. The solutions were transferred to a glass bomb equipped with a stir bar and rinsed with another 0.5 ml n-octane. Sodium hydride (14.9 mg, 0.62 mmol, 1.3 equiv) was added to the glass bomb. The content of glass bomb was put under hydrogen atmosphere using the Schlenk line as discussed. The vessel was heated to 120 °C for 14 h during which white solids precipitated. The n-octane soluble fraction was filtered through Celite and rinsed with diethyl ether. GC-MS analysis of the n-octane soluble fraction indicated that only p-xylene and solvents were present. Water (0.1 ml) and 0.5M HCl solution (2 ml) were added in sequence dropwise to the remaining solid. Diethyl ether was used to extract the organic compounds from aqueous layer three times. The organic layer was dried over  $\text{Na}_2\text{SO}_4$  and the diethyl ether was removed *in vacuo* to afford a white solid (59.1 mg, 92%). The solid was identified as p-methylbenzoic acid.  $^1\text{H}$  NMR (300 MHz,  $\text{CDCl}_3$ )  $\delta$  7.87 (m, 2H); 7.31 (m, 2H); 2.38 (s, 3H).  $^{13}\text{C}$  NMR (400 MHz,  $\text{CDCl}_3$ )  $\delta$  167.3 (C=O); 143.0 (Ar); 129.4 (Ar); 129.1 (Ar); 128.1 (Ar); 21.1 ( $\text{CH}_3$ ).

Control experiment for *p*-methylbenzaldehyde hydrogenation without  $\text{CaH}_2$



In a drybox, **8** (6.0 mg,  $5.5 \times 10^{-3}$  mmol, 2.0 mol% per cluster) and *p*-methylbenzaldehyde (32.8 mg, 0.27 mmol) were weighed into glass vials separately and dissolved in 0.5 ml *n*-octane. The solutions were transferred to a glass bomb equipped with a stir bar and rinsed with another 0.5 ml *n*-octane. The content of glass bomb was put under hydrogen atmosphere using the Schlenk line as discussed. The vessel was heated to 100 °C for 14 h. The *n*-octane soluble fraction was filtered through Celite and rinsed with diethyl ether. GC-MS analysis of the *n*-octane soluble fraction indicated the presence of *p*-methylbenzyl alcohol (94%) and *p*-xylene (6%).

## Experimental Section of Chapter 2

### General Procedures

For the aerobic oxidation reactions, the organic liquids used as substrates were dried over calcium hydride upon receipt from commercial providers. Unless previously degassed, the addition of liquids to reaction mixtures was performed in the fumehood. Frequently used substrates including ethylbenzene and cyclooctane were degassed by three freeze-pump-thaw cycles at high vacuum ( $10^{-5}$  mm Hg) and stored in the drybox.

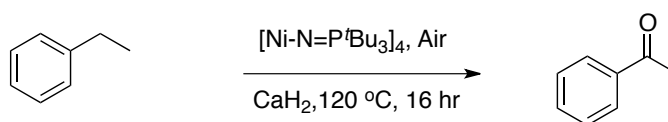
For organic liquids with boiling point above 120 °C, oxidation reactions were performed in Schlenk flasks either open to the air or under a flow of anhydrous molecular oxygen. All these reactions were performed at 120 °C by immersing the vessels into heated oil bath unless otherwise stated. A water-cooled condenser was connected to the Schlenk flask to maintain solvent/reactant reflux. The condenser was attached with a drying tube filled with Drierite for reactions using air as dioxygen source. If an oxygen tank was used to supply the continuous flow of dioxygen, the condenser was sealed with a fresh septum, pierced by a needle connecting to the rubber tube from oxygen tank. The septum was pierced by another needle as outlet to release the oxygen flow. Teflon sleeves were used to seal the joints between all the glassware if pure oxygen is used as oxidant. *The use of grease was avoided to prevent any potential fire accidents.*

Alternatively, oxidation of volatile liquid or solid substrates was conducted in sealed glass bombs filled with dioxygen. The addition of metal catalysts and substrates to the glass bomb was performed in the drybox. The glass bomb was then immersed in liquid nitrogen bath to freeze the reaction mixture, and was subsequently placed under vacuum for at least 10 minutes. Pure molecular oxygen was subsequently back-filled into the glass bomb. This

procedure was performed in less than three seconds to prevent oxygen condensation. The glass bomb was sealed and allowed to warm to room temperature, before it was immersed into an oil bath at 120 °C or otherwise stated temperature. The reaction mixture was stirred at a speed of 1500 rpm.

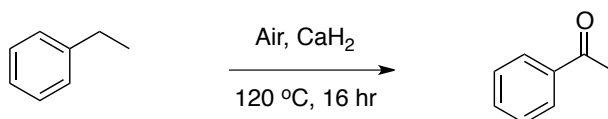
## Detailed Experimental Procedures for Chapter 2

### *First attempt for aerobic alkane oxidation*



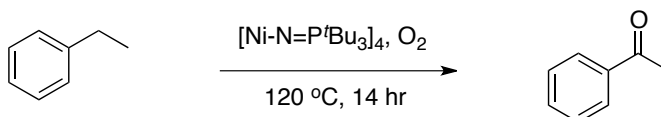
In a drybox, nickel catalyst **8** (9.4 mg,  $8.5 \times 10^{-3}$  mmol), ethylbenzene (2.0 g, 18.8 mmol) and powdered calcium hydride (800 mg, 19.0 mmol) were weighed into a glass flask equipped with a stir bar. The flask was connected to a water-cooled condenser that open to air through a drying tube full of Drierite. The vessel was heated to 120 °C for 16 h. Water (0.1 ml) and 0.5M HCl solution (2 ml) were added dropwise in sequence to quench the solution. The organic layer was extracted and submitted for GC-MS analysis. The GC-MS results indicated the presence of ethylbenzene (65.1%) and acetophenone (33.1%). Based on the initial mass of ethylbenzene, this represents a total of 732 catalyst turnovers during the 16 h reaction, for an average TOF of  $45.8 \text{ h}^{-1}$ . Crude  $^1\text{H}$  NMR was obtained with the organic layer confirming the presence of ethylbenzene and acetophenone.

*Control experiment for aerobic ethylbenzene oxidation*



In a drybox, ethylbenzene (2.1 g, 19.8 mmol) and powdered calcium hydride (800 mg, 19.0 mmol) were weighed into a glass flask equipped with a stir bar. The flask was connected to a water-cooled condenser that was open to air through a drying tube full of drierite. The vessel was heated to 120 °C for 16 h. Water (0.1 ml) and 0.5M HCl solution (2 ml) were added dropwise in sequence to quench the remaining solid. The organic layer was submitted for GC-MS analysis. The GC-MS results indicated the presence of ethylbenzene (94.3%) and acetophenone (5.3%).

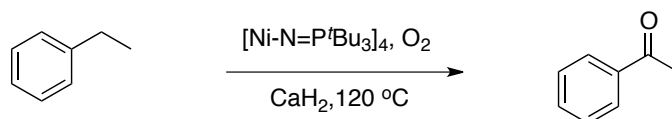
*Ethylbenzene oxidation without addition of base scavenger*



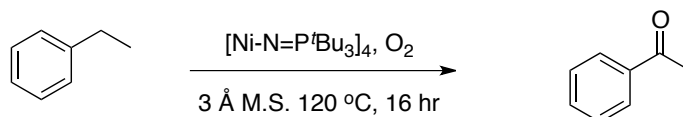
In the drybox, **8** (8.2 mg,  $7.5 \times 10^{-3}$  mmol), ethylbenzene (2.0 g, 18.8 mmol) were weighed into a glass flask equipped with a stir bar. The flask was connected to a water-cooled condenser that was attached to an oxygen tank. The flow from oxygen tank was adjusted to approximately 2 bubbles per second. The vessel was heated to 120 °C for 14 h. Water (0.1 ml) and 0.5M HCl solution (2 ml) were added dropwise in sequence to quench the remaining solid. The organic layer was submitted for GC-MS analysis. The GC-MS results indicated the presence of ethylbenzene (68%) and acetophenone (31%). Based on the

initial mass of ethylbenzene, this represents a total of 777 catalyst turnovers during the 14 h reaction, for an average TOF of 55.5 h<sup>-1</sup>.

*Comparison between CaH<sub>2</sub> and 3 Å molecular sieves as the scavenger*



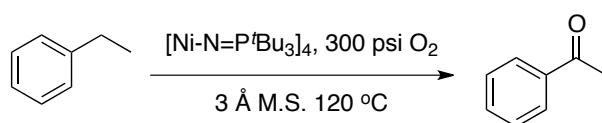
In the drybox, **8** (8.3 mg,  $7.5 \times 10^{-3}$  mmol), ethylbenzene (2.0 g, 18.8 mmol) and powdered calcium hydride (800 mg, 19.0 mmol) were weighed into a glass flask equipped with a stir bar. The flask was connected to a water-cooled condenser that was attached to an oxygen tank. The flow from oxygen tank was adjusted to approximately 2 bubbles per second. The vessel was heated to 120 °C for 14 h. Water (0.1 ml) and 0.5M HCl solution (2 ml) were added dropwise in sequence to quench the remaining solid. The organic layer was submitted for GC-MS analysis. The GC-MS results indicated the presence of ethylbenzene (38%) and acetophenone (53%). Based on the initial mass of ethylbenzene, this represents a total of 1328.5 catalyst turnovers during the 14 h reaction, for an average TOF of 94.9 h<sup>-1</sup>.



In a drybox, **8** (8.3 mg,  $7.5 \times 10^{-3}$  mmol), ethylbenzene (2.0 g, 18.8 mmol) and powdered 3 Å molecular sieve (900 mg) were weighed into a glass flask equipped with a stir bar. The flask was connected to a water-cooled condenser that was attached to an oxygen tank. The flow from oxygen tank was adjusted to approximately 2 bubbles per second. The vessel was heated to 120 °C for 14 h. Water (0.1 ml) and 0.5M HCl solution (2 ml) were added

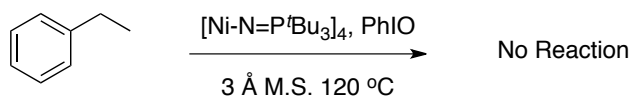
dropwise in sequence to quench the remaining solid. The organic layer was submitted for GC-MS analysis. The GC-MS results indicated the presence of ethylbenzene (48%) and acetophenone (51%). Based on the initial mass of ethylbenzene, this represents a total of 1278.4 catalyst turnovers during the 16 h reaction, for an average TOF of 79.9 h<sup>-1</sup>.

*Ethylbenzene oxidation under high pressure of molecular oxygen*

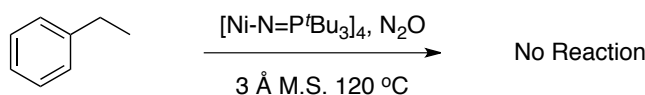


In a drybox, **8** (8.3 mg, 7.5×10<sup>-3</sup> mmol), ethylbenzene (2.0 mg, 18.8 mmol) and powdered 3 Å molecular sieve (900 mg) were weighed into a glass container equipped with a stir bar. The high-pressure steel reactor was assembled inside the drybox and pressured to 300 psi oxygen before conducting the reaction. The reactor was heated to 120 °C for 14 h. Water (0.1 ml) and 0.5M HCl solution (2 ml) were added dropwise in sequence to quench the remaining solid. The organic layer was submitted for GC-MS analysis. The GC-MS results indicated the presence of ethylbenzene (68.3%), 1-phenylethanol (11.4%) and acetophenone (8.1%). Based on the initial mass of ethylbenzene, this represents a total of 794.6 catalyst turnovers during the 14 h reaction, for an average TOF of 56.8 h<sup>-1</sup>.

*Ethylbenzene oxidation using other oxidants: iodosobenzene or nitrous oxide*



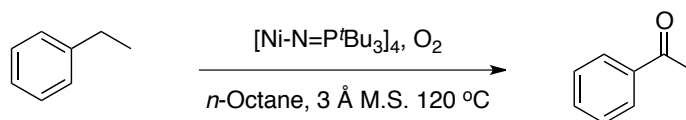
In a drybox, **8** (9.6 mg,  $8.7 \times 10^{-3}$  mmol), ethylbenzene (2.5 g, 23.5 mmol), iodosobenzene (250 mg, 1.14 mmol) and powdered 3 Å molecular sieve (1.0 g) were weighed into a glass bomb equipped with a stir bar. The flask was connected to a water-cooled condenser that was attached to an oxygen tank. The flow from oxygen tank was adjusted to approximately 2 bubbles per second. The vessel was heated to 120 °C for 14 h. Water (0.1 ml) and 0.5M HCl solution (2 ml) were added dropwise in sequence to quench the remaining solid. The organic layer was submitted for GC-MS analysis. The GC-MS results indicated the presence of only ethylbenzene (100%).



In a drybox, **8** (8.8 mg,  $8.0 \times 10^{-3}$  mmol), ethylbenzene (2.0 g, 18.8 mmol), and powdered 3 Å molecular sieve (1.0 g) were weighed into a glass flask equipped with a stir bar. The flask was connected to a water-cooled condenser that was attached to a tank of anhydrous nitrous oxide. The flow from the nitrous oxide tank was adjusted to approximately 2 bubbles per second. The vessel was heated to 120 °C for 14 h. Water (0.1 ml) and 0.5M HCl solution (2 ml) were added dropwise in sequence to quench the remaining solid. The organic layer was submitted for GC-MS analysis. The GC-MS results indicated the presence of only ethylbenzene (100%).

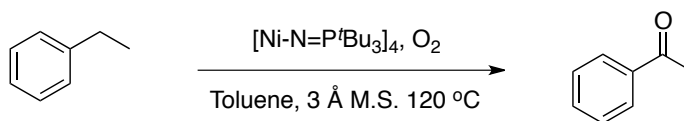
### *Introduction of various solvent systems for ethylbenzene oxidation*

#### *1. n-Octane*



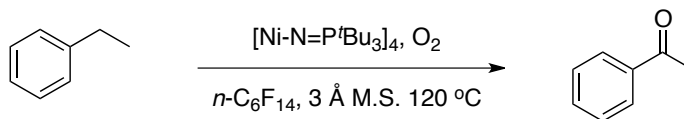
In a drybox, **8** (4.7 mg,  $4.3 \times 10^{-3}$  mmol), ethylbenzene (191.3 mg, 1.8 mmol), *n*-octane (1.5 ml) and powdered 3 Å molecular sieve (300 mg) were weighed into a glass flask equipped with a stir bar. The flask was connected to a water-cooled condenser that was attached to an oxygen tank. The flow from oxygen tank was adjusted to approximately 2 bubbles per second. The vessel was heated to 120 °C for 16 h. Water (0.1 ml) and 0.5M HCl solution (2 ml) were added dropwise in sequence to quench the remaining solid. The organic layer was submitted for GC-MS analysis. The GC-MS results indicated the presence of only ethylbenzene (100%) and solvent.

### 2. Toluene



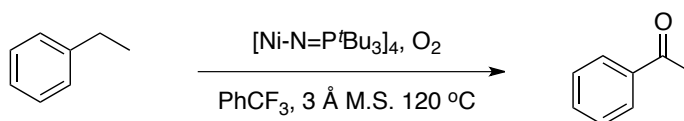
In the drybox, **8** (5.2 mg,  $4.7 \times 10^{-3}$  mmol), ethylbenzene (186.5 g, 1.76 mmol), toluene (1.5 ml) and powdered 3 Å molecular sieve (300 mg) were weighed into a glass flask equipped with a stir bar. The flask was connected to a water-cooled condenser that was attached to an oxygen tank. The flow from oxygen tank was adjusted to approximately 2 bubbles per second. The vessel was heated to 120 °C for 16 h. Water (0.1 ml) and 0.5M HCl solution (2 ml) were added dropwise in sequence to quench the remaining solid. The organic layer was submitted for GC-MS analysis. The GC-MS results indicated the presence of only ethylbenzene (100%) and solvent.

### 3. Perfluorohexane



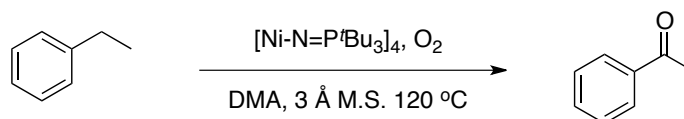
In a drybox, **8** (5.4 mg,  $4.9 \times 10^{-3}$  mmol), ethylbenzene (189.4 mg, 1.78 mmol), perfluorohexane (1.5 ml) and powdered 3 Å molecular sieve (300 mg) were weighed into a glass flask equipped with a stir bar. The flask was connected to a water-cooled condenser that was attached to an oxygen tank. The flow from oxygen tank was adjusted to approximately 2 bubbles per second. The vessel was heated to 120 °C for 16 h. Water (0.1 ml) and 0.5M HCl solution (2 ml) were added dropwise in sequence to quench the remaining solid. The organic layer was submitted for GC-MS analysis. The GC-MS results indicated the presence of ethylbenzene (98.6%), acetophenone (1.4%) and solvent. Based on the initial mass of ethylbenzene, this represents a total of 5.1 catalyst turnovers during the 16 h reaction, for an average TOF of  $0.3 \text{ h}^{-1}$ .

#### 4. Trifluoromethylbenzene



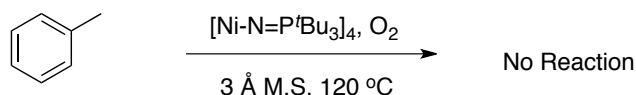
In a drybox, **8** (6.2 mg,  $5.6 \times 10^{-3}$  mmol), ethylbenzene (219.0 mg, 2.06 mmol), trifluoromethylbenzene (1.0 ml) and powdered 3 Å molecular sieve (300 mg) were weighed into a glass flask equipped with a stir bar. The flask was connected to a water-cooled condenser that was attached to an oxygen tank. The flow from oxygen tank was adjusted to approximately 2 bubbles per second. The vessel was heated to 120 °C for 16 h. Water (0.1 ml) and 0.5M HCl solution (2 ml) were added dropwise in sequence to quench the remaining solid. The organic layer was submitted for GC-MS analysis. The GC-MS results indicated the presence of ethylbenzene (99.9%), acetophenone (0.1%) and solvent. Based on the initial mass of ethylbenzene, this represents a total of 0.4 catalyst turnovers during the 16 h reaction, for an average TOF of  $0.02 \text{ h}^{-1}$ .

### 5. Dimethylacetamide



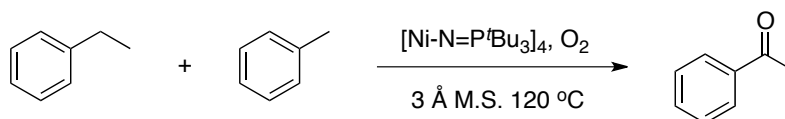
In a drybox, **8** (7.8 mg,  $7.1 \times 10^{-3}$  mmol), ethylbenzene (277.1 mg, 2.61 mmol), dimethylacetamide (1.8 ml) and powdered 3 Å molecular sieve (300 mg) were weighed into a glass flask equipped with a stir bar. The flask was connected to a water-cooled condenser that was attached to an oxygen tank. The flow from oxygen tank was adjusted to approximately 2 bubbles per second. The vessel was heated to 120 °C for 17 h. Water (0.1 ml) and 0.5M HCl solution (2 ml) were added dropwise in sequence to quench the remaining solid. The organic layer was submitted for GC-MS analysis. The GC-MS results indicated the presence of only ethylbenzene (100%) and solvent.

### Toluene oxidation under optimized conditions



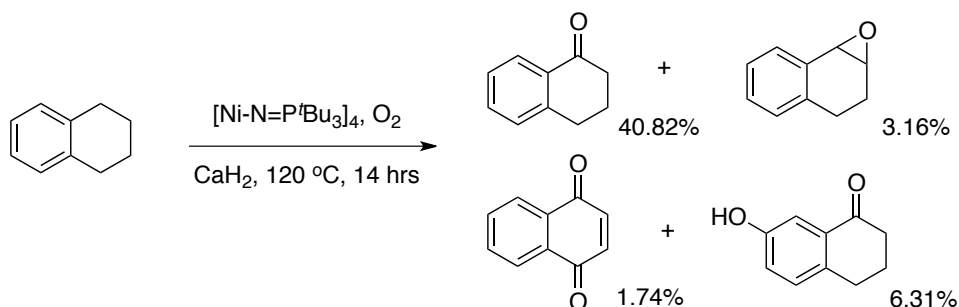
In a drybox, **8** (9.2 mg,  $8.4 \times 10^{-3}$  mmol), toluene (2.1 g, 22.8 mmol), and powdered 3 Å molecular sieve (900 mg) were weighed into a glass flask equipped with a stir bar. The flask was connected to a water-cooled condenser that was attached to an oxygen tank. The flow from oxygen tank was adjusted to approximately 2 bubbles per second. The vessel was heated to 120 °C for 14 h. Water (0.1 ml) and 0.5M HCl solution (2 ml) were added dropwise in sequence to quench the remaining solid. The organic layer was submitted for GC-MS analysis. The GC-MS results indicated the presence of only toluene (100%).

*Selective oxidation of ethylbenzene in the presence of toluene with about 1:1 ratio*



In a drybox, **8** (5.5 mg,  $5.0 \times 10^{-3}$  mmol), toluene (370.0 mg, 4.02 mmol), ethylbenzene (420.3 mg, 3.96 mmol) and powdered 3 Å molecular sieve (600 mg) were weighed into a glass flask equipped with a stir bar. The flask was connected to a water-cooled condenser that was attached to an oxygen tank. The flow from oxygen tank was adjusted to approximately 2 bubbles per second. The vessel was heated to 120 °C for 19 h. Water (0.1 ml) and 0.5M HCl solution (2 ml) were added dropwise in sequence to quench the remaining solid. The organic layer was submitted for GC-MS analysis. The GC-MS results indicated the presence of toluene, ethylbenzene (74.9%) and acetophenone (25.1%). Based on the initial mass of ethylbenzene, this represents a total of 198.8 catalyst turnovers during the 19 h reaction, for an average TOF of  $10.5 \text{ h}^{-1}$ .

*Tetralin oxidation under optimized conditions*

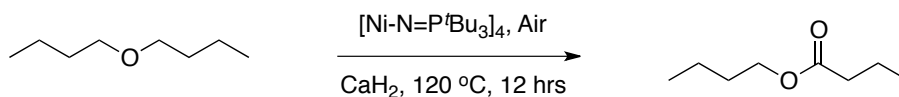


In a drybox, **8** (4.2 mg,  $3.8 \times 10^{-3}$  mmol), tetralin (3.0 g, 22.7 mmol) and powdered calcium hydride (600 mg, 14.3 mmol) were weighed into a glass flask equipped with a stir bar. The



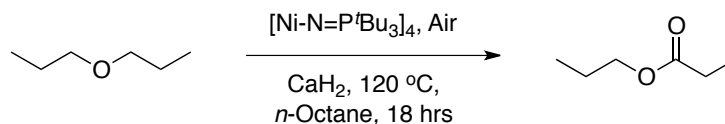
17 h reaction, for an average TOF of 76.6 h<sup>-1</sup>. 3,4-dihydroisocoumarin: <sup>1</sup>H NMR (300 MHz, CDCl<sub>3</sub>) δ 8.11 (m, 1H), 7.55 (m, 1H), 7.40 (m, 1H), 7.26 (m, 1H), 4.55 (t, *J* = 6.0 Hz, 2H), 3.07 (t, *J* = 6.0 Hz, 2H). 1,1'-oxodiisochromane: <sup>1</sup>H NMR (300 MHz, CDCl<sub>3</sub>) δ 7.24 (m, 6H), 7.15 (m, 2H), 6.14 (s, 2H), 4.37 (dt, *J* = 11.8, 3.2 Hz, 2H), 4.10 (ddd, *J* = 11.1, 6.1, 1.1 Hz, 2H), 3.14 (m, 2H), 2.67 (dd, *J* = 16.5, 2.6 Hz, 2H). <sup>13</sup>C NMR (125 MHz, CDCl<sub>3</sub>) δ 134.2, 133.9, 128.4, 128.0, 127.6, 126.3, 92.8, 58.3, 28.3.

### Dibutylether oxidation



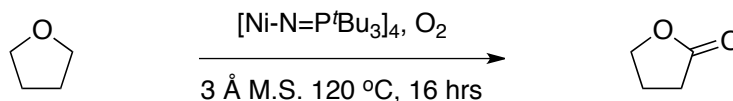
In a drybox, **8** (5.6 mg, 5.1 × 10<sup>-3</sup> mmol), di-*n*-butyl ether (2.2 g, 16.9 mmol), and powdered calcium hydride (600 mg, 14.3 mmol) were weighed into a glass flask equipped with a stir bar. The flask was connected to a water-cooled condenser that was open to air through a drying tube full of drierite. The vessel was heated to 120 °C for 12 h. Water (0.1 ml) and 0.5M HCl solution (2 ml) were added dropwise in sequence to quench the remaining solid. The organic layer was submitted for GC-MS analysis. The GC-MS results indicated the presence of di-*n*-butyl ether (88.6%), *n*-butyl butyrate (3.6%), butyl formate (4.3%), 1-butanol (1.2%), *n*-butoxyl-3-butanone (0.2%) and 1-butoxyl-4-butanol (0.2%). Based on the yield of the oxidized product, the turnover number for the nickel cluster was 397.2, for an average TOF of 33.1 h<sup>-1</sup>.

### Dipropylether oxidation



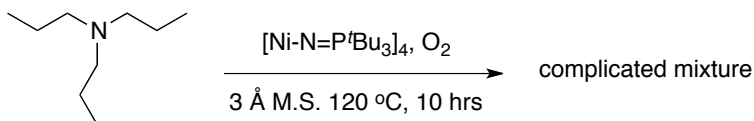
In a drybox, **8** (4.5 mg,  $4.1 \times 10^{-3}$  mmol), di-*n*-propyl ether (1.2 g, 11.7 mmol), *n*-octane (2.0 ml) and powdered calcium hydride (350 mg, 8.3 mmol) were weighed into a Schlenk flask equipped with a stir bar. The flask was connected to a water-cooled condenser and refluxed for 18 h. The reaction mixture was submitted for GC-MS analysis. The result indicated the presence of di-*n*-propyl ether (94%) and *n*-propyl propionate (5.8%). Based on the yield of the oxidized product, the turnover number for the nickel cluster was 171.0, for an average TOF of  $9.5 \text{ h}^{-1}$ .

#### *Tetrahydrofuran oxidation*



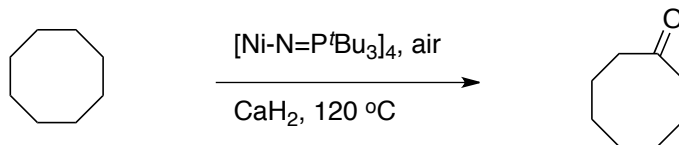
In a drybox, **8** (3.6 mg,  $3.3 \times 10^{-3}$  mmol), THF (2.0 ml), and powdered 3 Å molecular sieve (500 mg) were weighed into a glass bomb equipped with a stir bar. The glass bomb was kept under vacuum for at least 10 minutes while immersed in liquid nitrogen bath to freeze the reaction mixture. Afterwards the glass bomb was back-filled with dioxygen, sealed and warmed to room temperature. The glass bomb was heated to 120 °C for 16 h. The reaction mixture was submitted for GC-MS analysis. The result indicate the presence of  $\gamma$ -butyrolactone (5.3%) 2-hydroxyltetrahydrofuran (1.2%), the dimeric 2,2'-bis ether (0.6%) and THF (91%). Based on the yield of the oxidized product, the turnover number for the nickel cluster was 672.5, for an average TOF of  $42.0 \text{ h}^{-1}$ .

### Tributylamine oxidation



In a drybox, **8** (7.8 mg,  $7.1 \times 10^{-3}$  mmol), tri-*n*-butyl amine (1.13 g, 6.1 mmol), and powdered 3 Å molecular sieve (1.0 g) were weighed into a glass flask equipped with a stir bar. The flask was connected to a water-cooled condenser that was attached to an oxygen tank. The flow from oxygen tank was adjusted to approximately 2 bubbles per second. The vessel was heated to 120 °C for 10 h. Water (0.1 ml) and 0.5M HCl solution (2 ml) were added dropwise in sequence to quench the remaining solid. The organic layer was submitted for GC-MS analysis. The GC-MS results indicated the presence of tri-*n*-propyl amine (74.4%) and other minor impurities.

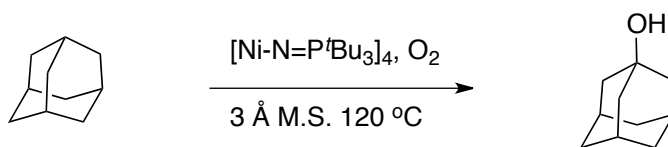
### Cyclooctane oxidation



In a drybox, **8** (7.3 mg,  $6.6 \times 10^{-3}$  mmol), cyclooctane (2.06 g, 18.4 mmol), and powdered calcium hydride (1.0 g, 23.8 mmol) were weighed into a glass flask equipped with a stir bar. The flask was connected to a water-cooled condenser that was open to air through a drying tube full of drierite. The vessel was heated to 120 °C for 12 h. Water (0.1 ml) and 0.5M HCl solution (2 ml) were added dropwise in sequence to quench the remaining solid. The organic layer was submitted for GC-MS analysis. The GC-MS results indicated the presence of cyclooctane (84.5%), cyclooctanol (2.2%) and cyclooctanone (8.9%). Based on the initial

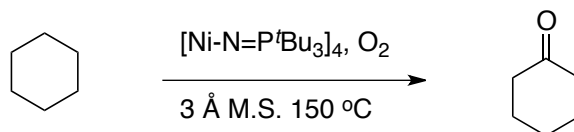
mass of cyclooctane, this represents a total of 441.5 catalyst turnovers during the 16 h reaction, for an average TOF of 27.6 h<sup>-1</sup>.

#### *Adamantane oxidation*



In a drybox, **8** (11 mg, 10.0×10<sup>-3</sup> mmol), adamantane (780 mg, 5.7 mmol), hexane (0.5 ml), and powdered 3 Å molecular sieve (300 mg) were weighed into a glass bomb equipped with a stir bar. The glass bomb was kept under vacuum for at least 10 minutes while immersed in liquid nitrogen bath to freeze the reaction mixture. Afterwards the glass bomb was back-filled with dioxygen, sealed and warmed to room temperature. The glass bomb was heated to 120 °C for 21 h. The reaction mixture was submitted for GC-MS analysis. The GC yields for 1-adamantanol, 2-adamantanol and 2-adamantanone were 7.8%, 1.3% and 1.0%, respectively. Based on the initial mass of adamantane, this represents a total of 57.6 catalyst turnovers during the 21 h reaction, for an average TOF of 2.7 h<sup>-1</sup>.

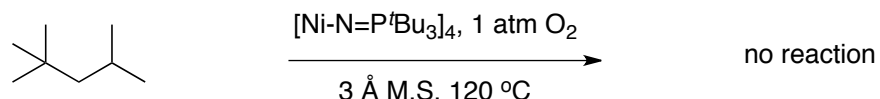
#### *Cyclohexane oxidation*



In a drybox, **8** (5.2 mg, 4.7×10<sup>-3</sup> mmol), cyclohexane (1.5 g, 17.8 mmol), and powdered 3 Å molecular sieve (450 mg) were weighed into a glass bomb equipped with a stir bar. The glass bomb was kept under vacuum for at least 10 minutes while immersed in liquid nitrogen bath to freeze the reaction mixture. Afterwards the glass bomb was back-filled

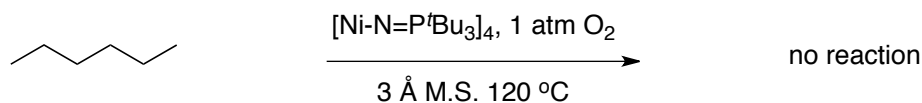
with dioxygen, sealed and warmed to room temperature. The glass bomb was heated to 150 °C for 20 h. The reaction mixture was submitted for GC-MS analysis. The result indicates the presence of cyclohexane (96.7%) and cyclohexanone (3.3%). Based on the initial mass of cyclohexane, this represents a total of 125.0 catalyst turnovers during the 20 h reaction, for an average TOF of 6.3 h<sup>-1</sup>.

### 2,2,4-trimethylpentane oxidation



In a drybox, **8** (9.0 mg, 8.2×10<sup>-3</sup> mmol), 2,2,4-trimethylpentane (2.3 g, 20.1 mmol), and powdered 3 Å molecular sieve (700 mg) were weighed into a glass flask equipped with a stir bar. The flask was connected to a water-cooled condenser that was attached to an oxygen tank. The flow from oxygen tank was adjusted to approximately 2 bubbles per second. The vessel was heated to 120 °C for 14 h. The reaction mixture was submitted for GC-MS analysis. The GC-MS results indicated the only presence of 2,2,4-trimethylpentane (100%).

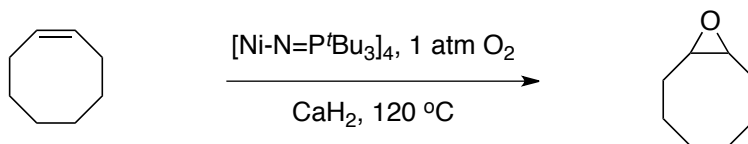
### Hexane oxidation



In a drybox, **8** (8.8 mg, 8.0×10<sup>-3</sup> mmol), hexane (1.8 g, 20.9 mmol), and powdered 3 Å molecular sieve (550 mg) were weighed into a glass bomb equipped with a stir bar. The

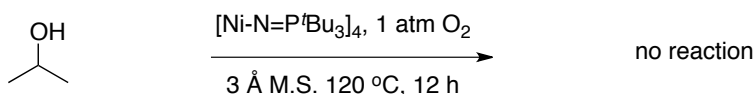
glass bomb was kept under vacuum for at least 10 minutes while immersed in liquid nitrogen bath to freeze reaction mixture. Afterwards the glass bomb was back-filled with dioxygen, sealed and warmed to room temperature. The glass bomb was heated to 120 °C for 14 h. The reaction mixture was submitted for GC-MS analysis. The GC-MS results indicated the only presence of *n*-hexane (100%).

### *Cyclooctene oxidation*



In a drybox, **8** (8.0 mg,  $7.3 \times 10^{-3}$  mmol), cyclooctene (2.1 g, 19.3 mmol), and powdered calcium hydride (850 mg, 20.2 mmol) were weighed into a glass flask equipped with a stir bar. The flask was connected to a water-cooled condenser that was attached to an oxygen tank. The flow from oxygen tank was adjusted to approximately 2 bubbles per second. The vessel was heated to 120 °C for 16 h. The reaction mixture was purified by column chromatography, giving pure cyclooctene oxide (1.09 g, 45%).

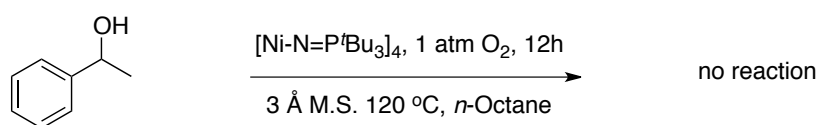
### *Isopropanol oxidation*



In a drybox, **8** (3.7 mg,  $3.4 \times 10^{-3}$  mmol), isopropanol (1.5 g, 25.0 mmol), and powdered 3 Å molecular sieve (350 mg) were weighed into a glass bomb equipped with a stir bar. The glass bomb was kept under vacuum for at least 10 minutes while immersed in liquid

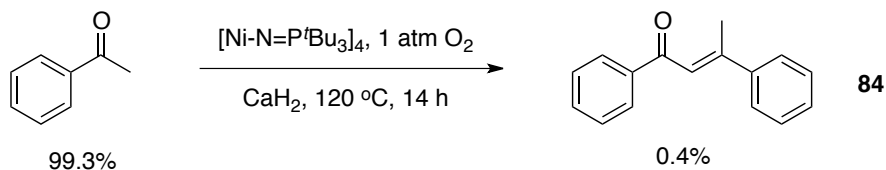
nitrogen bath to freeze the reaction mixture. Afterwards the glass bomb was back-filled with dioxygen, sealed and warmed to room temperature. The glass bomb was heated to 120 °C for 12 h. The reaction mixture was submitted for GC-MS analysis. The result indicated the only presence of isopropanol (100%).

### 1-phenylethanol oxidation



In a drybox, **8** (4.7 mg,  $4.3 \times 10^{-3}$  mmol), 1-phenylethanol (164 mg, 1.34 mmol), *n*-octane (2.5 ml) and powdered 3 Å molecular sieve (300 mg) were weighed into a glass flask equipped with a stir bar. The flask was connected to a water-cooled condenser that was attached to an oxygen tank. The flow from oxygen tank was adjusted to approximately 2 bubbles per second. The vessel was heated to 120 °C for 12 h. The reaction mixture was acidified by diluted HCl and submitted for GC-MS analysis. The GC-MS results indicated the presence of 1-phenylethanol (64.1%), 1-chloroethyl benzene (35.9%).

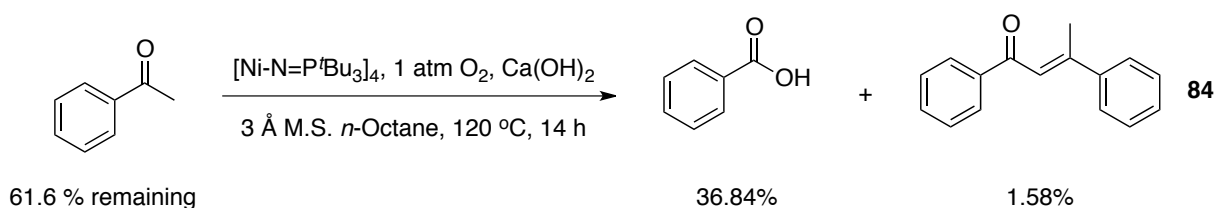
### Acetophenone oxidation



In a drybox, **8** (8.0 mg,  $7.3 \times 10^{-3}$  mmol), acetophenone (2.4 g, 20.0 mmol), and powdered calcium hydride (800 mg, 19.0 mmol) were weighed into a glass flask equipped with a stir

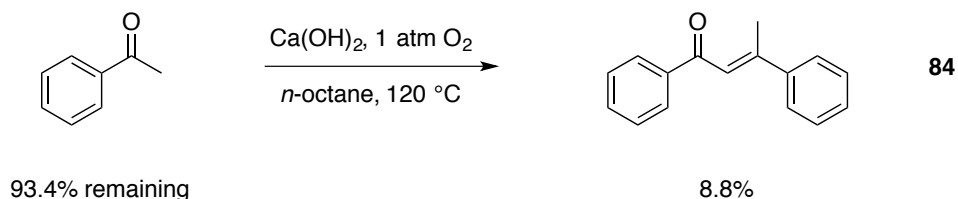
bar. The flask was connected to a water-cooled condenser that was attached to an oxygen tank. The flow from oxygen tank was adjusted to approximately 2 bubbles per second. The vessel was heated to 120 °C for 16 h. The reaction mixture was submitted for GC-MS analysis. The GC-MS results indicated the presence of acetophenone (99.3%), enone (0.4%).

#### Effect of $\text{Ca}(\text{OH})_2$ to acetophenone oxidation



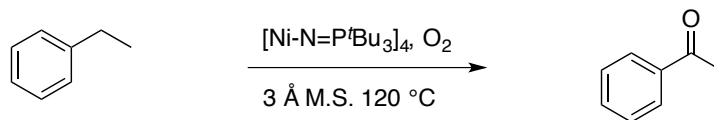
In a drybox, **8** (6.7 mg,  $6.1 \times 10^{-3}$  mmol), acetophenone (140 mg, 1.17 mmol), *n*-octane (1 ml), calcium hydroxide (148 mg, 2.0 mmol), and powdered 3 Å molecular sieves (150 mg) were weighed into a glass flask equipped with a stir bar. The flask was connected to a water-cooled condenser that was attached to an oxygen tank. The flow from oxygen tank was adjusted to approximately 2 bubbles per second. The vessel was heated to 120 °C for 19 h. The reaction mixture was submitted for GC-MS analysis. The GC-MS results indicated the presence of acetophenone (62%), benzoic acid (37%), enone (1.6%).

#### Control experiment between acetophenone and $\text{Ca}(\text{OH})_2$



Acetophenone (5.232 g, 44.3 mmol), *n*-octane (8 ml), and powdered calcium hydroxide (0.8 g, 10.8 mmol) were weighed into a glass flask equipped with a stir bar. The flask was connected to a water-cooled condenser that was attached to an oxygen tank. The flow from oxygen tank was adjusted to approximately 2 bubbles per second. The vessel was heated to 120 °C for 15 h. The reaction mixture was submitted for GC-MS analysis. The GC-MS results indicated the presence of acetophenone (93.5%), enone (5.8%).

*Monitor of ethylbenzene oxidation by <sup>1</sup>H NMR spectroscopy*

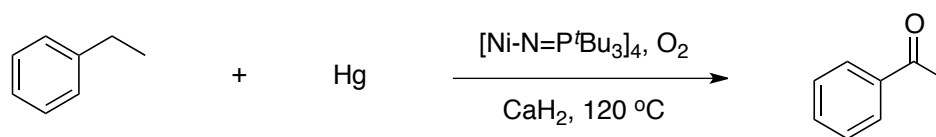


In a drybox, **8** (19.8 mg, 0.018 mmol), ethylbenzene (4.22 g, 39.7 mmol), and powdered **3** (2.15 g) were weighed into a three-neck round-bottom flask equipped with a stir bar. Two side necks were sealed with glass stoppers. Meanwhile, the flask was connected to a water-cooled condenser that was attached to an oxygen tank. The flow from oxygen tank was adjusted to approximately 2 bubbles per second. The vessel was then placed in an oil bath that had already been heated to 120 °C. After every one hour of heating, a drop of sample was taken by a pipet from a side arm. The sample was then dissolved in CDCl<sub>3</sub> and analyzed by <sup>1</sup>H NMR spectroscopy. The integration ratio between ethylbenzene, acetophenone and 1-phenylethanol was obtained from <sup>1</sup>H NMR spectrum and converted the composition percentage. The results were summarized in a table as following.

Time (Hour)	Ethylbenzene (%)	Acetophenone (%)	1-phenylethanol (%)
1	100	0	0
2	100	0	0
3	98.0	2.0	0

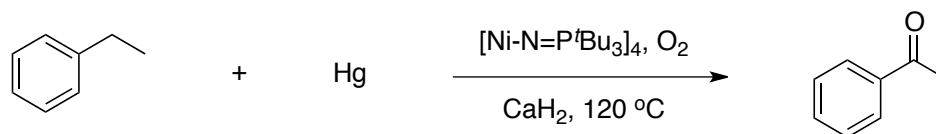
4	90.2	6.2	3.6
5	85.7	10.9	3.4
6	82.6	14.0	3.3
7	79.4	17.4	3.2
8	77.5	19.4	3.1
9	75.6	21.4	3.0
10	72.8	23.5	3.6
11	64.9	31.2	3.9

*Addition of mercury (566 equiv) to the ethylbenzene oxidation*



In a drybox, **8** (4.9 mg,  $4.5 \times 10^{-3}$  mmol), ethylbenzene (2.1 g, 19.6 mmol), mercury (510.7 mg, 2.55 mmol) and powdered calcium hydride (600 mg, 14.3 mmol) were weighed into a glass flask equipped with a stir bar. The flask was connected to a water-cooled condenser that was attached to an oxygen tank. The flow from oxygen tank was adjusted to approximately 2 bubbles per second. The vessel was heated to 120 °C for 16 h. The reaction mixture was submitted for GC-MS analysis. The GC-MS results indicated the presence of acetophenone (49.7%), ethylbenzene (35.4%), benzaldehyde (0.3%) and benzoic acid (7.3%). Based on the yield of the oxidized products, the turnover number for the nickel cluster was 2813.7, for an average TOF of 175.9 h<sup>-1</sup>.

*Addition of mercury (29 equiv) to the ethylbenzene oxidation*

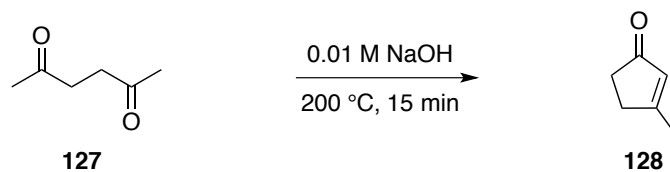


In a drybox, **8** (9.7 mg,  $8.8 \times 10^{-3}$  mmol), ethylbenzene (2.9 g, 27.3 mmol), mercury (34.0 mg, 0.17 mmol) and powdered calcium hydride (600 mg, 14.3 mmol) were weighed into a glass flask equipped with a stir bar. The flask was connected to a water-cooled condenser that was attached to an oxygen tank. The flow from oxygen tank was adjusted to approximately 2 bubbles per second. The vessel was heated to 120 °C for 17 h. The reaction mixture was submitted for GC-MS analysis. The GC-MS results indicated the presence of acetophenone (61.2%), ethylbenzene (37.0%) and benzaldehyde (1.8%). Based on the yield of the oxidized products, the turnover number for the nickel cluster was 1739.7, for an average TOF of 102.3 h<sup>-1</sup>.

## Chapter 3. Experimental Section.

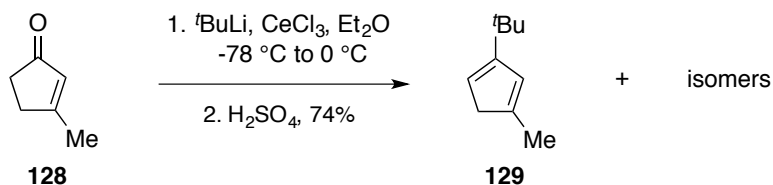
### Detailed Experimental Procedures for Chapter 3

#### Preparation of 3-methyl-2-cyclopente-1-one **128**



3-methyl-2-cyclopente-1-one was prepared according to literature method.<sup>180</sup>

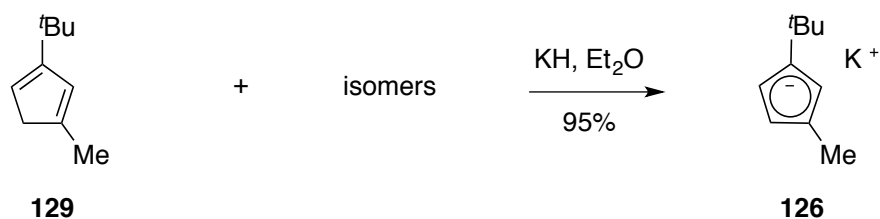
#### Synthesis of 1-methyl-3-tert-butylcyclopentadiene **129**



Prior to usage, cerium chloride was desiccated in a vacuum oven (ca. 50 mtorr) at 100 °C for overnight. A Schlenk flask equipped with a stir bar was placed under a nitrogen atmosphere. After the subsequent addition of anhydrous cerium chloride (8.3 g, 33.7 mmol) and diethyl ether (30 ml), the flask was immersed into an acetone/dry ice bath (-78 °C). Dropwise addition of *tert*-butyllithium (20 ml, 34.1 mmol) to the flask was conducted over a period of 10 minutes. The mixture was kept stirring at -78 °C for 4 h. 3-methyl-2-cyclopente-1-one **128** (2.2 g, 21.3 mmol) was then added dropwise by syringe. The solution was slowly warmed to 0 °C over a period of 4 h. The solution was later quenched by dilute

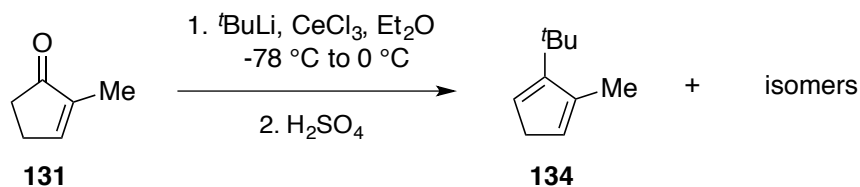
sulfuric acid (10%) and extracted with diethyl ether three times. The solvent was removed *in vacuo* to afford a yellow oily compound (2.31 g, 74%). The product was subjected to  $^1\text{H}$  NMR spectroscopy analysis, however due to the presence of various isomers, the  $^1\text{H}$  NMR spectrum appeared complicated and the material was taken without further purification or characterization.

*Synthesis of 1-methyl-3-tert-butylcyclopentadienyl potassium 126*



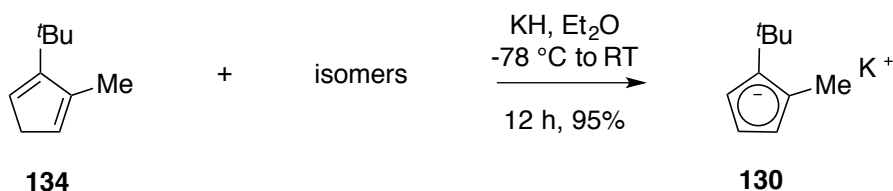
In a drybox, hexane-washed potassium hydride (0.64 g, 16.0 mmol) was weighed into a Schlenk flask. The flask was then connected to a Schlenk line and placed under a nitrogen atmosphere. To the flask, diethyl ether (30 ml) was added, followed by dropwise addition of a mixture of 1-methyl-3-*tert*-butylcyclopentadiene **129** (2.05 g, 15.0 mmol). The reaction was left for 12 h to afford a yellow solution. The solvent was removed *in vacuo* to afford a yellow solid (2.48 g, 95%). The solid was further rinsed with pentane in the drybox. The product was analyzed by  $^1\text{H}$  NMR spectroscopy only.  $^1\text{H}$  NMR (300 MHz, D<sub>8</sub>-THF)  $\delta$  5.03 (s, 2H), 4.92 (s, 1H), 1.73 (s, 3H), 0.86 (s, 9H).

### Synthesis of 1-methyl-2-tert-butylcyclopentadiene **134**



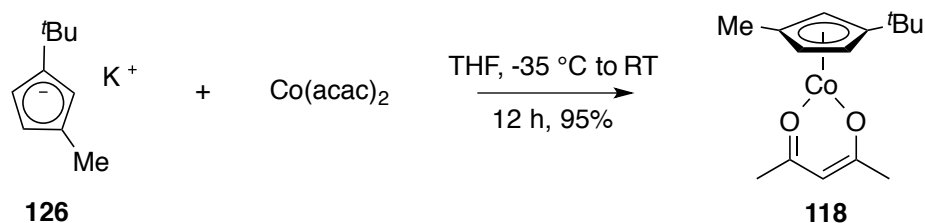
Prior to usage, cerium chloride was desiccated in vacuum oven at  $100\text{ }^\circ\text{C}$  for overnight. A Schlenk flask equipped with a stir bar was placed under a nitrogen atmosphere. After the subsequent addition of anhydrous cerium chloride (7.7 g, 31.2 mmol) and diethyl ether (30 ml), the flask was immersed to an acetone/dry ice bath ( $-78\text{ }^\circ\text{C}$ ). Dropwise addition of *tert*-butyllithium (18.5 ml, 31.5 mmol) to the flask was conducted over a period of 10 minutes. The mixture was kept stirring at  $-78\text{ }^\circ\text{C}$  for 4 h. 2-methyl-2-cyclopent-1-one **131** (2.0 g, 20.8 mmol) was then added dropwise with a syringe. The solution was slowly warmed to  $0\text{ }^\circ\text{C}$  over a period of 4 h. The solution was later quenched by dilute sulfuric acid (10%) and extracted with diethyl ether three times. The solvent was removed *in vacuo* to afford a yellow oily compound (2.12 g, 75%). The product was subjected to  $^1\text{H}$  NMR spectroscopy analysis, however due to the presence of various isomers, the  $^1\text{H}$  NMR spectrum appeared complicated and the material was taken on without further purification or characterization.

### Synthesis of 1-methyl-2-tert-butylcyclopentadienyl potassium **130**



In a drybox, hexane-washed potassium hydride (0.32g, 8.0 mmol) was weighed to a Schlenk flask. The flask was then connected to a Schlenk line and placed under a nitrogen atmosphere. To the flask, diethyl ether (15 ml) was added, followed by dropwise addition of a mixture of 1-methyl-2-*tert*-butylcyclopentadiene **134** (1.02 g, 7.50 mmol). The reaction was left for 12 h to afford a yellow solution. The solvent was removed *in vacuo* to afford a yellow solid (1.24 g, 95%). The solid was further rinsed with pentane in the drybox. The product was analyzed by <sup>1</sup>H NMR spectroscopy. <sup>1</sup>H NMR (300 MHz, D<sub>8</sub>-THF) δ 5.04 (m, 1H), 4.93 (m, 1H), 4.83 (m, 1H), 1.89 (s, 3H), 0.90 (s, 9H).

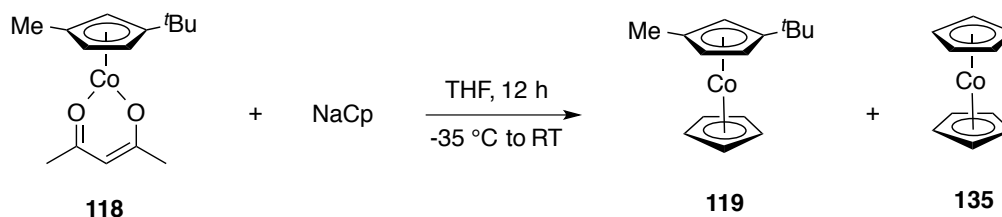
*Synthesis of 1-methyl-3-*tert*-butylcyclopentadienyl cobalt(II) acetylacetonate 118*



In a drybox, 1-methyl-3-*tert*-butylcyclopentadienyl potassium **126** (43.0 mg, 0.25 mmol) and THF (2.0 ml) were added into a 5-dram glass vial. Bis(acetylacetonate)cobalt (131.1 mg, 0.51 mmol) and THF were added into another 5-dram vial equipped with a stir bar. Both vials were stored in the -35 °C freezer for 30 minutes. The 1-methyl-3-*tert*-butylcyclopentadienyl potassium **126** solution in THF was added dropwise to the vial containing bis(acetylacetonate)cobalt. The reaction was left for 12 h to warm slowly to room temperature. During the reaction, the solution turned to brown, with the formation of pink precipitate. The solvent was removed *in vacuo* and pentane was used to extract 1-methyl-3-*tert*-butylcyclopentadienyl cobalt(II) acetylacetonate **118**, which appeared as a brown oily compound after removing pentane. The paramagnetic product was analyzed by

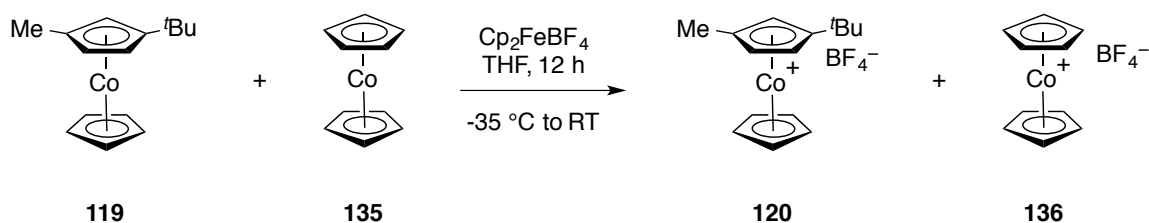
HR-MS spectroscopy. MS  $m/z$  calculated for  $C_{15}H_{22}O_2Co$  ( $M^+$ ): 293.0952; found: 293.0948 (63.0%).

*Synthesis of 1-methyl-3-tert-butylcyclopentadienyl cobalt(II) cyclopentadienyl 119*



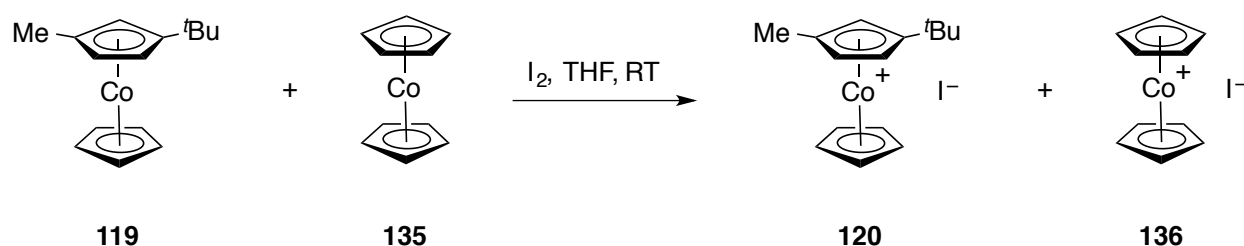
In a drybox, cyclopentadienyl sodium (25.5 mg, 0.29 mmol), recrystallized from THF, was dissolved in 1.0 ml THF in a 5 dram glass vial. 1-methyl-3-*tert*-butylcyclopentadienyl cobalt(II) acetylacetonate **118** (85.0 mg, 0.29 mmol) and THF were added to another 5 dram vial equipped with a stir bar. Both vials were stored in the -35 °C freezer for 30 minutes. The cyclopentadienyl sodium solution in THF was added dropwise to the vial containing 1-methyl-3-*tert*-butylcyclopentadienyl cobalt(II) acetylacetonate **118**. The reaction was left for 12 h to allow slow warm to room temperature. During the reaction, the solution remained brown, with the formation of pink precipitate. The solvent was removed *in vacuo* and pentane was used to extract 1-methyl-3-*tert*-butylcyclopentadienyl cobalt(II) cyclopentadienyl **119**, which appeared as a brown oily compound after removing pentane. The product was analyzed by HR-MS spectroscopy. MS  $m/z$  calculated for  $C_{15}H_{20}Co$  ( $M^+$ ): 259.0897; found: 259.0898 (10.5%);  $m/z$  calculated for  $C_{10}H_{10}Co$  ( $M^+$ ): 189.0114; found: 189.1135 (100%).

Oxidation of cobaltocene derivatives using ferrocenium tetrafluoroborate



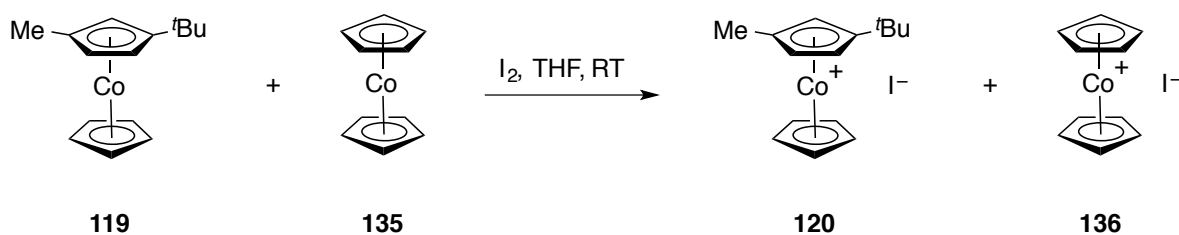
In a drybox, 1-methyl-3-*tert*-butylcyclopentadienyl cobalt(II) cyclopentadienyl **119** (37.3 mg, 0.14 mmol) was added to a 5 dram vial equipped with a stir bar and dissolved in 2.0 ml THF. Ferrocenium tetrafluoroborate (40.9 mg, 0.15 mmol) was weighed into another 5 dram vial and dissolved in 2.0 ml THF. Both vials were stored in the -35 °C freezer for 30 minutes. [Cp<sub>2</sub>Fe][BF<sub>4</sub>] solution was added to the vial containing 1-methyl-3-*tert*-butylcyclopentadienyl cobalt(II) cyclopentadienyl. Though the brown solution changed to yellow within a few minutes, the reaction was left stirring for 12 h. The solvent was removed *in vacuo* and washed with pentane to remove ferrocene. The remaining solid was further purified by the column chromatography to afford **120** (21.4 mg, 43%) and **136** (14.3 mg, 36%). The product was analyzed by <sup>1</sup>H NMR spectroscopy. For unsymmetrical cobaltocenium compound **120**: <sup>1</sup>H NMR (300 MHz, CDCl<sub>3</sub>) δ 6.05 (s, 1H), 5.78 (s, 5H), 5.63 (s, 1H), 5.59 (s, 1H), 2.29 (s, 3H), 1.33 (s, 9H). ESI MS *m/z* calculated for C<sub>15</sub>H<sub>20</sub>Co (M<sup>+</sup>): 259.0892; found: 259.0892. For cobaltocenium compound **136**: <sup>1</sup>H NMR (300 MHz, CDCl<sub>3</sub>) δ 5.93 (s, 10 H). ESI MS *m/z* calculated for C<sub>10</sub>H<sub>10</sub>Co (M<sup>+</sup>): 189.0109; found: 189.0111.

*Oxidation of cobaltocene derivatives using solid iodine at room temperature*



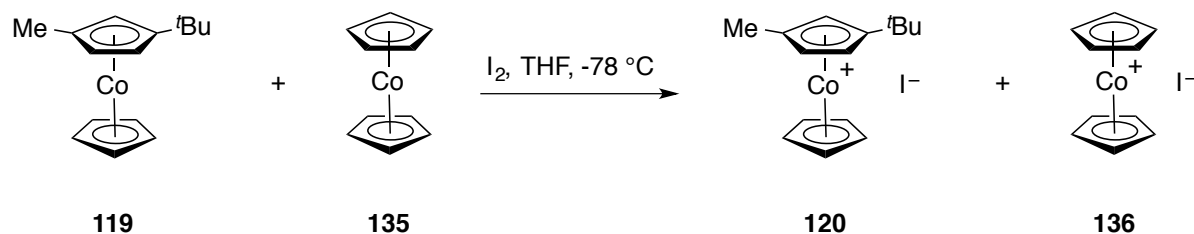
In a drybox, 1-methyl-3-*tert*-butylcyclopentadienyl cobalt(II) cyclopentadienyl **119** (37.4 mg, 0.14 mmol) was added to a Schlenk flask equipped with a stir bar and dissolved in 2.0 ml THF. The flask was connected to a Schlenk line and placed under a nitrogen atmosphere. At the room temperature, iodine (17.8 mg, 0.14 mmol) was added to the flask and the brown solution changed to yellow within a few minutes. The solvent was removed *in vacuo* and the remaining solid was further purified by the column chromatography to afford **120** (20.5 mg, 38%) and **136** (16.4 mg, 37%). For unsymmetrical cobaltocenium compound **120**:  $^1H$  NMR (300 MHz,  $CDCl_3$ )  $\delta$  6.05 (s, 1H), 5.77 (s, 1H), 5.65 (s, 1H), 5.56 (s, 1H), 2.28 (s, 3H), 1.29 (s, 9H). For cobaltocenium compound **136**:  $^1H$  NMR (300 MHz,  $CDCl_3$ )  $\delta$  5.93 (s, 10H).

*Oxidation of cobaltocene derivatives using iodine/ether solution at room temperature*



In a drybox, 1-methyl-3-*tert*-butylcyclopentadienyl cobalt(II) cyclopentadienyl **119** (37.4 mg, 0.14 mmol) was added to a Schlenk flask equipped with a stir bar and dissolved in 2.0 ml THF. The flask was connected to a Schlenk line and placed under a nitrogen atmosphere. Iodine (8.9 mg, 0.07 mmol) was dissolved in 1.0 ml diethyl ether. The iodine solution was then added dropwise to the flask at room temperature and the brown solution changed to yellow gradually. The solvent was removed *in vacuo* and the remaining solid was further purified by the column chromatography to afford **120** (9.2 mg, 17%) and **136** (14.6 mg, 33%). For unsymmetrical cobaltocenium compound **120**:  $^1\text{H NMR}$  (300 MHz,  $\text{CDCl}_3$ )  $\delta$  6.05 (s, 1H), 5.77 (s, 1H), 5.65 (s, 1H), 5.56 (s, 1H) 2.28 (s, 3H), 1.29 (s, 9H). For cobaltocenium compound **136**:  $^1\text{H NMR}$  (300 MHz,  $\text{CDCl}_3$ )  $\delta$  5.93 (s, 10H).

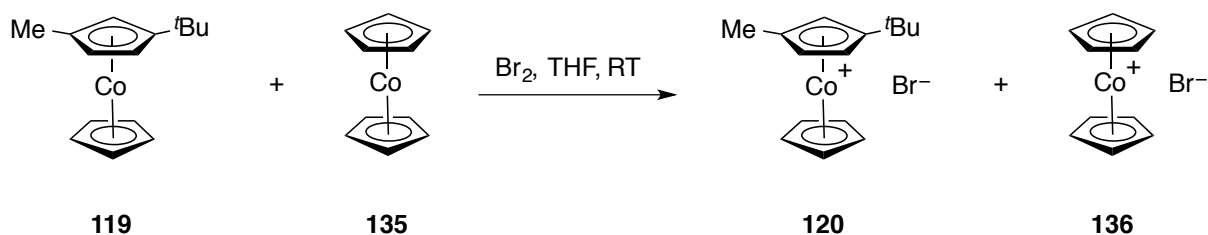
*Oxidation of cobaltocene derivatives using iodine/ether solution at -78 °C*



In a drybox, 1-methyl-3-*tert*-butylcyclopentadienyl cobalt(II) cyclopentadienyl **119** (37.8 mg, 0.14 mmol) was added to a Schlenk flask equipped with a stir bar and dissolved in 2.0 ml THF. The flask was connected to a Schlenk line and placed under a nitrogen atmosphere. Iodine (8.9 mg, 0.07 mmol) was dissolved in 1.0 ml diethyl ether. The iodine solution was then added dropwise to the flask at  $-78\text{ }^\circ\text{C}$ . The reaction mixture was maintained at  $-78\text{ }^\circ\text{C}$  for 1 h and allowed to warm slowly to room temperature. The solvent was removed *in vacuo* and the remaining solid was further purified by the column chromatography to afford **120** (5.4 mg, 10%) and **136** (22.1 mg, 50%). For unsymmetrical cobaltocenium

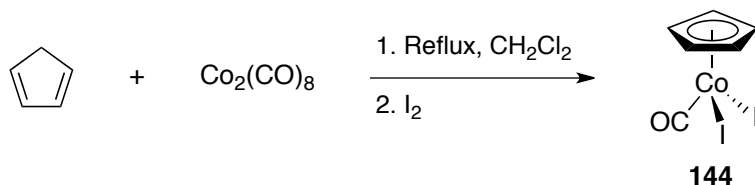
compound **120**:  $^1\text{H NMR}$  (300 MHz,  $\text{CDCl}_3$ )  $\delta$  6.05 (s, 1H), 5.77 (s, 1H), 5.65 (s, 1H), 5.56 (s, 1H) 2.28 (s, 3H), 1.29 (s, 9H). For cobaltocenium compound **136**:  $^1\text{H NMR}$  (300 MHz,  $\text{CDCl}_3$ )  $\delta$  5.93 (s, 10H).

*Oxidation of cobaltocene derivatives using bromine at room temperature*



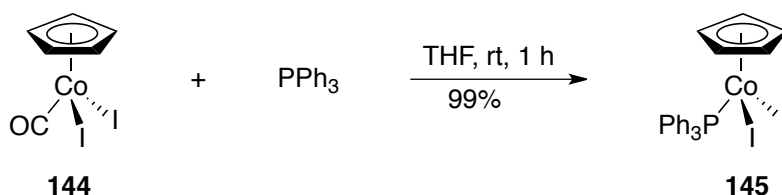
In a drybox, 1-methyl-3-*tert*-butylcyclopentadienyl cobalt(II) cyclopentadienyl **119** (37.5 mg, 0.14 mmol) was added to a Schlenk flask equipped with a stir bar and dissolved in 2.0 ml THF. The flask was connected to a Schlenk line and placed under a nitrogen atmosphere. At the room temperature, bromine (5.6 mg, 0.07 mmol) was added to the flask and the brown solution changed to yellow within a few minutes. The solvent was removed *in vacuo* and the remaining solid was further purified by the column chromatography to afford **120** (14.2 mg, 30%) and **136** (16.9 mg, 45%). The product was analyzed by  $^1\text{H NMR}$  spectroscopy. For unsymmetrical cobaltocenium compound **120**:  $^1\text{H NMR}$  (300 MHz,  $\text{CDCl}_3$ )  $\delta$  6.04 (s, 1H), 5.76 (s, 5H), 5.58 (s, 1H), 5.52 (s, 1H), 2.25 (s, 3H), 1.30 (s, 9H). For cobaltocenium compound **136**:  $^1\text{H NMR}$  (300 MHz,  $\text{CDCl}_3$ )  $\delta$  5.84 (s, 10H).

### Synthesis of CpCoI<sub>2</sub>CO **144**



$\text{CpCo}(\text{CO})_2$  was synthesized from the literature preparation.<sup>189</sup> After the formation of  $\text{CpCo}(\text{CO})_2$  *in situ*, the reaction flask was immersed into an acetone/dry ice bath ( $-78\text{ }^\circ\text{C}$ ). Iodine (363.5 mg, 1.43 mmol, 1.2 equiv) was added *slowly* to the flask, as carbon monoxide evolved *rapidly* from the solution. The reaction was stirred for another 30 minutes. The product was purified by column chromatography to afford **144** (435.2 mg, 90%). The product was analyzed by  $^1\text{H}$  NMR spectroscopy.  $^1\text{H}$  NMR (300 MHz,  $\text{CDCl}_3$ )  $\delta$  5.69 (s, 5H).

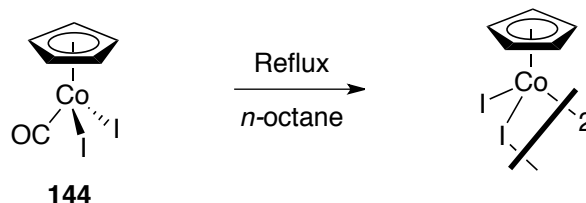
### Synthesis of CpCoI<sub>2</sub>PPh<sub>3</sub> **145**



To the Schlenk flask equipped with a stir bar,  $\text{CpCoI}_2\text{CO}$  **144** (309.2 mg, 0.76 mmol) and THF (3 ml) were added. Triphenylphosphine (199.5 mg, 0.76 mmol) was dissolved in 3 ml THF and added to the flask dropwise over a period of 5 minutes. The reaction was stirred for an hour, during which evolution of carbon monoxide was observed. The product was purified by column chromatography to afford **145** (481.6 mg, 99%). The product was analyzed by  $^1\text{H}$  NMR spectroscopy.  $^1\text{H}$  NMR (300 MHz,  $\text{CDCl}_3$ )  $\delta$  7.77 (m, 6H); 7.40 (m, 9H);

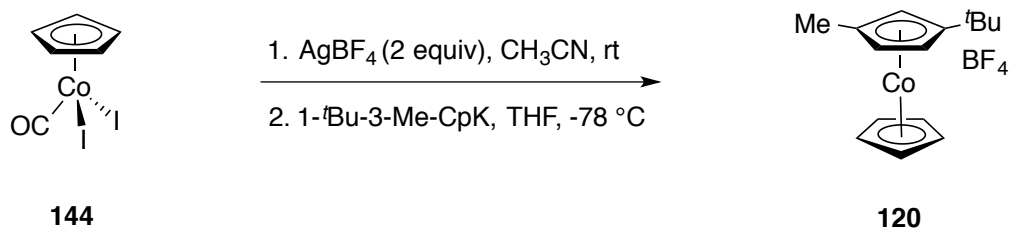
5.11 (s, 5H). IR (KBr Solid,  $\text{cm}^{-1}$ ) 3118.5 (s), 3106.7 (m), 3082.8 (m), 3074.0 (w), 3054.2 (w), 3024.0 (w), 1585.5 (w), 1574.1 (w), 1479.1 (s), 1436.8 (s).

*Synthesis of CpCoI<sub>2</sub> dimer*



To a Schlenk flask equipped with a stir bar, CpCoI<sub>2</sub>CO **144** (2.3 g, 5.7 mmol) and *n*-octane (15 ml) were added. The flask was connected with a water-cooled condenser. The solution was heated to reflux for 12 h, during which evolution of carbon monoxide was observed. A black precipitate was formed and cleaned by rinsing with dichloromethane. The product was analyzed by elemental analysis (calculated: C, 15.8; H, 1.3; I, 67.2; Found: C, 16.4; H, 1.4; I, 66.8.)

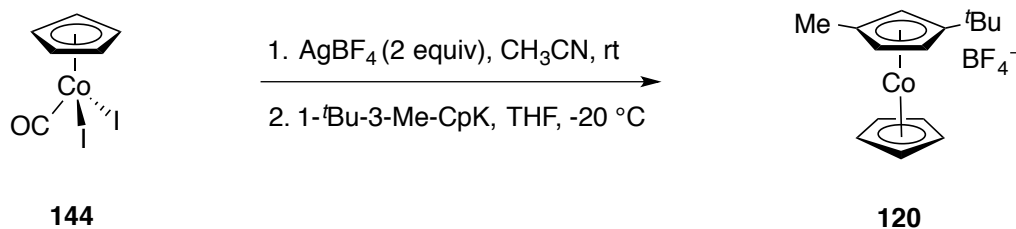
*Synthesis of 1-methyl-3-tert-butylcobaltocenium tetrafluoroborate **120** at -78 °C*



CpCoI<sub>2</sub>CO **144** (1.06 g, 2.59 mmol) and acetonitrile (10 ml) were charged to a Schlenk flask equipped with a stir bar. Silver tetrafluoroborate (1.01 g, 5.18 mmol) was added to the

flask slowly. The reaction mixture was kept stirring for 8 h, during which color changed gradually from brown to deep red. The solution was immersed into an acetone/dry ice bath (-78 °C). In a drybox, 1-methyl-3-*tert*-butylcyclopentadienyl potassium (0.45 g, 2.59 mmol) and 5 ml THF were charged into another Schlenk flask. The THF solution was transferred dropwise to the first flask containing [CpCo(CH<sub>3</sub>CN)<sub>3</sub>][BF<sub>4</sub>]<sub>2</sub> solution using a cannula. The mixture was remained stirring for 12 h at -78 °C. The solvent was removed *in vacuo* to afford a yellow residue, which was further purified by column chromatography to obtain a golden solid (268.9 mg, 30%). Single crystals were obtained from ether/hexane recrystallization and the X-ray structure was obtained (Appendix 1). The product was analyzed by <sup>1</sup>H NMR spectroscopy. <sup>1</sup>H NMR (300 MHz, CDCl<sub>3</sub>) δ 5.75 (s, 1H), 5.64 (s, 5H), 5.48 (s, 2H), 2.18 (s, 3H), 1.29 (s, 9H). <sup>13</sup>C NMR (125 MHz, CDCl<sub>3</sub>) δ 120.1, 103.7, 85.1, 83.2, 81.0, 79.5, 30.9, 13.8. IR (cast film, cm<sup>-1</sup>) 3120.1 (m), 2968.0 (s), 2934.8 (m), 2873.7 (w), 1706.2 (w), 1490.9 (s), 1072.6 (s). ESI MS *m/z* calculated for C<sub>15</sub>H<sub>20</sub>Co (M<sup>+</sup>): 259.0892; found: 259.0889.

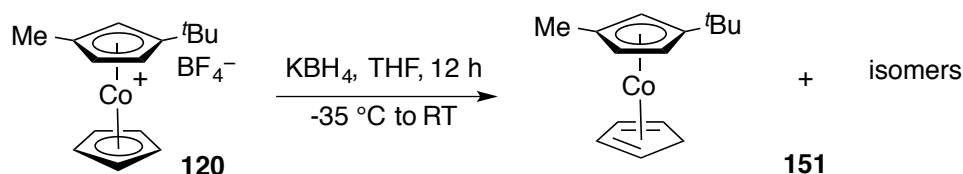
*Synthesis of 1-methyl-3-tert-butylcobaltocenium tetrafluoroborate 120 at -20 °C*



CpCoI<sub>2</sub>CO **144** (1.05 g, 2.59 mmol) and acetonitrile (10 ml) were charged into a Schlenk flask equipped with a stir bar. Silver tetrafluoroborate (1.0 g, 5.18 mmol) was added to the flask slowly. The reaction mixture was kept stirring for 8 h, during which color changed gradually from brown to deep red. The solution was immersed into a NaCl/ ice bath (-20

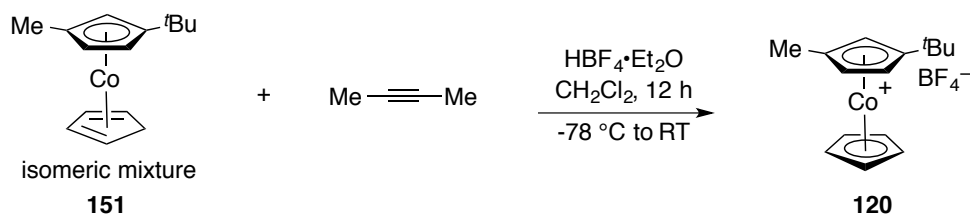
°C). In a drybox, 1-methyl-3-*tert*-butylcyclopentadienyl potassium (0.45 g, 2.59 mmol) and 5 ml THF were charged into another Schlenk flask. The THF solution was transferred dropwise to the first flask containing  $[\text{CpCo}(\text{CH}_3\text{CN})_3][\text{BF}_4]_2$  solution using a cannula. The mixture was stirred for 12 h at -20 °C. The solvent was removed *in vacuo* to afford a yellow residue, which was further purified by column chromatography to obtain a golden solid (609.5 mg, 68%). The product was analyzed by  $^1\text{H}$  NMR spectroscopy.  $^1\text{H}$  NMR (300 MHz,  $\text{CDCl}_3$ )  $\delta$  5.75 (s, 1H), 5.64 (s, 5H), 5.48 (s, 2H), 2.18 (s, 3H), 1.29 (s, 9H).  $^{13}\text{C}$  NMR (125 MHz,  $\text{CDCl}_3$ )  $\delta$  120.1, 103.7, 85.1, 83.2, 81.0, 79.5, 30.9, 13.8. ESI MS  $m/z$  calculated for  $\text{C}_{15}\text{H}_{20}\text{Co}$  ( $\text{M}^+$ ): 259.0892; found: 259.0889.

*Synthesis of ( $\eta^5$ -1-methyl-3-*tert*-butylcyclopentadienyl) cobalt(II) ( $\eta^4$ -cyclopentadiene) **151***



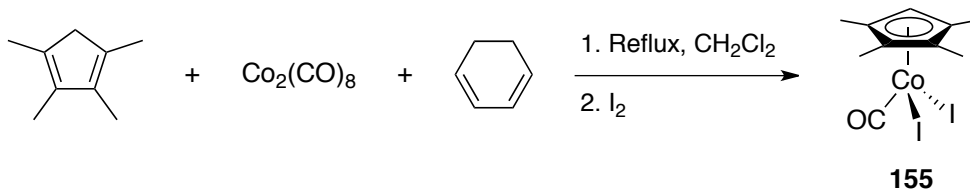
In a drybox, 1-methyl-3-*tert*-butylcobaltocenium tetrafluoroborate **120** (45.4 mg, 0.13 mmol) was dissolved in 2.0 ml THF in a 5 dram glass vial equipped with a stir bar. The vial was stored in the -35 °C freezer for 30 minutes. Potassium borohydride (7.0 mg, 0.13 mmol) was added slowly to the THF solution. The reaction mixture was kept stirring for 12 h to warm to room temperature. During the reaction, the color of the solution changed from yellow to brown. The solvent was removed *in vacuo* and pentane was used to extract the product. The product appeared as a brown oily compound after removing pentane and was analyzed by  $^1\text{H}$  and  $^{13}\text{C}$  NMR spectroscopy. The product was subjected to  $^1\text{H}$  NMR spectroscopy analysis, however due to the presence of various isomers, the  $^1\text{H}$  NMR spectrum appeared complicated and was not further interpreted.

### Attempted ring-expansion reaction



In a drybox, ( $\eta^5$ -1-methyl-3-*tert*-butylcyclopentadienyl) cobalt(I) ( $\eta^4$ -cyclopentadiene) **151** (30.5 mg, 0.12 mmol) was added to a Schlenk flask equipped with a stir bar. The flask was placed under a nitrogen atmosphere and immersed in an acetone/dry ice bath (-78 °C).  $\text{CH}_2\text{Cl}_2$  (2.5 ml), 2-butyne (0.2 ml, 2.5 mmol) and fluoroboric acid diethyl ether complex (16  $\mu\text{l}$ , 0.12 mmol) were added subsequently to the flask. The reaction mixture was kept stirring for 15 h to warm to room temperature. During the reaction, the color of the solution changed from brown to yellow. The solvent was removed *in vacuo* and the residue was further purified by column chromatography. The product was analyzed by  $^1\text{H}$  NMR spectroscopy.  $^1\text{H}$  NMR (300 MHz,  $\text{CDCl}_3$ )  $\delta$  5.75 (s, 1H), 5.64 (s, 5H), 5.48 (s, 2H), 2.18 (s, 3H), 1.29 (s, 9H).  $^{13}\text{C}$  NMR (125 MHz,  $\text{CDCl}_3$ )  $\delta$  120.1, 103.7, 85.1, 83.2, 81.0, 79.5, 30.9, 13.8.

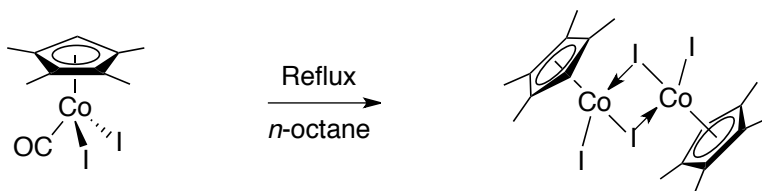
### Synthesis of carbonyl( $\eta^5$ -tetramethylcyclopentadienyl)diiodocobalt **154**



In a drybox, dicobalt octacarbonyl (1.15 g, 3.36 mmol) was charged to a Schlenk flask equipped with a stir bar. The flask was then placed under a nitrogen gas using a Schlenk

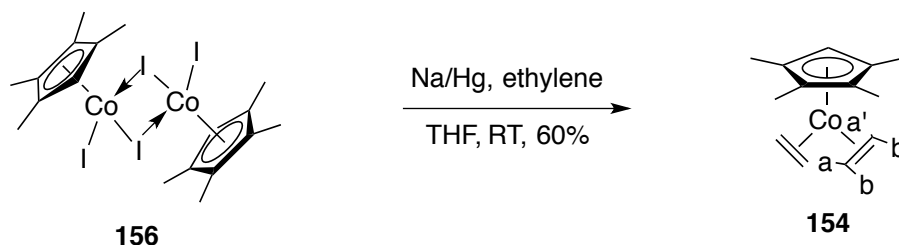
line. Dichloromethane (10 ml) and tetramethylcyclopentadiene (0.83 g, 6.80 mmol) were added to the flask. A water-cooled condenser was attached to the flask and the whole apparatus was wrapped with aluminum foil. The reaction mixture was heated at reflux for 12 h. After immersing the flask into an ice bath, iodine (1.71 g, 6.74 mmol) was *slowly* added to the solution. During the reaction, the sash of the fume hood was kept as low as possible, as carbon monoxide was released *rapidly*. The solvent was removed *in vacuo* and the residue was purified by column chromatography to obtain 3.05 g purple solid. The product was analyzed by  $^1\text{H}$  NMR spectroscopy.  $^1\text{H}$  NMR (300 MHz,  $\text{CDCl}_3$ )  $\delta$  5.20 (s, 1H); 2.31 (s, 6H); 2.23 (s, 6H).  $^{13}\text{C}$  NMR (125 MHz,  $\text{CDCl}_3$ )  $\delta$  198.8, 104.9, 99.5, 89.3, 12.7, 11.7.

*Synthesis of ( $\eta^5$ -tetramethylcyclopentadienyl)diiodocobalt dimer **156***



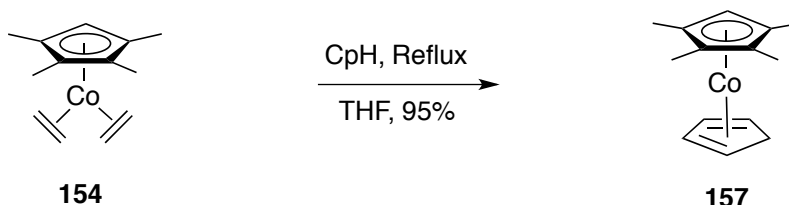
Carbonyl( $\eta^5$ -tetramethylcyclopentadienyl)diiodocobalt **154** (1.0 g, 2.17 mmol) and *n*-octane (20 ml) was charged into a Schlenk flask equipped with a stir bar. A water-cooled condenser was connected to the flask. The solution was refluxed for 12 h, during which black solid precipitated (0.85 g, 91%). The solid was isolated and rinsed with anhydrous pentane. The product was analyzed by IR spectroscopy, which revealed no carbonyl remained. IR (solid,  $\text{cm}^{-1}$ ) 3389.5 (w), 3081.1 (w), 2980.5 (w), 2960.0 (w), 2906.9 (w), 1486.7 (m), 1467.6 (m), 1418.7 (m), 1474.9 (s), 1148.9 (w), 1011.8 (s).

Synthesis of ( $\eta^5$ -tetramethylcyclopentadienyl) cobalt(I) bisethylene **154**



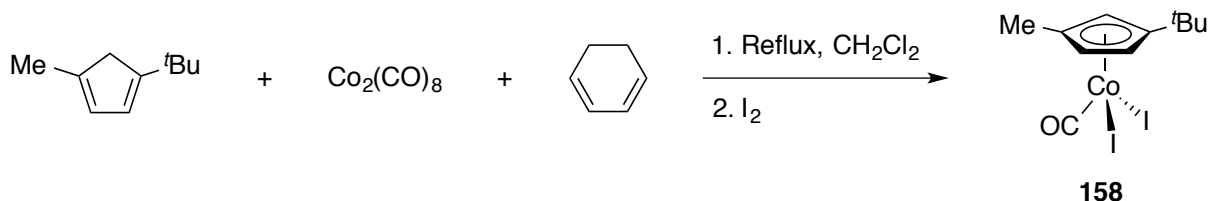
In a drybox, ( $\eta^5$ -tetramethylcyclopentadienyl)diiiodocobalt dimer **156** (280.2 mg, 0.65 mmol) and THF (10.0 ml) was charged into a Schlenk flask equipped with a stir bar. Sodium amalgam (3%) was prepared *in situ* by adding sodium (148.4 mg, 6.4 mmol) to mercury (4.9 g). Sodium amalgam was added to the flask, when it was placed under a nitrogen atmosphere using a Schlenk line. An ethylene tank was connected to the flask with the needle tip immersed under the THF solution. Ethylene was bubbled into the THF solution at a rate of one bubble per second. The reaction was stirred at room temperature for 2 h to afford a red solution with black precipitates. The solvent was removed *in vacuo* and transferred into drybox *as quickly as possible*. The product was dissolved in pentane and filtered through Celite. A red solid (93.3 mg, 60%) was obtained after removing pentane *in vacuo*. The product decomposes slowly at room temperature and must be stored in the freezer. The product was analyzed by  $^1\text{H}$  NMR spectroscopy.  $^1\text{H}$  NMR (300 MHz,  $\text{C}_6\text{D}_6$ )  $\delta$  4.28 (s, 1H); 1.87 (m, 4H, H<sub>b</sub>,b'); 1.46 (s, 6H); 1.27 (s, 6H); 0.97 (m, 4H, H<sub>a</sub>, a').  $^{13}\text{C}$  NMR (125 MHz,  $\text{C}_6\text{D}_6$ )  $\delta$  94.5, 92.1, 83.8, 43.5, 10.1, 8.9.

Synthesis of ( $\eta^5$ -tetramethylcyclopentadienyl) cobalt(I) ( $\eta^4$ -cyclopentadiene) **157**



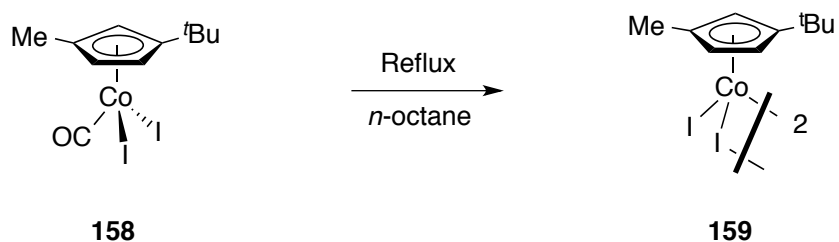
In a drybox, ( $\eta^5$ -tetramethylcyclopentadienyl) cobalt(I) bisethylene **154** (60.2 mg, 0.25 mmol) and THF (5.0 ml) was charged into a Schlenk flask equipped with a stir bar. The flask was placed under a nitrogen atmosphere using Schlenk line. Freshly-cracked monomeric cyclopentadiene (0.20 ml, 2.4 mmol) was added using a 1.0 ml syringe. The flask was then attached to a water-cooled condenser. The reaction mixture was refluxed for 45 minutes with a continuous purge of nitrogen gas. The solvent was removed *in vacuo* to afford a red solid (65.6 mg, 95%). The product was analyzed by  $^1\text{H}$  NMR spectroscopy.  $^1\text{H}$  NMR (300 MHz,  $\text{C}_6\text{D}_6$ )  $\delta$  4.87 (s, 2H,  $\text{H}_{2,3}$ ); 4.28 (s, 1H,  $\text{C}_5\text{HMe}_4$ ); 2.65 (d,  $J=13.7$  Hz, 1H,  $\text{H}_{5a}$ ); 2.22 (d,  $J=13.7$  Hz, 1H,  $\text{H}_{5b}$ ); 1.88 (s, 2H,  $\text{H}_{1,4}$ ).

Synthesis of carbonyl( $\eta^5$ -1-methyl-3-tert-butylcyclopentadienyl)diiodocobalt **158**



In a drybox, dicobalt octacarbonyl (2.01 g, 5.88 mmol) was charged into a Schlenk flask equipped with a stir bar. The flask was then placed under a nitrogen gas using a Schlenk line. Dichloromethane (20 ml), 1-methyl-3-*tert*-butylcyclopentadiene (1.60 g, 11.8 mmol) and cyclohexadiene (0.47 ml, 5.87 mmol) were subsequently added to the flask. A water-cooled condenser was attached to the flask and the whole apparatus was wrapped with aluminum foil. The reaction mixture was left refluxing for 15 h. The flask was then cooled down by immersing into an ice bath. Iodine (2.98 g, 11.7 mmol) was added *slowly* to the solution. Since carbon monoxide was released *rapidly*, the sash of fume hood was kept as low as possible. The solvent was removed *in vacuo* and the residue was purified by column chromatography to obtain a purple solid (4.09 g, 71%). The product was analyzed by  $^1\text{H}$  and  $^{13}\text{C}$  NMR spectroscopy.  $^1\text{H}$  NMR (300 MHz,  $\text{CDCl}_3$ )  $\delta$  5.52 (s, 1H); 5.42 (s, 1H); 5.03 (s, 1H); 2.59 (s, 3H); 1.32 (s, 9H).  $^{13}\text{C}$  NMR (100 MHz,  $\text{CDCl}_3$ )  $\delta$  115.4, 104.6, 94.2, 93.5, 80.5, 31.3, 15.0. IR (cast film,  $\text{cm}^{-1}$ ) 3086.5 (m), 2965.4 (s), 2911.0 (m), 2870.9 (m), 2528.4 (w), 2056.7 (s), 1734.5 (w), 1693.8 (w), 1480.9 (s), 1372.1 (s), 1217.2 (m).

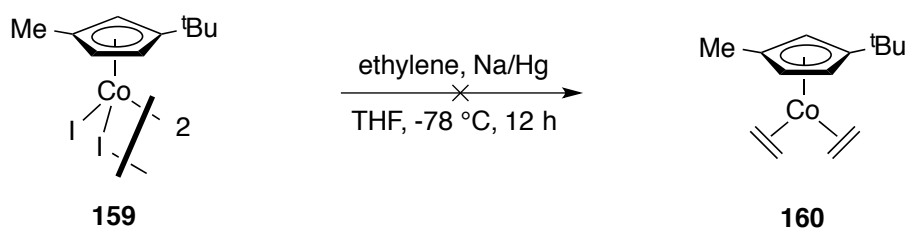
*Synthesis of ( $\eta^5$ -1-methyl-3-*tert*-butylcyclopentadienyl)diiodocobalt dimer 159*



Carbonyl( $\eta^5$ -1-methyl-3-*tert*-butylcyclopentadienyl)diiodocobalt **158** (2.4 g, 5.4 mmol) and *n*-octane (20 ml) was charged to a Schlenk flask equipped with a stir bar. A water-cooled condenser was connected to the flask. The solution was refluxed for 15 h, during which black solid precipitated out. The solid (2.18 g, 90%) was isolated and rinsed with

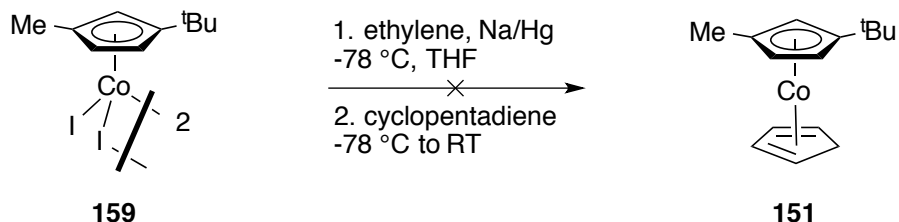
anhydrous pentane. Due to its insolubility in non-coordinating solvents and instability in coordinating solvents, the product was not analyzed by NMR and MS spectroscopy. Elemental analysis of the product was performed. (calculated: C, 26.8; H, 3.4; I, 56.7; found: C, 26.9; H, 3.5; I, 56.5.)

*Attempted synthesis of ( $\eta^5$ -1-methyl-3-tert-butylcyclopentadienyl) cobalt(I) bisethylene **160***



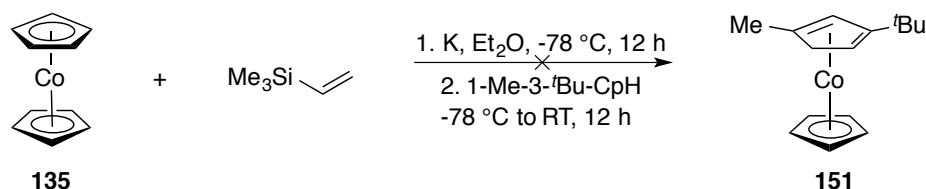
In the drybox, ( $\eta^5$ -1-methyl-3-tert-butylcyclopentadienyl)diodocobalt dimer **159** (120.5 mg, 0.27 mmol) and THF (5.0 ml) was charged into a Schlenk flask equipped with a stir bar. Sodium amalgam (3%) was prepared *in situ* by adding sodium (60 mg, 2.5 mmol) metal to mercury (1.9 g). Sodium amalgam was added into the flask under the protection of a nitrogen atmosphere using a Schlenk line. An ethylene tank was connected to the flask with needle tip kept immersed under the THF solution. Ethylene was bubbled into the THF solution at a rate of one bubble per second. The reaction was stirred at -78 °C for 12 h to afford a brown solution with black precipitates. The solvent was removed *in vacuo* and transferred into a drybox *as quickly as possible*. The product was dissolved in pentane and filtered through Celite. A brown residue was obtained after removing pentane *in vacuo*. The product was analyzed by  $^1\text{H}$  NMR spectroscopy, however the spectrum appeared complicated and uninterpretable, so no conclusion can be made.

Attempted synthesis of ( $\eta^5$ -1-methyl-3-*tert*-butylcyclopentadienyl) cobalt(I) ( $\eta^4$ -cyclopentadiene) **151** by trapping bisethylene intermediate **160**



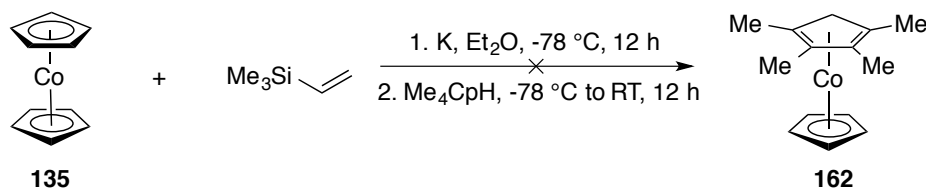
In a drybox, ( $\eta^5$ -1-methyl-3-*tert*-butylcyclopentadienyl)diiodocobalt dimer **159** (66.4 mg, 0.15 mmol) and THF (2.5 ml) was charged into a Schlenk flask equipped with a stir bar. The flask was immersed in an acetone/dry ice bath (-78 °C). Solid sodium amalgam (3%) was prepared *in situ* by adding sodium (34.3 mg, 1.5 mmol) into mercury (1.1 g). Sodium amalgam was added to the flask under the protection of a nitrogen atmosphere using a Schlenk line. An ethylene tank was connected to the flask with the needle tip immersed under the THF solution. Ethylene was bubbled into the THF solution at a rate of one bubble per second. The reaction was stirred at -78 °C for 12 h to afford a brown solution with black precipitates. Cyclopentadiene (0.13 ml, 1.5 mmol) was added to the flask using a 1.0 ml syringe. The reaction mixture was further stirred at -78 °C for 12 h. After removing the solvent *in vacuo*, the product was dissolved in pentane and filtered through Celite. A brown residue was obtained after removing pentane *in vacuo*. The product was analyzed by  $^1\text{H}$  NMR spectroscopy, however the spectrum appeared complicated and uninterpretable, so no conclusion can be made.

Attempted synthesis of ( $\eta^5$ -1-methyl-3-*tert*-butylcyclopentadienyl) cobalt(I) ( $\eta^4$ -cyclopentadiene) **151** by trapping  $\text{CpCo}(\text{H}_2\text{C}=\text{CHSiMe}_3)_2$  **161**



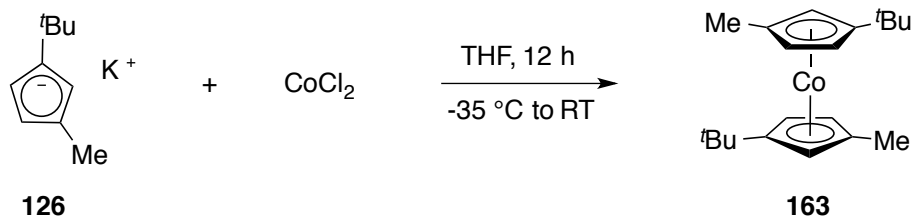
In a drybox, cobaltocene (62.8 mg, 0.33 mmol), potassium (13.1 mg, 0.33 mmol) and diethyl ether (2.0 ml) was charged into a Schlenk flask equipped with a stir bar. The flask was placed under a nitrogen atmosphere using a Schlenk line and immersed in an acetone/dry ice bath ( $-78\text{ }^\circ\text{C}$ ). Vinyltrimethylsilane (0.15 ml, 1.0 mmol) was added into the flask using a 1.0 ml syringe. The reaction was stirred at  $-78\text{ }^\circ\text{C}$  for 12 h to afford a red solution with dark precipitates. 1-methyl-3-*tert*-butylcyclopentadiene (0.1 ml) was added with a syringe. The reaction mixture was further stirred for 12 h slowly warming up to room temperature. The solvent was removed *in vacuo* and the product was filtered through Celite using pentane. A brown residue was obtained after removing pentane *in vacuo*. The product was analyzed by  $^1\text{H}$  NMR spectroscopy, however the spectrum appeared messy and no conclusion can be made.

Attempted synthesis of ( $\eta^5$ -cyclopentadienyl) cobalt(I) ( $\eta^4$ -tetramethylcyclopentadiene) **162** by trapping  $\text{CpCo}(\text{H}_2\text{C}=\text{CHSiMe}_3)_2$  **161**



In a drybox, cobaltocene (62.9 mg, 0.33 mmol), potassium (13.0mg, 0.33 mmol) and diethyl ether (2.0 ml) was charged into a Schlenk flask equipped with a stir bar. The flask was placed under a nitrogen atmosphere using a Schlenk line and immersed into an acetone/dry ice bath (-78°C). Vinyltrimethylsilane (0.15 ml, 1.0 mmol) was added to the flask using a 1 ml syringe. The reaction was stirred at -78 °C for 12 h to afford a red solution with dark precipitates. Tetramethylcyclopentadiene (0.15 ml) was added by a 1 ml syringe. The reaction mixture was further stirred for 12 h warming up slowly to room temperature. The solvent was removed *in vacuo* and the product was filtered through Celite using pentane. A brown residue (72.3 mg) was obtained after removing pentane *in vacuo*. The product was analyzed by <sup>1</sup>H NMR spectroscopy, however the spectrum appeared messy and no conclusion can be made.

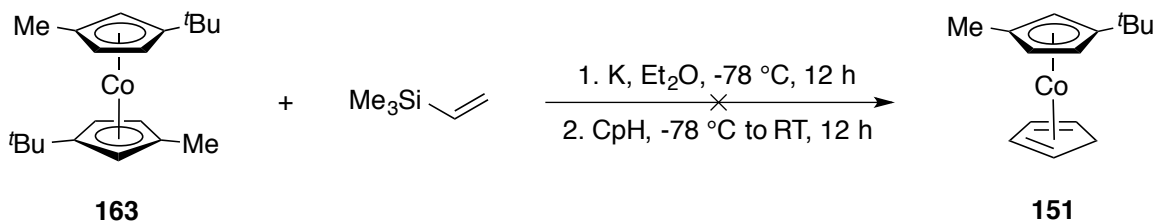
*Synthesis of bis(1-methyl-3-tert-butylcyclopentadienyl)cobalt 163*



In a drybox, 1-methyl-3-*tert*-butylcyclopentadienyl potassium (154.5 mg, 0.89 mmol) and THF (2.0 ml) were added into a 5 dram glass vial. Cobalt(II) chloride (56.7 mg, 0.44 mmol) and THF (1.0 ml) were added into another 5 dram vial equipped with a stir bar. Both vials were stored in the -35 °C freezer for 30 minutes. The 1-methyl-3-*tert*-butylcyclopentadienyl potassium solution in THF was added dropwise to the vial containing cobalt(II) chloride. The reaction was left for 12 h to slowly warm up to room temperature. During the reaction, the solution turned to brown, while dark precipitate was

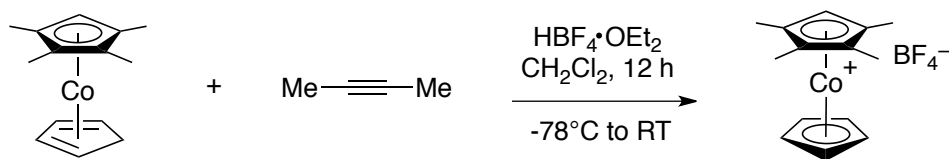
formed. The solvent was removed *in vacuo* and pentane was used to extract the product. The product (193.5 mg) appeared as a brown oily compound after removing pentane and was analyzed by HR-MS spectroscopy. MS  $m/z$  calculated for  $C_{20}H_{30}Co$  ( $M^+$ ): 329.1680; found: 259.1687 (100%).

*Attempted synthesis of ( $\eta^5$ -1-methyl-3-tert-butylcyclopentadienyl) cobalt(I) ( $\eta^4$ -cyclopentadiene) **151** by trapping ( $\eta^5$ -1-Me-3-*t*BuCp)Co( $H_2C=CHSiMe_3$ )<sub>2</sub>*



In a drybox, cobaltocene **163** (58.9 mg, 0.18 mmol), potassium (7.0 mg, 0.18 mmol) and diethyl ether (2.0 ml) was charged into a Schlenk flask equipped with a stir bar. The flask was placed under a nitrogen atmosphere using a Schlenk line and immersed in an acetone/dry ice bath (-78°C). Vinyltrimethylsilane (0.15 ml, 1.0 mmol) was added to the flask. The reaction was stirred at -78 °C for 12 h to afford a red solution with dark precipitates. Monomeric cyclopentadiene (0.15 ml, 1.8 mmol) was added by a 1 ml syringe. The reaction mixture was further stirred for 12 h to slowly warm up to room temperature. The solvent was removed *in vacuo* and the product was filtered through Celite using pentane. A brown residue (64.5 mg) was obtained after removing pentane *in vacuo*. The product was analyzed by  $^1\text{H}$  NMR spectroscopy, however the spectrum appeared messy and no conclusion can be made.

*Attempted ring-expansion reaction*

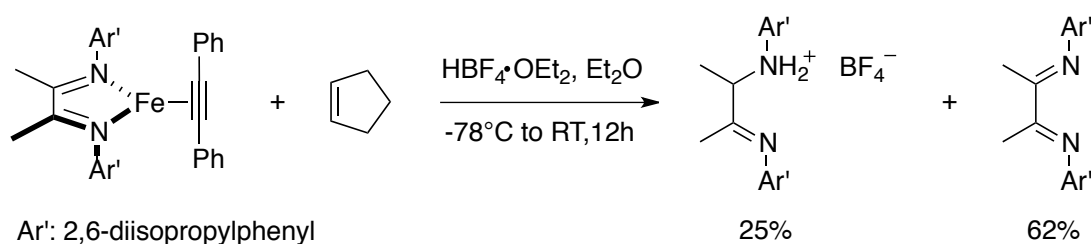


In a drybox, ( $\eta^5$ -tetramethylcyclopentadienyl) cobalt(I) ( $\eta^4$ -cyclopentadiene) **157** (37.6 mg, 0.15 mmol) was added into a Schlenk flask equipped with a stir bar. The flask was placed under a nitrogen atmosphere and immersed in an acetone/dry ice bath ( $-78^\circ\text{C}$ ). Methylene chloride (2.0 ml), 2-butyne (0.25 ml, 10 equiv) and fluoroboric acid diethyl ether complex (21  $\mu\text{l}$ , 0.15 mmol) were added subsequently to the flask. The reaction mixture was kept stirring for 12 h to warm up slowly to room temperature. During the reaction, the color of the solution changed from brown to yellow. The solvent was removed *in vacuo* and the residue was further purified by column chromatography. The product was analyzed by  $^1\text{H}$  and  $^{13}\text{C}$  NMR spectroscopy and confirmed as  $[\text{Me}_4\text{CpCo(III)Cp}][\text{BF}_4]$ .  $^1\text{H}$  NMR (300 MHz,  $\text{CDCl}_3$ )  $\delta$  5.55 (s, 1H); 5.37 (s, 5H); 2.07 (s, 12H).

## Experimental section of Chapter 4.

Di-imine ligand **175**,<sup>198</sup> di-imine iron(II) complex **172**,<sup>199</sup> and iron(0) alkyne **173**<sup>171</sup> were prepared according to the literature procedures.

### Attempted ring-expansion reaction



In a drybox, diimine iron(0) diphenylacetylene **173** (75.3 mg, 0.14 mmol) was dissolved in 1.5 ml diethyl ether in a 5 dram glass vial equipped with a stir bar. The vial was stored in the -78 °C freezer for 30 minutes. Cyclopentene (47.7 mg, 0.70 mmol) and fluoroboric acid diethyl ether complex (20.0  $\mu$ l, 0.14 mmol) were added to the diethyl ether solution. The reaction mixture was kept stirring for 12 h to warm up slowly to room temperature. During the reaction, the color of the solution changed from brown to yellow. The solvent was removed *in vacuo* to afford a yellowish solid. Pentane was used to wash the product and 62.0% of the diimine ligand was recovered. The remaining solid was recrystallized from cold diethyl ether solution. X-ray analysis identified the crystal as an ammonium compound **176**.

Appendix 1

STRUCTURE REPORT

XCL Code: JMS1029

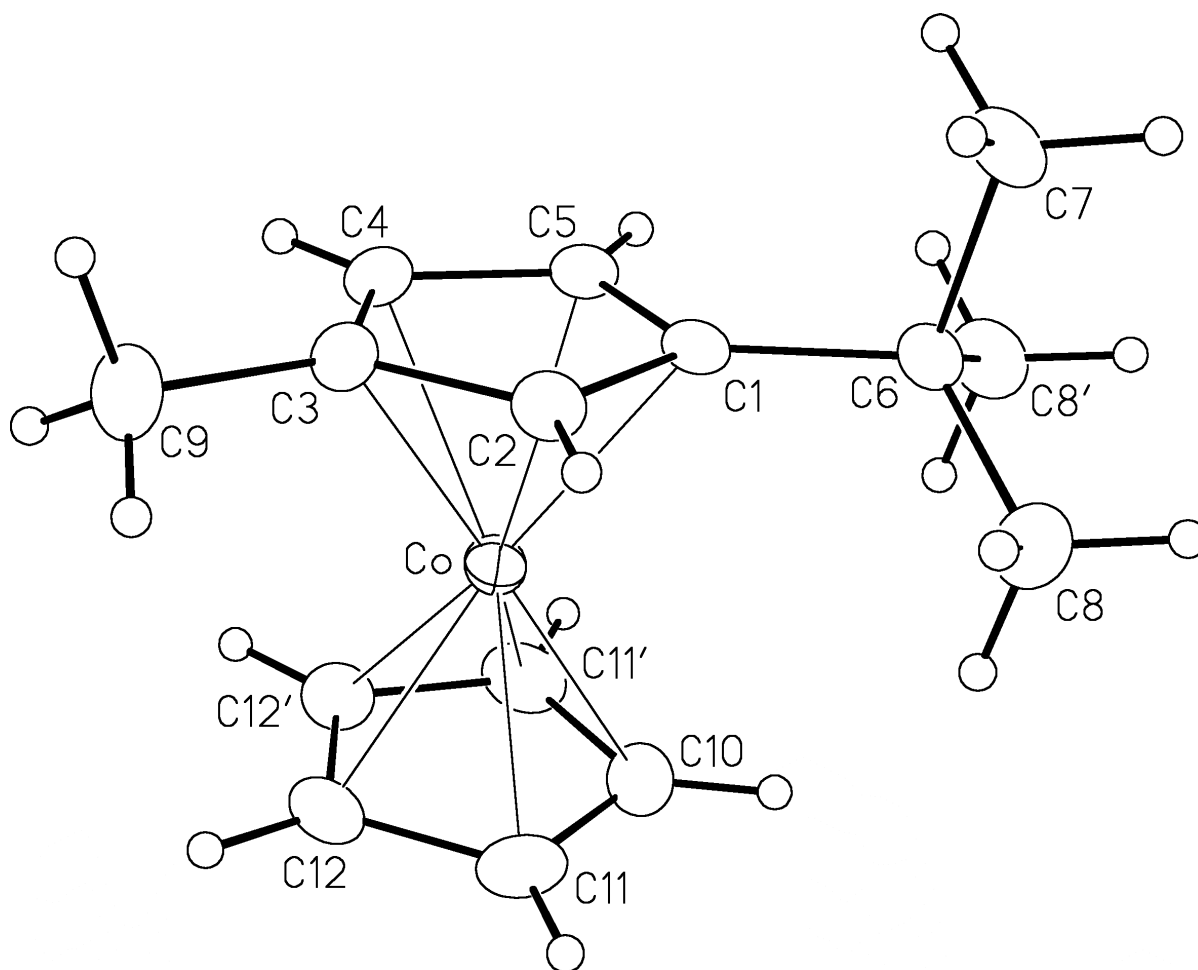
Date: 16 April 2010

Compound:  $[(\eta^5-1-t\text{-Butyl-3-methylcyclopentadienyl)CoCp][BF_4]$

Formula:  $C_{15}H_{20}BCoF_4$

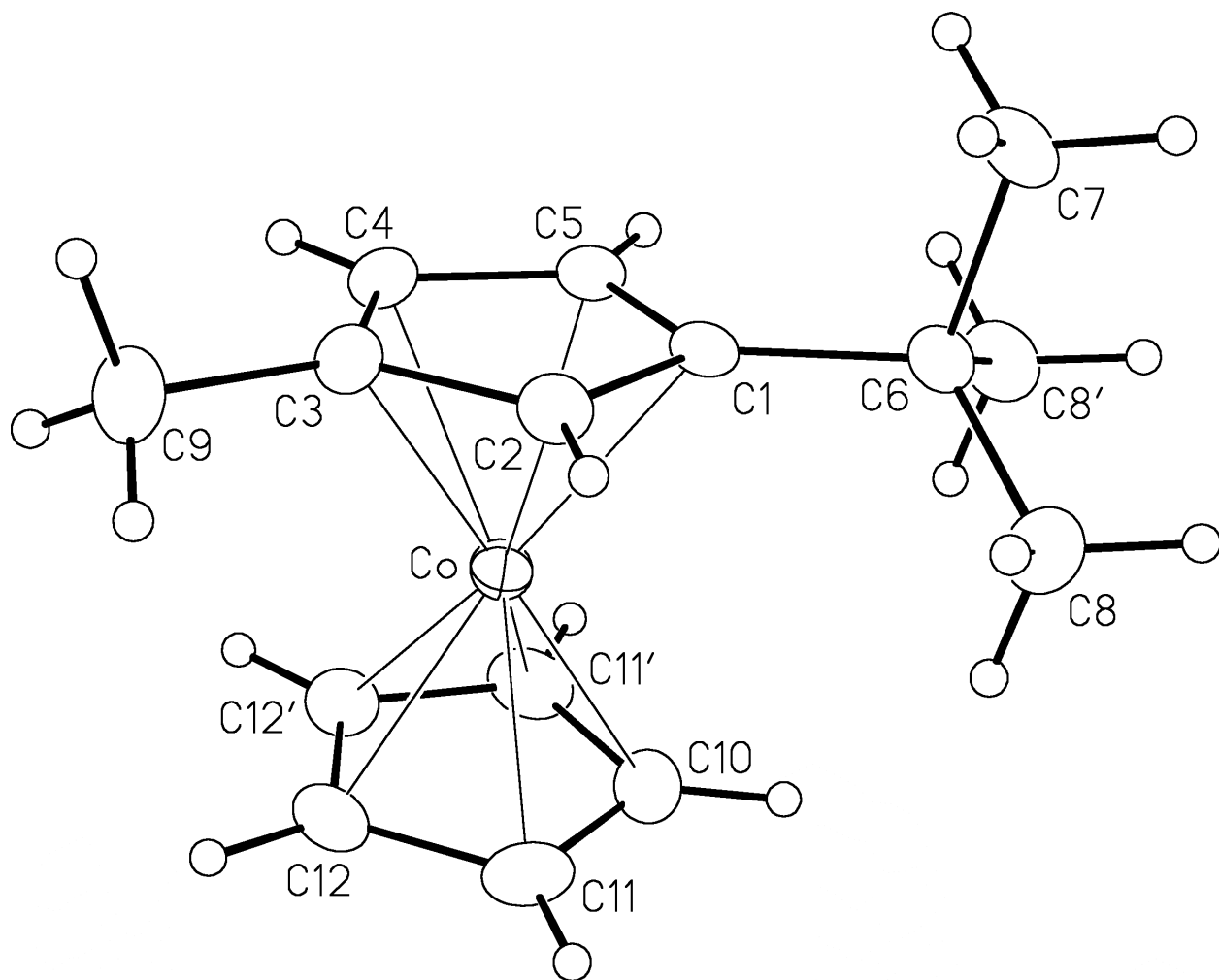
Supervisor: J. M. Stryker

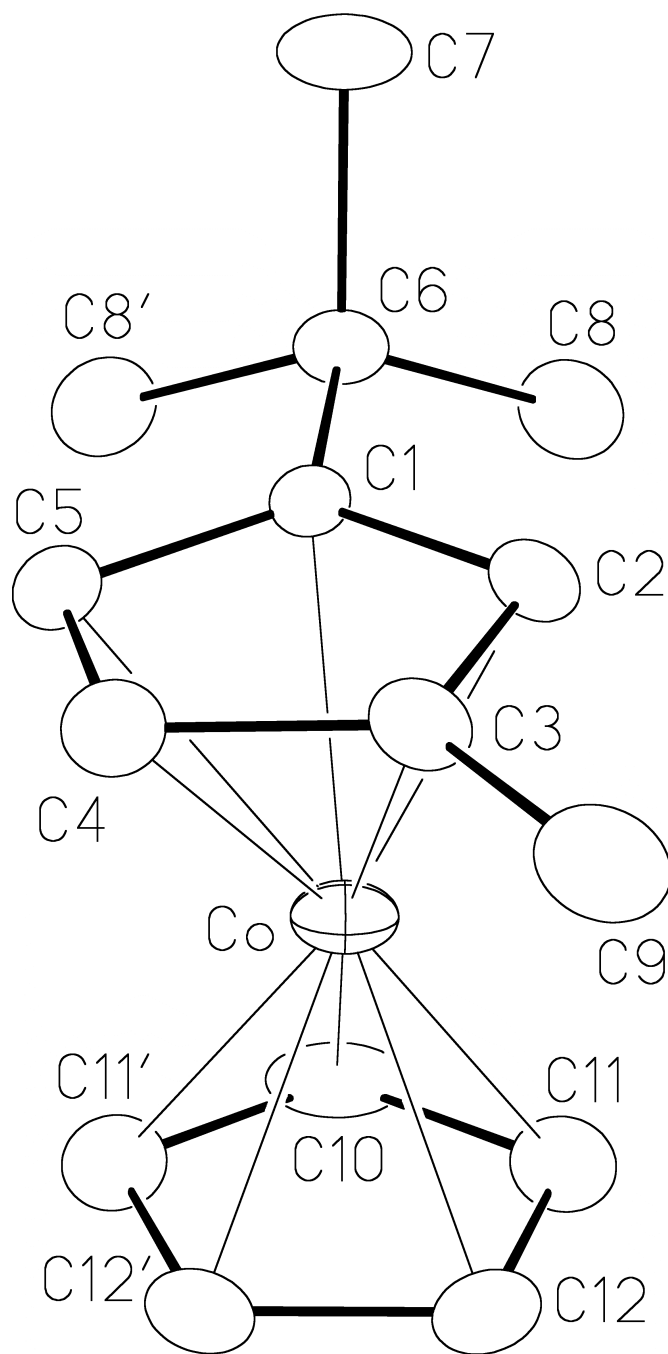
Crystallographer: R. McDonald



## Figure Legends

- Figure 1.** Perspective view of the  $[(\eta^5\text{-}1\text{-}t\text{-butyl-3-methylcyclopentadienyl})\text{CoCp}]^+$  complex ion showing the atom labelling scheme. Non-hydrogen atoms are represented by Gaussian ellipsoids at the 20% probability level. Hydrogen atoms are shown with arbitrarily small thermal parameters. Primed atoms are related to unprimed ones via the crystallographic mirror plane ( $x, 1/4, z$ ) upon which the Co, C6, C7, and C10 atoms are located. The ring carbons (C1–C5) and methyl group (C9) of the 1-*t*-butyl-3-methylcyclopentadienyl group are disordered across this mirror plane.
- Figure 2.** Alternate view of the molecule. Hydrogen atoms are not shown.





## List of Tables

- Table 1.** Crystallographic Experimental Details
- Table 2.** Atomic Coordinates and Equivalent Isotropic Displacement Parameters
- Table 3.** Selected Interatomic Distances
- Table 4.** Selected Interatomic Angles
- Table 5.** Torsional Angles
- Table 6.** Least-Squares Planes
- Table 7.** Anisotropic Displacement Parameters
- Table 8.** Derived Atomic Coordinates and Displacement Parameters for Hydrogen Atoms

**Table 1.** Crystallographic Experimental Details*A. Crystal Data*

formula	C <sub>15</sub> H <sub>20</sub> BCoF <sub>4</sub>
formula weight	346.05
crystal dimensions (mm)	0.42 × 0.34 × 0.16
crystal system	orthorhombic
space group	<i>Pnma</i> (No. 62)
unit cell parameters <sup>a</sup>	
<i>a</i> (Å)	16.909 (3)
<i>b</i> (Å)	9.6164 (19)
<i>c</i> (Å)	9.6425 (19)
<i>V</i> (Å <sup>3</sup> )	1567.9 (5)
<i>Z</i>	4
$\rho_{\text{calcd}}$ (g cm <sup>-3</sup> )	1.466
$\mu$ (mm <sup>-1</sup> )	1.124

*B. Data Collection and Refinement Conditions*

diffractometer	Bruker D8/APEX II CCD <sup>b</sup>
radiation ( $\lambda$ [Å])	graphite-monochromated Mo K $\alpha$ (0.71073)
temperature (°C)	-100
scan type	$\omega$ scans (0.3°) (15 s exposures)
data collection $2\theta$ limit (deg)	55.14
total data collected	13288 ( $-21 \leq h \leq 21$ , $-12 \leq k \leq 12$ , $-12 \leq l \leq 12$ )
independent reflections	1917 ( $R_{\text{int}} = 0.0156$ )
number of observed reflections ( <i>NO</i> )	1777 [ $F_o^2 \geq 2\sigma(F_o^2)$ ]
structure solution method	Patterson/structure expansion ( <i>DIRDIF-2008</i> <sup>c</sup> )
refinement method	full-matrix least-squares on $F^2$ ( <i>SHELXL-97</i> <sup>d</sup> )
absorption correction method	Gaussian integration (face-indexed)
range of transmission factors	0.8406–0.6483
data/restraints/parameters	1917 / 0 / 149
goodness-of-fit ( <i>S</i> ) <sup>e</sup> [all data]	1.072
final <i>R</i> indices <sup>f</sup>	
<i>R</i> <sub>1</sub> [ $F_o^2 \geq 2\sigma(F_o^2)$ ]	0.0318
<i>wR</i> <sub>2</sub> [all data]	0.0850
largest difference peak and hole	0.297 and -0.428 e Å <sup>-3</sup>

<sup>a</sup>Obtained from least-squares refinement of 9941 reflections with  $4.82^\circ < 2\theta < 54.80^\circ$ .

<sup>b</sup>Programs for diffractometer operation, data collection, data reduction and absorption correction were those supplied by Bruker.

(continued)

**Table 1.** Crystallographic Experimental Details (continued)

<sup>c</sup>Beurskens, P. T.; Beurskens, G.; de Gelder, R.; Smits, J. M. M; Garcia-Granda, S.; Gould, R. O. (2008). The *DIRDIF-2008* program system. Crystallography Laboratory, Radboud University Nijmegen, The Netherlands.

<sup>d</sup>Sheldrick, G. M. *Acta Crystallogr.* **2008**, *A64*, 112–122.

<sup>e</sup> $S = [\Sigma w(F_o^2 - F_c^2)^2 / (n - p)]^{1/2}$  ( $n$  = number of data;  $p$  = number of parameters varied;  $w = [\sigma^2(F_o^2) + (0.0431P)^2 + 0.4924P]^{-1}$  where  $P = [\text{Max}(F_o^2, 0) + 2F_c^2]/3$ ).

<sup>f</sup> $R_1 = \Sigma ||F_o| - |F_c|| / \Sigma |F_o|$ ;  $wR_2 = [\Sigma w(F_o^2 - F_c^2)^2 / \Sigma w(F_o^4)]^{1/2}$ .

**Table 2.** Atomic Coordinates and Equivalent Isotropic Displacement Parameters*(a) atoms of the  $[(\eta^5-1-t\text{-butyl-3-methylcyclopentadienyl})\text{CoCp}]^+$  ion*

Atom	<i>x</i>	<i>y</i>	<i>z</i>	$U_{\text{eq}}, \text{\AA}^2$
Co	0.171787(15)	0.2500	0.06541(3)	0.04696(13)*
C1 <sup>a</sup>	0.07029(14)	0.2682(14)	0.1811(3)	0.039(2)*
C2 <sup>a</sup>	0.0691(3)	0.1589(5)	0.0804(5)	0.0459(9)*
C3 <sup>a</sup>	0.0764(2)	0.2188(4)	-0.0542(4)	0.0458(13)*
C4 <sup>a</sup>	0.0829(2)	0.3630(5)	-0.0367(4)	0.0507(8)*
C5 <sup>a</sup>	0.0793(3)	0.3946(5)	0.1078(6)	0.0466(10)*
C6	0.05778(12)	0.2500	0.3369(2)	0.0493(5)*
C7	-0.03248(16)	0.2500	0.3584(3)	0.0769(8)*
C8	0.09369(13)	0.1206(2)	0.4034(2)	0.0725(5)*
C9 <sup>a</sup>	0.0775(2)	0.1422(5)	-0.1893(4)	0.0674(10)*
C10	0.26758(13)	0.2500	0.1907(3)	0.0725(8)*
C11	0.26793(11)	0.1318(2)	0.1052(2)	0.0694(5)*
C12	0.26951(10)	0.1781(2)	-0.0325(2)	0.0599(4)*

*(b) tetrafluoroborate ion atoms*

Atom	<i>x</i>	<i>y</i>	<i>z</i>	$U_{\text{eq}}, \text{\AA}^2$
F1 <sup>a</sup>	0.38304(16)	0.270(3)	0.6722(3)	0.134(5)*
F2 <sup>a</sup>	0.25868(18)	0.2329(18)	0.6318(3)	0.144(3)*
F3 <sup>a</sup>	0.3540(5)	0.1436(7)	0.4885(7)	0.144(3)*
F4 <sup>a</sup>	0.3191(4)	0.3652(5)	0.4854(7)	0.105(2)*
B	0.3298(3)	0.2500	0.5708(4)	0.0731(10)*

Anisotropically-refined atoms are marked with an asterisk (\*). The form of the anisotropic displacement parameter is:  $\exp[-2\pi^2(h^2a^{*2}U_{11} + k^2b^{*2}U_{22} + l^2c^{*2}U_{33} + 2klb^*c^*U_{23} + 2hla^*c^*U_{13} + 2hka^*b^*U_{12})]$ . <sup>a</sup>Refined with an occupancy factor of 0.5.

**Table 3.** Selected Interatomic Distances (Å)*(a) within the  $[(\eta^5-1-t\text{-butyl-3-methylcyclopentadienyl})\text{CoCp}]^+$  ion*

Atom1	Atom2	Distance	Atom1	Atom2	Distance
Co	C1	2.054(3)	C1	C6	1.527(4)
Co	C2	1.950(5)	C2	C3	1.426(6)
Co	C3	2.005(3)	C3	C4	1.401(7)
Co	C4	2.100(3)	C3	C9	1.497(5)
Co	C5	2.133(5)	C4	C5	1.428(6)
Co	C10	2.021(2)	C6	C7	1.540(3)
Co	C11	2.0202(18)	C6	C8	1.526(2)
Co	C11'	2.0202(18)	C6	C8'	1.526(2)
Co	C12	2.0247(17)	C10	C11	1.404(3)
Co	C12'	2.0247(17)	C10	C11'	1.404(3)
C1	C2	1.431(11)	C11	C12	1.400(3)
C1	C5	1.415(11)	C12	C12'	1.384(4)

Primed atoms are related to unprimed ones via the crystallographic mirror plane ( $x, 1/4, z$ ).

*(b) within the tetrafluoroborate ion*

Atom1	Atom2	Distance	Atom1	Atom2	Distance
F1	B	1.343(6)	F3	B	1.357(7)
F2	B	1.349(5)	F4	B	1.392(6)

**Table 4.** Selected Interatomic Angles (deg)*(a) within the  $[(\eta^5-1-t\text{-butyl-3-methylcyclopentadienyl})\text{CoCp}]^+$  ion*

Atom1	Atom2	Atom3	Angle	Atom1	Atom2	Atom3	Angle
C1	Co	C2	41.8(3)	C11	Co	C11'	68.46(12)
C1	Co	C3	69.71(15)	C11	Co	C12	40.49(8)
C1	Co	C4	67.2(2)	C11	Co	C12'	67.91(8)
C1	Co	C5	39.4(3)	C11'	Co	C12	67.91(8)
C1	Co	C10	110.17(11)	C11'	Co	C12'	40.49(8)
C1	Co	C11	128.1(2)	C12	Co	C12'	39.96(11)
C1	Co	C11'	121.4(3)	Co	C1	C2	65.2(3)
C1	Co	C12	164.6(4)	Co	C1	C5	73.3(3)
C1	Co	C12'	154.9(4)	Co	C1	C6	129.8(2)
C2	Co	C3	42.22(17)	C2	C1	C5	107.1(4)
C2	Co	C4	68.29(17)	C2	C1	C6	125.6(9)
C2	Co	C5	68.0(2)	C5	C1	C6	127.2(8)
C2	Co	C10	132.01(16)	Co	C2	C1	73.0(3)
C2	Co	C11	116.71(15)	Co	C2	C3	71.0(2)
C2	Co	C11'	162.77(17)	C1	C2	C3	108.6(5)
C2	Co	C12	127.41(16)	Co	C3	C2	66.8(2)
C2	Co	C12'	156.16(17)	Co	C3	C4	73.8(2)
C3	Co	C4	39.82(19)	Co	C3	C9	124.4(3)
C3	Co	C5	67.54(17)	C2	C3	C4	107.3(4)
C3	Co	C10	171.33(10)	C2	C3	C9	126.5(4)
C3	Co	C11	132.24(12)	C4	C3	C9	126.2(4)
C3	Co	C11'	147.19(12)	Co	C4	C3	66.4(2)
C3	Co	C12	109.71(12)	Co	C4	C5	71.5(2)
C3	Co	C12'	116.07(12)	C3	C4	C5	108.9(4)
C4	Co	C5	39.43(18)	Co	C5	C1	67.3(3)
C4	Co	C10	148.66(13)	Co	C5	C4	69.1(2)
C4	Co	C11	162.95(13)	C1	C5	C4	108.0(4)
C4	Co	C11'	111.96(14)	C1	C6	C7	105.7(2)
C4	Co	C12	122.85(13)	C1	C6	C8	116.8(4)
C4	Co	C12'	100.88(12)	C1	C6	C8'	105.4(4)
C5	Co	C10	118.24(15)	C7	C6	C8	109.74(14)
C5	Co	C11	157.02(16)	C7	C6	C8'	109.74(14)
C5	Co	C11'	100.78(15)	C8	C6	C8'	109.3(2)
C5	Co	C12	155.62(15)	Co	C10	C11	69.65(12)
C5	Co	C12'	117.72(14)	Co	C10	C11'	69.65(12)
C10	Co	C11	40.67(7)	C11	C10	C11'	108.1(2)
C10	Co	C11'	40.67(7)	Co	C11	C10	69.69(12)
C10	Co	C12	67.94(9)	Co	C11	C12	69.93(10)
C10	Co	C12'	67.94(9)	C10	C11	C12	107.46(18)

**Table 4.** Selected Interatomic Angles (continued)

Atom1	Atom2	Atom3	Angle	Atom1	Atom2	Atom3	Angle
Co	C12	C11	69.58(10)	C11	C12	C12'	108.52(12)
Co	C12	C12'	70.02(6)				

Primed atoms are related to unprimed ones via the crystallographic mirror plane ( $x, 1/4, z$ ).

*(b) within the tetrafluoroborate ion*

Atom1	Atom2	Atom3	Angle	Atom1	Atom2	Atom3	Angle
F1	B	F2	107.3(3)	F2	B	F3	115.5(8)
F1	B	F3	109.5(9)	F2	B	F4	103.8(7)
F1	B	F4	113.6(10)	F3	B	F4	107.0(3)

**Table 5.** Torsional Angles (deg)

Atom1	Atom2	Atom3	Atom4	Angle	Atom1	Atom2	Atom3	Atom4	Angle
C2	Co	C1	C5	-118.5(4)	C12'	Co	C2	C3	-28.9(5)
C2	Co	C1	C6	116.7(12)	C1	Co	C3	C2	-39.1(4)
C3	Co	C1	C2	39.5(3)	C1	Co	C3	C4	78.4(4)
C3	Co	C1	C5	-78.9(3)	C1	Co	C3	C9	-158.5(5)
C3	Co	C1	C6	156.2(10)	C2	Co	C3	C4	117.5(4)
C4	Co	C1	C2	82.4(3)	C2	Co	C3	C9	-119.4(4)
C4	Co	C1	C5	-36.1(3)	C4	Co	C3	C2	-117.5(4)
C4	Co	C1	C6	-160.9(11)	C4	Co	C3	C9	123.1(5)
C5	Co	C1	C2	118.5(4)	C5	Co	C3	C2	-81.6(2)
C5	Co	C1	C6	-124.8(11)	C5	Co	C3	C4	36.0(3)
C10	Co	C1	C2	-131.2(3)	C5	Co	C3	C9	159.1(4)
C10	Co	C1	C5	110.3(2)	C10	Co	C3	C2	51.7(9)
C10	Co	C1	C6	-14.5(10)	C10	Co	C3	C4	169.2(7)
C11	Co	C1	C2	-88.8(3)	C10	Co	C3	C9	-67.7(9)
C11	Co	C1	C5	152.7(2)	C11	Co	C3	C2	84.4(3)
C11	Co	C1	C6	27.8(11)	C11	Co	C3	C4	-158.0(2)
C11'	Co	C1	C2	-175.0(3)	C11	Co	C3	C9	-34.9(4)
C11'	Co	C1	C5	66.6(3)	C11'	Co	C3	C2	-156.0(3)
C11'	Co	C1	C6	-58.3(11)	C11'	Co	C3	C4	-38.5(4)
C12	Co	C1	C2	-51.2(5)	C11'	Co	C3	C9	84.6(4)
C12	Co	C1	C5	-169.6(3)	C12	Co	C3	C2	124.4(2)
C12	Co	C1	C6	65.5(12)	C12	Co	C3	C4	-118.0(2)
C12'	Co	C1	C2	147.9(3)	C12	Co	C3	C9	5.1(4)
C12'	Co	C1	C5	29.4(4)	C12'	Co	C3	C2	167.5(2)
C12'	Co	C1	C6	-95.4(10)	C12'	Co	C3	C4	-75.0(3)
C1	Co	C2	C3	117.3(5)	C12'	Co	C3	C9	48.1(3)
C3	Co	C2	C1	-117.3(5)	C1	Co	C4	C3	-85.2(4)
C4	Co	C2	C1	-79.6(4)	C1	Co	C4	C5	36.1(4)
C4	Co	C2	C3	37.7(2)	C2	Co	C4	C3	-39.9(3)
C5	Co	C2	C1	-37.0(4)	C2	Co	C4	C5	81.4(3)
C5	Co	C2	C3	80.3(2)	C3	Co	C4	C5	121.3(4)
C10	Co	C2	C1	71.8(4)	C5	Co	C4	C3	-121.3(4)
C10	Co	C2	C3	-170.84(16)	C10	Co	C4	C3	-176.9(2)
C11	Co	C2	C1	118.3(4)	C10	Co	C4	C5	-55.6(4)
C11	Co	C2	C3	-124.4(2)	C11	Co	C4	C3	70.7(5)
C11'	Co	C2	C1	14.7(7)	C11	Co	C4	C5	-168.0(4)
C11'	Co	C2	C3	132.0(4)	C11'	Co	C4	C3	158.7(2)
C12	Co	C2	C1	164.9(4)	C11'	Co	C4	C5	-80.0(3)
C12	Co	C2	C3	-77.8(2)	C12	Co	C4	C3	81.5(3)
C12'	Co	C2	C1	-146.2(4)	C12	Co	C4	C5	-157.2(2)

**Table 5.** Torsional Angles (continued)

Atom1	Atom2	Atom3	Atom4	Angle	Atom1	Atom2	Atom3	Atom4	Angle
C12'	Co	C4	C3	117.9(2)	C4	Co	C11	C10	132.4(4)
C12'	Co	C4	C5	-120.8(2)	C4	Co	C11	C12	14.0(5)
C1	Co	C5	C4	-121.3(4)	C5	Co	C11	C10	-27.8(4)
C2	Co	C5	C1	39.2(3)	C5	Co	C11	C12	-146.2(3)
C2	Co	C5	C4	-82.1(3)	C10	Co	C11	C12	-118.41(18)
C3	Co	C5	C1	84.9(3)	C11'	Co	C11	C10	37.64(14)
C3	Co	C5	C4	-36.3(3)	C11'	Co	C11	C12	-80.77(13)
C4	Co	C5	C1	121.3(4)	C12	Co	C11	C10	118.41(18)
C10	Co	C5	C1	-87.9(3)	C12'	Co	C11	C10	81.40(14)
C10	Co	C5	C4	150.8(2)	C12'	Co	C11	C12	-37.01(12)
C11	Co	C5	C1	-67.7(4)	C1	Co	C12	C11	-47.8(5)
C11	Co	C5	C4	171.0(3)	C1	Co	C12	C12'	-167.6(5)
C11'	Co	C5	C1	-127.2(3)	C2	Co	C12	C11	-88.6(2)
C11'	Co	C5	C4	111.6(2)	C2	Co	C12	C12'	151.66(19)
C12	Co	C5	C1	173.3(3)	C3	Co	C12	C11	-132.86(15)
C12	Co	C5	C4	52.1(5)	C3	Co	C12	C12'	107.41(12)
C12'	Co	C5	C1	-166.4(3)	C4	Co	C12	C11	-175.14(18)
C12'	Co	C5	C4	72.3(3)	C4	Co	C12	C12'	65.13(15)
C1	Co	C10	C11	125.5(4)	C5	Co	C12	C11	148.3(3)
C1	Co	C10	C11'	-115.1(4)	C5	Co	C12	C12'	28.5(3)
C2	Co	C10	C11	83.1(3)	C10	Co	C12	C11	38.20(11)
C2	Co	C10	C11'	-157.5(2)	C10	Co	C12	C12'	-81.53(4)
C3	Co	C10	C11	37.9(9)	C11	Co	C12	C12'	-119.73(11)
C3	Co	C10	C11'	157.3(8)	C11'	Co	C12	C11	82.25(18)
C4	Co	C10	C11	-155.4(2)	C11'	Co	C12	C12'	-37.48(8)
C4	Co	C10	C11'	-36.1(3)	C12'	Co	C12	C11	119.73(11)
C5	Co	C10	C11	168.08(18)	Co	C1	C2	C3	-62.4(3)
C5	Co	C10	C11'	-72.6(2)	C5	C1	C2	Co	61.7(2)
C11	Co	C10	C11'	119.3(2)	C5	C1	C2	C3	-0.7(4)
C11'	Co	C10	C11	-119.3(2)	C6	C1	C2	Co	-122.5(3)
C12	Co	C10	C11	-38.04(12)	C6	C1	C2	C3	175.1(3)
C12	Co	C10	C11'	81.31(14)	Co	C1	C5	C4	57.1(3)
C12'	Co	C10	C11	-81.31(14)	C2	C1	C5	Co	-56.6(3)
C12'	Co	C10	C11'	38.04(12)	C2	C1	C5	C4	0.5(4)
C1	Co	C11	C10	-76.1(4)	C6	C1	C5	Co	127.7(3)
C1	Co	C11	C12	165.5(4)	C6	C1	C5	C4	-175.2(3)
C2	Co	C11	C10	-124.3(2)	Co	C1	C6	C7	-169.9(7)
C2	Co	C11	C12	117.3(2)	Co	C1	C6	C8	-47.5(10)
C3	Co	C11	C10	-172.81(17)	Co	C1	C6	C8'	74.0(9)
C3	Co	C11	C12	68.78(19)	C2	C1	C6	C7	-84.2(4)

**Table 5.** Torsional Angles (continued)

Atom1	Atom2	Atom3	Atom4	Angle	Atom1	Atom2	Atom3	Atom4	Angle
C2	C1	C6	C8	38.2(4)	C2	C3	C4	C5	-0.3(5)
C2	C1	C6	C8'	159.7(3)	C9	C3	C4	Co	-121.0(4)
C5	C1	C6	C7	90.8(3)	C9	C3	C4	C5	-180.0(4)
C5	C1	C6	C8	-146.9(4)	Co	C4	C5	C1	-56.0(3)
C5	C1	C6	C8'	-25.4(4)	C3	C4	C5	Co	55.9(3)
Co	C2	C3	C4	-63.1(3)	C3	C4	C5	C1	-0.1(5)
Co	C2	C3	C9	116.6(4)	Co	C10	C11	C12	60.00(13)
C1	C2	C3	Co	63.7(3)	C11'	C10	C11	Co	-59.26(17)
C1	C2	C3	C4	0.6(5)	C11'	C10	C11	C12	0.7(3)
C1	C2	C3	C9	-179.7(3)	Co	C11	C12	C12'	59.39(6)
Co	C3	C4	C5	-59.0(3)	C10	C11	C12	Co	-59.84(14)
C2	C3	C4	Co	58.6(3)	C10	C11	C12	C12'	-0.46(17)

Primed atoms are related to unprimed ones via the crystallographic mirror plane ( $x, 1/4, z$ ).

**Table 6.** Least-Squares Planes

Plane	Coefficients <sup>a</sup>			Defining Atoms with Deviations (Å) <sup>b</sup>			
1	16.816(5)	-0.80(2)	0.602(14)	1.079(8)			
				C1	-0.0035(19)	C2	0.004(2)
				C3	-0.003(3)	C4	0.001(3)
				C5	0.002(2)		
				<u>C</u> <sub>o</sub>	1.6482(14)	<u>C</u> <sub>6</sub>	-0.106(5)
				<u>C</u> <sub>9</sub>	-0.005(7)		
2	16.906(3)	-0.0000(0)	0.159(12)	4.5500(16)			
				C10	0.0043(16)	C11	-0.0034(13)
				C12	0.0013(5)	C11'	-0.0034(13)
				C12'	0.0013(5)		
				<u>C</u> <sub>o</sub>	-1.6353(12)		

Dihedral angle between planes 1 and 2: 5.48(4)°

<sup>a</sup>Coefficients are for the form  $ax+by+cz = d$  where  $x$ ,  $y$  and  $z$  are crystallographic coordinates.

<sup>b</sup>Primed atoms are related to unprimed ones via the crystallographic mirror plane ( $x, 1/4, z$ ).

Underlined atoms were not included in the definition of the plane.

**Table 7.** Anisotropic Displacement Parameters ( $U_{ij}$ , Å<sup>2</sup>)

Atom	$U_{11}$	$U_{22}$	$U_{33}$	$U_{23}$	$U_{13}$	$U_{12}$
Co	0.02947(17)	0.0686(2)	0.04281(19)	0.000	0.00098(10)	0.000
C1	0.0278(9)	0.040(7)	0.0501(12)	-0.0063(18)	0.0009(8)	-0.0001(12)
C2	0.0353(18)	0.047(3)	0.055(3)	0.000(2)	0.0016(15)	-0.0100(18)
C3	0.0380(14)	0.055(4)	0.0449(14)	0.0004(15)	-0.0048(10)	-0.0082(14)
C4	0.0435(17)	0.057(2)	0.052(2)	0.0095(18)	-0.0042(13)	0.0062(17)
C5	0.0392(19)	0.045(2)	0.055(2)	0.0037(19)	0.0018(16)	0.0085(18)
C6	0.0398(11)	0.0607(13)	0.0475(11)	0.000	0.0062(9)	0.000
C7	0.0454(13)	0.117(2)	0.0689(17)	0.000	0.0188(12)	0.000
C8	0.0722(12)	0.0760(12)	0.0694(11)	0.0204(10)	0.0032(10)	-0.0008(10)
C9	0.064(2)	0.088(3)	0.0499(18)	-0.0120(18)	-0.0028(15)	-0.0208(19)
C10	0.0290(10)	0.135(3)	0.0532(13)	0.000	-0.0034(10)	0.000
C11	0.0459(9)	0.0691(11)	0.0931(14)	0.0199(11)	0.0002(9)	0.0091(8)
C12	0.0427(8)	0.0697(10)	0.0674(10)	-0.0115(9)	0.0091(7)	0.0047(8)
F1	0.0850(16)	0.230(13)	0.0881(15)	0.041(6)	-0.0220(13)	-0.027(5)
F2	0.0893(17)	0.229(8)	0.114(2)	-0.060(6)	-0.0121(16)	-0.027(5)
F3	0.234(9)	0.100(4)	0.098(4)	-0.017(3)	0.043(5)	0.049(4)
F4	0.175(5)	0.0417(15)	0.099(3)	-0.0087(16)	-0.057(3)	0.004(2)
B	0.099(3)	0.0616(18)	0.0587(18)	0.000	-0.0028(16)	0.000

The form of the anisotropic displacement parameter is:

$$\exp[-2\pi^2(h^2a^2U_{11} + k^2b^2U_{22} + l^2c^2U_{33} + 2klb^*c^*U_{23} + 2hla^*c^*U_{13} + 2hka^*b^*U_{12})]$$

**Table 8.** Derived Atomic Coordinates and Displacement Parameters for Hydrogen Atoms

Atom	<i>x</i>	<i>y</i>	<i>z</i>	$U_{\text{eq}}, \text{\AA}^2$
H2 <sup>a</sup>	0.0643	0.0624	0.1000	0.055
H4 <sup>a</sup>	0.0887	0.4291	-0.1093	0.061
H5 <sup>a</sup>	0.0824	0.4848	0.1478	0.056
H7A	-0.0443	0.2500	0.4579	0.092
H7B <sup>a</sup>	-0.0553	0.1668	0.3155	0.092
H7C <sup>a</sup>	-0.0553	0.3332	0.3155	0.092
H8A	0.0840	0.1223	0.5035	0.087
H8B	0.1508	0.1190	0.3861	0.087
H8C	0.0694	0.0373	0.3632	0.087
H9A <sup>a</sup>	0.0237	0.1378	-0.2271	0.081
H9B <sup>a</sup>	0.0974	0.0476	-0.1744	0.081
H9C <sup>a</sup>	0.1120	0.1909	-0.2549	0.081
H10	0.2672	0.2500	0.2892	0.087
H11	0.2672	0.0377	0.1352	0.083
H12	0.2704	0.1203	-0.1124	0.072

<sup>a</sup>Included with an occupancy factor of 0.5.

## References

- (1) Samojłowicz, C.; Bieniek, M.; Grela, K. *Chem. Rev.* **2009**, *109*, 3708–3742.
- (2) Li, H.; Johansson Seechurn, C. C. C.; Colacot, T. J. *ACS Catal.* **2012**, *2*, 1147–1164.
- (3) Camacho-Bunquin, J.; Ferguson, M. J.; Stryker, J. M. *J. Am. Chem. Soc.* **2013**, *135*, 5537–5540.
- (4) Camacho-Bunquin, J.; Stryker, J. M. *Unpubl. results* **2013**.
- (5) Choudhary, T. V.; Phillips, C. B. *Appl. Catal., A* **2011**, *397*, 1–12.
- (6) Leung, D. Y. C.; Wu, X.; Leung, M. K. H. *Appl. Energy* **2010**, *87*, 1083–1095.
- (7) Lasekan, O.; Abbas, K. A. *Crit. Rev. Food Sci. Nutr.* **2012**, *52*, 726–735.
- (8) Ravindranath, K.; Mashelkar, R. A. *Chem. Eng. Sci.* **1986**, *41*, 2197–2214.
- (9) Brown, H. C.; Krishnamurthy, S. *Tetrahedron* **1979**, *35*, 567–607.
- (10) Nystrom, R. F.; Chaikin, S. W.; Brown, W. G. *J. Am. Chem. Soc.* **1949**, *71*, 3245–3246.
- (11) Spindler, F.; Blaser, H. In *Top Organomet Chem*; 2012; pp. 65–102.
- (12) Periasamy, M.; Thirumalaikumar, M. *J. Organomet. Chem.* **2000**, *609*, 137–151.
- (13) Cheng, C.; Brookhart, M. *Angew. Chem. Int. Ed.* **2012**, *51*, 9422–9424.
- (14) Mäki-Arvela, P.; Hájek, J.; Salmi, T.; Murzin, D. Y. *Appl. Catal., A* **2005**, *292*, 1–49.
- (15) Pez, G. P.; Grey, R. A.; Corsi, J. *J. Am. Chem. Soc.* **1981**, *103*, 7528–7535.
- (16) Grey, R. A.; Pez, G. P.; Wallo, A. *J. Am. Chem. Soc.* **1981**, *103*, 7536–7542.
- (17) Matteoli, U.; Bianchi, M.; Menchi, G.; Prediani, P.; Piacenti, F. *J. Mol. Catal.* **1984**, *22*, 353–362.
- (18) Matteoli, U.; Menchi, G.; Bianchi, M.; Piacenti, F. *J. Organomet. Chem.* **1986**, *299*, 233–238.
- (19) Nomura, K.; Ogura, H.; Imanishi, Y. *J. Mol. Catal. A Chem.* **2002**, *178*, 105–114.
- (20) T. Teunissen, H.; J. Elsevier, C. *Chem. Commun.* **1997**, 667–668.
- (21) Zhang, J.; Leitius, G.; Ben-David, Y.; Milstein, D. *Angew. Chem. Int. Ed.* **2006**, *45*, 1113–1115.
- (22) Saudan, L. A.; Saudan, C. M.; Debieux, C.; Wyss, P. *Angew. Chem. Int. Ed.* **2007**, *46*, 7473–7476.
- (23) Takebayashi, S.; Bergens, S. H. *Organometallics* **2009**, *28*, 2289–2291.
- (24) Wylie, W. N. O.; Morris, R. H. *ACS Catal.* **2013**, *3*, 32–40.
- (25) Spasyuk, D.; Smith, S.; Gusev, D. G. *Angew. Chem. Int. Ed.* **2012**, *51*, 2772–5.
- (26) Pouilloux, Y.; Autin, F.; Piccirilli, A.; Guimon, C.; Barrault, J. *Appl. Catal., A* **1998**, *169*, 65–75.
- (27) Sánchez, M. A.; Mazzieri, V. A.; Sad, M. R.; Pieck, C. L. *Reac. Kinet. Mech. Cat.* **2012**, *107*, 127–139.
- (28) Egan, R. R.; Earl, G. W.; Ackerman, J.; Chemical, S. *J. Am. Oil Chem. Soc.* **1984**, *61*, 324–329.
- (29) Bodnar, B. S.; Vogt, P. F. *J. Org. Chem.* **2009**, *74*, 2598–600.

- (30) Kreutzer, U. R. *J. Am. Oil Chem. Soc.* **1984**, *61*, 343–348.
- (31) Rieke, R. D.; Thakur, D. S.; Roberts, B. D.; White, G. T. *J. Am. Oil Chem. Soc.* **1997**, *74*, 333–339.
- (32) Narasimhan, C. S.; Deshpande, V. M.; Ramnaryan, K. *Appl. Catal.* **1989**, *48*, L1–L6.
- (33) Sauer, J.; Adkins, H. *J. Am. Chem. Soc.* **1937**, *59*, 1–3.
- (34) Narasimhan, C. S.; Deshpande, V. M.; Ramnarayan, K. *Ind. Eng. Chem. Res.* **1989**, *28*, 1110–1112.
- (35) Knothe, G. *Top. Catal.* **2010**, *53*, 714–720.
- (36) Atabani, A. E.; Silitonga, A. S.; Badruddin, I. A.; Mahlia, T. M. I.; Masjuki, H. H.; Mekhilef, S. *Renew. Sustain. Energy Rev.* **2012**, *16*, 2070–2093.
- (37) Şenol, O.; Viljava, T.-R.; Krause, A. O. I. *Catal. Today* **2005**, *100*, 331–335.
- (38) Kubička, D.; Kaluža, L. *Appl. Catal., A* **2010**, *372*, 199–208.
- (39) Şenol, O. İ.; Viljava, T. R.; Krause, A. O. I. *Catal. Today* **2005**, *106*, 186–189.
- (40) Dundich, V. O.; Khromova, S. A.; Ermakov, D. Y.; Lebedev, M. Y.; Novopashina, V. M.; Sister, V. G.; Yakimchuk, A. I.; Yakovlev, V. A. *Kinet. Catal.* **2010**, *51*, 704–709.
- (41) Snåre, M.; Kubickova, I.; Maki-Arvela, P.; Eranen, K.; Murzin, D. Y. *Ind. Eng. Chem. Res.* **2006**, *45*, 5708–5715.
- (42) Nimmanwudipong, T.; Aydın, C.; Lu, J.; Runnebaum, R. C.; Brodwater, K. C.; Browning, N. D.; Block, D. E.; Gates, B. C. *Catal. Lett.* **2012**, *142*, 1190–1196.
- (43) Donniss, B.; Egeberg, R. G.; Blom, P.; Knudsen, K. G. *Top. Catal.* **2009**, *52*, 229–240.
- (44) Santillan-Jimenez, E.; Crocker, M. J. *Chem. Technol. Biotechnol.* **2012**, *87*, 1041–1050.
- (45) Kubičková, I.; Snåre, M.; Eränen, K.; Mäki-Arvela, P.; Murzin, D. Y. *Catal. Today* **2005**, *106*, 197–200.
- (46) Smith, M. B.; March, J. *March's Advanced Organic Chemistry: Reactions, Mechanisms, and Structure, 5th Edition*; Wiley-Interscience, 2001; p. 569.
- (47) Perosa, A.; Tundo, P.; Zinovyev, S. *Green Chem.* **2002**, *4*, 492–494.
- (48) Werner, T.; Koch, J. *Eur. J. Org. Chem.* **2010**, 6904–6907.
- (49) Houston, B. Houston Thesis, University of Alberta, 2013.
- (50) Pregel, M. J.; Dunn, E. J.; Nagelkerke, R.; Thatcher, G. R. J.; Buncl, E. *Chem. Soc. Rev.* **1995**, *24*, 449–455.
- (51) Wang, B.; Sun, H.-X.; Sun, Z.-H.; Lin, G.-Q. *Adv. Synth. Catal.* **2009**, *351*, 415–422.
- (52) Anslyn, E. V.; Dougherty, D. A. *Modern Physical Organic Chemistry*; University Science, 2005; p. 1095.
- (53) Pawar, D. M.; Khalil, A. A.; Hooks, D. R.; Collins, K.; Elliott, T.; Stafford, J.; Smith, L.; Noe, E. A. **1998**, 7863, 2108–2112.
- (54) Rickborn, B. *Org. React. (Hoboken, NJ, United States)* **1998**, *53*, No pp. given.
- (55) Kamiguchi, S.; Mori, T.; Watanabe, M.; Suzuki, A.; Kodomari, M.; Nomura, M.; Iwasawa, Y.; Chihara, T. *J. Mol. Catal. A Chem.* **2006**, *253*, 176–186.
- (56) Peter, G. In *Oxidation of Organic Compounds*; American Chemical Society, 1968; Vol. 75, pp. 282–287.
- (57) Khoo, L. E.; Lee, H. H. *Tetrahedron Lett.* **1968**, *41*, 4351–4354.

- (58) Ishizu T.; Yamamoto, A.; Yamamoto, A. *Chem. Lett.* **1976**, 1091–1094.
- (59) Yamamoto, T.; Ishizu, J.; Kohara, T.; Komiya, S.; Yamamoto, A. *J. Am. Chem. Soc.* **1980**, *102*, 3758–3764.
- (60) Bing-Tao Guan Bi-Jie Li, Da-Gang Yu, Zhang-Jie Shi, Y. W. *J. Am. Chem. Soc.* **2008**, *130*, 14468.
- (61) Li S.-L.; Fu, Y.; Guo, Q.-X.; Liu, L., Z. *J. Am. Chem. Soc.* **2009**, *131*, 8815–8823.
- (62) Trost, B. M.; Murphy, D. J. *Organometallics* **1985**, *4*, 1143–1145.
- (63) Ittel, S. D.; Tolman, C. A.; English, A. D.; Jesson, J. P. *J. Am. Chem. Soc.* **1978**, *100*, 7577.
- (64) Pettit, G. R.; Piatak, D. M. *J. Org. Chem.* **1962**, *27*, 2127–2130.
- (65) Tsurugi, J.; Ren, N.; Tsugio Fukumoto *J. Am. Chem. Soc.* **1969**, *91*, 4587–4588.
- (66) Yato, M.; Homma, K.; Ishida, A. *Tetrahedron* **2001**, *57*, 5353–5359.
- (67) Sakai, N.; Moriya, T.; Fujii, K.; Konakahara, T. *Synthesis (Stuttg.)* **2008**, *21*, 3533–3536.
- (68) Sakai, N.; Moriya, T.; Konakahara, T. *J. Org. Chem.* **2007**, *72*, 5920–5922.
- (69) Matsubara, K.; Iura, T.; Maki, T.; Nagashima, H. *J. Org. Chem.* **2002**, *67*, 4985–8.
- (70) Mao, Z.; Gregg, B. T.; Cutler, A. R. *J. Am. Chem. Soc.* **1995**, *117*, 10139–10140.
- (71) Labet, M.; Thielemans, W. *Chem. Soc. Rev.* **2009**, *38*, 3484–3504.
- (72) Namekawa, S.; Uyama, H.; Kobayashi, S. *Proc. Japan Acad.* **1998**, *74*, 65–68.
- (73) Nicolaou, K. C.; Hwang, C. K.; Marron, B. E.; DeFrees, S. A.; Couladouros, E. A.; Abe, Y.; Carroll, P. J.; Snyder, J. P. *J. Am. Chem. Soc.* **1990**, *112*, 3040–3054.
- (74) Rastetter, W. H.; Phillion, D. P. *J. Org. Chem.* **1981**, *46*, 3209–3214.
- (75) Kurihara, T.; Nakajima, Y.; Mitsunobu, O. *Tetrahedron Lett.* **1976**, 2455–2458.
- (76) Dale, J.; Schwartz, J.-E. *Acta Chem. Scand. B.* **1986**, *B40*, 559–567.
- (77) Tischtschenko, W. *J. Russ. Phys. Chem. Soc.* **1906**, *38*, 482.
- (78) Seki, T.; Nakajo, T.; Onaka, M. *Chem. Lett.* **2006**, *35*, 824–829.
- (79) Crabtree, R. H. *Chem. Rev.* **2012**, *112*, 1536–1554.
- (80) Wong, O. A.; Shi, Y. *Chem. Rev.* **2008**, *108*, 3958–3987.
- (81) Mallat, T.; Baiker, A. *Chem. Rev.* **2004**, *104*, 3037–3058.
- (82) Zhan, B.-Z.; Thompson, A. *Tetrahedron* **2004**, *60*, 2917–2935.
- (83) Tohma, H.; Kita, Y. *Adv. Synth. Catal.* **2004**, *346*, 111–124.
- (84) Li, J. J. *Name Reactions: A Collection of Detailed Mechanisms and Synthetic Applications*; Springer, 2009; p. 643.
- (85) Clayden, J.; Greeves, N.; Warren, S.; Wothers, P. *Organic Chemistry*; Oxford University Press, USA, 2000; p. 638.
- (86) Parmeggiani, C.; Cardona, F. *Green Chem.* **2012**, *14*, 547.
- (87) Emsley, J. *Nature's Building Blocks: An A-Z Guide to the Elements*; Oxford University Press, USA, 2011; p. 592.
- (88) Atkins, P. W.; Paula, J. D. *Atkins' Physical Chemistry*; 6th ed.; Oxford University Press, 2001; p. 1180.
- (89) Cramer, P. L.; Campbell, J. M. *Ind. Eng. Chem.* **1949**, *41*, 893–897.

- (90) Solomons, T. W. G.; Fryhle, C. B. *Organic Chemistry Eighth Edition Solomons & Fryhle Wiley Student Edition*; 8th ed.; Wiley, 2004; pp. 498–499.
- (91) Mahajan, S. S.; Sharma, M. M.; Sridhar, T. *Ind. Eng. Chem. Res.* **2007**, *46*, 3057–3062.
- (92) Mahajan, S. S.; Sharma, M. M.; Sridhar, T. *Ind. Eng. Chem. Res.* **2004**, *43*, 3289–3296.
- (93) Singh, R.; Ishar, M. P. S.; Girdhar, N. K.; Velmurugan, D.; Pandi, A. S. *Eur. J. Org. Chem.* **2002**, 3734–3739.
- (94) Shi, Z.; Zhang, C.; Tang, C.; Jiao, N. *Chem. Soc. Rev.* **2012**, *41*, 3381–3430.
- (95) Gowrisankar, S.; Neumann, H.; Beller, M. *Angew. Chem. Int. Ed.* **2011**, *50*, 5139–5143.
- (96) Wang, Y.; Zhu, D.; Tang, L.; Wang, S.; Wang, Z. *Angew. Chem. Int. Ed.* **2011**, *50*, 8917–8921.
- (97) Zhu, J.; Liu, J.; Ma, R.; Xie, H.; Li, J.; Jiang, H.; Wang, W. *Adv. Synth. Catal.* **2009**, *351*, 1229–1232.
- (98) Cahiez, G.; Moyeux, A.; Buendia, J.; Duplais, C. *J. Am. Chem. Soc.* **2007**, *129*, 13788–13789.
- (99) Zhang, S.-Y.; Zhang, F.-M.; Tu, Y.-Q. *Chem. Soc. Rev.* **2011**, *40*, 1937–1949.
- (100) Song, G.; Wang, F.; Li, X. *Chem. Soc. Rev.* **2012**, *41*, 3651–3678.
- (101) Lucas, H. R.; Li, L.; Sarjeant, A. A. N.; Vance, M. A.; Solomon, E. I.; Karlin, K. D. *J. Am. Chem. Soc.* **2009**, *131*, 3230–3245.
- (102) Zhang, C.; Jiao, N. **2010**, *2*, 28–29.
- (103) Gajan, D.; Guillois, K.; Delichère, P.; Basset, J.-M.; Candy, J.-P.; Caps, V.; Copéret, C.; Lesage, A.; Emsley, L. *J. Am. Chem. Soc.* **2009**, *131*, 14667–14669.
- (104) Wang, H.; Wang, Y.; Liang, D.; Liu, L.; Zhang, J.; Zhu, Q. *Angew. Chem. Int. Ed.* **2011**, *50*, 5678–5681.
- (105) Jensen, K. H.; Pathak, T. P.; Zhang, Y.; Sigman, M. S. *J. Am. Chem. Soc.* **2009**, *131*, 17074–17075.
- (106) Pathak, T. P.; Gligorich, K. M.; Welm, B. E.; Sigman, M. S. *J. Am. Chem. Soc.* **2010**, *132*, 7870–7871.
- (107) Chiba, S.; Zhang, L.; Lee, J.-Y. *J. Am. Chem. Soc.* **2010**, *132*, 7266–7267.
- (108) Morrison, R. T.; Boyd, R. N. *Organic Chemistry, 6th Edition*; Prentice Hall, 1992; p. 1360.
- (109) Froment, G. F. *Chem. Eng. Sci.* **1981**, *36*, 1271–1282.
- (110) Mulhaupt, R. *Macromol. Chem. Phys.* **2003**, *204*, 289–327.
- (111) Mondal, P.; Dang, G. S.; Garg, M. O. *Fuel Process. Technol.* **2011**, *92*, 1395–1410.
- (112) Crabtree, R. H. *Chem. Rev.* **1995**, *95*, 987–1007.
- (113) Shilov, A. E.; Shul'pin, G. B. *Chem. Rev.* **1997**, *97*, 2879–2932.
- (114) Levedahl, W. J.; Howard, F. L. *Ind. Eng. Chem.* **1951**, *43*, 2805–2814.
- (115) Raja, R.; Sankar, G.; Thomas, J. M. *Angew. Chem. Int. Ed.* **2000**, *39*, 2313–2316.
- (116) Crabtree, R. H. *J. Organomet. Chem.* **2004**, *689*, 4083–4091.
- (117) Labinger, J. A.; Bercaw, J. E. *Nature* **2002**, *417*, 507–514.
- (118) Gol'dshleger, N. F.; Tyabin, M. B.; Shilov, A. E.; Shteinman, A. A. *Zh. Fiz. Khim.* **1969**, *43*, 2174.

- (119) Gol'dshleger, N. F.; Es'kova, V. V.; Shilov, A. E.; Shteinman, A. A. *Zh. Fiz. Khim. (Engl. Transl.)* **1972**, *46*, 785.
- (120) Zhu, H.; Ziegler, T. *J. Organomet. Chem.* **2006**, *691*, 4486–4497.
- (121) Luinstra, G. a.; Wang, L.; Stahl, S. S.; Labinger, J. a.; Bercaw, J. E. *J. Organomet. Chem.* **1995**, *504*, 75–91.
- (122) Freund, M. S.; Labinger, J. A.; Lewis, N. S.; Bercaw, J. E. *J. Mol. Catal.* **1994**, *87*, L11–L15.
- (123) Geletii, Y. V.; Shilov, A. E. *Kinet. Catal. Engl. Trans.* **1983**, *24*, 413–416.
- (124) Lin, M.; Shen, C.; Garcia-Zayas, E. A.; Sen, A. *J. Am. Chem. Soc.* **2001**, *123*, 1000–1001.
- (125) Arndtsen, B. A.; Bergman, R. G. *Science (80-. )*. **1995**, *270*, 1970–1973.
- (126) Foley, P.; Whitesides, G. M. *J. Am. Chem. Soc.* **1979**, *101*, 2732–2733.
- (127) Crabtree, R. H.; Mihelcic, J. M.; Quirk, J. M. *J. Am. Chem. Soc.* **1979**, *101*, 7738–7740.
- (128) Hoyano, J. K.; Graham, W. A. G. *J. Am. Chem. Soc.* **1982**, *3*, 3123–3125.
- (129) Jaanowicz, A. H.; Bergman, Robert, G. *J. Am. Chem. Soc.* **1982**, *104*, 352–354.
- (130) Gretz, E.; Oliver, T. F.; Sen, A. *J. Am. Chem. Soc.* **1987**, *109*, 8109–8111.
- (131) Kao, L.-C.; Hutson, A. C.; Sen, A. *J. Am. Chem. Soc.* **1991**, *113*, 700–701.
- (132) Periana, Roy, A.; Taube, Douglas, J.; Evitt, Eric, R.; Loffler, Daniel, G.; Wentreck, Paul, R.; Voss, G.; Masuda, T. *Science (80-. )*. **1993**, *259*, 340–343.
- (133) Periana, R. A.; Taube, D. J.; Gamble, S.; Taube, H.; Satoh, T.; Fujii, H. *Science (80-. )*. **1998**, *280*, 560–564.
- (134) Periana, R. A.; Mironov, O.; Taube, D.; Bhalla, G.; Jones, C. J. *Science (80-. )*. **2003**, *301*, 814–818.
- (135) Bordeaux, M.; Galarneau, A.; Drone, J. *Angew. Chem. Int. Ed.* **2012**, *51*, 10712–10723.
- (136) Sono, M.; Roach, M. P.; Coulter, E. D.; Dawson, J. H. *Chem. Rev.* **1996**, *96*, 2841–2888.
- (137) Staijen, I. E.; Hatzimanikatis, V.; Witholt, B. *Eur. J. Biochem.* **1997**, *244*, 462–470.
- (138) Grogan, G. *Curr. Opin. Chem. Biol.* **2011**, *15*, 241–248.
- (139) Barton, D. H. R.; Boivin, J.; Gastiger, M.; Morzycki, J.; Hay-motherwell, R. S.; Motherwell, W. B.; Ozbalik, N.; Schwartzentruber, K. M. *J. Chem. Soc. Perkin Trans. I* **1986**, 947–955.
- (140) Barton, D. H. R.; Gastiger, M. J.; Motherwell, W. B. *J. Chem. Soc., Chem. Commun.* **1983**, 41–43.
- (141) Barton, D. H. R.; Doller, D. *Acc. Chem. Res.* **1992**, *25*, 504–512.
- (142) Hill, C. L. *Wiley: Activation and Functionalization of Alkanes*; 1989; p. 296.
- (143) Che, C.; Lo, V. K.; Zhou, C.; Huang, J. *Chem. Soc. Rev.* **2011**, *40*, 1950–1975.
- (144) Punniyamurthy, T.; Velusamy, S.; Iqbal, J. *Chem. Rev.* **2005**, *105*, 2329–2363.
- (145) Cavani, F.; Trifirò, F. *Appl. Catal., A* **1992**, *88*, 115–135.
- (146) Li, X.; Chen, J.; Wang, X.; Sun, J.; Antonietti, M. *J. Am. Chem. Soc.* **2011**, *133*, 8074–8077.
- (147) Ishii, Y.; Sakaguchi, S.; Iwahama, T. *Adv. Synth. Catal.* **2001**, *343*, 393–427.
- (148) Camacho-Bunquin, J. Bunquin Thesis, University of Alberta, 2013.
- (149) Yu, S.; Han, C.; Stryker, J. M. *Unpubl. results*.

- (150) Riess, J. G.; Blanc, M. *Le Angew. Chem. Int. Ed. Engl.* **1978**, *17*, 621–700.
- (151) Pina, C. Della; Falletta, E.; Rossi, M. *Chem. Soc. Rev.* **2012**, *41*, 350–369.
- (152) McMillen, D. F.; Golden, D. M. *Annu. Rev. Phys. Chem.* **1982**, *33*, 493–532.
- (153) Shaabani, A.; Mirzaei, P.; Naderi, S.; Lee, D. G. *Tetrahedron* **2004**, *60*, 11415–11420.
- (154) Xu, Y.-C.; Lebeau, E.; Gillard, J. W.; Attardo, G. *Tetrahedron Lett.* **1993**, *34*, 3841–3844.
- (155) Eikawa, M.; Sakaguchi, S.; Ishii, Y. *J. Org. Chem.* **1999**, *64*, 4676–4679.
- (156) George, M. W.; Hall, M. B.; Portius, P.; Renz, A. L.; Sun, X.-Z.; Towrie, M.; Yang, X. *Dalt. Trans.* **2011**, *40*, 1751.
- (157) Hirashima, S.; Nobuta, T.; Tada, N.; Itoh, A. *Synlett* **2009**, *2009*, 2017–2019.
- (158) Bjørsvik, H.-R.; Liguori, L.; Vedia Merinero, J. A. *J. Org. Chem.* **2002**, *67*, 7493–500.
- (159) Minisci, F.; Recupero, F.; Fontana, F.; Bjørsvik, H.-R.; Liguori, L. *Synlett* **2002**, *2002*, 0610–0612.
- (160) Saiman, M. I. bin; Brett, G. L.; Tiruvalam, R.; Forde, M. M.; Sharples, K.; Thetford, A.; Jenkins, R. L.; Dimitratos, N.; Lopez-Sanchez, J. A.; Murphy, D. M.; Bethell, D.; Willock, D. J.; Taylor, S. H.; Knight, D. W.; Kiely, C. J.; Hutchings, G. J. *Angew. Chem. Int. Ed.* **2012**, *51*, 5981–5985.
- (161) Halpern, J. *Acc. Chem. Res.* **1982**, *15*, 238–244.
- (162) Ruhland, K. *Eur. J. Org. Chem.* **2012**, *2012*, 2683–2706.
- (163) Murakami, M.; Takahashi, K.; Amii, H.; Ito, Y. *J. Am. Chem. Soc.* **1997**, *119*, 9307–9308.
- (164) Crabtree, R. H.; Dion, R. P.; Gibboni, D. J.; Mccrath, D. V.; Holt, E. M. *J. Am. Chem. Soc.* **1986**, *108*, 7222–7227.
- (165) Gozin, M.; Welsman, Al.; Ben-David, Y.; Milstein, D. *Nature* **1993**, *364*, 699–701.
- (166) Jun, C.-H. *Chem. Soc. Rev.* **2004**, *33*, 610–618.
- (167) Seiser, T.; Cramer, N. *Angew. Chem. Int. Ed.* **2008**, *47*, 9294–9297.
- (168) Dzwiniel, T. L.; Etkin, N.; Stryker, J. M. *J. Am. Chem. Soc.* **1999**, *121*, 10640–10641.
- (169) Dzwiniel, T. L.; Stryker, J. M. *J. Am. Chem. Soc.* **2004**, *126*, 9184–9185.
- (170) Nguyen, T.; Hartmann, J.; Enders, D. *Synthesis (Stuttg.)* **2013**, *45*, 845–873.
- (171) Bart, S. C.; Hawrelak, E. J.; Lobkovsky, E.; Chirik, P. J. *Organometallics* **2005**, *24*, 5518–5527.
- (172) Schore, N. E. *Chem. Rev.* **1988**, *88*, 1081–1119.
- (173) Lautens, M.; Klute, W.; Tam, W. *Chem. Rev.* **1996**, *96*, 49–92.
- (174) Schwiebert, K. E.; Stryker, J. M. *J. Am. Chem. Soc.* **1995**, *117*, 8275–8276.
- (175) Etkin, N.; Dzwiniel, T. L.; Schwiebert, K. E.; Stryker, J. M. *J. Am. Chem. Soc.* **1998**, *120*, 9702–9703.
- (176) Lehmkuhl, H.; Nehl, H. F. *Chem. Ber.* **1984**, *117*, 3443–3456.
- (177) Dzwiniel, T. L. Seven-membered carbocycle synthesis by cobalt-mediated [3 + 2 + 2] allyl/alkyne cycloaddition reactions and novel [5 + 2] cyclopentadiene/alkyne ring expansions, University of Alberta, 1999, pp. 1–461.
- (178) Chan, B. C. K. Cobalt(III)-Mediated Cycloalkenyl-Alkyne Cycloaddition and Cycloexpansion Reactions, University of Alberta, 2010, pp. 1–294.

- (179) Roe, D. M.; Maitlis, P. M. *J. Chem. Soc. A* **1970**, 3173–3175.
- (180) An, J.; Bagnell, L.; Cablewski, T.; Strauss, C. R.; Trainor, R. W. *J. Org. Chem.* **1997**, *62*, 2505–2511.
- (181) Imamoto, T.; Kusumoto, T.; Tawarayama, Y.; Sugiura, Y.; Mita, T.; Hatanaka, Y.; Yokoyama, M. *J. Org. Chem.* **1984**, *53*, 3904–3912.
- (182) Yamabe, S.; Tsuchida, N.; Yamazaki, S. *J. Chem. Theory Comput.* **2005**, *1*, 944–952.
- (183) Tsuji, J.; Nisar, M.; Shimizu, I.; Minami, I. *Synthesis (Stuttg.)*. **1984**, *12*, 1009–1009.
- (184) Wilkinson, G. *J. Am. Chem. Soc.* **1952**, *74*, 6148–6149.
- (185) Sheats, J. E.; Rausch, M. D. *J. Org. Chem.* **1970**, *35*, 3245–3249.
- (186) Gesing, E. R. F.; Tane, J. P.; Vollhardt, K. P. C. *Angew. Chem. Int. Ed.* **1980**, *19*, 1023–1024.
- (187) Heck, R. F. *Inorg. Chem.* **1989**, *4*, 855–857.
- (188) Knizhnikov, V. A.; Shirokii, V. L.; Ryabtsev, A. N.; Maier, N. A. *J. Organomet. Chem.* **1997**, *537*, 181–189.
- (189) Rausch, M. D.; Genetti, R. A. *J. Org. Chem.* **1970**, *35*, 3888–3897.
- (190) Kuhn, N.; Broggemann, H.; Winter, M. *J. Organomet. Chem.* **1987**, *320*, 391–400.
- (191) Tane, J. P.; Vollhardt, K. P. C. *Angew. Chem. Int. Ed.* **1982**, *21*, 617–618.
- (192) Weding, N.; Hapke, M. *Chem. Soc. Rev.* **2011**, *40*, 4525–4538.
- (193) Nicholls, J. C.; Spencer, J. L. *Inorg. Synth.* **1990**, *28*, 278–280.
- (194) Jonas, K.; Deffense, E.; Habermann, D. *Angew. Chem. Int. Ed. Engl.* **1983**, *22*, 716–717.
- (195) Hapke, M.; Weding, N.; Spannenberg, A. *Organometallics* **2010**, *29*, 4298–4304.
- (196) Ammal, S.; Nakamura, E.; Stryker, J. M. *Unpubl. results*.
- (197) Hardesty, J. H.; Koerner, J. B.; Albright, T. A.; Lee, G.-Y. *J. Am. Chem. Soc.* **1999**, *121*, 6055–6067.
- (198) Tempel, D. J.; Johnson, L. K.; Huff, R. L.; White, P. S.; Brookhart, M. *J. Am. Chem. Soc.* **2007**, *122*, 6686–6700.
- (199) Dieck, H. T.; Bruder, H. *Chem. Commun.* **1977**, 24–25.
- (200) Rieke, R. D. *Science* **1989**, *246*, 1260–1264.
- (201) Groth, P. *Acta Chem. Scand. A*. **1985**, *39*, 659–670.